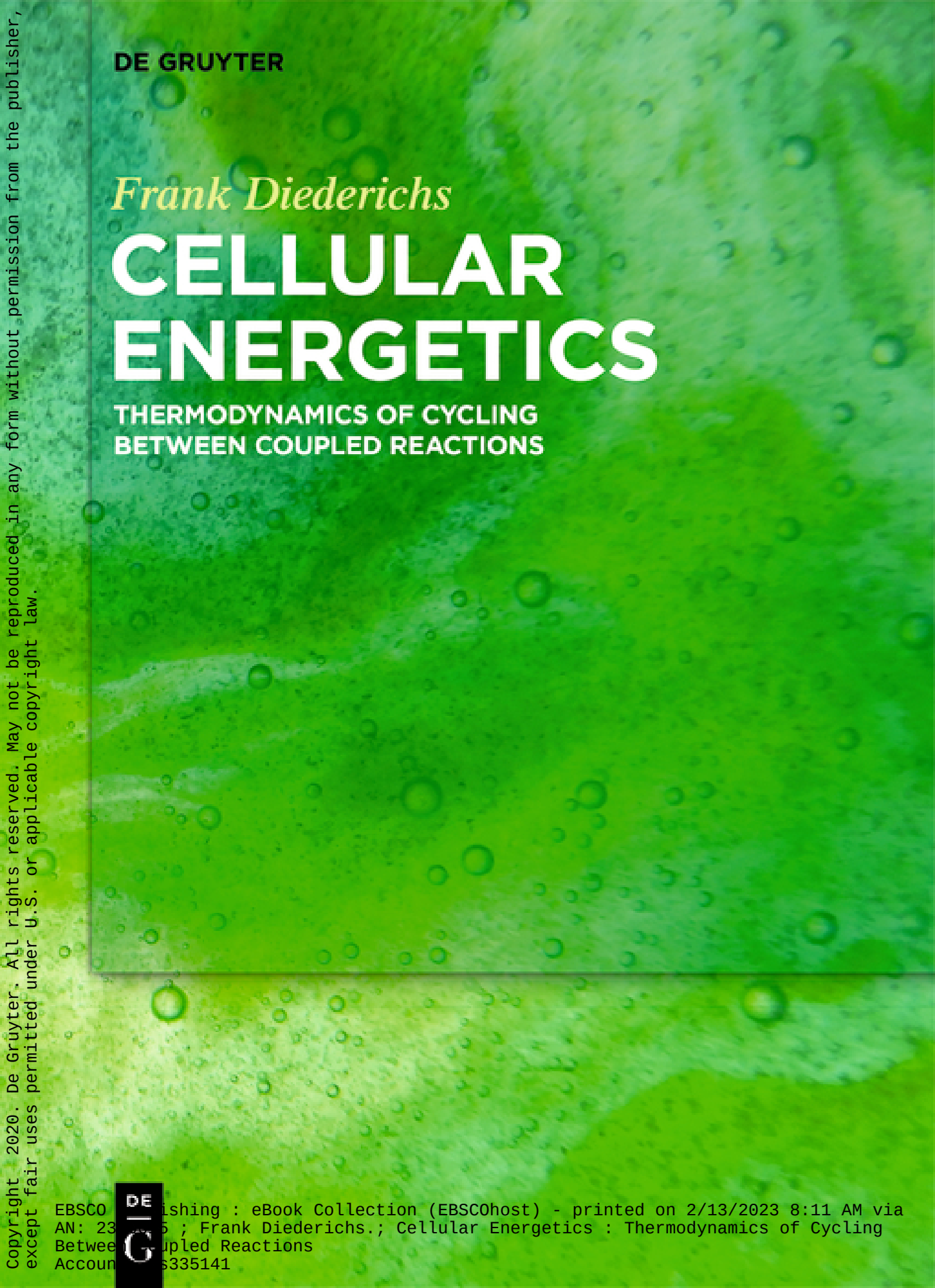

Frank Diederichs

Cellular Energetics

Also of interest

Multiscale Thermo-Dynamics.
Introduction to GENERIC
Pavelka, Klika, Grmela, 2018
ISBN 978-3-11-035094-4, e-ISBN 978-3-11-035095-1

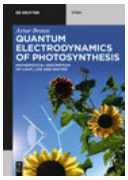

Quantum Electrodynamics of Photosynthesis.
Mathematical Description of Light, Life and Matter
Braun, 2020
ISBN 978-3-11-062692-6, e-ISBN 978-3-11-062994-1

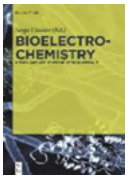

Bioelectrochemistry.
Design and Applications of Biomaterials
Cosnier (Ed.), 2019
ISBN 978-3-11-056898-1, e-ISBN 978-3-11-057052-6

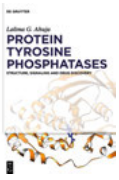

Protein Tyrosine Phosphatases.
Structure, Signaling and Drug Discovery
Ahuja, 2018
ISBN 978-3-11-049137-1, e-ISBN 978-3-11-049398-6

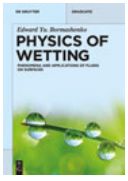

Physics of Wetting.
Phenomena and Applications of Fluids on Surfaces
Bormashenko, 2017
ISBN 978-3-11-044480-3, e-ISBN 978-3-11-044481-0

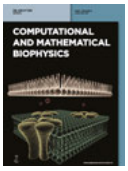

Computational and Mathematical Biophysics.
Edited by Julie Mitchell, Shan Zhao
Editor-in-Chief: Guowei Wei
e-ISSN 2544-7297

Frank Diederichs

Cellular Energetics

Thermodynamics of Cycling Between Coupled Reactions

DE GRUYTER

Author
Frank Diederichs
fwkh.diederichs@gmail.com

ISBN 978-3-11-064837-9
e-ISBN (PDF) 978-3-11-065050-1
e-ISBN (EPUB) 978-3-11-064860-7

Library of Congress Control Number: 2019944995

Bibliographic information published by the Deutsche Nationalbibliothek
The Deutsche Nationalbibliothek lists this publication in the Deutsche Nationalbibliografie; detailed bibliographic data are available on the Internet at http://dnb.dnb.de.

Cover image: Shannon Kohn/iStock/Getty Images Plus
Typesetting: Integra Software Services Pvt. Ltd.
Printing and binding: CPI books GmbH, Leck

www.degruyter.com

Preface

This book is written primarily with biochemists and biophysicists in mind; however, it does not claim to be a textbook. The most important basics of chemical thermodynamics for biochemical processes are summarized in the first five chapters so that readers who are less familiar with this area of science have the opportunity to tackle this material without any need to laboriously read through the appropriate textbooks to gather this information. For this reason, the term exact differential is comprehensively derived in the first chapter and is explained with the aid of calculated examples. At the same time, it is assumed that the reader knows how to handle partial differentiation. A deep understanding of this term in particular is indispensable because potential functions and their differentials do exist, particularly in thermodynamics, on the basis of which systems can be described and characterized. In connection with this, a particular value is placed on expressing entropy change through two different changes, namely through the entropy exchanged between the system and surroundings, and through the entropy produced by the system, as described in *Modern Thermodynamics: From Heat Engines to Dissipative Structures* (Dilip Kondepudi and Ilja Prigogine).

When introducing the terms of affinity and dissipation function, which are important for the thermodynamics of irreversible processes, the terminology used by the above-mentioned authors and the authors of the book *Bioenergetics and Linear Nonequilibrium Thermodynamics: The Steady State* (S. Roy Caplan and Alvin Essig) has been adopted. For the description of flux equations for coupled reactions, however, these are amended insofar as only one conductance emerges in the equations, namely, the coupling conductance. Uncoupling is described by two newly introduced parameters. The resulting equations are easier to survey with regard to the coupled reactions occurring in metabolism, and are therefore easier to cope with the application.

One of the main objectives of this book is to describe metabolic processes and coupled reactions in particular, through these thermodynamic flux equations, which can be solved in their entirety as a set of differential equations with the aid of a Solver. In this context, the mathematical structure of such an equation is of particular importance. The usual form of flux equations in the thermodynamics of irreversible processes defines the flux as a product of conductance and affinity, where the former is a constant and the latter can be variable. This form of equation, however, cannot fulfil the demands of the enzyme activity controlled by reactions in the metabolism of a cell. The possibilities of activation and inhibition are lacking. To eliminate this disadvantage, variable conductances were introduced by the author to provide the flux with very similar kinetic properties as they emerge with enzyme-catalyzed reactions. On the basis of such flux equations, the energy metabolism of muscle cells, for instance, can be simulated for almost every situation.

As the analogy to Ohm's law could be shown also for a metabolic pathway gone through at steady state, an electrical analogue is introduced for the energy

https://doi.org/10.1515/9783110650501-202

metabolism in the form of two batteries connected at opposite directions. Such a simple circuit can be evaluated even without the aid of a simulation. In this way, readers who are less familiar with cellular metabolic processes are given a quick introduction into the principles arising from such a constellation.

One of the most important results is that the ATP cycle, in analogy with a charging cycle in the battery model, takes place practically without entropy production. This also applies to other cycles, for instance, the proton cycle at the inner mitochondrial membrane or the cross-bridge cycle of muscular contraction.

To understand the metabolic processes described in this book, it is of course advantageous if the reader already possessed some knowledge of biochemistry. However, to the author's opinion this is not absolutely necessary. An ample range of biochemistry textbooks exists, covering the most important pathways of metabolism in clear graphic detail, which can be referenced with minimum effort. Thus, physicists and engineers interested in cellular processes should have the opportunity to penetrate the biophysics of living systems without needing to swot up on the whole subject of metabolic biochemistry.

Contents

1 State functions and exact differentials

1.1 State functions

The state function is a significant term in natural sciences and especially in chemical thermodynamics. The state of a system is defined as follows:

A system is a spatially limited area in which physical processes or chemical or biochemical reactions can occur separately. The system boundaries separate the interior of the system from the environment. Due to different characteristics of the borders, three categories can be distinguished: (1) *isolated systems* cannot exchange energy or matter with the environment, (2) *closed systems* can exchange energy but not matter with the environment and (3) *open systems* are able to exchange both energy and matter with the environment.

The state of a system such as that of an ideal gas in a cylinder closed by a movable piston is characterized by its state variables such as temperature T, volume V, pressure P and number of moles n. If one or more of these variables are changed, it is completely irrelevant in which way or on which (reaction) path these quantities are changed, only the difference between the final and initial state counts. It is always the same, provided that the considered function such as the energy content of an ideal gas is a state function.

In the following, we discuss the prerequisites that need to be fulfilled for such a function to characterize it as a state function. Determining this is important because, in such cases, handling of system changes is greatly simplified. Here, the line integral is of particular importance.

1.2 Exact differentials and line integrals

The following two situations explain the origin of a line or path integral. A body is moved by a force along a given path. If the force belongs to a potential field such as the gravitational field of the earth, its differential work can be represented as the scalar product of two vectors $\vec{F} \cdot d\vec{r} = (F_x \vec{i} + F_y \vec{j}) \cdot (dx\vec{i} + dy\vec{j})$ (arrows indicate vectors).

An exact differential,

$$dW = \frac{\partial W}{\partial x}\, dx + \frac{\partial W}{\partial y}\, dy, \tag{1.1}$$

obviously exists if $F_x \vec{i} + F_y \vec{j}$ is the gradient of the function W, that is

$$F_x \vec{i} + F_y \vec{j} = \text{grad}\, W = \frac{\partial W}{\partial x}\vec{i} + \frac{\partial W}{\partial y}\vec{j}.$$

https://doi.org/10.1515/9783110650501-001

This results in the exact differential from

$$\left(\frac{\partial W}{\partial x}\vec{i}+\frac{\partial W}{\partial y}\vec{j}\right)\cdot\left(dx\vec{i}+dy\vec{j}\right)=\frac{\partial W}{\partial x}\,dx+\frac{\partial W}{\partial y}\,dy=dW.$$

As described later, dW must have exactly this structure in order to be treated as an exact differential.

In a number of thermodynamic processes such as chemical reactions, potential fields are not involved with corresponding gradients; rather, chemical energies and the resulting work, if any, are implemented. Vector analysis is not applicable to such processes. However, even with these energy changes, functions with exact differentials (state functions) occur, which should be identified as such. Hence, slightly cumbersome nonvectorial derivation is treated in detail so as to emphasize the importance of nonexact differentials.

The nonvectorial work carried out differs from the above scalar product of two vectors. On the one hand, there is no potential field in which the direction of force as the tangential force component comes into effect; on the other, the path is not a vectorially describable function of path, but a possible direction of a process or a reaction. The differential work with infinitesimal progression of the process [dW in Joule (J)] is always given by the product of two conjugated variables such as $-PdV$ (volume work), consisting of an intensive variable such as pressure P and an extensive variable such as the infinitesimal volume change dV. The intensive variable represents the potential of a certain form of potential energy (P = volume energy/unit volume ($J/m^3 = N/m^2$)). The product of that potential and its extensive variable always has the dimension of an energy (in J). Other conjugate variables are, for example, the electrical potential ϕ [electrical energy/charge unit (J/C, C = Coulomb)] and the electric charge $q(C)$, also $\phi\,dq(J)$, or the chemical potential μ [chemical energy/unit of quantity (J/mol)] and the particle quantity n (mol), that is, $\mu\,dn(\mathrm{J})$.

The overall work results from the integral over the execution of the process in question (path). In this way, for example, volume work is given through

$$W=\int_{path}-P\,dV. \tag{1.2}$$

Often W depends on several variables. The integrand is composed of several summands of conjugated variable pairs. For two variables (x and y), it is usual to describe the integrand with $P(x,y)dx+Q(x,y)dy$, so that W can be formulated as

$$W=\int_{path}(Pdx+Qdy). \tag{1.3}$$

In order to be able to calculate such an integral, the course of the path must be given in the form of a function $y(x)$. The following examples are intended to explain this.

The integral $I = \int (3ydx + (4x + 2y)dy)$ is to be calculated as a line integral between the starting point $P_i(0.4, 2.0)$ and the final point $P_f(2.4, 2.8)$ along two different paths. Path 1 is given by $y(x) = a\,x + b\,(a = 0.4,\ b = 1.84)$. Both points must be on the path function $y(x)$. For this path, $dy = f'(x)\,dx = 0.4\ dx$ applies. Used in I this results in

$$I = \int\limits_{path1} (3(0.4x + 1.84)dx + (4x + 2(0.4x + 1.84))0.4\,dx).$$

Thus, the line integral is transformed into an ordinary definite integral, which can be solved based on the known rules. It is

$$\int\limits_{0.4}^{2.4} (3.12\,x + 6.992)dx = \left[\frac{3.12}{2}x^2 + 6.992\,x\right]_{0.4}^{2.4},$$

and therefore $I = 21.6$.

Path 2 leads from $P_i(0.4, 2.0)$ parallel to the X-axis at a distance of $y_\mathrm{i} = 2.0$ from $x_\mathrm{i} = 0.4$ to $x_\mathrm{f} = 2.8$ and from there along the Y-coordinate to P_f. The functions for this path composed of path sections $A = x_\mathrm{f} - x_\mathrm{i}$ and $B = y_\mathrm{f} - y_\mathrm{i}$ are given through $y = 2.0$ (parallel to the X-axis at a distance of $y_i = 1.5$), and $x = 2.4$ (parallel to a Y-axis at a distance of $x_\mathrm{f} = 2.4$). Parallel to the X-axis is $dy = 0$, and parallel to the Y-axis is $dx = 0$. For path A this leads to

$$I_A = \int\limits_A (3 \cdot 2.0 \cdot dx + (4x + 2 \cdot 2.0) \cdot 0) = \int\limits_{0.4}^{2.4} 6.0\,dx = [6.0\,x]_{0.4}^{2.4} = 22.72,$$

and for path B to

$$I_B = \int\limits_B (3y \cdot 0 + (4 \cdot 2.4 + 2y)dy) = \int\limits_2^{2.8} (9.6 + 2y)dy = \left[9.6y + y^2\right]_2^{2.8} = 220.32.$$

The result is $I = I_A + I_B = 243.04$.

For these integrands, it is evident that different values for both line integrals result from different paths. If this is changed in $3ydx + (3x + 2y)dy$, for unchanged initial and final points as well as the same paths, the surprising result is that at this time both paths produce the same value for their line integral. With the slightly changed integrand ($3x$ instead of $4x$), the line integral is now

$$I = \int (3ydx + (3x + 2y)dy).$$

On path 1, this yields with $y(x) = 0.4\,x + 1.84$

$$I = \int_{path1} (3(0.4x + 1.84)dx + (3x + 2(0.4x + 1.84))0.4\,dx)$$
$$= \int_{0.4}^{2.4} (2.72\,x + 6.992)dx = \left[\frac{2.72}{2}\,x^2 + 6.992\,x\right]_{0.4}^{2.4} = 21.6,$$

and on path 2 with the two path sections A and B,

$$I_A = \int_A (3 \cdot 2.0 \cdot dx + (3x + 2 \cdot 2.0) \cdot 0) = \int_0^4 6\,dx = [6\,x]_{0.4}^{2.4} = 12.0,$$

$$I_B = \int_B (3y \cdot 0 + (3 \cdot 2.4 + 2y)dy) = \int_2^{2.8} (7.2 + 2y)dy = \left[7.2y + y^2\right]_2^{2.8} = 9.6 \text{ and}$$

$$I = I_A + I_B = 21.6.$$

For the above integrand, all integration paths give the same value I = 21.6. This obviously has to be related to the structure of the integrand. For, as has been shown, even a slight change of it can nullify this property of path independence. The question therefore immediately arises as to which mathematical structure the integrand must possess in order to produce always the same and thus path-independent line integrals despite different integration paths. The answer is: the integrand must represent the exact (or total) differential of a function. For a function $W(x, y)$ of two variables, this is

$$dW = \frac{\partial W}{\partial x}dx + \frac{\partial W}{\partial y}dy,$$

and for n variable

$$dW(x_1, x_2, x_3, ..., x_n) = \frac{\partial W}{\partial x_1}dx_1 + \frac{\partial W}{\partial x_2}dx_2 + \frac{\partial W}{\partial x_3}dx_3 + \cdots + \frac{\partial W}{\partial x_n}dx_n. \tag{1.4}$$

$\partial W/\partial x$ and $\partial W/\partial y$ are the partial derivatives of the function $W(x, y)$. They are considered as functions $P(x, y)$ or $Q(x, y)$, respectively, so that dW can be formulated in the form shown earlier:

$$dW = Pdx + Qdy.$$

Now the usually unknown primitive should be found by indefinite integration of its partial derivatives. The primitive is given here in order to understand the calculation better:

$$W(x, y) = 3xy + y^2 + C.$$

Its differential is

$$dW = 3y\,dx + (3x + 2y)dy,$$

$$P(x,y) = \frac{\partial W}{\partial x} = 3y, \text{ and } Q(x,y) = \frac{\partial W}{\partial y} = 3x + 2y.$$

From these data, $W(x,y)$ can be determined by indefinite integration in the following manner. Once as

$$W = \int 3y\,dx = 3yx + f_1(y),$$

and additionally as

$$W = \int (3x + 2y)dy = 3xy + y^2 + f_2(x).$$

The functions $f_1(y)$ or $f_2(x)$ must be added to the respective function $W(x,y)$, because the former has been found by integration of the corresponding partial differential, and thus there is the possibility that the solutions thus found have lost the dependence on the respective other variable.

Since both results must be the same, it can be found by comparison that

$$W(x,y) = 3xy + y^2 + C,$$

with $f_1(y) = y^2 + C$ and $f_2(x) = 0$.

Another way to get to the primitive is to start again from

$W = \int 3y\,dx = 3yx + f_1(y)$. This expression is now differentiated with respect to y, which leads to $\partial W/\partial y = 3x + f_1'(y)$. On the other hand, $Q(x,y) = \partial W/\partial y = 3x + 2y$. Again by comparison it can be seen that $f_1'(y) = 2y$ must be true; thus,

$$f_1(y) = \int (2y\,dy) = y^2 + C.$$

The line integrals of this differential have already been determined for several paths. They all resulted in the same value. Since in addition there is the primitive obtained by integration, which corresponds to the specification, the above numerical result can be checked by inserting the coordinates of the final and the starting points into it. It is $W_\mathrm{f} - W_\mathrm{i} = W(2.4, 2.8) - W(0.4, 2.0) = 21.6$,

which agrees with the above calculations.

The last example shows that only an integrand can produce a path independence of the line integral, which is an exact differential of the primitive. In order to be able to specify the corresponding exact differential correctly, a given primitive has been assumed. In general, the primitive is not known; hence, you cannot be sure that the expression to be integrated really represents an exact differential, even if it has the form $Pdx + Qdy$. However, there is a way to test whether the integrand is actually an exact differential.

As $P = \partial W/\partial x$ and $Q = \partial W/\partial y$,

for repeated partial differentiation of $P(x,y)$ with respect to y and $Q(x,y)$ with respect to x, the following expressions are produced:

$$\frac{\partial P}{\partial y} = \frac{\partial^2 W}{\partial x\,\partial y} \text{ and } \frac{\partial Q}{\partial x} = \frac{\partial^2 W}{\partial y\,\partial x},$$

that is,

$$\frac{dP}{dy} \equiv \frac{dQ}{dx}.$$

This result is the content of the sentence established by *Schwartz* and named after him. It represents the integrability condition that must be satisfied for the existence of an indefinite integral. This exists if and only if the integrand is the exact differential of a primitive.

In the last example, $\partial P/\partial y = 3$ and $\partial Q/\partial x = 3$, which means that the integrand represents an exact differential, and the terms $P(x,y)$ and $Q(x,y)$ are actually the partial differential quotients of a primitive that can be determined by integration. If $\partial P/\partial y \neq \partial Q/\partial x$, the integrand is not an exact differential, and the indefinite integral cannot be solved. However, the line integral within specified limits can be determined, but it is now dependent on the chosen path of integration, such that different integration values are generated by different paths, although the two points connected by the paths remained the same. For both exact and nonexact differentials, their total integral has to disappear over the forward and reverse paths, if both paths are identical except for the direction of path. For the exact integral, however, it also applies that the forward and reverse paths do not have to be identical in order to make the total integral disappear. If a state variable is brought from an initial state via various intermediate states back to the initial state, then the line integral must vanish. If this condition is not fulfilled, then the relevant variable is not a state variable.

In the following, the application of Schwartz's theorem is demonstrated using the example of the ideal gas. For such a gas applies for T = const.

PV = const., with

$$d(P\,V) = \frac{\partial(PV)}{\partial V}\,dV + \frac{\partial(PV)}{\partial P}\,dP = PdV + Vdp = 0$$

and

$$PdV = -VdP.$$

According to Schwartz,

$$\frac{\partial P}{\partial P} \equiv \frac{\partial V}{\partial V} = 1.0,$$

the differential $d(PV)$ is thus exact, and the variables P and V are state variables with the associated state function $PV = \text{const.}$

If T is also a variable (only n = const.), then the general gas equation applies

$$PV = nRT.$$

For $P(V,T) = nR(T/V)$, the result is

$$dP = \frac{\partial P}{\partial V}\,dV + \frac{\partial P}{\partial T}\,dT = -\frac{nRT}{V^2}\,dV + \frac{nR}{V}\,dT$$

and

$$\frac{\partial\left(\left(-nRT\right)/V^2\right)}{\partial T} \equiv \frac{\partial(nR/V)}{\partial V} = -\frac{nR}{V^2}.$$

For $V(P,T) = nR(T/P)$, the result is

$$dV = \frac{\partial V}{\partial P}dP + \frac{\partial V}{\partial T}dT = \frac{-nRT}{P^2}dP + \frac{nR}{P}dT$$

and

$$\frac{\partial\left(\left(-nRT\right)/P^2\right)}{\partial T} \equiv \frac{\partial(nR/P)}{\partial P} = -\frac{nR}{P^2}.$$

For $T(P,V) = PV/nR$, the result is

$$dT = \frac{\partial T}{\partial P}dP + \frac{\partial T}{\partial V}dV = \frac{1}{nR}\left(VdP + PdV\right)$$

and

$$\frac{\partial V}{\partial V} \equiv \frac{\partial P}{\partial P}.$$

All variables are considered as state variables with the state function $PV = nRT$. Of course, this can also be found by integration. For

$$z(P,V) = PV = \text{const.}$$

$$\frac{\partial z}{\partial P} = V \text{ and } \frac{\partial z}{\partial V} = P$$

are obtained, which leads to

$$z = V\int \partial P = VP + f_a(V)$$

and

$$z = P\int \partial V = PV + f_b(P).$$

$z \equiv z$ is the result for

$$f_a(V) = f_b(P) = 0.$$

For $V(P,T) = nR(T/P)$, the result is

$$\frac{\partial V}{\partial P} = -nR\frac{T}{P^2} \text{ and } \frac{\partial V}{\partial T} = nR\frac{1}{P}$$

yielding

$$V = -nRT\int\left(\frac{\partial P}{P^2}\right) = nR\frac{T}{P} + f_1(T)$$

and

$$V = \frac{nR}{P}\int \partial T = nR\frac{T}{P} + f_2(P).$$

The last two determinative equations of V are identical for $f_1(T) = f_2(P) = 0$.

For $P(V,T) = nR(T/V)$, the result is

$$\frac{\partial P}{\partial V} = -nR\frac{T}{V^2}$$

and

$$\frac{\partial P}{\partial T} = nR\frac{1}{V};$$

therefore,

$$P = -nRT\int\left(\frac{\partial V}{V^2}\right) = nR\frac{T}{V} + f_3(T),$$

as well as

$$P = \frac{nR}{V}\int \partial T = nR\frac{T}{V} + f_4(V).$$

Identity arises for

$$f_3(T) = f_4(V) = 0.$$

As expected when Schwartz's theorem holds, the integrals exist for all conditions and result in the respective (given here) primitives.

As a rule, the infinitesimal change (dW) and the actual, finite change (ΔW) clearly differ, so integration of dW becomes inevitable in order to determine W. For the definite integral over $dW = Pdx + Qdy$,

$$W = \int_{x_0}^{x_0+\Delta x} P(x,y)\,dx + \int_{y_0}^{y_0+\Delta y} Q(x,y)\,dy$$

applies. For the above primitive

$$W(x,y) = 3xy + y^2 + C,$$

the result is (with $x_0 = 0.4$, $y_0 = 2.0$, as well as $\Delta x = 5.0\,x_0$, $\Delta y = 0.4\,y_0$ and $C = -2.0$) $W(x_0, y_0) = 4.4$ and $W(x_0 + \Delta x, y_0 + \Delta y) = 26.0$; therefore, $\Delta W = 21.6$.

The primitive also produces

$$\begin{aligned}\Delta W &= 3\,(x+\Delta x)(y+\Delta y) + (y+\Delta y)^2 + C - \left(3\,x_0 y_0 + {y_0}^2 + C\right)\\ &= 3y_0\,\Delta x + (3x_0 + 2y_0)\Delta y + 3\Delta x\Delta y + \Delta y^2 = 21.6.\end{aligned}$$

For comparison, the differential dW

$$dW = 3y_0\,\Delta x + (3x_0 + 2y_0)\Delta y = 16.6$$

shows a significantly lower value.

The integration of this differential, however, yields also

$$\Delta W = \Delta W_P + \Delta W_Q = \int_{x_0}^{x_0+\Delta x} (3y)\,dx + \int_{y_0}^{y_0+\Delta y} (3x+2y)\,dy = 21.6.$$

If $y = y_0$ is assumed in the first integral, $x = x_0 + \Delta x$ must be set in the second integral, which results in $\Delta W_P = 12.0$, $\Delta W_Q = 9.6$ and $\Delta W = 21.6$. If $x = x_0$ is assumed in the second integral, then $y = y_0 + \Delta y$ must be set in the first. Now $\Delta W_P = 16.8$, $\Delta W_Q = 4.8$, and ΔW is again equal to 21.6.

Figure 1.1 should clarify the integration process. The above function $W(x,y)$ represents a slightly curved surface in the considered range. Integration starts from the lower left corner point (0.4, 2.0, 4.4) through the lower right corner point (2.4, 2.0, 16.4) and then from this point to the upper right corner point (2.4, 2.8, 26.0). From the figure, however, it is not clear where the surfaces to be added come from. These are the respective areas under the two functions $P(x,y) = 3y_0$ (12.0) and $Q(x,y) = 3(x_0 + \Delta x) + 2y$ (9.6). The figure illustrates that the second integral must necessarily be continued from the point at which the first was ended, since all points of the integration path must fulfil the function, that is, must lie on the surface. Since the variables are independent of each other, $W(x,y)$ must change in the same way regardless of whether both variables change at the same time or successively.

The following example from geometry is particularly illustrative. Let us consider the volume change of a cylinder. With $r_0 = 5.0$ cm and $h_0 = 8.0$ cm, the initial volume is given by

$$V_0 = \pi r_0^2 h_0 = 628.3185 \text{ cm}^3.$$

With $\Delta r = 4.0$ cm and $\Delta h = 6.0$ cm, this leads to

$$V_1 = \pi (r_0 + \Delta r)^2 (h_0 + \Delta h) = 3,562.566 \text{ cm}^3$$

and thus to the volume increase

$$\Delta V = V_1 - V_0 = 2,934.248 \text{ cm}^3.$$

From $\partial V / \partial r = 2\pi r h$ and $\partial V / \partial h = \pi r^2$, the result by indefinite integration is given by

$$V = 2\pi h \int r \, dr = \pi h r^2 + f_1(h)$$

as well as

$$V = \pi r^2 \int dh = \pi r^2 h + f_2(r).$$

Apparently applies $f_1(h) = f_2(r) = 0$.

Furthermore,

$$\frac{\partial^2 V}{\partial r \, \partial h} \equiv \frac{\partial^2 V}{\partial h \, \partial r} = 2\pi r.$$

The calculation using definite integration yields,

$$\Delta V_r = 2\pi (h_0 + \Delta h) \int_{r_0}^{r_0 + \Delta r} r \, dr = \pi (h_0 + \Delta h) \left((r_0 + \Delta r)^2 - r_0^2 \right) = 2,463.009 \text{ cm}^3$$

(ΔV_r is the volume change caused solely by variable r), and

$$\Delta V_h = \pi r_0^2 \int_{h_0}^{h_0 + \Delta h} dh = \pi r_0^2 \Delta h = 471.2389 \text{ cm}^3$$

(ΔV_h is the volume change caused solely by the variable h). The sum of both volume increases results in

$$\Delta V = \Delta V_r + \Delta V_h = 2,934.248 \text{ cm}^3$$

and

$$V = V_0 + \Delta V = 3,562.566 \text{ cm}^3.$$

Another integration path gives

$$\Delta V_{ra} = 2\pi h_0 \int_{r_0}^{r_0+\Delta r} r\,dr = \pi h_0 \left((r_0 + \Delta r)^2 - r_0^2 \right) = 1,407.434 \text{ cm}^3,$$

and

$$\Delta V_{ha} = \pi (r_0 + \Delta r)^2 \int_{h_0}^{h_0+\Delta h} dh = \pi (r_0 + \Delta r)^2 \Delta h = 1,526.814 \text{ cm}^3,$$

$$\Delta V = \Delta V_{ra} + \Delta V_{ha} = 2,934.248 \text{ cm}^3.$$

Of course, this last mentioned approach must obtain the same result as the earlier method, to generate a certain integral by means of a path function, which can then be solved like an ordinary integral. But the latter procedure might be much more illustrative.

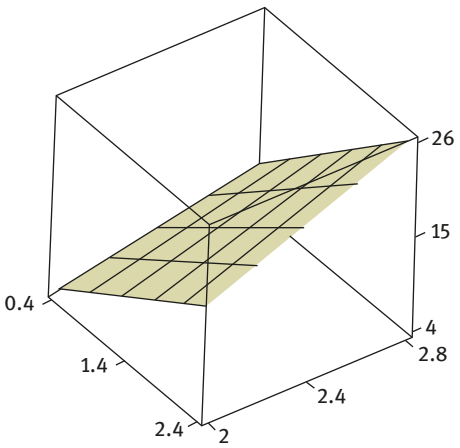

Figure 1.1: Three-dimensional surface plot of $W(x, y)$. Coordinates: x values from 0.4 to 2.4, and y values from 2.0 to 2.8.

2 State functions in thermodynamics

2.1 Energy of the system

One of the most important state functions of thermodynamics is the internal energy U of a system. It can be changed by the uptake or release of heat and/or work. In an infinitesimal form, the equation underlying this fact is

$$dU = dQ + dW \text{ (in J)}. \tag{2.1}$$

This formulation reflects the content of the first fundamental theorem of thermodynamics. It states that the total energy of the energies converted by a process is always preserved, regardless of whether identical or different forms of energy are generated during the implementation. This fact is not only an empirical principle, but a law of nature, as could be evidenced by the work of Noether [1].

On the basis of dU, further differentials, such as enthalpy dH, can be formulated. If dW is given by the volume work of a gas, then

$$dU = dQ - PdV, \tag{2.2}$$

or

$$dU = dQ - PdV - VdP + VdP = dQ - d(PV) + VdP,$$

and from there

$$dU + d(PV) = dQ + VdP.$$

The left-hand side of the equation can be summarized to a new function, the enthalpy H. The result is

$$d(U + PV) = dH = dQ + VdP. \tag{2.3}$$

This procedure, known as Legendre transformation, is necessary so that the new primitive $H = U + PV$ can be read directly from the differential $d(U + PV)$.

If the pressure of the system can be kept constant, eq. (2.3) (due to $VdP = 0$) simplifies to $dH = dQ$. Under these conditions ($P = \text{const.}$ ($\underline{\text{P}}$)), $dH = dU + \underline{P}dV$ (from $dH = dU + d(PV)$).

From the equation, it can be seen that when volume work is delivered at constant system pressure, dH is by the amount of $\underline{P}dV$ more positive than dU. At variable system pressure, for an ideal gas $d(PV) = 0$ (T and $n = \text{const.}$), and consequently $dH = dU$ (this is also apparent from $VdP = -PdV$).

The following examples demonstrate this connection:

A certain amount of heat is removed from a mixture of liquid water and ice at 273.15 K (K = degrees Kelvin), so that 1.0 mol of ice is newly formed. As a result, the volume of the system increases because the density of the ice ($\rho_s = 918 \text{ kg/m}^3$) is

https://doi.org/10.1515/9783110650501-002

lower than that of the liquid water ($\rho_l = 999.84$ kg/m^3). Increasing the volume of the system against the constant pressure of atmosphere (1 bar = 10^5 N/m^2 or Pascal) will release work from the system to the environment. This is given through

$$W = \underline{P}\left(V_s^{H_2O} - V_l^{H_2O}\right).$$

With $V_l^{H_2O} = m/\rho_l = 1.8018 \times 10^{-5}$ and $V_s^{H_2O} = m/\rho_s = 1.9624 \times 10^{-5}$ m^3, the work released is $W = -0.16$ J.

When compared with the heat of fusion that must be removed from the system to form 1.0 mol of ice (ΔH = −6.008 kJ/mol), this amount is negligible, so that the difference between ΔH and ΔU is insignificant (the value for ΔU due to $\Delta U = \Delta H - \underline{P}(V_s^{H_2O} - V_l^{H_2O}) = -6,008 - 0.16 = -6,008.16$ J under these conditions).

If a gas is produced or consumed at constant pressure, the difference between ΔH and ΔU can be much more pronounced, as the generation of, for example, 1.0 mol of gas ($\Delta n = 1.0$) is associated with a volume increase of 0.022414 m^3 (=molar volume at 273.15 K). At 1.01325 bar external pressure and constant system pressure of 1.01325 bar, then $W = \underline{P}\Delta V = \Delta n RT = -2.2711$ kJ ($T = 273.15$K) would have to be performed. ΔH would then be more positive than ΔU by the amount of 2.2711 kJ.

The derivation of the Legendre transformation used here is based on the product rule of differential calculus. If a function $f(x)$ exists as the product of two functions of the same independent variable $f(x) = u(x)v(x)$, $f'(x)$ is given as

$$f'(x) = v\,\frac{du}{dx} + u\,\frac{dv}{dx}.$$

Therefore, the differential of $f(x)$ is $df = d(u\,v) = v\,du + u\,dv$, and $-v\,du = -d(u\,v) + u\,dv$.

In eq. (2.2), $-PdV = -d(P\,V) + VdP$ of the above equation corresponds to $-v\,du = -d(u\,v) + u\,dv$.

In the transformation of the internal energy U into the enthalpy H, only the conjugated variable pair $-P\,dV$ (P = intensive variable, V = extensive variable) is converted into VdP by exchanging the variable so that V now represents the intensive variable and P the extensive variable.

From $dH = dU + \underline{P}dV = dQ - \underline{P}dV + \underline{P}dV = dQ$, it can be seen that at constant pressure of the system, the differential of volume work in dH is eliminated. All other terms of the differential dU, except $-PdV$, remain unchanged and must therefore agree with those of the differential dH under the same conditions (e.g., T = const.). Therefore, $\partial U/\partial T = \partial H/\partial T$ or $\partial U/\partial n = \partial H/\partial n = \mu$ (μ = chemical potential, see below).

The exact differential of $U(T, V)$ is given by

$$dU = \frac{\partial U}{\partial T}dT + \frac{\partial U}{\partial V}dV,$$

with $dQ = \partial U/\partial T \times dT$ and $dW = \partial U/\partial V \times dV$.

When V = const., $dQ_V = \partial U/\partial T \times dT$, and with $C_V = dQ_V/dT$, $C_V = \partial U/\partial T$.

For finite changes, the change is

$$\int dQ = Q_V = \int_{T_0}^{T_1} C_V \, dT = C_V \, \Delta T.$$

C_V is referred to as the heat capacity of a substance at constant volume. It is often constant over a wide temperature range.

At constant pressure, the result is

$$dQ_P = dU + \underline{P}dV = \frac{\partial U}{\partial T}dT + \frac{\partial U}{\partial V}dV + \underline{P}\,dV = \frac{\partial U}{\partial T}dT + \left(\frac{\partial U}{\partial V} + \underline{P}\right) dV.$$

For ideal gases, this results in the following due to $\partial U/\partial V = 0$:

$$dQ_P = C_V \, dT + \underline{P}\, dV.$$

Furthermore, because of $.\underline{P}dV = nR\,dT$ (T variable), $dQ_P/dT = C_P = C_V + nR$, and consequently $C_P - C_V = nR$.

Under these conditions, $dU_P = dQ_P - \underline{P}dV = C_V\,dT$ and $dH = C_V\,dT + \underline{P}dV$, so that $dH - dU = nR\,dT$.

The term $\underline{P}dV$ is equal to heat that must be additionally supplied to the system at constant pressure to achieve the same temperature change as at constant volume. However, the internal energy U does not change because exactly the same amount of energy is released into the environment in the form of mechanical work $-\underline{P}dV$. This fact should be clarified by the following numerical example:

One mole of an ideal gas (n = 1.0) in a cylinder closed by a movable piston is brought from $T_0 = 298.15$ K to $T_1 = 310.15$ K by supplying heat. The gas experiences a temperature change of 12.0 K and expands against a constant atmospheric pressure of $P_0 = nRT_0/V_0 = \underline{P} = 1.01325 \times 10^5 \mathrm{N/m^2} (= \mathrm{Pascal(Pa)})$. The volume at T_1 is given through $V_0 = V_M T_1/T_0 = 0.024465$ m^3 (molar volume $V_M = 0.022414$ m^3 at 273.15 K). The work delivered by the system during the expansion is $W_{\mathrm{Vol}} = -\underline{P}\Delta V$, so that the energy change of the system caused by heat supply in this case is given as

$$Q_P = \int_{T_0}^{T_1} C_V \, dT + \int_{V_0}^{V_1} \underline{P}dV = n\,Cm_V\,\Delta T + \underline{P}\Delta V.$$

($Cm_V = 12.4715\ J/mol\,K$ = molar heat capacity at V = const.). $\underline{P}\Delta V$ is the heat energy that is consumed by the expansion work.

ΔV results from

$$\int dV = \Delta V = \frac{nR}{\underline{P}} \int_{T_0}^{T_1} dT = \frac{nR}{\underline{P}}\,\Delta T = 9.846895 \times 10^{-4} \mathrm{m^3};$$

therefore, $Q_P = 12.4715 \times 12 + 1.01325 \times 10^5 \times 9.846895 \times 10^{-4} = 249.4317$ J. The result from that is $Cm_P = Q_P/\Delta T = 249.4317/12 = 20.78598\ J/mol\,K$ as well as $Cm_P - Cm_V = 20.78598 - 12.4715 = 8.31447\ J/mol\,K = R$.

Under these conditions, the change in internal energy is given by

$$\Delta U_P = Q_P - \underline{P}\Delta V = n\,Cm_V\,\Delta T = 149.658\,\text{J},$$

and the change of enthalpy by

$$\Delta H = Q_P = 249.4317\ \text{J}.$$

The following three terms must have identical values:

$$\Delta H - \Delta U = \underline{P}\Delta V = nR\,\Delta T.$$

In fact,

$$249.4317 - 149.658 = 1.01325 \times 10^5 \times 9.846895 \times 10^{-4} = 8.31447 \times 12.0 = 99.7737\ \text{J}.$$

2.2 Reversible and irreversible processes

In the last example, the volume work of an ideal gas delivered by the system was treated at constant pressure $-\underline{P}\Delta V$. However, this is not the only way for a gas to expand. The question is essential as to whether there is a possibility that allows the gain of maximum work from a given expansion of the gas. The maximum work ($W_{\max}$) is released from the gas whenever the expansion is reversible. This will be explained again with an example.

A cylinder with a piston contains 1 mol of an ideal gas in the state $T_0 = 310.15$ K, $V_1 = 0.0153\ \text{m}^3$ and $P_1 = 1.6852 \times 10^5 \text{N/m}^2$ (see previous example). This time, the gas should be brought at a constant temperature from the initial volume V_1 and the initial pressure P_1 to the volume $V_0 = 0.02545\ \text{m}^3$ and the pressure $P_0 = 1.01325\ 10^5 \text{N/m}^2$. This expansion at constant temperature can be accomplished in various ways.

It is noteworthy that the delivered volume work has a different value for each path, although the values of the state variables (T, V, P) remain the same in the initial and final states of the gas. The difference in paths is that the expansion with temperature compensation can be carried out either in a single step from V_1 to V_0 or in a multitude of steps over a great number of gradually increasing volumes.

Between these extremes every other possibility is conceivable. This dependence on the number of expansion steps (N_V) is represented by the following equation (Figure 2.1: red = expansion, blue = compression):

$$W(N_V) = \sum_{i=1}^{N_V} \left(-P(V_1 + i\,\Delta V/N_V)\,\frac{\Delta V}{N_V} \right), \text{ with } \Delta V = V_0 - V_1, \text{ and } i = 1,2,3,\ldots,N_V.$$

When $N_V \to \infty$, $-P(V_1 + i\,\Delta V/N_V)$ is transformed into $-P(V)$, and $\Delta V/N_V$ into dV and thus the above sums into the definite integral

$$\int_{V_1}^{V_0} -P(V)dV = -nRT \int_{V_1}^{V_0} (dV/V)$$

with the known solution

$$W = -nRT \ln\left(\frac{V_0}{V_1}\right) = -1.3118 \text{ kJ (expansion)},$$

$$W(1)/W = 0.7838,\ W(4)/W = 0.93789,\ W(32)/W = 0.9919 \text{ and } W(128)/W = 0.998.$$

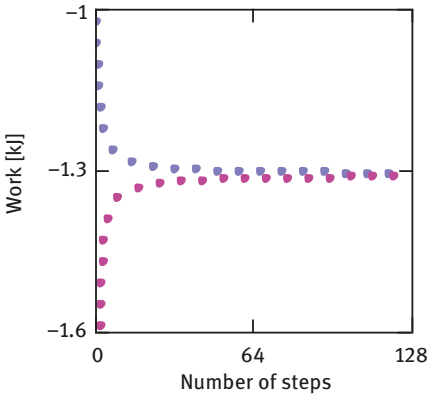

Figure 2.1: Reversible work. Blue points: expansion work; red points: compression work (with reversed sign). Reversibility of both processes is reached when the curves meet after about 128 steps at the point of reversible work of – 1,311.8 J.

Figure 2.1 shows that as the number of steps increases, the value of summation changes to that of the integral. At $N_V = 4$ around 94.0 and at $N_V = 128$, approximately 99.8% of the integral value is reached (with a cylinder radius of r = 0.1 m, this would correspond to a displacement of the piston of 2.524 mm during each expansion step). In the expansion process, the system apparently delivers the maximum work exactly when the step size becomes infinitesimal, as in the case of integration. Under such conditions, compression to initial values requires a minimum amount of work to be delivered to the system. Both works are opposite and equal under these conditions, so that $W_{\text{Exp}} + W_{\text{Comp}} = 0$. Such a process is therefore considered to be reversible. It must be assumed that rapid temperature compensation between the system and the environment can occur across the system boundaries. Even with such a small volume change under these reversible conditions, work is released at the expense of the kinetic energy of all particles of the gas, which leads to an infinitesimal temperature change dT ($dT < 0$ on expansion), which is compensated by heat input from the environment. This means that the amount of energy that disappears in the form of work from the system is made

available to the system by an equal amount of energy in the form of heat again. The internal energy of the system does not change in such a process, and $\Delta U = 0$ applies (at a constant temperature of an ideal gas). During compression, work is done on the system, and an equal amount of heat is released. Also for this $\Delta U = 0$ applies.

If the gas is left in just one step to expand from V_1 to V_0, the gas would only deliver the work needed to compress the atmosphere at constant pressure ($\underline{P}_0$) to $\Delta V = V_0 - V_1 = 10.15 = 10.15 \times 10^{-3}\text{m}^3$. This work is given by $-\underline{P}_0 \Delta V = -1,028.5\text{J}$ and is significantly lower than the work that has been obtained with the reversibly led process. Although each of all state variables has the same values, a considerably less amount of work has been carried out on the irreversible (one-step expansion) path at this time, and a considerably less amount of heat (1,028.5 J) has been absorbed. Even with the compression performed in just one step, the output values are obtained. The work done on this irreversible path is given by the piston work $\underline{P}_1 \Delta V = 1,711.0\text{J}$. In contrast to the reversible process, the sum of the working amount exchanged on the forward and reverse paths is positive, and the sum of the exchanged amounts of heat is negative ($W_{\text{Exp}} + W_{\text{Comp}} = 682.5$ J, $Q_{\text{Exp}} + Q_{\text{Comp}} = -682.5$ J). The sum of the two forms of energy results in zero, so that even in this irreversible process, $\Delta U = 0$ must be true.

The implication of these results must therefore be that only dU can be an exact differential, because ΔU disappears on the closed path, that is

$$\Delta U = \oint dU = 0.$$

This does not apply for dW and dQ, because their respective amounts,

$$W = \oint \delta W > 0 \text{ and } Q = \oint \delta Q < O$$

do not disappear in the cycle and are therefore marked with "δ" as nonexact differentials. Equation (2.1) is thus

$$dU = \delta Q + \delta W.$$

With the same forward and reverse paths and reversible processing, both Q and W disappear. This is achieved simply by the fact that the respective integrals are identical on the forward and reverse paths except for the direction of integration and as a result must vanish. Under these special conditions, therefore, the amounts of nonexact differentials can also be zero.

The fact that the differential of the work δW depends on the path that has gained tremendous importance, especially in technology, because of this property thermal engines could be developed. The working principle of such machines is described by the Carnot cycle, named after its discoverer Sadi Carnot. At high temperature T_{h} a certain amount of heat energy Q_{h} is absorbed by the system (e.g., an ideal gas) and by reversible expansion at T_{h} = const. is converted into volume work. Thereafter, the system is brought to a lower temperature T_{c} and reversibly compressed at this

temperature to a certain volume, whereby work must be performed on the system, and a corresponding amount of heat Q_c is delivered to the environment at $T_c = \text{const.}$. These isothermal works are $W_h = -nRT_h \ln(V_2/V_1)$ and $W_c = -nRT_c \ln(V_3/V_4)$. The resulting reversible work must be negative and thus usable because T_h is greater than T_c. Due to the reversible processing, W_h ($T = \text{const.}$) represents the maximum expansion work and W_c the minimum compression work.

To reach the lower temperature, the gas must adiabatically expand, that is, without heat exchange with the environment, T_h decreases to T_c. The initial temperature T_h is restored by adiabatic compression from T_c to T_h. The two adiabatic works are given by $W_{adexp} = C_V \Delta T < 0$ (due to $\Delta T < 0$ with adiabatic expansion) and $W_{adcom} = C_V \Delta T > 0$. Since both ΔTs are opposite and equal, $W_{adexp} + W_{adcom} = 0$, which means that both adiabatic works disappear in the work balance of the cycle, so that this is given solely by the isothermal steps $W_{Car} = W_h + W_c$.

The following volumes are processed clockwise in a cyclic way:

1. $V_1 \rightarrow V_2$ isotherm,
2. $V_2 \rightarrow V_3$ adiabatic,
3. $V_3 \rightarrow V_4$ isotherm and
4. $V_4 \rightarrow V_1$ adiabatic (Figure 2.2).

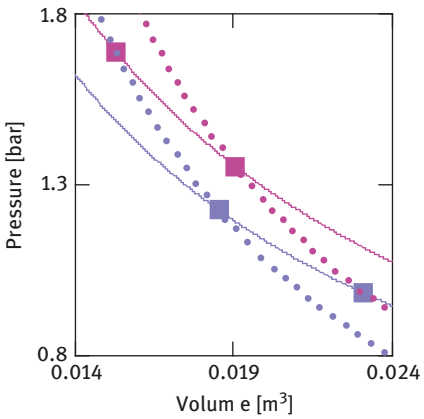

Figure 2.2: Carnot cycle. The cycle starts on the forward path (isothermally at $T_h = 310.15$ K: red line; adiabatically: red points) at point $P1$(1.6852, 0.0153) through $P2$(1.3523, 0.01907) to $P3$ (0.9844, 0.02307), and runs on the return path (isothermally at $T_c = 213.15$ K: blue line; adiabatically: blue points) from there through $P4$(1.2267, 0.01851) back to $P1$. The enclosed area corresponds to the work done by the system under reversible conditions.

The same applies to pressures. After completion of a cycle, the initial values T_h V_1 and P_1 are reached again. As expected, the values for heat and work changes of the respective isothermal work operations do not disappear. With reversible process operation, a particularly noteworthy fact emerges. The quotients of exchanged

thermal energy and temperature of the respective isothermal heat transfer are opposite and equal, that is, in the cycle, these expressions must disappear. Then the following applies:

$$\frac{Q_\mathrm{h}}{T_\mathrm{h}} + \frac{Q_\mathrm{c}}{T_\mathrm{c}} = 0 \ (Q_c < 0).$$

For the efficiency of the cycle the following applies, due to

$$T_\mathrm{h}\, V_2^{\gamma-1} = T_\mathrm{c}\, V_3^{\gamma-1}, \text{ and } T_h\, V_1^{\gamma-1} = T_c\, V_4^{\gamma-1};$$

hence,

$$V_2/V_1 = V_3/V_4,$$

$$\eta_\mathrm{Car} = -\frac{W_\mathrm{Car}}{Q_\mathrm{h}} = \frac{Q_\mathrm{h} + Q_\mathrm{c}}{Q_\mathrm{h}} = 1 + \frac{-nRT_\mathrm{c}\ln(V_3/V_4)}{nRT_\mathrm{h}\ln(V_2/V_1)} = 1 - \frac{T_\mathrm{c}}{T_\mathrm{h}} \tag{2.4}$$

2.3 Entropy of the system

The quantity $\delta Q/T$ is evidently independent of the path, as it becomes zero on the closed path of the cycle. According to R. Clausius, this quantity is defined as a new variable and called entropy S (in J/K). Its exact differential is $dS = \delta Q/T$. For reversible conditions, therefore

$$\Delta S = \oint \frac{\delta Q}{T} = \oint dS = 0$$

applies.

In mathematics, $1/T$ is known as the integrating factor, which transforms the nonexact differential δQ into the exact differential dS.

The following numerical examples are intended to illustrate and explain the influence of the irreversibly conducted process on the work delivered, the heat energies exchanged with the environment and the entropies associated therewith:

Under reversible conditions, the work delivered by the system (ideal gas) after passing through a cycle is

$$W_\mathrm{Car} = W_\mathrm{h} + W_\mathrm{c} = -nR\ 310.15\ \ln\left(\frac{0.015302}{0.019107}\right) + (-)nR\ 273.15\ \ln\left(\frac{0.01851}{0.02307}\right) = -67.7\ \mathrm{J},$$

thereby $W_\mathrm{h} = -567.5$ J and $W_\mathrm{c} = 499.8$ J. The heat exchanged with the environment is $Q_\mathrm{h} = -W_\mathrm{h}$ and $Q_\mathrm{c} = -W_\mathrm{c}$. Thus, the following applies:

$$\Delta S_\mathrm{Car} = \frac{Q_\mathrm{h}}{T_\mathrm{h}} + \frac{Q_\mathrm{c}}{T_\mathrm{c}} = \frac{567.5}{310.15} + \frac{-499.8}{273.15} = 0\ \mathrm{J/K}.$$

Under partially irreversible conditions, this result changes considerably. The irreversibility is brought about by replacing the expansion in infinitesimal steps with

one in just one step. It is expanded from the beginning against the respective constant final pressure, or compressed with the respective constant final pressure. The cycle should run through the same volumes as under reversible conditions. The result for the partially irreversible, isothermal expansion (310.15 K) is

$$W_{\mathrm{h}}^{\mathrm{parirr}} = -\underline{P}_2(V_2 - V_1) = -509.4\,\mathrm{J}\ (\text{reversible: } -567.5\ \mathrm{J}).$$

The partially irreversible, isothermal compression (273.15 K) is given by

$$W_{\mathrm{c}}^{\mathrm{parirr}} = -\underline{P}_4\,(V_4 - V_3) = 559.1\,\mathrm{J}\ (\text{reversible: } 499.8).$$

The adiabatic work steps should be carried out reversibly, so that the entire delivered work is given also under these conditions by the two isothermal steps:

$$W_{\mathrm{Car}}^{\mathrm{parirr}} = W_{\mathrm{h}}^{\mathrm{parirr}} + W_{\mathrm{c}}^{\mathrm{parirr}} = +\ 49.7\ \mathrm{J}.$$

The positive value means that in contrast to the reversible cycle, where the compression work is entirely from expansion work, extra work has to be done from the environment to operate it. The entropy change due to the reversibly exchanged heat (only expansion and compression are partially irreversible) is

$$\Delta_{\mathrm{e}}S = \frac{Q_{\mathrm{h}}^{\mathrm{parirr}}}{T_{\mathrm{h}}} + \frac{Q_{\mathrm{c}}^{\mathrm{parirr}}}{T_{\mathrm{c}}} = -0.4043\ \mathrm{J/K}$$

(the index "e" in $\Delta_{\mathrm{e}}S$ refers to exchanged entropy). The nonzero value indicates that under irreversible conditions, the entropies exchanged with the environment do not disappear, so their differential cannot be exact. To yield $\oint dS = \Delta S = 0$, the opposite and equal value would have to be added, which results from the difference of the respective reversible and irreversible works: $\Delta W_{\mathrm{h}}^{\mathrm{diss}} = W_{\mathrm{h}} - W_{\mathrm{h}}^{\mathrm{irr}} = -58.1\ \mathrm{J}$ and $\Delta W_{\mathrm{c}}^{\mathrm{diss}} = W_{\mathrm{c}} - W_{\mathrm{c}}^{\mathrm{irr}} = -59.26\ \mathrm{J}$.

The difference thus obtained is equal to the work dissipated in the irreversible process. By means of division with the respective temperature that entropy change is achieved, which evidently results directly from the irreversibly conducted process. For this irreversibly produced entropy change

$$\Delta_{\mathrm{i}}S = \frac{-\Delta W_{\mathrm{h}}^{\mathrm{diss}}}{T_{\mathrm{h}}} + \frac{-\Delta W_{\mathrm{c}}^{\mathrm{diss}}}{T_{\mathrm{c}}} = 0.4043\ \mathrm{J/K}$$

applies (the index "i" in $\Delta_{\mathrm{i}}S$ denotes the entropy produced by the irreversible process). Also $d_{\mathrm{i}}S$ is not an exact differential. It is seen, however, that the sum of the entropy changes disappears, so that the change in the total entropy of the cycle is

$$\Delta S_{\mathrm{Car}} = \Delta_{\mathrm{e}}S + \Delta_{\mathrm{i}}S = 0.$$

While $\Delta_{\mathrm{e}}S$ of the system is always compensated by an oppositely equal value of the entropy change of the environment $\Delta_{\mathrm{e}}S = -\Delta_{\mathrm{e}}S_{\mathrm{sur}}$, $\Delta_{\mathrm{i}}S$ remains uncompensated.

Since $\Delta_i S$ is calculated from the dissipated work, it seems plausible to make it directly responsible for the production of entropy. Obviously, work becomes always dissipated whenever an amount of work going beyond the level of work required is used to drive the process. During reversible expansion, the pressure associated with each infinitesimal amount of work is only infinitesimally greater than the counter pressure applied to the piston. In the case of irreversible expansion, this equilibrium pressure on the piston is lowered by a non-infinitesimal step below that of the gas. The gas has a much higher pressure than the piston, so that the expansion is now inevitably carried out with an excess of energy. This excess energy expenditure is lost for the expansion work and therefore cannot influence the internal energy of the gas. Though the gas particles release less kinetic energy to the piston under these conditions, they also take less kinetic energy in the form of heat from the environment. While under reversible conditions, the gas particles give off a maximum of kinetic energy as expansion work via the piston to the environment and absorb a maximum of heat to keep the temperature constant, this exchange of work against heat is reduced in the case of partially irreversible expansion. However, the state of the gas is the same under both conditions, meaning that V, P, T and S are identical at the end of the two differently conducted processes.

Under partially irreversible conditions, less work is released into the environment during expansion compared to the fully reversible process control, and accordingly less heat energy is taken up by the system. The environment thus holds back more heat energy. During compression, however, more work is put into the system and accordingly more heat energy is delivered to the environment. This difference obtained in relation to reversible conditions is generated in the system and equals the sum of both works dissipated there. In the environment they appear with opposite and equal amounts as heat.

In this connection, also such a Carnot cycle must be considered, which does not produce net work. For this purpose, the isothermal working steps must also be equal. This can be realized by conducting the expansion process partially irreversibly with $W_h = -W_c$, thereby the net work of the cycle vanishes. The work that could be gained under reversible conditions becomes dissipated, which is equal to the heat

$$Q = -W_{Car} = Q_h + Q_c = 67.7 \text{ J } (Q_c < 0).$$

This amount of heat remains in the hot reservoir. Only an amount of 499.8 J goes from the hot reservoir via Carnot cycle to the cold one. The entropy change produced by dissipation is

$$\Delta_{Ri}S = \frac{Q}{T_h} = 67.7/310.15 = 0.2183 \text{ J/K}.$$

It equals that entropy production, which is generated by an irreversible heat transfer from a hot to a cold reservoir without contribution of a Carnot cycle (at same temperatures, $Q_h < 0$, $Q_c > 0$):

$$\Delta_{Ri}S = \frac{Q_h}{T_h} + \frac{Q_c}{T_c} = -499.8/310.15 + 499.8/273.15 = 0.2183 \text{ J/K}.$$

Under these special conditions, mechanical work is cycled at $W_{Car} = 0$, so that no net work can be produced. It follows that dW must be an exact differential for that special cycle. It will be shown that in living cells similar cycling processes occur (at $T = const.$) between coupled reactions.

The irreversible or partially irreversible process is characterized by a remarkable difference compared to the reversible process. This is given by the respective speed with which both are gone through. While the process rate approaches zero under reversible conditions, it can reach very significant levels in the event of irreversible events and, as a result, can be accompanied by an equally significant output. The associated generation of $\Delta_i S$ multiplied by the respective temperature, $T\Delta_i S = -\Delta W_{diss}$, indicates the degree of irreversibility of the process. This entropy production, in contrast to the exchanged entropy, which can have both positive and negative values, is always positive. This is the content of the second law of thermodynamics, which can be summarized as follows [2, 3]:

$$\Delta_i S \geq 0. \tag{2.5}$$

The fastest process in the expansion is achieved when the gas can freely expand, which means it can expand completely without work. Then, the power output also equals zero. A gas that is in a cylinder closed by a movable piston must not transmit any kinetic energy to the piston. Of course, this can only be verified in thought experiments. After the free expansion, the gas has a larger volume and a correspondingly reduced pressure, its temperature (strictly speaking, only for ideal gases) does not change due to the expansion in the absence of work output ($W = 0$), so that also no heat exchange has to take place $(Q = 0)$.

For this completely irreversible expansion $\Delta W_{diss} = W_{max}$ applies. The result is $\Delta_i S = (-\Delta W_{diss})/T = -W_{max}/T$, and therefore for an ideal gas,

$$\Delta S = \Delta_i S = nR \ln\left(\frac{V_2}{V_1}\right) \tag{2.6}$$

(completely irreversible expansion with $\Delta_e S = 0$).

The question of which molecular mechanism of entropy production is the basis was answered by Ludwig Boltzmann. The starting point of his theory was the idea that the particles of a system such as that of an ideal gas, depending on its state variables, have different energies, which are distributed over a certain number of possible energy levels. Different distributions are possible, but not all are equally likely. One of the possible distributions has the maximum probability. This thermodynamic probability or multiplicity Ω differs from the mathematical probability, in which the latter can assume values between 0 and 1, while Ω is always given by a very large number. This number of all possible distributions can be determined in

principle with the means of combinatorics. In order to simplify the calculation, its natural logarithm is used to determine the maximum. $\ln(\Omega_{max})$ can be related to the entropy of the system according to the following formula:

$$S = k_B \ln(\Omega_{max}) \ (k_B = \text{Boltzmann constant in J/K}).$$

This is Boltzmann's famous formula. It combines the macroscopic quantity of the entropy with the greatest possible multiplicity of the molecular components forming the system. The relationship with eq. (2.6) becomes clear by comparison. First, $\Delta_i S = nR \ln(V_2/V_1)$ merges by means of expansion with N_A (Avogadro's number $N_A = 6.022142 \times 10^{23}$ particle/mol) in the expression $\Delta_i S = k_B \ln (V_2/V_1)^N$ ($N = nN_A$ = particle number). The change of entropy according to Boltzmann is given by $\Delta S = k_B \ln(\Omega_2/\Omega_1)$. The comparison shows that $\Omega_2/\Omega_1 = (V_2/V_1)^N$.

As already shown, one can obtain from $U(S, V)$ by a Legendre transformation with respect to V the new function $H(S, P)$ and

$$dH = d(U + PV) = Td_eS + VdP. \tag{2.7}$$

In the above equation δQ has been replaced by Td_eS. The prerequisite for this is that the heat exchange between the system and the environment is reversible, because only then does $d_eS = \delta Q/T$ apply.

dU and dH can also be transformed with respect to the variable S. By means of this the new functions $A(T, V)$ (Helmholtz energy) and $G(T, P)$ (Gibbs energy) are created. Thus, eqs. (2.2) and (2.3) are first transformed to

$$\begin{aligned} dU &= Td_eS + Td_iS - Td_iS - PdV \\ &= TdS - Td_iS - PdV \end{aligned}$$

(with $dS = d_eS + d_iS$), and

$$\begin{aligned} dH &= Td_eS + Td_iS - Td_iS + VdP \\ &= TdS - Td_iS + VdP \end{aligned}$$

The Legendre transformation of dU or dH with respect to S yields

$$dA = d(U - TS) = -SdT - Td_iS - PdV \text{ with } A = U - TS, \tag{2.8}$$

$$dG = d(H - TS) = -SdT - Td_iS + VdP \text{ with } G = H - TS. \tag{2.9}$$

The transformation to dA or to dG occurs by subtraction of $d(TS)$ from both sides of the equations for dU and dH, respectively. Through this the reversibly exchanged heat Td_eS from both dU and dH is eliminated. In contrast to dU and dH, which are related to actual energy changes, dA and dG are related to the maximum possible working ability, which contains both the actually performed and the dissipated work. Therefore, $Td_iS = -\delta W_{diss}$ must be included in the equations for dA and dG.

For T = const.,

$$dA = dU - TdS = -Td_iS - PdV, \tag{2.10}$$

$$dG = dH - TdS = -Td_iS + VdP. \tag{2.11}$$

Inserting dU or dH into the left side of the respective equation confirms the correctness of the derivation. For dG, for example, the following applies:

$$Td_eS + VdP - T(d_eS + d_iS) \equiv -Td_iS + VdP.$$

By means of some examples, the terms $\Delta U$and ΔH, as well as ΔA and ΔG are explained.

In the reversible isothermal expansion of an ideal gas from V_1 to V_2 (first step in the Carnot cycle), the maximum expansion work is given by the integral

$$W_h^{iso} = -nRT_h \int_{V_1}^{V_2} \frac{dV}{V} = -nRT_h \ln\left(\frac{V_2}{V_1}\right) = = -567.495 \text{ J}.$$

The heat energy required by the system is $Q_h = T\Delta_eS = -W_h = 567.495$ J, so that $\Delta U = Q + W = 0$ is obtained.

As $\Delta H = \Delta U + \Delta(PV)$ and $\Delta(PV) = 0$ with $T = \text{const.}$, $\Delta H = 0$: $\Delta G = W_h = -567.495$ J.

Also $\Delta G = \Delta H - T_h(\Delta_eS + \Delta_iS)$ leads to this result, because $\Delta G = 0 - Q_h - 0 = -567.5$ J and $\Delta_eS + \Delta_iS = Q_h/T_h + 0 = 1.8297$ J/K.

The same applies for the reversible isothermal compression (third step in the Carnot cycle), $\Delta U = \Delta H = 0$, because even with isothermal compression, work and heat compensate each other. Under reversible conditions, the compression work is minimal. It is given by $\Delta G = -nRT_c \ln(V_4/V_3) = 499.795$ J, with $Q_c = -W_c = -499.795$ J:

$$\Delta G = \Delta H - T_c(\Delta_eS + \Delta_iS) = 0 - (-499.795) + 0 = 499.795 \text{ J},$$

$$\Delta_eS + \Delta_iS = Q_c/T_c + 0 = -1.8297 \text{ J/K}.$$

In the case of partially irreversible isothermal expansion, the work is given by $W_h^{parirr} = -\underline{P}_2(V_2 - V_1) = -509.391$J. The amount of heat absorbed is $Q_h^{parirr} = T_h\,\Delta_eS = -W_h^{parirr} = 509.391$ J.

Even under these conditions, the work released is energetically compensated by the absorbed thermal energy, so that $\Delta U = \Delta H = 0$ must also apply here. The dissipated work for this is $\Delta W_{diss} = W_{max} - W_h^{parirr} = -58.104$ J.

Since $\Delta G = W_{max} = W_h^{parirr} + \Delta W_{diss}$, this results in $\Delta G = -509.391 + (-)58.104 = -567.495$ J, or $\Delta G = \Delta H - T(\Delta_eS + \Delta_iS) = 0 - 509.391 - 58.104 = -567.495$ J (with $\Delta W_{diss} = -T\Delta_iS$) and $\Delta_eS + \Delta_iS = Q_h^{parirr}/T_h + (-\Delta W_{diss})/T_h = 1.642402 + 0.1873416 = 1.8297$ J/K.

The last result shows that ΔG does not depend on the reversibly or irreversibly conducted process, that is, it is independent of the path. The same applies for ΔA.

An adiabatic process (second step in the Carnot cycle) is characterized by the fact that only work but no heat can be exchanged with the surroundings. That is, $dU = C_V dT = -PdV$. Dividing by $T = PV/nR$ yields

$$\frac{dT}{T} = -\frac{nR}{C_V}\frac{dV}{V}, \text{ or with } \gamma = C_P/C_V$$

$$\ln\left(\frac{T_2}{T_1}\right) = n(\gamma - 1)\ln\left(\frac{V_1}{V_2}\right),$$

which leads to $T_2\, {V_2}^{n(\gamma-1)} = T_1\, {V_1}^{n(\gamma-1)}$ or $P_2\, {V_2}^{n\gamma} = P_1\, {V_1}^{n\gamma}$.

The following integrals apply (for $n = 1.0$):

$$W_{\text{ad23}} = -P_2\, {V_2}^{\gamma} \int_{V_2}^{V_3} V^{-\gamma} dV = -\frac{P_2\, {V_2}^{\gamma}}{1-\gamma}\left({V_3}^{(1-\gamma)} - {V_2}^{(1-\gamma)}\right) = -461.45 \text{ J}$$

and

$$W_{\text{ad41}} = \frac{P_1\, {V_1}^{\gamma}}{1-\gamma}\left({V_4}^{(1-\gamma)} - {V_1}^{(1-\gamma)}\right) = 461.45 \text{ J}.$$

Obviously, both adiabatic work processes are opposite equal and therefore cancel. This is shown as follows:

The above equations can be written as

$$-\frac{P_2\, {V_2}^{\gamma}}{1-\gamma}\left({V_3}^{(1-\gamma)} - {V_2}^{(1-\gamma)}\right) = -\frac{P_2\, V_2}{1-\gamma}\left(\frac{{V_2}^{\gamma-1}}{{V_3}^{\gamma-1}} - 1\right)$$

and

$$\frac{P_1\, {V_1}^{\gamma}}{1-\gamma}\left({V_4}^{(1-\gamma)} - {V_1}^{(1-\gamma)}\right) = \frac{P_1\, V_1}{1-\gamma}\left(\frac{{V_1}^{(1-\gamma)}}{{V_4}^{(1-\gamma)}} - 1\right).$$

Because

$$\frac{T_c}{T_h} = \left(\frac{V_2}{V_3}\right)^{1-\gamma} = \left(\frac{V_1}{V_4}\right)^{1-\gamma}$$

and

$$P_2\, V_2 = P_1\, V_1,\ W_{\text{ad23}} = -W_{\text{ad41}}.$$

The adiabatic work is equal to the change in the internal energy of the system, and hence, it can be also expressed as

$$\Delta U = C_V \Delta T = 12.4715\ (-37.0) = -461.45 \text{ J}, \text{ with } Q = Td_eS = 0.$$

The fact that d_eS becomes zero in adiabatic processes can also be shown by the following derivation:

$$\frac{dQ}{T} = \frac{dU}{T} + nR\frac{dV}{V} \text{ or } d_eS = C_V\frac{dT}{T} + nR\frac{dV}{V}.$$

The integration results in

$$\Delta_eS = C_V \ln\left(\frac{T_2}{T_1}\right) + nR\ln\left(\frac{V_3}{V_2}\right);$$

therefore,

$$\Delta_eS = 12.4715\ \ln\left(\frac{273.15}{310.15}\right) + 8.3145\ \ln\left(\frac{0.023072}{0.019069}\right) = 0\ \text{J/K}.$$

$\Delta G = W_{max} = C_V\Delta T = -461.45$ J, with which $\Delta_eS + \Delta_iS = 0$ J/K leads to $\Delta H = \Delta G = -461.45$ J.

For the partially irreversible isothermal compression (third step in the Carnot cycle), the following applies:

$$\Delta U = \Delta H = 0 \text{ and } \Delta G = W_{min} = W + \Delta W_{diss} = 559.055 + (-)59.26 = 499.795\ \text{J},$$

or

$$\Delta G = \Delta H - T_c(\Delta_eS + \Delta_iS) = 0 - 273.15\ (-2.046696 + 0.2169504) = 499.795\ \text{J}.$$

$$\Delta_eS + \Delta_iS = -2.046696 + 0.2169504 = -1.829746\ \text{J/K}.$$

For reversible adiabatic expansion (fourth step in the Carnot cycle), the result is with $\Delta U = C_V\Delta T = 12.4715\ (+37.0) = 461.45$ J, $\Delta G = W_{max} = C_V\Delta T = 461.45$ J, $\Delta H = \Delta G = 461.45$ J and $\Delta_eS + \Delta_iS = 0$ J/K.

For the respective line integrals concerning the closed path of the cycle (=sum of the four steps, either all reversible, or first and third step partially irreversible) applies,

reversible as irreversible:

$$\sum_{i=1}^{4}\Delta U_i = 0 + (-461.495) + 0 + 461.495 = 0\ \text{J},$$

reversible as irreversible:

$$\sum_{i=1}^{4}\Delta H_i = 0 + (-461.495) + 0 + 461.495 = 0\ \text{J},$$

reversible as irreversible:

$$\sum_{i=1}^{4}\Delta G_i = -567.495 + (-461.495) + 499.795 + 461.495 = -67.7\ \text{J}$$

or

$$\sum_{i=1}^{4} \Delta G_i = \sum_{i=1}^{4} \Delta H_i - \left(T_\mathrm{h}\left(\Delta_\mathrm{e}S_\mathrm{h} + \Delta_i S_\mathrm{h}\right) + T_\mathrm{c}\left(\Delta_\mathrm{e}S_\mathrm{c} + \Delta_i S_\mathrm{c}\right)\right)$$
$$= 0 - 310.15\ (1.642401 + 0.1873416) - 273.15\ (-2.046696 + 0.2169504)$$
$$= -67.7\ \mathrm{J}.$$

As for each step, $\Delta U = \Delta H$ is fulfilled, also $\Delta A = \Delta G$ must apply.

Reversible:

$$\sum_{i=1}^{4} \Delta S_i = \Delta_\mathrm{e}S_\mathrm{h} + \Delta_\mathrm{e}S_\mathrm{c} = 1.829746 + (-)1.829746 = 0\ \mathrm{J/K},$$

irreversible:

$$\sum_{i=1}^{4} \Delta S_\mathrm{i} = \left(\Delta_\mathrm{e}S_\mathrm{h} + \Delta_i S_\mathrm{h}\right) + \left(\Delta_\mathrm{e}S_\mathrm{c} + \Delta_i S_\mathrm{c}\right) = 1.829746 + (-1.829746) = 0\ \mathrm{J/K}, \text{ with}$$
$$\sum_{i=1}^{4} \Delta_\mathrm{e}S_\mathrm{i} = \Delta_\mathrm{e}S_\mathrm{h} + \Delta_\mathrm{e}S_\mathrm{c} = 1.642401 + -2.046696 = -0.404295, \text{ and}$$
$$\sum_{i=1}^{4} \Delta_i S_i = \Delta_i S_\mathrm{h} + \Delta_i S_\mathrm{c} = 0.1873416 + 0.2169504 = 0.404292.$$

Reversible:

$$\sum_{i=1}^{4} W_i = \sum_{i=1}^{4} W_{\mathrm{max}i} = \sum_{i=1}^{4} \Delta G_i = -567.495 + (-461.495) + 499.795 + 461.495 = -67.7\ \mathrm{J}.$$

Partially irreversible:

$$\sum_{i=1}^{4} W_i = -509.391 + (-461.495) + 559.055 + 461.495 = 49.664\ \mathrm{J}.$$

The positive value of the (net) work indicates that, due to irreversibility, work from outside has to be fed into the system to make the cycle progress.

The results show that dU and dH are exact differentials. The sum concerning ΔG_i does not result in zero, so the line integral does not disappear. As a result, dG and dA are not exact differentials with respect to the Carnot cycle. This behavior is caused by the fact that this process has to go through different temperatures.

Also $dS = d_\mathrm{e}S + d_\mathrm{i}S$ is an exact differential, the differentials $d_\mathrm{e}S$ and $d_\mathrm{i}S$, on the other hand, are not, because they do not disappear in the irreversible course of the Carnot cycle. $d_\mathrm{e}S$ is exact only under fully reversible conditions.

Under isothermal conditions dG and dA are, in contrast to the working differential δW, exact differentials. This can be shown by the following consideration. The

expansion of a gas takes place at a given temperature T completely irreversible from V_1 to V_2. This changes G by $\Delta G = -RT\ln(V_2/V_1)$. On the return path from V_2 to V_1, the gas is reversibly compressed at the same temperature. In the process, G changes by $\Delta G = -RT\ln(V_1/V_2)$. The total change ΔG_{cyc} for this cycle disappears. In contrast, W_{cyc} does not become zero but is given by $W_{cyc} = W_{exp} + W_{comp} = 0 - RT\ln(V_1/V_2) > 0$.

Based on this example, the interrelation of $\Delta_e S$ and $\Delta_i S$ is particularly clearly demonstrated. The completely irreversible gas expansion (T = const.) occurs without work and heat exchange. Accordingly $\Delta_e S = 0$, while for $\Delta_i S$, $\Delta_i S = -W_{max}/T = -\Delta G_{exp}/T$ applies.

The reversible compression (T = const.) results in $\Delta_e S = -W_{min}/T = -\Delta G_{comp}/T$ and $\Delta_i S = 0$.

Over the closed path, is

$$\sum \Delta S = \sum \Delta_e S + \sum \Delta_i S = [0 - R\ln(V_2/V_1)] + [R\ln(V_2/V_1) + 0] = 0.$$

ΔS equals zero, therefore, dS must be an exact differential. Neither $\Delta_i S$ nor $\Delta_e S$ disappear, but are opposite equal, so that they cancel out in the sum. $d_i S$ and $d_e S$, therefore, do not represent exact differentials for such a process.

3 Chemical potentials

So far, the number of moles n has been kept constant. However, if this is also a variable, the exact differential of a system consisting of several substance components $dU(S, V, n_1, ..., n_n) = (\partial U/\partial S)dS + (\partial U/\partial V)dV + \sum_i (\partial U/\partial n_i)dn_i$ applies.

When $(\partial U/\partial S) = T$, $(\partial U/\partial V) = -P$ and $(\partial U/\partial n_i) = \mu_i$, the following is obtained:

$$dU = Td_eS - PdV + \sum_i \mu_i dn_i. \tag{3.1}$$

The new quantity μ (in J/mol) is called chemical potential. Analogous to Td_eS and $-PdV$ this is conjugated with the infinitesimal change of the corresponding number of moles, so that this product also has the dimension of an energy.

The general antiderivative of 3.1 is given by

$$U = ST - PV + \sum_i n_i\mu_i$$

This follows from the fact that the function U (S, V, n) depends on extensive variables, so that it can be treated according to Euler's theorem with the above result. The completely developed differential of this latter equation is

$$dU = SdT + Td_eS - (VdP + PdV) + \sum_i (n_i d\mu_i + \mu_i dn_i). \tag{3.2}$$

The comparison of expressions (3.1) and (3.2) shows that some terms must disappear in the above equation, so that both formulations agree for dU. This leads to the Gibbs–Duhem relationship

$$SdT - VdP + \sum_i n_i d\mu_i = 0. \tag{3.3}$$

If only one substance component is considered, and if, in addition, the temperature is kept constant ($dT = 0$), $n_i d\mu_i = V_i dP_i$ is obtained.

For an ideal gas mixture then $n_i \int_{\mu_i^\circ}^{\mu_i} d\mu_i = n_i(\mu_i - \mu_i^\circ) = n_i RT \int_{P_i^\circ}^{P_i} dP_i/P_i$ applies; therefore,

$$\mu_i - \mu_i^\circ = RT \ln\left(\frac{P_i}{P_i^\circ}\right) \quad \text{or } \mu_i = \mu_i^\circ + RT \ln\left(\frac{P_i}{P_i^\circ}\right). \tag{3.4}$$

The P_i° represents a reference or standard pressure at the standard temperature of 298.15 K. μ_i° is the standard chemical potential at P_i° and standard temperature. Expediently, P_i° is set equal to the pressure unit of 1.0 bar, so that in the argument of the logarithm only the dimensionless numerical value of P_i must be specified.

https://doi.org/10.1515/9783110650501-003

Equation (3.6) can also be formulated for concentrations. Then

$$\mu_i = \mu_i^\circ + RT \ln\left(\frac{c_i}{c_i^\circ}\right) \text{ applies.} \tag{3.5}$$

c_i° is the reference or standard concentration of 1.0 mol/L, and μ_i° is the standard chemical potential at this unit concentration and a standard temperature of 298.15 K.

The completely irreversible gas expansion and the associated entropy production $\Delta_i S$ can also be derived from the chemical potential. Instead of the movable piston, the cylinder containing the ideal gas is provided with a rigid partition dividing the total volume (V_2) into the volumes V_1 and $V_d = V_2 - V_1$. At the beginning of the process, the total amount of gas in V_1 is same as in the piston experiment. After removal of the partition, the gas expands into the evacuated volume V_d without performing work. It takes on the volume V_2 at the end of the process, just like in the piston experiment. The chemical potential μ_1 of the gas in V_1 decreases continuously, while that in $V_d(\mu_d)$ increases until equilibrium is reached. At equilibrium $\mu_d = \mu_1$ applies. As there is no mechanical work, pressure changes in the system are irrelevant. Therefore, the following applies:

$$dG = \sum_i \mu_i dn_i = -Td_iS \,(P = \text{const.}). \tag{3.6}$$

For gas expansion, $\text{Gas}_1 \rightarrow \text{Gas}_d$; therefore, $\mu_d - \mu_1 = \frac{\partial G_d}{\partial n_d} - \frac{\partial G_1}{\partial n_1}$.

When $-\partial n_1 = \partial n_d = \partial n$ and $\partial G_d + \partial G_1 = \partial G$,

$$\frac{\partial G}{\partial n} = RT(\ln(c_d) - \ln(c_1)) = RT \ln\left(\frac{c_d}{c_1}\right) = RT\left(\ln\left(\frac{c_d}{c_{\text{eq}}}\right) - \ln\left(\frac{c_1}{c_{\text{eq}}}\right)\right) \tag{3.7}$$

(the standard potentials are the same in both compartments and disappear accordingly).

c_{eq} is the concentration that remains the same in both compartments after reaching equilibrium. The integration is based on the following formulation:

$$\frac{\partial G}{\partial n} = RT \ln\left(c_d^i + \frac{n}{V_d}\right) - RT \ln\left(c_1^i - \frac{n}{V_1}\right).$$

The integral over ∂G is

$$\Delta G = RT \int_0^n \left(\ln\left(c_d^i + \frac{n}{V_d}\right) - \ln\left(c_1^i - \frac{n}{V_1}\right)\right) dn.$$

As a solution,

$$\Delta G = RT\left(\begin{array}{c} \dfrac{\left(c_d^i + \dfrac{n}{V_d}\right)\left(\ln\left(c_d^i + \dfrac{n}{V_d}\right) - 1\right)}{\dfrac{1}{V_d}} - \dfrac{c_d^i\left(\ln\left(c_d^i\right) - 1\right)}{\dfrac{1}{V_d}} \\ - \left(\dfrac{(-1)\left(c_1^i - \dfrac{n}{V_1}\right)\left(\ln\left(c_1^i - \dfrac{n}{V_1}\right) - 1\right)}{\dfrac{1}{V_1}} - \dfrac{(-1)c_1^i\left(\ln\left(c_1^i\right) - 1\right)}{\dfrac{1}{V_1}}\right) \end{array}\right)$$

is obtained. When $n = n_{\mathrm{eq}}$, the following is obtained:

$$\Delta G = RT\left[\begin{array}{c} \left(n_d^{\mathrm{eq}}\right)\left(\ln\left(c_d^{\mathrm{eq}}\right) - 1\right) - n_d^i\left(\ln\left(c_d^i\right) - 1\right) \\ - \left[(-1)\left(n_1^{\mathrm{eq}}\right)\left(\ln\left(c_1^{\mathrm{eq}}\right) - 1\right) - (-1)n_1^i\left(\ln\left(c_1^i\right) - 1\right)\right] \end{array}\right].$$

Since $n_1^i - n_1^{\mathrm{eq}} + n_d^i - n_d^{\mathrm{eq}} = 0$, this leads to

$$\Delta G = RT\left[n_d^{\mathrm{eq}}\ln\left(c_d^{\mathrm{eq}}\right) - n_d^i\ln\left(c_d^i\right) + n_1^{\mathrm{eq}}\ln\left(c_1^{\mathrm{eq}}\right) - n_1^i\ln\left(c_1^i\right)\right].$$

Therefore, $c_1^{\mathrm{eq}} = c_d^{\mathrm{eq}}$ as well as $n_1^{\mathrm{eq}} + n_d^{\mathrm{eq}} = n_1^i + n_d^i$ yields

$$\Delta G = n_1^i RT\ln\left(\frac{c_1^{\mathrm{eq}}}{c_1^i}\right) + n_d^i RT\ln\left(\frac{c_d^{\mathrm{eq}}}{c_d^i}\right).$$

When $n_d^i = 0$, the following is obtained:

$$\Delta G = n_1^i RT\ln\left(\frac{c_1^{\mathrm{eq}}}{c_1^i}\right) = n_1^i RT\ln\left(\frac{c_1^i\,\frac{V_1}{V_1+V_d}}{c_1^i}\right) = -n_1^i RT\ln\left(\frac{V_1+V_d}{V_1}\right) \equiv W_{\max}.$$

This proves that the irreversible expansion of an ideal gas in a vacuum is equivalent to the free expansion (volume increase without work) in the piston experiment.

The above equation ($n_d^i = 0$) can be interpreted as follows: In the irreversible expansion of an ideal gas from volume V_1 to $V_2 = V_1 + V_d$ n_{eq} moles (in the following example, $n_{\mathrm{eq}} = 0.1975$ mol) the potential difference $\Delta_R G(n)$ is obtained, which continuously decreases to zero (equilibrium). The n_{eq} is obtained from the equilibrium condition $c_d^i + \left(n_{\mathrm{eq}}/V_d\right) = c_1^i - \left(n_{\mathrm{eq}}/V_1\right)$, n_{eq} = 0.1975 mol.

The integral of this process yields $\Delta G = n_1^i RT\ln\left(c_d^{\mathrm{eq}}/c_1^i\right)$. The integrative process can obviously be equated in this case ($c_d^i = 0$) with the passage of n_1^i moles through the constant potential difference with the concentrations $c_d^{\mathrm{eq}} = c_1^{\mathrm{eq}}$ and c_1^i. If, in addition, as in the example $n_1^i = 1.0$ mol, numerical equality results between $\Delta G = n_1^i RT\ln\left(c_d^{\mathrm{eq}}/c_1^i\right)$ and $\Delta_R G = RT\ln\left(c_d^{\mathrm{eq}}/c_1^i\right)$, which means that 1.0 mol goes through the above potential difference, as it corresponds to the definition of a potential itself. It should not be overlooked, however, that ΔG and $\Delta_R G$ have different dimensions (J or J/mol). The above formula does not apply to any n, but only to $n = n_{\mathrm{eq}}$ for the specific case.

c^i indicates the initial concentrations of the gas. For example, in compartment 1, $c_1^i = n_1^i / V_1 = 1.0/0.0153 = 65.35\ \text{mol/m}^3$, while compartment d is set to $c_d^i = 10^{-12}\ \text{mol/m}^3$, which is practically zero, and $c_d^i = 19.605\ \text{mol/m}^3$ (Figure 3.1). The corresponding ΔG processes go through a minimum, which represents the respective equilibrium state. At values $n_{\text{eq}}^{\text{min1}} = 0.1975$ mol and $n_{\text{eq}}^{\text{min2}} = 0.1383$ mol, the concentrations in both compartments are the same.

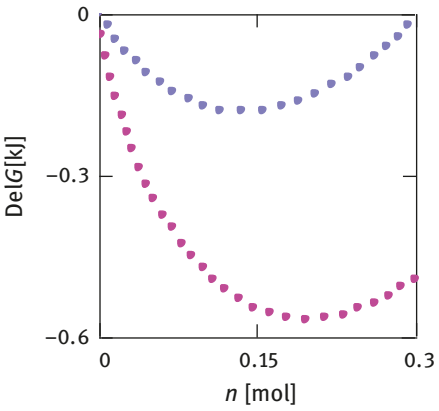

Figure 3.1: Irreversible expansion of an ideal gas. Del $G = \Delta G$ in kJ (integrated). Red points: initially no gas present; blue points: initial gas concentration 19.605 mol/m^3.

In the absence of volume work, $dG = \sum_i \mu_i dn_i = -Td_iS$ (T and P const.) and $d_iS = -(1/T)\sum_i \mu_i dn_i$, which leads $c_d^i = 0$ to

$$\Delta_i S = -\frac{\Delta G}{T} = nR\ln\left(\frac{c_1^i}{c_{\text{eq}}}\right) = nR\ln\left(\frac{V_1 + V_d}{V_1}\right),$$

and $c_d^i \neq 0$ to

$$\Delta_i S = n_1^i R\ \ln\left(\frac{c_1^i}{c_{\text{eq}}}\right) + n_d^i R \ln\left(\frac{c_d^i}{c_{\text{eq}}}\right).$$

Based on this equation, the entropy production of mixing two ideal gases can be determined. As an example, the following task (see Atkins, example 5.2 [4]) is calculated: a container with two equal compartments of volume $V_1 = V_d = 0.0153$ m^3 contains $n_{\text{H}_2} = 3.0$ mol of the ideal gas H_2 in V_1 and $n_{\text{N}_2} = 1.0$ mol of the gas N_2 in V_d. The initial concentrations of $[\text{H}_2]_{\text{i}} = 3.0/0.0153 = 196.08$ and $[\text{N}_2]_{\text{i}} = 1.0/0.0153 = 65.36\ \text{mol/m}^3$, which results in $c_d^i + \frac{n}{V_d} = c_1^i - \frac{n}{V_1}$ and $n = c_i \frac{V_d V_1}{V_d + V_1}$ (1.5 mol H_2 and 0.5 mol N_2), $[\text{H}_2]_{\text{eq}} = 98.025121\ \text{mol/m}^3$ and $\Delta G_{\text{H}_2} = n_{\text{H}_2} RT \ln\left(\frac{[\text{H}_2]_{\text{eq}}}{[\text{H}_2]_{\text{i}}}\right) = -5.1549$ kJ ($T = 298.15$ K).

For ΔG_{N_2} with $[\text{N}_2]_{\text{eq}} = 32.68\ \text{mol/m}^3$, the following is obtained:

$$\Delta G_{N_2} = n_{N_2} RT \ln\left(\frac{[N_2]_{eq}}{[N_2]_i}\right) = -1.7183 \text{ kJ}$$

therefore, $\Delta G_{H_2} + \Delta G_{N_2} = -6.873$ kJ.

However, the value –6,873 kJ is too negative because it contains ΔG_{unif} that is obtained from different concentrations. For its calculation, both ideal gases are combined into a single gas, which results in

$$\Delta G_{unif} = 3.0\, RT \ln\left(\frac{2.0/V_1}{3.0/V_1}\right) + 1.0\, RT \ln\left(\frac{2.0/V_d}{1.0/V_d}\right) = -1.297 \text{ kJ}.$$

Then for mixing alone results

$$\Delta G_{mix} = \Delta G_{H_2} + \Delta G_{N_2} - \Delta G_{unif} = -5.576 \text{ kJ}.$$

Both ΔU and ΔH are zero for this irreversible process. When $\Delta G = \Delta H - T(\Delta_e S + \Delta_i S)$, during mixing, neither work is performed nor is heat exchanged:

$$\Delta_i S = -\frac{\Delta G}{T} = 5.576\ 10^3/298.15 = 18.702 \text{ J/K}.$$

4 Chemical reactions

The treatment of completely irreversible processes with the help of chemical potentials is indicated above all because they are identical to ΔG at constant temperature and pressure. It is shown that an ideal gas spontaneously passes without an energy change from an unlikely to a more probable arrangement of its components. The latter is characterized by a larger volume. The improbability of the arrangement can therefore be regarded as a prerequisite that the gas can perform volume work. The actual work delivery can occur under isothermal conditions only by simultaneous heat absorption. Such behavior is not observed in spontaneous chemical and biochemical reactions. Heat is always generated in such an irreversible reaction. This can be reduced if the considered reaction is coupled to another, which in the absence of coupling would spontaneously proceed with heat production in the opposite direction. By the coupling, the coupled reaction (index "1") is forced into the direction of the input reaction (index "2"), as long as the sum of chemical potentials of both reactions is negative. At equilibrium, this sum equals zero. This corresponds to the coupling of an ideal gas in the cylinder/piston system, insofar as the gas is prevented from irreversible expansion by means of the oppositely equal pressure from a piston. It is also possible to obtain a maximum of work from a chemical reaction, if infinitesimal changes are applied progressively to induce successive equilibria as in the case of reversible gas expansion. This consists of bringing the chemical potentials of the coupled reaction (1) to more positive values. Unlike gas, this does not happen as a result of the consumption of kinetic energy, which must be returned to the system as heat from the environment ($T = \text{const.}$). In chemical reactions, the necessary energy comes from the difference in potential energies between products and reactants. Therefore, under irreversible conditions, the amount of energy that must be released could have been extracted as work in the reversible case. This release of energy takes place in the irreversible case in the form of heat energy, which can be understood as the dissipated reaction work

$$\Delta W_{\text{diss}} = -Q_{\text{irr}} = -T\Delta_i S$$

of the chemical reaction concerned. In contrast to the ideal gas, the entropy production $\Delta_i S$ in chemical reactions is always accompanied through the associated heat production with an actual change of energy.

The potential energy released by the reaction changes with the changing chemical potential differences in the course of the reaction. This energy, which was distributed to reactants and products before the reaction started, can now be distributed via the heat energy produced to a considerably larger number of possible states, which is accompanied by an increase in the probability of the newly arising energy distribution. The entropy increase $\Delta_i S$ is therefore of particular importance in a spontaneous chemical reaction. In the course of the reaction, potential energy is transformed into kinetic energy as in a conservative force field in which a potential gradient provides

https://doi.org/10.1515/9783110650501-004

the driving and directional force of the transformation. However, since a comparable force field between products and reactants does not exist, it follows that chemical reactions are not driven by such a gradient. However, the presence of a difference of potential chemical energy is essential because, according to the first law, the production of heat energy can only originate from such a difference of potential energy between products and reactants.

The reason why chemical reactions can proceed spontaneously, is due to the increasing probability associated with a redistribution of energies of all involved particles. This is connected with a reduction of reactant and an increase of product concentrations, whereby the difference of potential energy is concomitantly decreased. It appears as heat energy, which is released from the system into surroundings ($T = const.,\ Q_{irr} = T\Delta_i S$). When this difference reaches zero, no more potential energy can be dissipated as heat and, as a result, the probability of energy distribution cannot be increased further by the reaction. At this stage, a further progressing of the reaction becomes extremely unlikely, and the process is at equilibrium. The sum of the chemical potentials of products is then oppositely equal to the sum of the chemical potentials of reactants, that is, the stoichiometric sum of all chemical potentials involved in the reaction is equal to zero. It follows, that for the spontaneous progression of a reaction, a difference of potential energy between products and reactants must first be present, and that, in addition, a possibility (reaction path) must exist, to increase the probability of the momentary energy distribution. The fulfilment of the first condition is a necessary prerequisite, while the fulfilment of the second condition is sufficient to allow a chemical or biochemical reaction to run spontaneously.

The difference in the irreversible expansion of a gas evidently consists of the fact that in the case of gas, the vehicle for the increase in probability already exists in the form of kinetic energy, whereas in the chemical reaction, this must first be produced by the reaction itself.

Also, the heat exchange ($T\Delta_e S$) occurring in the course of isothermal chemical reactions is significantly different from the exchange observed with the expanding gas. While the ideal gas only compensates for changes in the kinetic energy of the system, in chemical reactions the difference in thermal energy content between products and reactants is compensated by heat transfer. This is explained by the example of the following reaction:

$$\mathrm{Glu(s) + 6O_2(g) \rightarrow 6CO_2(g) + 6H_2O(l)}, \tag{R4.1}$$

where Glu represents glucose, s represents solid, g is gas, l is liquid.

During progression of the reaction in a closed system, the reactants Glu plus 6 O_2 are continuously consumed and replaced by products 6 CO_2 plus 6 H_2O. At a given temperature, each of the compounds involved contains a certain amount of heat energy. This corresponds exactly to the amount of energy that would be supplied to a certain amount (e.g., 1.0 mol) of the substance in question in order to bring its temperature from 0 to 298.15 K.

At the beginning of the reaction, all reactants are in thermal equilibrium. After an extent of reaction of, for example, $\xi = 1.0$ mol, 1.0 mol Glu plus 6.0 mol O_2 are consumed, leaving just the amount of heat that was required to bring the sum of the reactants to 298.15 K. The new products resulting from the reaction 6.0 mol CO_2 plus 6.0 mol H_2O must absorb heat energy in order to reach the specified temperature. This can be done first by taking up the heat energy from reactants. In principle, this amount of heat cannot be equated with that which would have to be applied for heating the products from 0 to 298.15 K. In the above example, it is too small, so additional heat must be absorbed from the environment to bring the products into thermal equilibrium with the system temperature of 298.15 K. This heat exchanged with the environment is equal to $T\Delta_e S$ (with $\Delta_e S > 0$ for the above reaction).

On the other hand, if the reactants had released more heat energy than the newly created products needed, heat would have to be given off by the system to maintain the given temperature. In this case, it would be $\Delta_e S < 0$. The so-called third law entropies (S_m°) present in $\Delta_e S$ can be regarded as absolute quantities because they have been calculated from $T = 0$ K up to the standard temperature $T = 298.15$ K. They are largely independent of concentration. These values must be used in the stoichiometric sum of the reaction (R4.1) to obtain $\Delta_e S$ (for $T = 298.15$ K):

$$\Delta_e S = 6\, S_m^{CO_2} + 6\, S_m^{H_2O} - \left(S_m^{Glu} + 6\, S_m^{O_2}\right) = 259.072\ \mathrm{J/mol\ K}.$$

The differentials for the internal energy and the enthalpy in chemical and biochemical reactions that result from (without volume work) $dU = Td_eS + \sum_i \mu_i dn_i$ and $dH = Td_eS + \sum_i \mu_i dn_i$ apply.

Unlike gases, the Legendre transformation can be applied to Td_eS alone. This yields the differential of the Helmholtz energy,

$$dA = d(U - TS) = dU - Td_eS = \sum_i \mu_i dn_i \ (V \text{ and } T = \text{const.}), \tag{4.1}$$

and for that of the Gibbs energy,

$$dG = d(H - TS) = dH - Td_eS = \sum_i \mu_i dn_i \ (P \text{ and } T = \text{const.}). \tag{4.2}$$

The reason why the sum of both entropy differentials (d_eS plus d_iS) does not enter the transformation but only d_eS is given by the fact that in spontaneous reactions always the entire maximum work is dissipated and is delivered to the environment as heat energy at $T = \text{const}$. In contrast to the irreversible expansion of a gas, this reduces the actual energy content of the system, which must be accompanied by a decrease in U or H.

As for chemical reactions in the absence of volume work $dG = \sum_i \mu_i dn_i = -Td_iS$ applies, it follows, with

$$dG = dH - Td_eS, \tag{4.3}$$

that

$$dH = Td_eS - Td_iS. \tag{4.4}$$

Equations can also be related to the respective extent of reaction ξ rather than to n. This results in the case that only one reaction takes place in the system,

$$dG = \sum \mu \, d\xi, \; with \; \mu = \frac{\partial G}{\partial \xi}$$

The sum sign represents the stoichiometric sum of products and reactants of this reaction, resulting in

$$\frac{dG}{d\xi} = \sum \mu \tag{4.5}$$

and

$$\frac{dH}{d\xi} = T\frac{d_eS}{d\xi} + \sum \mu. \tag{4.6}$$

The same applies to the differentials dA or dU.

The differential quotients $dG/d\xi$, $dH/d\xi$ and $d_eS/d\xi$ are usually shown in abbreviated notation as Δ_RG, Δ_RH and $\Delta_{Re}S$. They indicate the infinitesimal change of the respective quantity per infinitesimal extent of reaction in J/mol and in J/K mol, respectively. The differential quotient is also referred to as the driving force $DF = -\Delta_RG$ of a reaction or a process. For the distinction between differential quotient (e.g., Δ_RG) and difference (ΔG), the integration over Δ_RG is used. With

$$\frac{dG}{d\xi} = \Delta_RG; \tag{4.7}$$

and $dG = \Delta_R G \, d\xi$, the integration results in

$$\int_0^\xi dG = \Delta G = \int_0^\xi \sum \mu \, d\xi.$$

From eqs. (4.3), (4.5) and (4.6)

$$\Delta_RG = \Delta_RH - T\Delta_{Re}S \tag{4.8}$$

can be obtained.

Δ_RG can be calculated by means of the chemical potentials of the substances involved in the reaction. The following reaction is considered:

$$A + B \rightarrow C + D$$

Insertion of the chemical potentials into the stoichiometric sum yields

$$\Delta_R G = \mu_C + \mu_D - (\mu_A + \mu_B);$$

furthermore,

$$\Delta_R G = \mu_C^\circ + \mu_D^\circ - (\mu_A^\circ + \mu_B^\circ) + RT \ln\left(\frac{[C]\,[D]}{[A]\,[B]}\right). \tag{4.9}$$

With $$\Delta_R G^\circ = \mu_C^\circ + \mu_D^\circ - \left(\mu_A^\circ + \mu_B^\circ\right),$$

$$\Delta_R G = \Delta_R G^\circ + RT \ln\left(\frac{[C]\,[D]}{[A]\,[B]}\right) \tag{4.10}$$

(square brackets indicate a concentration).

At equilibrium $\Delta_R G$ vanishes, and

$$\Delta_R G^\circ = -RT \ln\left(\frac{[C]_{eq}\,[D]_{eq}}{[A]_{eq}\,[B]_{eq}}\right) \tag{4.11}$$

is obtained.

With $\Gamma_{eq} = \frac{[C]_{eq}\,[D]_{eq}}{[A]_{eq}\,[B]_{eq}}$ and $\Gamma = \frac{[C]\,[D]}{[A]\,[B]}$, the following is obtained:

$$\Delta_R G = -RT \ln\left(\Gamma_{eq}\right) + RT \ln(\Gamma) \tag{4.12}$$

or

$$\Delta_R G = RT \ln\left(\frac{\Gamma}{\Gamma_{eq}}\right).$$

Γ_{eq} is identical to K_{eq}, the equilibrium constant of the mass action law.

$\Delta_R G^\circ$ can be also obtained by setting $\Gamma = 1.0$, that is, the reaction would extend at constant concentrations of 1.0 mol/L.

Equations (4.10) and (4.11) can be converted to

$$\Delta_R G = RT\left(\ln\left(\frac{[C]}{[C]_{eq}}\right) + \ln\left(\frac{[D]}{[D]_{eq}}\right) - \left(\ln\left(\frac{[A]}{[A]_{eq}}\right) + \ln\left(\frac{[B]}{[B]_{eq}}\right)\right)\right)$$

The comparison with eq. (3.7) reveals the close relationship between the expansion of an ideal gas and the progression of a chemical reaction. While during the expansion process $\ln\left(K_{eq}\right)$ due to $K_{eq} = 1.0$ disappears and is thus irrelevant; however, the equilibrium constant in a chemical reaction must be considered. Its value significantly influences the course of the reaction as will be shown. It is possible to calculate $\Delta_R G$ also

with the help of the last formula. For this, however, the corresponding equilibrium concentrations must be determined for each initial condition. They result from the relation

$$\left([C] + \xi_{eq}/V\right)\left([D] + \xi_{eq}/V\right) / \left([A] - \xi_{eq}/V\right)\left([B] - \xi_{eq}/V\right) = K_{eq}.$$

They change with each change of an initial concentration, but always result in K_{eq}.

The entropy $\Delta_e S$ exchanged in the course of the reaction is of far less importance for the spontaneous reaction, since it is not involved in the maximization process. The entropy $\Delta_{Re}S^{Sur}$ exchanged with the environment is always opposite and equal to the entropy change occurring in the system $\Delta_{Re}S$, so that their sum disappears and consequently cannot be maximized.

The above ideas will be explained below using the example of Glu oxidation (R4.1).

The standard values of the molar reaction enthalpies and Gibbs energies, $\Delta_R H^\circ$ or $\Delta_R G^\circ$, are often tabulated or can be determined from the standard values of the molar enthalpies and Gibbs energies of formation ([4], 298.15 K):

$$\Delta_R H^\circ = 6\,\Delta H_{CO_2}(g) + 6\,\Delta H_{H_2O}(l) - \left(\Delta H_{Glu}(s) + 6\,\Delta H_{O_2}(g)\right) = -2,808.04 \text{ kJ/mol},$$

as well as

$$\Delta_R G^\circ = 6\,\Delta G_{CO_2}(g) + 6\,\Delta G_{H_2O}(l) - \left(\Delta G_{Glu}(s) + 6\,\Delta G_{O_2}(g)\right) = -2,878.94 \text{ kJ/mol}.$$

Due to $\Delta_R G^\circ = \Delta_R H^\circ - T\Delta_{Re}S$ the following also applies:

$$\Delta_{Re}S = \frac{\Delta_R H^\circ - \Delta_R G^\circ}{T} = 237.8 \text{ J/mol K}.$$

If a reaction is initiated by other than the standard values, then the result is, for example, for Glu oxidation with initial values Glu(s) = 1.0, $P_{O_2} = 1.6$ and $P_{CO_2} = 0.03612$ bar ($T = 298.15$ K):

$$\Delta_R H = \Delta_R H^\circ + RT \ln\left(\frac{(P_{CO_2})^6}{\text{Glu}\ (P_{O_2})^6}\right) = -2,864.43 \text{ kJ/mol},$$

$$\Delta_R G = -T\Delta_{Ri}S = \Delta_R G^\circ + RT \ln\left(\frac{(P_{CO_2})^6}{\text{Glu(s)}\ (P_{O_2})^6}\right) = -2,935.33 \text{ kJ/mol},$$

$$\Delta_{Re}S = \frac{\Delta_R H - \Delta_R G}{T} = 237.8 \text{ J/K mol and } \Delta_{Ri}S = -\frac{\Delta_R G}{T} = 9,845.13 \text{ J/K mol}.$$

$\Delta_R H$ is also given by $\Delta_R H = T(\Delta_{Re}S - \Delta_{Ri}S) = -2,864.43$ kJ/mol. In practice, it is important that the units used for the standard values are identical to those of Γ.

Figure 4.1 shows the curves of ΔG, ΔG° and ΔH resulting from integration of eqs. (4.11) and (4.12), respectively, in terms of the extent of reaction ξ (mol).

Integrals such as

$$I_{\text{plus}} = 6\int_0^{\xi}\left(\ln\left([\text{CO}_2]_{\text{in}} + 6\frac{\xi}{V}\right)\right)d\xi \text{ and } I_{\text{minus}} = 6\int_0^{\xi}\left(\ln\left([\text{O}_2]_{in} - 6\frac{\xi}{V}\right)\right)d\xi,$$

have the solutions

$$I_{\text{plus}} = \left([\text{CO}_2]_{\text{in}} + 6\frac{\xi}{V}\right)\left(\ln\left([\text{CO}_2]_{\text{in}} + 6\frac{\xi}{V}\right) - 1\right) - \left([\text{CO}_2]_{\text{in}}\right)\left(\ln\left([\text{CO}_2]_{\text{in}}\right) - 1\right)$$

or

$$I_{\text{minus}} = (-1)\left([\text{O}_2]_{in} - 6\frac{\xi}{V}\right)\left(\ln\left([\text{O}_2]_{in} - 6\frac{\xi}{V}\right) - 1\right) - (-1)\left([\text{O}_2]_{in}\right)\left(\ln\left([\text{O}_2]_{in}\right) - 1\right),$$

where V is the unit volume of 10^{-3} m^3, and the stoichiometric coefficients of CO_2 or O_2 are both equal to 6.0 according to (R4.1). If the initial conditions are given in pressure units, these must be converted into concentration units.

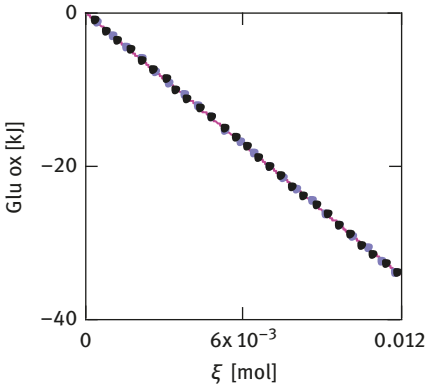

Figure 4.1: Glucose oxidation. Red line:ΔG; blue points: ΔH; black points:ΔG°. The integrated quantity ΔG° is given by $\Delta G^\circ = \Delta_R G^\circ \times \xi$.

In the specified range, all functions are almost linear and almost identical. At a strongly negative standard potential, ΔG differs only slightly from $\Delta_R G^\circ \times \xi$. $\Delta_R G$ and $\Delta_R H$ can be recovered by differentiation, so both represent the respective slopes of the tangents to ΔG or ΔH. For example, $\Delta_R G(\xi = 0) = -2,935.33$ kJ/mol. This is the value of $\Delta_R G$ at the given initial concentrations, whereas $\Delta_R G(5 \times 10^{-3}) = -2,926.05$ kJ/mol represents the value at concentrations changed from initial values by an extent of reaction of $\xi = 5.0\ 10^{-3}$ mol. At this ξ, $\Delta G(5 \times 10^{-3}) = 14.651$ kJ.

Analogously, $\Delta_R G^\circ$ can be determined as that of $\Delta_R G$, which results from the standard concentrations and/or pressures. $\Delta_R G^\circ$ is given by the slope at that point of the ΔG function, where $\Gamma = 1.0$ ($\Delta_R G^\circ = -2,878.94$ kJ/mol). It is not at all identical to a value of ΔG, which would result from $\xi = 1.0$ mol.

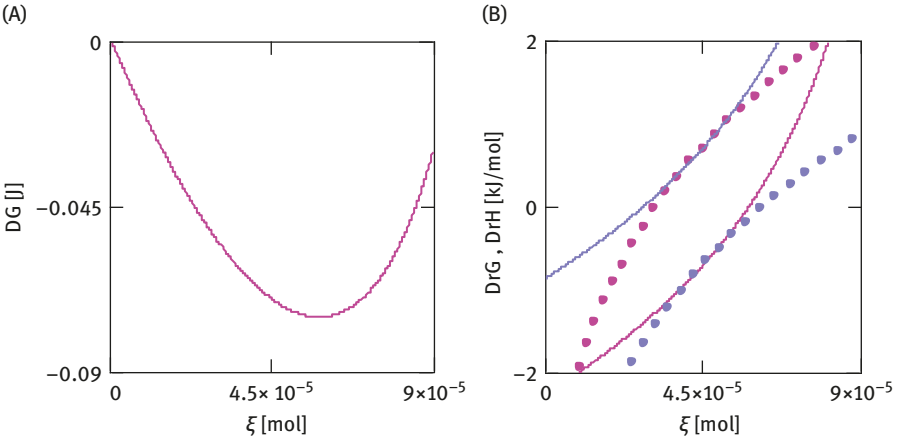

Figure 4.2: Phosphocreatine reaction near equilibrium. (A) Course of ΔG in J; (B) red line (forward): $\Delta_R G$; blue line (forward): $\Delta_R H$; red points (reverse): $\Delta_R G$; blue points (reverse): $\Delta_R H$. Initial concentrations for the forward reaction: [PCr] = 22.0 mM, [ADP] = 0.1 mM, [Cr] = 18.0 mM, [ATP] = 8.9 mM. Initial concentrations for the reverse reaction: [Cr] = 18.0 + 9.0 10^{-2} mM, [ATP] = 8.9 + 9.0 10^{-2} mM, [PCr] = 22.0–9.0 10^{-2} mM and [ADP] = 0.1–9.0 10^{-2} mM.

Figure 4.2 shows the course of ADP phosphorylation by phosphocreatine:

$$\mathrm{PCr} + \mathrm{ADP} \rightleftharpoons \mathrm{Cr} + \mathrm{ATP} \tag{R4.2}$$

where PCr represents phosphocreatine, Cr represents creatine (biochemical notation, see Section 10.1). In contrast to the Glu oxidation with a $\Delta_R G^\circ$ of –2,878.94 kJ/mol, this reaction has a $\Delta_R G^\circ$ of only –13.35 kJ/mol. This relatively low value causes $\Delta_R G$ and $\Delta_R G^\circ$ to differ significantly, for example, $\Delta_R G$ of (R4.2) is at the point $\xi = 4.5 \times 10^{-5}$ mol $\Delta_R G(4.5 \times 10^{-5}) = -0.07$ J/mol.

Figure 4.2 is intended to demonstrate the energetic behavior of the reaction at near equilibrium. The forward reaction (lines) occurs spontaneously only until reaching the minimum of $\Delta G\,(-0.0748\ \mathrm{J})$ at $\xi^{\mathrm{f}}_{\mathrm{min}} = 5.794574 \times 10^{-5}$ mol (A). $\Delta_R G$ is zero at this point and would become positive if the reaction could proceed beyond this ξ value. At ξ^{f} = 7.0 10^{-5} mol (in forward direction), for example, $\Delta_R G$ would be clearly positive (877.57 J/mol), but negative in the direction of the reverse reaction (ξ^{r} = 2.0 × 10^{-5}, –877.57 J/mol, A and B), so that the reaction now in this direction can be spontaneous. This opposite course is shown by the points, red and blue, which is calculated for the reverse reaction and becomes zero at $\xi^{\mathrm{r}}_{\mathrm{min}} = 9.0 \times 10^{-5} - \xi^{\mathrm{f}}_{\mathrm{min}} = 3.2054 \times 10^{-5}$ mol.

When the reaction direction is reversed, the sign of $\Delta_{\mathrm{Re}} S$ must change. Near equilibrium applies to the forward and the reverse reactions, $\Delta_R H \approx T\,\Delta_{\mathrm{Re}} S$, so that in this range both $\Delta_R H$ values are practically opposite equal (at $\Delta_R G \approx 0$, Figure 4.2B). The corresponding $\Delta_R G$ values, on the other hand, must be negative for both the spontaneous forward reaction and the spontaneously occurring reverse

reaction. Also under near-equilibrium conditions, heat cannot be absorbed by a reaction. This would lead to $\Delta_{Ri}S < 0$, which is incompatible with the second law. But heat can be exchanged. In this case, near-equilibrium heat is taken up by the forward reaction ($\Delta_R H \approx 1.42$ kJ/mol), because $\Delta_{Re}S > 0$ and is released by the reverse reaction ($\Delta_R H \approx -1.42$ kJ/mol), because $\Delta_{Re}S < 0$.

For the formulation of the second law, the equation

$$\Delta_R G = \Delta_R H - T\Delta_{Re}S$$

is frequently used. It has often been misinterpreted, with regard to the Glu oxidation, it could be concluded for example that $\Delta_R G$ is more negative than $\Delta_R H$ because $\Delta_{Re}S$ is positive for this reaction. However, such a conclusion would be wrong, although this reading does not contradict the above formula. $\Delta_R G$ has independent meaning. Its value is independent of the reversible heat $T\,\Delta_{Re}S$ exchanged with the reaction, which in this case is positive and in principle does not depend on concentration. $T\,\Delta_{Re}S$ is eliminated from $\Delta_R H$ by means of the Legendre transformation and as a result is not present in $\Delta_R G$. The above formula thus only describes the fact that $\Delta_R G$ is obtained, if $T\,\Delta_{Re}S$ is subtracted from $\Delta_R H$, whereas both $\Delta_R G$ and $T\,\Delta_{Re}S$ are contained in $\Delta_R H$.

Equation (4.12) appears trivial and therefore should not be used to formulate the second law. For chemical reactions, this theorem is adequately described (see eq. (2.5) for comparison) by the inequality

$$\Delta_{Ri}S \geq 0. \tag{4.13}$$

In older textbooks, the second law is sometimes interpreted as follows: $\Delta_R H$ is compared with a gross income that cannot be fully used because a tax is payable. This duty should correspond to $T\Delta_{Re}S$ while the remainder would correspond to the so-called free enthalpy $\Delta_R G$.

This explanation is wrong. As already mentioned, $\Delta_R H$ has been freed from $T\Delta_{Re}S$ by a Legendre transformation. However, this mathematical operation should not be interpreted as meaning that the generation of useful work by the reaction can only occur if it gives off a certain proportion of its $\Delta_R H$, namely $T\Delta_{Re}S$, so that only the remainder $\Delta_R G$ remains freely available for use.

Rather, it is correct that the production of useful work is achieved by dissipating at least part of the Gibbs energy ($\Delta_R G$) of the reaction. Spontaneous chemical reactions are usually uncoupled, so their course is completely irreversible. Under these conditions, $\Delta_R G$ is always completely dissipated, producing the irreversible heat $T\Delta_{Ri}S$ $(= -\Delta_R G)$ and the associated entropy change $\Delta_{Ri}S > 0$, respectively. The reversibly exchanged heat $T\Delta_{Re}S$ has nothing to do with it, at the first instance. However, it is inextricably linked to the extending reaction, regardless of whether it runs reversible or irreversible.

This fact should be explained by the following examples:

A spontaneously occurring reaction absorbs heat from the environment at a constant temperature, so it can be described as endothermic. Its $\Delta_R G$ is negative, meaning that the reaction produces the irreversible heat $Q_{irr} = T\Delta_{Ri}S$, then it would have to be released by the system if no simultaneous reversible heat exchange $Q_{rev} = T\Delta_{Re}S$ occurred. As already described, this results from the difference in the contents of heat energy or the entropy contents between products and reactants. If, for example, the heat energy from the reactants is insufficient to bring the products to the specified temperature, the system must absorb heat from the environment in order to keep the system's temperature constant. In such an endothermic reaction, the exchanged heat is positive but reduced by the amount $T\Delta_{Ri}S$ with respect to $T\Delta_{Re}S$, which can be seen from equation $\Delta_R H = T\,\Delta_{Re}S - T\Delta_{Ri}S$.

As $\Delta_{Ri}S$ is always positive, in this case $\Delta_{Re}S$ must be sufficiently positive, so that also $\Delta_R H > 0$. In exothermic reactions, a strong negative $\Delta_R G = -T\Delta_{Ri}S$ usually predominates, so that even if $T\Delta_{Re}S$ is positive, the result is $\Delta_R H < 0$.

In the next example the melting of ice

$$H_2O(s) \rightleftharpoons H_2O(l)$$

at 273.15 K is investigated. At this temperature, $\Delta_R G = 0$, that is, $\Delta_{Ri}S = 0$ also must be true, and it remains so as long as the reaction is reversible. For the melting process to proceed, heat must be reversibly added to the system. This exchanged heat $T\Delta_{Re}S$ is required, because the heat energy left behind by the disappearing reactant $H_2O(s)$ is insufficient to bring the continuously evolving product $H_2O(l)$ to 273.15 K. It is $\Delta_R H = T\Delta_{Re}S - T\,\Delta_{Ri}S = 273.15(22.0 - 0) = 6.01\ \mathrm{kJ/mol}$.

In the reverse process, the same amount of heat energy is given off because under these conditions $\Delta_{Re}S < 0$.

In summary, it can be stated that the introduction of chemical potentials by Josiah W. Gibbs has greatly increased the understanding of chemical reactions and their energetics. For such a phenomenological approach, although it enables calculations of energy and entropy changes, it cannot give an insight into the molecular mechanism of a reaction. So, it is not possible to explain on a molecular level, by which mechanism the concentration dependence of $\Delta_R G$ is brought about.

5 The temperature dependence of $\Delta_R G$

The derivation of the Gibbs–Helmholtz equation is based on the definition equation $G = H - TS = H(T) + T((\partial G(T))/\partial T)$ [4]. $\partial G(T)/\partial T = -S(T)$ is obtained from the differential of $G(T)$. Dividing by T results in

$$\frac{G(T)}{T} = \frac{H(T)}{T} + \frac{\partial G(T)}{\partial T}.$$

The differentiation from $G(T)/T$ with respect to T using the chain rule yields

$$\frac{\partial\left(\frac{G(T)}{T}\right)}{\partial T} = -\frac{\partial_i S(T)}{\partial T} = \frac{1}{T}\frac{\partial G(T)}{\partial T} + \frac{\partial\left(\frac{1}{T}\right)}{\partial T}\, G(T) = \frac{1}{T}\frac{\partial G(T)}{\partial T} - \frac{1}{T^2}\, G(T) \cdot$$
$$= \frac{1}{T}\left(\frac{\partial G(T)}{\partial T} - \frac{1}{T}\, G(T)\right) \cdot$$

As

$$\frac{\partial G(T)}{\partial T} - \frac{1}{T}\, G(T) = -\frac{H(T)}{T}$$

the following Gibbs–Helmholtz equation is obtained:

$$\frac{\partial\left(\frac{G(T)}{T}\right)}{\partial T} = -\frac{H(T)}{T^2}. \tag{5.1}$$

On second differentiation with respect to ξ leads to

$$\frac{\partial\left(\frac{dG(T)}{d\xi\, T}\right)}{\partial T} = -\frac{d\left(\frac{H(T)}{d\xi}\right)}{T^2}$$

or

$$\frac{\partial\left(\frac{\Delta_R G(T)}{T}\right)}{\partial T} = -\frac{\Delta_R H(T)}{T^2}.$$

To derive the closely related van't Hoff equation, it is assumed that $\Delta_R G^\circ(T) = -RT\, \ln\left(K_{eq}(T)\right)$.

The differentiation with respect to T leads to

$$-\frac{\partial\left(\frac{\Delta_R G^\circ(T)}{R\, T}\right)}{\partial T} = \frac{\partial \ln\left(K_{eq}(T)\right)}{\partial T}.$$

https://doi.org/10.1515/9783110650501-005

With

$$\Delta_R G^\circ(T) = \Delta_R G(T) - RT\ln(\Gamma) \text{ and } \frac{\Delta_R G^\circ(T)}{T} = \frac{\Delta_R G(T)}{T} - R\ln(\Gamma),$$

this yields after differentiation with respect to T:

$$\frac{\partial\left(\frac{\Delta_R G^\circ(T)}{T}\right)}{\partial T} = \frac{\partial\left(\frac{\Delta_R G(T)}{T}\right)}{\partial T} = -\frac{\Delta_R H(T)}{T^2}.$$

It follows that

$$\frac{\partial \ln\left(K_{eq}(T)\right)}{\partial T} = \frac{\Delta_R H(T)}{R\,T^2}, \tag{5.2}$$

and with

$$\partial\left(\frac{1}{T}\right) = -\frac{1}{T^2}\partial T,$$

$$\frac{\partial \ln\left(K_{eq}(T)\right)}{\partial(1/T)} = -\frac{\Delta_R H(T)}{R} \tag{5.3}$$

can be obtained.

The above derivation differs from the van't Hoff equation,

$$\frac{\partial \ln\left(K_{eq}(T)\right)}{\partial T} = -\frac{\Delta_R H^\circ(T)}{RT^2}$$

since the latter refers to $\Delta_R H^\circ$ instead of $\Delta_{Re} S$. This deviation can be distinguished as follows:

$$\int_{T_1}^{T_x} \partial\left(\frac{\Delta_R G(T)}{T}\right) = \frac{\Delta_R G(T_x)}{T_x} - \frac{\Delta_R G(T_1)}{T_1} = \int_{T_1}^{T_x}\left(\frac{-\Delta_R H(T)}{T^2}\right)dT$$

and

$$\Delta_R G(T_x) = \frac{\Delta_R G(T_1)}{T_1}T_x + T_x\int_{T_1}^{T_x}\left(\frac{-\Delta_R H(T)}{T^2}\right)dT.$$

Also,

$$\int_{T_1}^{T_x} \partial\left(\frac{\Delta_R G^\circ(T)}{T}\right) = \frac{\Delta_R G^\circ(T_x)}{T_x} - \frac{\Delta_R G^\circ(T_1)}{T_1} = \int_{T_1}^{T_x}\left(\frac{-\Delta_R H(T)}{T^2}\right)dT$$

must apply, and

$$\Delta_R G^\circ(T_x) = \frac{\Delta_R G^\circ(T_1)}{T_1} T_x + T_x \int_{T_1}^{T_x} \left(\frac{-\Delta_R H(T)}{T^2} \right) dT.$$

With

$$\Delta_R G(T_x) - \Delta_R G^\circ(T_x) = R T_x \ln(\Gamma)$$

the result from the above two equations is $\frac{T_x}{T_1}(\Delta_R G^\circ(T_1) + RT_1 \ln(\Gamma) - \Delta_R G^\circ(T_1)) \equiv RT_x \ln(\Gamma)$.

This result can only be achieved by replacing $\Delta_R H^\circ(T)$ with $\Delta_R H(T)$ in van't Hoff's equation. For only then do the terms

$$T_x \int_{T_1}^{T_x} \left(\frac{-\Delta_R H(T)}{T^2} \right) dT$$

disappear, so that the relation $\Delta_R G(T) - \Delta_R G^\circ(T) = RT \ln(\Gamma)$ is fulfilled.

The following example should explain the relationships as follows:

The reaction enthalpies of a reaction are determined at different temperatures. The measured data are approximated by the function $\Delta_R H(T) = aT^2 + bT + c$ with the values $a = -0.47$, $b = 30.0$ and $c = -10^3$ with sufficient accuracy. From

$$\Delta_R H^\circ(T) = \Delta_R H(T) - RT \ln(\Gamma) \ (\Gamma = 10^{-4})$$

for example

$$\Delta_R H(298.15) = -3.3835\ 10^4 \ \text{J/mol}.$$

According to the above approximation formula,

$\Delta_R H^\circ(298.15) = -1.1003\ 10^4$ J/mol can be obtained, if $\Delta_R G^\circ(298.15) = -3.0 \times 10^4$ is known. This allows $\Delta_R G^\circ(T)$ to be calculated according to

$$\begin{aligned} \Delta_R G^\circ(T_x) &= \frac{\Delta_R G^\circ(T_1)}{T_1} T_x + T_x \int_{T_1}^{T_x} \left(\frac{-(aT^2 + bT + c)}{T^2} \right) dT \\ &= \frac{\Delta_R G^\circ(T_1)}{T_1} T_x + (-T_x) \left(a(T_x - T_1) + b \ln\left(\frac{T_x}{T_1}\right) + (-c)\left(\frac{1}{T_x} - \frac{1}{T_1}\right) \right) \end{aligned} \qquad (T_1 = 298.15\,K).$$

For example, when $T_x = 310.15$ K, the result is $\Delta_R G^\circ(310.15) = -2.9785\ 10^4$ J/mol.

When $\Delta_R G(T) = \Delta_R G^\circ(T) + RT \ln(\Gamma)$, $\Delta_R G(T)$ is given as follows, for example, $\Delta_R G(298.15) = -5.2832 \times 10^4$ and $\Delta_R G(310.15) = -5.353611 \times 10^4$ J/mol.

From $\Delta_{Re} S(T) = \frac{\Delta_R H(T) - \Delta_R G(T)}{T}$, the result is $\Delta_{Re} S(298.15) = 63.715$ and $\Delta_{Re} S(310.15) = 53.619$ J/(*mol K*).

If there is no functional connection available, and if, in addition, the temperature difference is sufficiently small, then $\Delta_R H(T)$ can be assumed to be constant for this range. This leads to

$$\Delta_R G_{app}(T_x) = \frac{\Delta_R G(T_1)}{T_1} T_x + T_x \, \Delta_R H(T_1) \left(\frac{1}{T_x} - \frac{1}{T_1} \right).$$

For example, at 294.15 K, $\Delta_R G(294.15) = -5.2571 \times 10^4$ J/mol. The approximated value is $\Delta_R G_{app}(294.15) = -5.212 \times 10^4$ J/mol.

If $\Delta_R H^\circ(T)$ would be included in the integration, this would yield

$$\Delta_R G^\circ_{vH}(T_x) = \frac{\Delta_R G^\circ(T_1)}{T_1} T_x + T_x \int_{T_1}^{T_x} \left(\frac{-\Delta_R H^\circ(T)}{T^2} \right) dT$$

$$= \frac{\Delta_R G^\circ(T_1)}{T_1} T_x + T_x \int_{T_1}^{T_x} \left(\frac{-(\Delta_R H(T) - RT \ln(\Gamma))}{T^2} \right) dT.$$

For $\Delta_R G^\circ_{vH}(310.15)$, for example, -3.0722×10^4 instead of $-2.9785\ 10^4$ J/mol would be obtained.

In Figure 5.1, $K_{eq}(T)$ (A), $\ln(K_{eq}(T))$ (B), $\Delta_R G(T)/T$ (C) and $\Delta_R G^\circ(T)/T$ (D) are shown as functions of T. The curve points fulfil the corresponding functions exactly because they were generated from them. In an experiment, of course, minor deviations have to be assumed.

The results of Figure 5.1D demonstrate that the $\Delta_R G(T)/T$ curves including $\Delta_R G^\circ/T(T)$ have all constant distances from each other and therefore possess equal slopes.

Different $\Delta_R G(T)/T$ functions of a specified reaction can be produced by different Γs. Although the temperature functions are shifted on the $\Delta_R G(T)/T$ axis, they must have the same slope at constant Γs at all corresponding temperatures. The same applies for $\Delta_R G^\circ/T(T)$ with $\Gamma = 1.0$. For this reason,

$$\frac{\partial\left(\frac{\Delta_R G^\circ(T)}{T}\right)}{\partial T} \text{ must be equal to } \frac{\partial\left(\frac{\Delta_R G(T)}{T}\right)}{\partial T}.$$

Both slopes must have the same value, namely $-\Delta_R H(T)/T^2$.

For example, $-\Delta_R H(298.15)/298.15^2 = 0.38063\,\mathrm{J/(mol\,K^2)}$.

In principle, this value may also be negative in another reaction (in endothermic reactions with a $\Delta_R H > 0$).

For

$$\frac{\Delta_R G(T)}{T} = -\Delta_{Ri} S(T),$$

a positive slope value does not mean that $\Delta_{Ri} S(T)$ must be negative and therefore the second law would be violated. A positive slope indicates that $\Delta_{Ri} S(T)$ has less positive values with increasing temperature. For example, $\Delta_{Ri} S(298.15) = 177.2$ and $\Delta_{Ri} S(310.15) = 172.61$ J/(*mol K*). For negative slopes, the reverse applies; then $\Delta_{Ri} S(T)$ assumes even more positive values with increasing temperature.

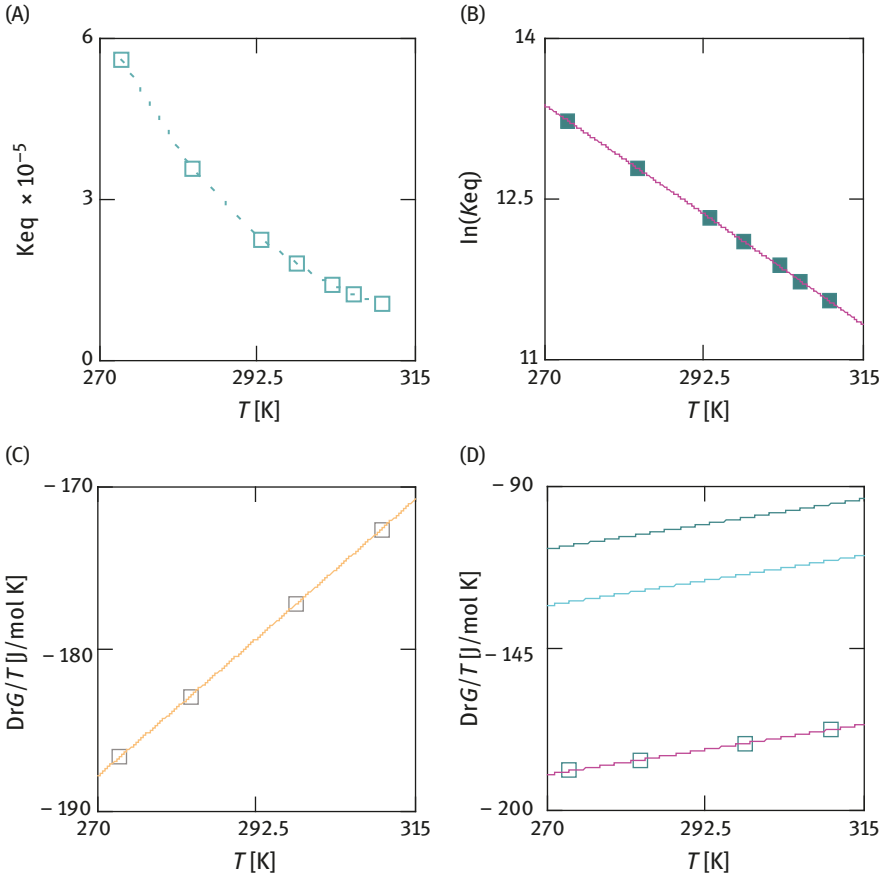

Figure 5.1: Temperature dependence of $\Delta_R G$-related parameters. (D) Red line shows the same function $\Delta_R G/T(T)$ as in (C); green line shows $\Delta_R G^\circ/T(T)$; cyan line shows $\Delta_R G^\circ/T(T)$ at the same $\Delta_R G/T(T)$ but with $\Gamma = 10^{-3}$ instead of 10^{-4}.

6 Thermodynamics of coupled reactions

6.1 Dissipation functions, fluxes and coupling

$\Delta_{Ri}S$ indicates the entropy production per mole of reaction in J/(mol K). The temporal change of entropy production is obtained by multiplying $\Delta_{Ri}S$ by the reaction rate $d\xi/dt$, that is

$$\Delta_{Ri}S\ \frac{d\xi}{dt} = \frac{d_iS}{d\xi}\ \frac{d\xi}{dt} = \frac{d_iS}{dt}\ \text{in J/(K s)}.$$

Due to $\Delta_{Ri}S = -\Delta_R G/T$ this yields

$$\frac{d_iS}{dt} = -\frac{\Delta_R G}{T}\ \frac{d\xi}{dt}$$

or

$$T\frac{d_iS}{dt} = A\,J\ \text{in J/s}. \tag{6.1}$$

For this, the affinity $A = -\Delta_R G = -dG/d\xi$ (in J/mol) and the reaction flux $J = d\xi/dt$ (in mol/s) have been introduced. For the product AJ, a new thermodynamic quantity has been defined. This is the dissipation function

$$\Phi = AJ\ (\text{in J/s}). \tag{6.2}$$

It gives the Gibbs energy dissipated per unit time and thus has the dimension of a power.

Formally, the following is obtained by expanding with A and J, respectively: $\Phi = JA\ (A/A) = LA^2$ or $\Phi = AJ(J/J) = RJ^2$, with $J/A = L$ (in $\text{mol}^2/\text{J s}$) and $R = 1/L$ (J s/mol^2).

Since $(\Phi/A) = J$, the following must apply for the flux:

$$J = L\,A\ (\text{in mol/s}). \tag{6.3}$$

For a constant ratio J/A, it is obvious that formulations (eq. (6.3)) are very similar to Ohm's law $I = G\,U$ or $I = (1/R)\,U$, known from electricity. Here I is the electric current (in A = Ampere = C/s), R is the electrical resistance (in Ω = Ohm and $G = 1/R$, respectively, in 1/Ω = Siemens or $\text{C}^2/\text{s J}$) and U is the voltage (in V = volts = J/C). In a chemical reaction, the (reaction) flux $J = L\,A$ corresponds to the charge flux $I = G\,U$. The affinity of the reaction $A = -\Delta_R G$ corresponds to the voltage U. For example, at a voltage of U = 1.0 V and an electrical conductance of $G = 1.0\ \text{A/V} = 1.0\ \text{C}^2/\text{Js}$, a current of I = 1.0 A flows through U. This current corresponds to a flux of $J = 1/96{,}485 \times \text{mol/s}$ through a chemical reaction with affinity A = 96,485 J/mol and conductance $L = 1/96{,}485^2 \times \text{mol}^2/\text{sJ}$ (for the calculation the Faraday constant F = 96,485 C/mol has been used).

https://doi.org/10.1515/9783110650501-006

In principle, $\Phi = IU = G\,U^2 = L\,A^2 = JA$ applies (all expressions in J/s). As $A = z\,F\,U$, this leads to $G\,U^2 = L\,U^2(zF)^2$; hence $G = L\,(zF)^2$.

For a chemical or biochemical reaction as well as for an electric current, Ohm's law is always valid if $J/A = \text{const.}$ or $I/U = \text{const.}$ is fulfilled. This condition prevails when the variables involved are in a steady state, which means that in the course of a chemical reaction both J and A have assumed constant values.

Coupling between two chemical or biochemical reactions is always present if an input reaction with positive input affinity A_2 drives another reaction with negative output affinity A_1, which – if uncoupled – would run spontaneously in the opposite direction of the input reaction, in the direction of the input reaction. This is only possible if the resulting affinity

$$A_{\text{res}} = A_1 + A_2 > 0. \tag{6.4}$$

If $A_1 = -A_2$, the coupled reaction would not be able to proceed, because then $A_{\text{res}} = -\Delta_{\text{R}}G_{\text{res}} = 0$.

6.2 Coupling in batteries

As an example of a coupled process, the reactions in a battery should be described. The battery fluid contains the reactants and products of a redox reaction

$$A_{\text{red}} + B_{\text{ox}} \rightleftharpoons A_{\text{ox}} + B_{\text{red}}, \tag{R6.1}$$

with

$$\Delta_{\text{R}}G_{\text{redox}} = \Delta_{\text{R}}G^{\circ}{}_{\text{redox}} + RT\ln\left(\frac{[A_{\text{ox}}][B_{\text{red}}]}{[A_{\text{red}}][B_{\text{ox}}]}\right).$$

The redox reaction is started by the introduction of a catalyst. The two electrodes function as such. Through this, the affinity A_{redox} of the redox reaction ($= -\Delta_{\text{R}}G_{\text{redox}}$) is coupled to the formation of an electrical potential difference $\Delta\phi$ at both electrodes. With an open circuit (no electrical connection of the electrodes), the reaction proceeds spontaneously and very quickly to equilibrium. Under these conditions, $A_{\text{res}} = A_1 + A_2 = \Delta\phi_{\text{eq}} + A_{\text{redox}} = 0$ applies.

Here A_{redox} represents the positive input affinity, and $\Delta\phi$ (in V) the negative output affinity. A_{redox} can also be expressed in electrical units as follows: $\text{EMF} = A_{\text{redox}}/z\,F = -\Delta\phi_{\text{eq}}$ (EMF = electromotive force in V, z = charge number).

If the two electrodes are connected via an external resistance, a constant current I can flow, which is given as

$$I = G_{\text{c}}(\Delta\phi + \text{EMF}),$$

where G_{c} is the conductance of the coupled process ($G_{\text{c}} = I/(\Delta\phi + \text{EMF})$). It is equal to the reciprocal of the internal resistance R_{c} of the battery. As the same current

flows through the battery and the outer branch at steady state, these currents can be equated yielding $G_c(\Delta\phi + \mathrm{EMF}) = G_{ex}\, U$ (G_{ex} = external conductance).

For U, $U = -\Delta\phi$ must hold, as I has to overcome the electric potential difference once in the forward direction ($\Delta\phi$), *quasi* uphill, and then to flow downhill via the same but oppositely directed potential jump ($-\Delta\phi = U$). Therefore, $\Delta\phi$ leads to

$$\Delta\phi = -\frac{G_c}{G_c + G_{ex}}\,\mathrm{EMF}.$$

The conductance G_c of the entire coupled process is composed of the conductances of the affinities involved in the overall process ($\Delta\phi$ and EMF). These partial conductances are denoted by G_{c1} and G_{c2}. They are associated with the output affinity A_1 (=$\Delta\phi$) and with the input affinity A_2 (EMF), respectively. These are obtained by expanding the equation $I = G_c(\Delta\phi + \mathrm{EMF})$ with $\Delta\phi$ or EMF:

$$I = G_c\left(\frac{\Delta\phi + \mathrm{EMF}}{\Delta\phi}\right)\Delta\phi = G_{c1}\,\Delta\phi$$

and

$$I = G_c\left(\frac{\Delta\phi + \mathrm{EMF}}{\mathrm{EMF}}\right)\mathrm{EMF} = G_{c2}\,\mathrm{EMF},$$

with

$$G_{c1} = G_c\left(\frac{\Delta\phi + \mathrm{EMF}}{\Delta\phi}\right) \tag{6.5}$$

and

$$G_{c2} = G_c\left(\frac{\Delta\phi + \mathrm{EMF}}{\mathrm{EMF}}\right). \tag{6.6}$$

The following applies:

$$G_c = \frac{1}{\frac{1}{G_{c1}} + \frac{1}{G_{c2}}} = \frac{1}{\frac{\Delta\phi}{G_c(\Delta\phi + \mathrm{EMF})} + \frac{\mathrm{EMF}}{G_c(\Delta\phi + \mathrm{EMF})}} \equiv G_c.$$

Also, it applies with$R_{c1} = 1/G_{c1}$ and $R_{c2} = 1/G_{c2}$:

$$R_c = R_{c1} + R_{c2}.$$

Hence, the sum of the resistances in the circuit must be equal to zero.

For the dissipation functions Ψ_1 and Ψ_2, which are related to the current flow through $\Delta\phi$ and through EMF, respectively, one obtains

$$\Psi_1 = G_c(\Delta\phi + \mathrm{EMF})\,\Delta\phi = G_c\left(\frac{\Delta\phi + \mathrm{EMF}}{\Delta\phi}\right)\Delta\phi^2 = G_{c1}\,\Delta\phi^2$$

and

$$\Psi_2 = G_c(\Delta\phi + \mathrm{EMF})\,\mathrm{EMF} = G_c\left(\frac{\Delta\phi + \mathrm{EMF}}{\mathrm{EMF}}\right)\mathrm{EMF}^2 = G_{c2}\,\mathrm{EMF}^2\,.$$

The resulting dissipation function of the entire coupled process is then given by

$$\Psi_{res} = \Psi_1 + \Psi_2 = G_c(\Delta\phi + \mathrm{EMF})^2.$$

The dissipation function of the external current branch with the conductance G_{ex} is

$$\Psi_{ex} = G_{ex}\,\Delta\phi^2 = G_c(\Delta\phi + \mathrm{EMF})\,(-\Delta\phi) = -G_{c1}\Delta\phi^2.$$

On comparison with $\Psi_1 = G_{c1}\,\Delta\phi^2$ shows that $G_{ex} = -G_{c1}$ must be true.

The dissipation function of the coupled process in the battery in addition to that of the external power branch is then due to $\Psi_1 = -\Psi_{ex}$

$$\Psi_{tot} = \Psi_1 + \Psi_2 + \Psi_{ex} = \Psi_2.$$

This result can be explained by the fact that the portion Ψ_1 of Ψ_{res} flows back again irreversibly, but now with the opposite sign, so that the initially saved dissipation is returned and the dissipation of the input (Ψ_2) alone is the determining factor.

The above derivations are again to be explained by means of a calculated example:

Consider a battery with the constant EMF of 12.0 V and the internal resistance $R_c = 0.5\ \Omega$ ($G_c = 2.0\ 1/\Omega$). The resistance of the outer branch is $R_{ex} = 2.5\ \Omega$ ($G_{ex} = 0.4\ 1/\Omega$). From these data, one obtains

$$\Delta\phi = -G_c/(G_c + G_{ex})\,\mathrm{EMF} = -2.0/2.4 \times 12.0 = -10.0\ \ \mathrm{V}$$

and

$$I = G_c(\Delta\phi + \mathrm{EMF}) = 2.0\ (-10.0 + 12.0) = 4.0\ \ \mathrm{A}.$$

$$G_{c1} = G_c\left(\frac{\Delta\phi + \mathrm{EMF}}{\Delta\phi}\right) = 2.0\ (-10.0 + 12.0)/(-10.0) = -0.4\ 1/\Omega$$

and

$$G_{c2} = G_c\left(\frac{\Delta\phi + \mathrm{EMF}}{\mathrm{EMF}}\right) = 2.0\ (-10.0 + 12.0)/(12.0) = 1/3\ 1/\Omega.$$

$R_c = R_{c1} + R_{c2} = 1/(-0.4) + 1/(1/3) = -2.5 + 3.0 \equiv 0.5\,\Omega$, as well as $R_{ex} = -R_{c1} = -1/(-0.4) \equiv 2.5\ \Omega$ and $R_{c1} + R_{ex} = -1/(-0.4) + 2.5 = 0\ \Omega$.

$\Psi_1 = G_{c1}\Delta\phi^2 = -0.4\ (-10.0)^2 = -40.0\ \mathrm{J/s}, \Psi_2 = G_{c2}\,\mathrm{EMF}^2 = 1/3\ \ 12.0^2 = 48.0\ \mathrm{J/s}$; therefore, $\Psi_{res} = 8.0\ \mathrm{J/s}$.

$U\,I = \Psi_{ex} = -\Psi_1 = 10.0 \times 4.0 = 40.0\ \mathrm{J/s}$ as well as $\Psi_1\ +\ \Psi_{ex} = 0\ \ \mathrm{J/s}$.

It follows that

$$\Psi_{tot} = \Psi_2 = -40.0 + 48.0 + 40.0 \equiv 48.0 \ \text{J/s}.$$

The above results show that in a closed circuit no electrical energy can be dissipated, and that the total resistance of the circuit disappears. The internal resistance of the battery is determined not only by its electrical partial resistance, but via coupling also by the partial resistance of the redox reaction. Furthermore, the sum of the energies dissipated by the coupled process and the outer branch must be equal to the chemical energy dissipated by the extending reaction alone.

Figure 6.1A shows the partial resistances (R_{c1} and R_{c2}) as a function of the external resistance (R_{ex}). Their sum results in the coupling resistance (=internal resistance) $R_c = R_{c1} + R_{c2}$, and due to $R_{ex} = -R_{c1}$, $R_{c2} = R_c + R_{ex}$ is obtained from it (A).

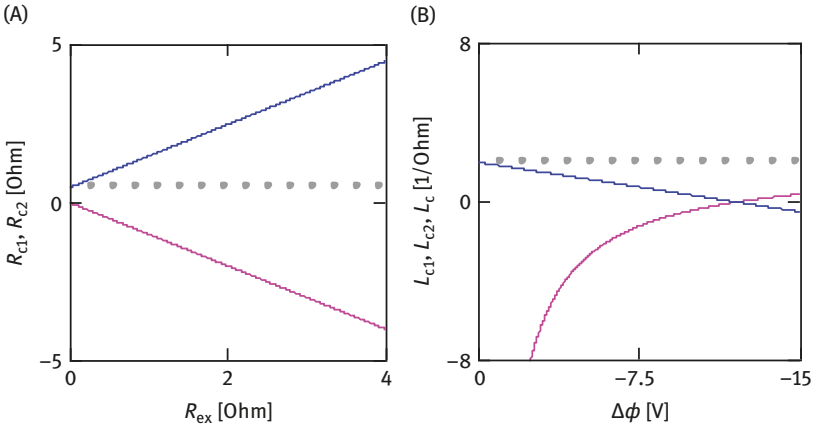

Figure 6.1: Simple circuit with battery and external resistance. (A) Resistances. Red line indicates partial resistance R_{c1}; blue line, partial resistance R_{c2}; gray points, inner resistance $R_c = R_{c1} + R_{c2}$. (B) Conductances. Red line indicates partial conductance G_{c1}; blue line, partial conductance G_{c2}; gray points, coupling conductance $G_c = 1/(1/G_{c1} + 1/G_{c2})$.

In Figure 6.1B, the partial conductivities (G_{c1} and G_{c2}) are shown as a function of the potential difference $\Delta\phi$ prevailing at the electrodes. For $\Delta\phi = -\text{EMF}$ (I = 0.0 A), G_{c1} and G_{c2} are equal to zero. At this point, L_c is not defined, but it retains the value 2.0 1/Ω with any approximation to $\Delta\phi$ = −12.0 V. For $\Delta\phi$ = 0.0 V the partial conductance G_{c1} goes against $-\infty$ 1/Ω, while R_{c1} goes against zero Ω. G_{c2} and R_{c2} have the values at this point 2.0 1/Ω and 0.5 Ω, respectively.

The electrical power that can be delivered to the outer branch is given by $P = \Psi_{ex} = -\Psi_1$.

The following applies:

$$P = G_c(\Delta\phi + \text{EMF})\,(-\Delta\phi) = G_c\left(-\Delta\phi^2 - \Delta\phi\,\text{EMF}\right).$$

The function $P(\Delta\phi)$ has a maximum that is derived from

$$\frac{dP(\Delta\phi)}{d(\Delta\phi)} = G_c(-2\Delta\phi - \mathrm{EMF}) = 0$$

and appears at

$$\Delta\phi_{max} = -\frac{\mathrm{EMF}}{2}.$$

The partial conductances for $\Delta\phi_{max}$ are

$$G_{c1max} = G_c\left(\frac{-\frac{1}{2}\mathrm{EMF} + \mathrm{EMF}}{-\frac{1}{2}\mathrm{EMF}}\right) = \frac{1}{2}G_c$$

and

$$G_{c2max} = G_c\left(\frac{-\frac{1}{2}\mathrm{EMF} + \mathrm{EMF}}{\mathrm{EMF}}\right) = \frac{1}{2}G_c.$$

Here the following also applies:

$$G_c = \frac{1}{\frac{1}{G_{c1max}} + \frac{1}{G_{c2max}}} = \frac{1}{\frac{1}{-G_c} + \frac{2}{G_c}} \equiv G_c.$$

Since $G_{ex} = -G_{c1}$ is true, which means that a battery always gives the maximum power when the conductance of the outer branch is equal to G_c, or when the external resistance R_{ex} is equal to the internal resistance R_c of the battery. The maximum power is thus given by $P_{max} = (1/R_c)(\mathrm{EMF}/2)^2$.

So, for example, a 12.0 V battery with an internal resistance of 0.5 Ω should deliver a maximum power of P_{max} = 1/0.5 (12.0/2)^2 = 72.0 J/s (or watt = W).

With $\Delta\phi = -G_c/(G_c + G_{ex})\,\mathrm{EMF}$, P can be described also as a function of G_{ex}. This leads to

$$P = G_c{}^2\left(\frac{G_{ex}}{(G_c + G_{ex})^2}\right)\mathrm{EMF}^2.$$

With $\Lambda = G_{ex}/ = 0.2$ results in

$$P = G_c\left(\frac{\Lambda}{(1+\Lambda)^2}\right)\mathrm{EMF}^2 = 2.0 \times 0.2/(1+0.2)^2 \times 12.0^2 = 40.0\ \mathrm{J/s}.$$

The maximum power is reached at $\Lambda_{max} = 1.0$, which confirms the above result ($G_{exmax} = G_c$):

$$P_{max} = G_c \frac{\Lambda_{max}}{(1+\Lambda_{max})^2} \text{EMF}^2 = 72.0 \text{ J/s}.$$

The efficiency η of a coupled reaction is defined as follows:

$$\eta = -\frac{\Psi_1}{\Psi_2} = -\frac{G_{c1}\,\Delta\phi^2}{G_{c2}\,\text{EMF}^2} = 0.8333.$$

Since

$$P = -G_{c1}\Delta\phi^2 = G_c\left(\frac{\Lambda}{(1+\Lambda)^2}\right)\text{EMF}^2 \text{ and } \Lambda = G_{ex}/G_c = 0.2.$$

The following is obtained:

$$\frac{\Delta\phi^2}{\text{EMF}^2} = \frac{1}{(1+\Lambda)^2};$$

therefore,

$$\eta = \frac{1}{1+\Lambda} = 0.8333.$$

If, instead of the resistance, a second battery is introduced into the outer current branch such that the electric poles (electrodes) of both batteries are connected to one another (plus to plus, and minus to minus), an electric current flows from the battery with the larger EMF (EMF_{Del}) to that with the lower EMF (EMF_{Dem}). In a sense, this leads to an energy demand by EMF_{Dem}, which is followed by energy delivery of EMF_{Del}.

Both EMFs are constant (e.g., $\text{EMF}_{Del} = 12.0$ V with $R_c^{Del} = 0.2\ \Omega$, and $\text{EMF}_{Dem} = -10.0$ V with $R_c^{Dem} = 0.3\ \Omega$). Then $G_c^{Del}\left(\Delta\phi_{Del} + \text{EMF}_{Del}\right) = G_c^{Dem}\left(\text{EMF}_{Dem} + \Delta\phi_{Dem}\right)$ is applied, and due to $\Delta\phi_{Del} = -\Delta\phi_{Dem}$:

$$\Delta\phi_{Dem} = \frac{G_c^{Del}\text{EMF}_{Del} - G_c^{Dem}\text{EMF}_{Dem}}{G_c^{Del} + G_c^{Dem}} = 11.2 \text{ V and } \Delta\phi_{Del} = -11.2 \text{ V}.$$

This results in a current of

$$1/0.2\ (-11.2 + 12.0) = 1/0.3\ (-10.0 + 11.2) = 4.0 \text{ A}.$$

The four partial conductances are

$$G_{c1}^{Del} = G_c^{Del}\frac{\Delta\phi_{Del} + \text{EMF}_{Del}}{\Delta\phi_{Del}} = -0.357143\ 1/\Omega,$$

$$G_{c2}^{Del} = G_c^{Del}\frac{\Delta\phi_{Del} + EMF_{Del}}{EMF_{Del}} = -0.333333\ \ 1/\Omega,$$

$$G_{c1}^{Dem} = G_c^{Dem}\frac{EMF_{Dem} + \Delta\phi_{Dem}}{EMF_{Dem}} = -0.4\ \ 1/\Omega$$

and

$$G_{c2}^{Dem} = G_c^{Dem}\frac{EMF_{Dem} + \Delta\phi_{Dem}}{\Delta\phi_{Dem}} = 0.357143\ \ 1/\Omega.$$

The conductances of the electrical circuit are determined by the partial conductances G_{c1}^{Del} and G_{c2}^{Del}. They are opposite equal also with the two batteries connected against each other. Consequently, the partial resistances must also be opposite equal ($R_{c1}^{Del} = -R_{c2}^{Dem}$), which means that the total resistance of the closed circuit must vanish.

The total dissipation is given through

$$\Psi_{tot}^{Del} + \Psi_{tot}^{Delm} = I\left(\Delta\phi_{Del} + EMF_{Del} + \Delta\phi_{Dem} + EMF_{Dem}\right) = I(EMF_{Del} + EMF_{Dem}) = 8.0\ J/s.$$

When $\Delta\phi_{Del} = -\Delta\phi_{Dem}$, the associated dissipation functions ($I\,\Delta\phi$) must also vanish, so that evidently no electrical energy is dissipated in this circuit either. This result was to be expected, since at $T = \text{const.}$ the line integral of electrical potential differences must disappear over a closed path.

The above result can also be derived as follows:

$$\Psi_1^{Del} = G_c^{Del}\left(\Delta\phi_{Del} + EMF_{Del}\right)\Delta\phi_{Del}$$

or

$$\Psi_1^{Del} = G_c^{Del}\left(\frac{G_c^{Dem}EMF_{Dem} - G_c^{Del}EMF_{Del}}{G_c^{Del} + G_c^{Dem}} + EMF_{Del}\right)\left(\frac{G_c^{Dem}EMF_{Dem} - G_c^{Del}EMF_{Del}}{G_c^{Del} + G_c^{Dem}}\right)$$

and

$$\Psi_1^{Del} = \frac{G_c^{Del}\,G_c^{Dem}}{G_c^{Del} + G_c^{Dem}}\ (EMF_{Del} + EMF_{Dem})\left(\frac{G_c^{Dem}EMF_{Dem} - G_c^{Del}EMF_{Del}}{G_c^{Del} + G_c^{Dem}}\right)$$
$$= 2.0 \times 2.0 \times (-11.2) = -44.8\ J/s.$$

For Ψ_2^{Dem}, $\Psi_2^{Dem} = G_c^{Dem}\left(EMF_{Dem} + \Delta\phi_{Dem}\right)\Delta\phi_{Dem}$ is applied or

$$\Psi_2^{Dem} = G_c^{Dem}\left(EMF_{Dem} - \frac{G_c^{Dem}EMF_{Dem} - G_c^{Del}EMF_{Del}}{G_c^{Del} + G_c^{Dem}}\right)\left(-\frac{G_c^{Dem}EMF_{Dem} - G_c^{Del}EMF_{Del}}{G_c^{Del} + G_c^{Dem}}\right)$$

and

$$\Psi_2^{\mathrm{Dem}} = \frac{G_c^{\mathrm{Del}}\, G_c^{\mathrm{Dem}}}{G_c^{\mathrm{Del}} + G_c^{\mathrm{Dem}}}\ (\mathrm{EMF}_{\mathrm{Del}} + \mathrm{EMF}_{\mathrm{Dem}})\left(- \frac{G_c^{\mathrm{Dem}}\mathrm{EMF}_{\mathrm{Dem}} - G_c^{\mathrm{Del}}\mathrm{EMF}_{\mathrm{Del}}}{G_c^{\mathrm{Del}} + G_c^{\mathrm{Dem}}}\right)$$
$$= 2.0 \times 2.0 \times 11.2 = 44.8\ \mathrm{J/s}.$$

It follows that,

$$\Psi_2^{\mathrm{Dem}} = G_{c2}^{\mathrm{Dem}} \left(\Delta\phi_{\mathrm{Dem}}\right)^2 = -\Psi_1^{\mathrm{Del}} = -G_{c1}^{\mathrm{Del}} \left(\Delta\phi_{\mathrm{Del}}\right)^2$$

from which $G_2^{\mathrm{Dem}} = -G_1^{\mathrm{Del}}$ is obtained.

The overall efficiency of both batteries results from the consideration that initially only the fraction η_{Del} of the chemical energy per unit time of the stronger battery is supplied as power to the weaker battery, and from this again only the fraction η_{Dem} can be converted into useful chemical energy per unit time, which is then available to the weaker battery to regenerate its EMF. The resulting efficiency is thus

$$\eta_{\mathrm{tot}} = \frac{-\Psi_1^{\mathrm{Del}}}{\Psi_2^{\mathrm{Del}}} \times \frac{-\Psi_1^{\mathrm{Dem}}}{\Psi_2^{\mathrm{Dem}}} = \frac{-I\,\Delta\phi_{\mathrm{Del}}}{I\,\mathrm{EMF}_{\mathrm{Del}}} \times \frac{-I\,\mathrm{EMF}_{\mathrm{Dem}}}{I\,\Delta\phi_{\mathrm{Dem}}} = \eta_{\mathrm{Del}} \times \eta_{\mathrm{Dem}} = -\frac{\mathrm{EMF}_{\mathrm{Del}}}{\mathrm{EMF}_{\mathrm{Dem}}}. \quad (6.7)$$

$\eta_{\mathrm{Del}} = -(-11.2)/12.0 = 0.9333,\ \eta_{\mathrm{Dem}} = -(-10.0)/11.2 = 0.89286$ and

$$\eta_{\mathrm{tot}} = \eta_{\mathrm{Del}} \times \eta_{\mathrm{Dem}} = -\frac{\mathrm{EMF}_{\mathrm{Del}}}{\mathrm{EMF}_{\mathrm{Dem}}} = 10.0/12.0 = 0.8333 (= 0.9333\ 0.89286).$$

So far it has been assumed that the coupling mechanism of a coupled process, as it is to be observed during the passage of current through a battery, always proceeds completely without losses, that is, no leak currents occur by complete coupling. With incomplete coupling, such currents and flows, respectively, cannot be avoided. In this regard, there exist two possibilities for a coupled reaction: on the one hand, the respective leak current can be caused by the uncoupled output affinity ($A_1 = \Delta\phi$) and on the other hand by the uncoupled input affinity ($A_2 = \mathrm{EMF}$). The flux going through A_1 is then given by

$$J_1 = L_c\,(A_1 + A_2) + L_{L1}\,A_1, \quad (6.8)$$

and the flux through A_2 by

$$J_2 = L_c\,(A_1 + A_2) + L_{L2}\,A_2. \quad (6.9)$$

As $A_1 < 0$, J_1 decreases by uncoupling, because the A_1-driven leak flux $J_{L1} = L_{L1}\,A_1$ runs in the opposite direction of the coupled flux ($L_c\,(A_1 + A_2)$). J_2, on the other hand, increases due to $A_2 > 0$. Hence, the A_2-driven leak flux $J_{L2} = L_{L2}\,A_2$ flows in the same direction as the coupled flux.

L_c is again the conductance of the coupled reaction, while L_L denotes the conductance of leak fluxes.

With $\lambda_1 = L_{L1}/L_c$ and $\lambda_2 = L_{L2}/L_c$, this leads to

$$J_1 = L_c\,(A_1 + A_2) + \lambda_1 L_c\,A_1 \;\; and \;\; J_2 = L_c\,(A_1 + A_2) + \lambda_2 L_c\,A_1$$

or

$$J_1 = L_c\,((1+\lambda_1)A_1 + A_2) \tag{6.10}$$

and

$$J_2 = L_c\,(A_1 + (1+\lambda_2)A_2). \tag{6.11}$$

The dissipation functions associated with these fluxes are

$$\Psi_1 = J_1 A_1 = L_c\,(A_1 + A_2) + \lambda_1 L_c\,{A_1}^2 = L_c\,((1+\lambda_1)A_1 + A_2)A_1 \tag{6.12}$$

and

$$\Psi_2 = J_2 A_2 = L_c\,(A_1 + A_2)A_2 + \lambda_2 L_c\,{A_2}^2 = L_c\,(A_1 + (1+\lambda_2)A_2)A_2, \tag{6.13}$$

$$\Psi_{tot} = \Psi_1 + \Psi_2 = L_c\left((A_1 + A_2)^2 + \lambda_1 {A_1}^2 + \lambda_2 {A_2}^2\right). \tag{6.14}$$

The efficiency results from this to

$$\eta = -\frac{\Psi_1}{\Psi_2} = -\frac{(1+\lambda_1)a + 1}{1 + \dfrac{(1+\lambda_2)}{a}}. \tag{6.15}$$

The above equation is obtained by substituting Ψ_1 and Ψ_2 by eqs. (6.12) and (6.13), respectively. By excluding A_2 in the numerator and A_1 in the denominator and with $a = A_1/A_2$, eq. (6.15) is obtained.

The efficiency can also be expressed as a function of the degree of coupling q. This is defined as

$$q = \frac{L_c}{\sqrt{(L_c + L_{L1})(L_c + L_{L2})}} = \frac{1}{\sqrt{(1+\lambda_1)(1+\lambda_2)}}. \tag{6.16}$$

q represents the ratio of coupling conductance L_c to the geometric mean of the respective sums of coupling conductance and leak conductance.

By factoring out $(1+\lambda_1)$ in the numerator (eq. (6.15)), and $(1+\lambda_2)$ in the denominator, first, one obtains for efficiency

$$\eta = -\frac{a + \dfrac{1}{1+\lambda_1}}{\dfrac{1}{1+\lambda_2} + \dfrac{1}{a}} \times \frac{1+\lambda_1}{1+\lambda_2}.$$

With $Z = \sqrt{\frac{1+\lambda_1}{1+\lambda_2}}$, this leads to

$$\eta = \frac{a + \dfrac{1}{1+\lambda_1} \times \dfrac{\sqrt{1+\lambda_2}}{\sqrt{1+\lambda_2}}}{\dfrac{1}{1+\lambda_2} \times \dfrac{\sqrt{1+\lambda_1}}{\sqrt{1+\lambda_1}} + \dfrac{1}{a}} \times Z^2 = -\frac{a + \dfrac{1}{Z}q}{Zq + \dfrac{1}{a}} \times \frac{Z}{\dfrac{1}{Z}} = -\frac{Za + q}{q + \dfrac{1}{Za}}. \tag{6.17}$$

With given λ_1 and λ_2 values, Z and q are given, and eqs. (6.15) and (6.17) are identical. Equation (6.17) can be maximized with respect to $Za = x$. It is

$$\frac{d\eta}{dx} = -\frac{q + \dfrac{1}{x} - \left(-\dfrac{1}{x^2}\right)(x+q)}{\left(q + \dfrac{1}{x}\right)^2},$$

and for $d\eta/dx = 0$ the result is

$$q + \frac{1}{x} + \frac{1}{x} + \frac{q}{x^2} = 0$$

or

$$x^2 + \frac{2}{q}x + 1 = 0.$$

This quadratic equation has the solution

$$x_{\max} = \frac{1}{q}\left(\sqrt{1-q^2} - 1\right),$$

from which

$$a_{\max} = \frac{x_{\max}}{Z} = \frac{\left(\sqrt{1-q^2} - 1\right)}{Zq}$$

can be obtained.

With $a_{\max}$ results for the maximum efficiency

$$\eta_{\max} = -\frac{\frac{1}{q}\left(\sqrt{1-q^2} - 1\right) + q}{q + \dfrac{1}{\sqrt{1-q^2} - 1}} = -\frac{q^2 + \sqrt{1-q^2} - 1}{q^2\sqrt{1-q^2}}\left(\sqrt{1-q^2} - 1\right).$$

By expanding with $\left(\sqrt{1-q^2} + 1\right)$,

$$\eta_{\max} = \frac{\sqrt{1-q^2} - (1-q^2)}{\sqrt{1-q^2} + (1-q^2)} = \frac{1 - \sqrt{1-q^2}}{1 + \sqrt{1-q^2}} = \frac{q^2}{\left(1 + \sqrt{1-q^2}\right)^2} \tag{6.18}$$

is obtained.

In nonequilibrium thermodynamics (NET), the fluxes J_1 and J_2 of a coupled reaction are shown in somewhat modified form [5–7]. The conductance of the coupled reaction (L_c) is denoted by L_{12} and the conductances ($L_c + L_{L1}$ and $L_c + L_{L2}$) containing both coupled plus leak conductances are denoted by L_{11} and L_{22}, respectively. Substituting in the flux equations (6.10) and (6.11), respectively, the result is $J_1 = L_{11}\,A_1 + L_{12}\,A_2$ and $J_2 = L_{12}\,A_1 + L_{22}\,A_2$.

The degree of coupling q and the quantity Z have as a result $q = L_{12}/\sqrt{L_{11}\,L_{22}}$ and $Z = \sqrt{L_{11}/L_{22}}$.

The potentials A_1 and A_2 are usually referred to as thermodynamic forces in the NET.

The above results for uncoupled processes are explained below using the example of two batteries connected against each other, but this time uncoupled. Uncoupling is caused by leak currents and leak fluxes (in electrical units), respectively. In both batteries, these can occur both at the electrical potential differences ($\Delta\phi_{\mathrm{Del}} = -\Delta\phi_{\mathrm{Dem}}$) and at the chemical potential differences ($\mathrm{EMF_{Del}}$ and $\mathrm{EMF_{Dem}}$). $\Delta\phi_{\mathrm{Del}}$ or $\Delta\phi_{\mathrm{Dem}}$ can be decoupled by short-circuiting the electrical poles via suitable resistors, while it is assumed for both redox reactions that they can proceed to a certain extent also uncoupled. The λ values associated with the respective leak currents or fluxes are $\lambda_1^{\mathrm{Del}} = 0.04$ (associated with $\Delta\phi_{\mathrm{Del}}$), $\lambda_2^{\mathrm{Del}} = 0.01$ (associated with $\mathrm{EMF_{Del}}$), $\lambda_1^{\mathrm{Dem}} = 0.012$ (associated with $\mathrm{EMF_{Dem}}$) and $\lambda_2^{\mathrm{Dem}} = 0.09$ (associated with $\Delta\phi_{\mathrm{Dem}}$).

$\Delta\phi_{\mathrm{Del}}$ (as a variable) is obtained from $I_1^{\mathrm{Del}} = I_2^{\mathrm{Dem}}$, which is given by $G_c^{\mathrm{Del}}\left(\Delta\phi_{\mathrm{Del}} + \mathrm{EMF_{Del}}\right) + \lambda_1^{\mathrm{Del}}\,G_c^{\mathrm{Del}}\,\Delta\phi_{\mathrm{Del}} = G_c^{\mathrm{Dem}}\left(\mathrm{EMF_{Dem}} + \left(-\Delta\phi_{\mathrm{Del}}\right)\right) + \lambda_1^{\mathrm{Dem}}G_c^{\mathrm{Dem}}\mathrm{EMF_{Dem}}$ yielding

$$\Delta\phi_{\mathrm{Del}} = \frac{G_c^{\mathrm{Dem}}\,\mathrm{EMF_{Dem}} - G_c^{\mathrm{Del}}\mathrm{EMF_{Del}}}{G_c^{\mathrm{Del}}\left(1+\lambda_1^{\mathrm{Del}}\right) - G_c^{\mathrm{Dem}}\left(1+\lambda_2^{\mathrm{Dem}}\right)} = -10.57\ \mathrm{V}.$$

The current going through $\Delta\phi_{\mathrm{Del}}$ ($A_1^{\mathrm{Del}} < 0$) is

$$I_1^{\mathrm{Del}} = G_c^{\mathrm{Del}}\left(\Delta\phi_{\mathrm{Del}} + \mathrm{EMF_{Del}}\right) + \lambda_1^{\mathrm{Del}}G_c^{\mathrm{Del}}\,\Delta\phi_{\mathrm{Del}} = 5.057\ \mathrm{A},$$

and the one through $\mathrm{EMF_{Del}}$ ($A_2^{\mathrm{Del}} > 0$) is

$$I_2^{\mathrm{Del}} = G_c^{\mathrm{Del}}\left(\Delta\phi_{\mathrm{Del}} + \mathrm{EMF_{Del}}\right) + \lambda_2^{\mathrm{Del}}G_c^{\mathrm{Del}}\,\mathrm{EMF_{Del}} = 7.77\ \mathrm{A}.$$

Through $\mathrm{EMF_{Dem}}$ ($A_1^{\mathrm{Dem}} < 0$) go

$$I_1^{\mathrm{Dem}} = G_c^{\mathrm{Dem}}\left(\mathrm{EMF_{Dem}} + (-)\Delta\phi_{\mathrm{Del}}\right) + \lambda_1^{\mathrm{Dem}}G_c^{\mathrm{Dem}}\,\mathrm{EMF_{Dem}} = 1.4868\ \mathrm{A},$$

and through $\Delta\phi_{\mathrm{Dem}}$ ($A_2^{\mathrm{Dem}} > 0$)

$$I_2^{\mathrm{Dem}} = G_c^{\mathrm{Dem}}\left(\mathrm{EMF_{Dem}} + (-)\Delta\phi_{\mathrm{Del}}\right) + \lambda_2^{\mathrm{Dem}}G_c^{\mathrm{Dem}}\left(-\Delta\phi_{\mathrm{Del}}\right) = 5.0566\ \mathrm{A}.$$

The dissipation functions are $\Psi_1^{\mathrm{Del}} = I_1^{\mathrm{Del}} \Delta\phi_{\mathrm{Del}} = -53.4283\ \mathrm{J/s}$,

$$\Psi_2^{\mathrm{Del}} = I_2^{\mathrm{Del}} \mathrm{EMF}_{\mathrm{Del}} = 93.238\ \mathrm{J/s} \text{ and}$$

$$\Psi_{\mathrm{tot}}^{\mathrm{Del}} = \Psi_1^{\mathrm{Del}} + \Psi_2^{\mathrm{Del}} = 39.81\ \mathrm{J/s}.$$

$$\Psi_1^{\mathrm{Dem}} = I_1^{\mathrm{Dem}}\ \mathrm{EMF}_{\mathrm{Dem}} = -14.868\ \mathrm{J/s},$$

$$\Psi_2^{\mathrm{Dem}} = I_2^{\mathrm{Dem}}\ \left(-\Delta\phi_{\mathrm{Del}}\right) = 53.4283\,\mathrm{J/s} \text{ and}$$

$$\Psi_{\mathrm{tot}}^{\mathrm{Dem}} = \Psi_1^{\mathrm{Dem}} + \Psi_2^{\mathrm{Dem}} = 38.56\,\mathrm{J/s}.$$

The total dissipation of both batteries is $\Psi_{\mathrm{tot}}^{\mathrm{Del}} + \Psi_{\mathrm{tot}}^{\mathrm{Dem}} = 78.37\ \mathrm{J/s}$. It is considerably larger than dissipation under fully coupled conditions (8.0 J/s). The dissipation functions Ψ_1^{Del} and Ψ_2^{Dem} are opposite equal also under uncoupled conditions.

The power delivery to the weaker battery is only slightly reduced by uncoupling under these conditions. The power on uncoupling is given by

$$P = -I_1^{\mathrm{Del}} \Delta\phi_{\mathrm{Del}} - I_{L2}^{\mathrm{Dem}} \left(-\Delta\phi_{\mathrm{Del}}\right).$$

The leak flux going through $-\Delta\phi_{\mathrm{Del}}$ of the weaker battery $I_{L2}^{\mathrm{Dem}} = \lambda_2^{\mathrm{Dem}} G_{\mathrm{c}}^{\mathrm{Dem}} \left(-\Delta\phi_{\mathrm{Del}}\right)$ is taken into consideration.

The replacement of $\Delta\phi_{\mathrm{Del}}$ through

$$\frac{G_{\mathrm{c}}^{\mathrm{Del}}\ \mathrm{EMF}_{\mathrm{Del}}}{G_{\mathrm{c}}^{\mathrm{Del}}\left(1+\lambda_{\Sigma\mathrm{Del}}\right) + G_{\mathrm{c2}}^{\mathrm{Dem}}} = -10.566\ \mathrm{V}$$

leads to

$$P = G_{\mathrm{c}}^{\mathrm{Del}} \frac{\Lambda}{\left(1+\lambda_{\Sigma\mathrm{Del}}+\Lambda\right)^2} \left(\mathrm{EMF}_{\mathrm{Del}}\right)^2 = 19.936\ \mathrm{J/s}.$$

For this purpose, the conductivities of the two leak fluxes are combined:

$$\lambda_{\Sigma\mathrm{Del}} = \left(G_{L1}^{\mathrm{Del}} + G_{L2}^{\mathrm{Dem}}\right) / G_{\mathrm{c}}^{\mathrm{Del}} = 0.1$$

Also under uncoupled conditions, the power output can be maximized. For this purpose, the function $P\left(\Delta\phi_{\mathrm{Del}}\right) = -G_{\mathrm{c}}^{\mathrm{Del}} \left(\left(1+\lambda_{\Sigma\mathrm{Del}}\right) \Delta\phi_{\mathrm{Del}}{}^2 + \mathrm{EMF}_{\mathrm{Del}}\, \Delta\phi_{\mathrm{Del}}\right)$ is assumed.

The maximum is at

$$\Delta\phi_{\mathrm{max}}^{\mathrm{Del}} = -\frac{\mathrm{EMF}_{\mathrm{Del}}}{2\left(1+\lambda_{\Sigma\mathrm{Del}}\right)} = -5.4546\ \mathrm{V}.$$

With $\Lambda = G_{\mathrm{c2}}^{\mathrm{Dem}} / G_{\mathrm{c}}^{\mathrm{Del}}$ and $G_{\mathrm{c2}}^{\mathrm{Dem}} = -G_{\mathrm{c}}^{\mathrm{Del}} \left(\left(1+\lambda_{\Sigma\mathrm{Del}}\right) \Delta\phi_{\mathrm{Del}}{}^2 + \mathrm{EMF}_{\mathrm{Del}}\, \Delta\phi_{\mathrm{Del}}\right) / \Delta\phi_{\mathrm{Del}}$ leads to

$\Lambda_{\mathrm{max}} = 1 + \lambda_{\Sigma\mathrm{Del}} = 1.1$ (1.0 without uncoupling) and

$P_{\mathrm{max}} = G_{\mathrm{c}}^{\mathrm{Del}} \left(\mathrm{EMF}_{\mathrm{Del}}/2\right)^2 /$ (180.0 J/s without uncoupling).

Figure 6.2A shows the corresponding power outputs for fully coupled and uncoupled processes. The increase in $\Delta\phi_{\mathrm{Del}}$ (from − 12.0 to −10.57 V, becomes less negative) and I_1^{Del} (from 4.0 to 5.0665 A) due to uncoupling is associated with a significant drop in performance from 44.8 to 19,936 J/s. The resulting reduction in performance under these conditions is mainly due to a drastic reduction of Λ (from 0.0714 to 0.0357). This change of Λ is ultimately caused by the leakage fluxes at the electrical potential difference, which means the appearance of the uncoupling parameter $\lambda_{\Sigma\mathrm{Del}}$.

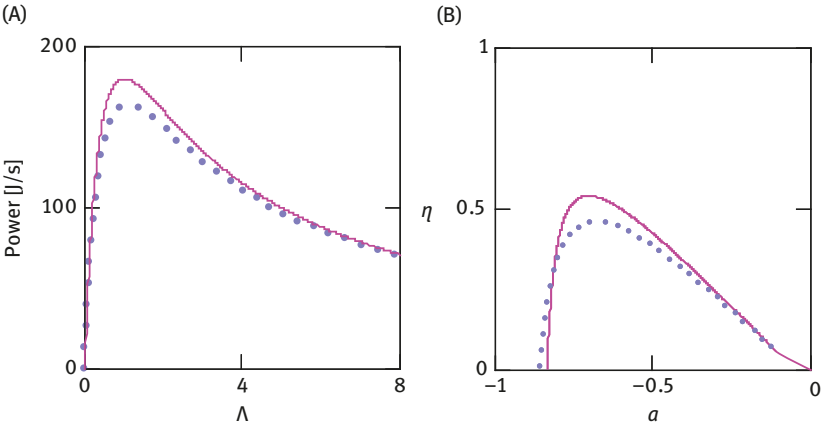

Figure 6.2: Power and efficiency. (A) Output power. Red line: under coupled conditions; blue points: partially uncoupled. (B) Efficiency. Red line: uncoupling at delivery sites; blue points: uncoupling at demand sites.

The efficiency of the coupled response of a battery that is short-circuited via a resistance in the outer branch must be zero because electrical power is supplied to $\Delta\phi$ at steady state at the same rate as it is dissipated. The insertion of $a = \Delta\phi/\mathrm{EMF} = -0.96154$ into eq. (6.15) results with $\lambda_1 = 0.04$ and $\lambda_2 = 0$

$$\eta = -\frac{(1+\lambda_1)a+1}{1+\frac{1}{a}} = 0.$$

When two batteries are connected against each other $\lambda_1^{\mathrm{Del}} = 0.04$, $\lambda_2^{\mathrm{Del}} = 0.01$, $\lambda_1^{\mathrm{Dem}} = 0.012$, $\lambda_2^{\mathrm{Del}} = 0.09$, as well as $a_{\mathrm{Del}} = \Delta\phi_{\mathrm{Del}}/\mathrm{EMF}_{\mathrm{Del}} = -0.88$ and $a_{\mathrm{Dem}} = \mathrm{EMF}_{\mathrm{Dem}}/\left(-\Delta\phi_{\mathrm{Del}}\right)\left(-\Delta\phi_{\mathrm{Del}}\right) = -0.946$. The efficiency functions are shown in Figure 6.2B:

$$\eta_{\mathrm{Del}} = -\frac{\left(1+\lambda_1^{\mathrm{Del}}\right)a_{\mathrm{Del}}+1}{1+\dfrac{\left(1+\lambda_2^{\mathrm{Del}}\right)}{a_{\mathrm{Del}}}} = 0.573$$

and

$$\eta_{\mathrm{Dem}} = -\frac{\left(1+\lambda_1^{\mathrm{Dem}}\right)a_{\mathrm{Dem}}+1}{1+\dfrac{\left(1+\lambda_2^{\mathrm{Dem}}\right)}{a_{\mathrm{Dem}}}} = 0.2783.$$

The result from this is $\eta_{\mathrm{Del}} \times \eta_{\mathrm{Dem}} = 0.1595$.

The latter result is also possible from

$$\eta_{\Sigma\mathrm{Del}} = -\frac{(1+\lambda_{\Sigma\mathrm{Del}})a_{\mathrm{Del}}+1}{1+\dfrac{\left(1+\lambda_2^{\mathrm{Del}}\right)}{a_{\mathrm{Del}}}} = 0.2138 \text{ and}$$

$$\eta_{\Sigma\mathrm{Dem}} = -\frac{\left(1+\lambda_1^{\mathrm{Dem}}\right)a_{\mathrm{Dem}}+1}{1+\frac{1}{a_{\mathrm{Dem}}}} = 0.7458.$$

Also this results in $\eta_{\Sigma\mathrm{Del}} \times \eta_{\Sigma\mathrm{Dem}} = 0.1595$.

The respective degrees of coupling are $q_{\mathrm{Del}} = 0.9757$, and $q_{\mathrm{Dem}} = 0.952$, the respective Z-values are $Z_{\mathrm{Del}} = 1.0147$ and $Z_{\mathrm{Dem}} = 0.9636$.

This results in the maximum efficiencies

$$\eta_{\mathrm{max}}^{\mathrm{Del}} = \frac{{q_{\mathrm{Del}}}^2}{\left(1+\sqrt{1-{q_{\mathrm{Del}}}^2}\right)^2} = 0.641$$

and

$$\eta_{\mathrm{max}}^{\mathrm{Dem}} = \frac{{q_{\mathrm{Dem}}}^2}{\left(1+\sqrt{1-{q_{\mathrm{Dem}}}^2}\right)^2} = 0.5318.$$

The corresponding a values are

$$a_{\mathrm{max}}^{\mathrm{Del}} = \frac{x_{\mathrm{max}}^{\mathrm{Del}}}{Z_{\mathrm{Del}}} = \frac{\left(\sqrt{1-{q_{\mathrm{Del}}}^2}-1\right)}{Z_{\mathrm{del}}\, q_{\mathrm{Del}}} = -0.7888$$

and

$$a_{\mathrm{max}}^{\mathrm{Dem}} = -0.7568.$$

With the two maximum efficiencies the overall efficiency $\eta_{max}^{Del} \times \eta_{max}^{Dem} = 0.34$ is obtained.

However, the above formulas only apply as long as EMF_{Del} and EMF_{Dem} do not change. Under real conditions, however, EMF_{Del} decreases continuously during charging, while EMF_{Dem} increases. The reaction comes to a halt when $EMF_{Del} = -EMF_{Dem}$. Then both redox reactions are at equilibrium.

7 Coupled transport processes at membranes

7.1 The Ca^{2+} ATPase of the sarco/endoplasmic reticulum

The Ca^{2+} concentration of the cytosol, $[Ca^{2+}]_c$, or sarcosol (in muscle cells) is an important activation parameter that is able to initiate vital processes such as muscle contraction or exocytosis. It is absolutely necessary for this Ca^{2+} that even very precise concentration values can be set. This is done in the cell mainly by the so-called Ca^{2+} pumps. Those of the sarco/endoplasmic reticulum (SR) are referred to as sarco/endoplasmic reticulum ATPase (SERCA). These are protein complexes that are embedded in the membrane of the reticulum. Their task is to transport Ca^{2+} ions of the cytosol into the lumen of the reticulum. This active transport reaction (reactions coupled to ATP hydrolysis are referred to as active) can be described by the following reaction equation:

$$MgATP^{2-} + H_2O + 2Ca_c{}^{2+} \rightarrow MgADP^{-} + H_2PO_4{}^{-} + 2Ca_r{}^{2+}. \qquad \text{(R7.1)}$$

This is apparently a coupled reaction in which the hydrolysis of 1.0 mol ATP in the cytosol is coupled to the transport of 2.0 mol Ca^{2+} from the cytosol into the reticulum (index "r"). Analogous to the coupling between the chemical potential difference of a redox reaction and the electrical potential difference in a battery, the chemical potential difference of the ATP hydrolysis here is coupled to the electrochemical potential difference of Ca^{2+} ions in the two compartments cytosol and reticulum. Accordingly, the following flux equation can be formulated:

The general formulation for the flux by a coupled reaction $J = L_c(A_1 + A_2)$ corresponds to $J_{ser} = L_c^{ser}\left(A_{ca}^{ser} + A_{ATP}^{c}\right)$.

The affinity of the output reaction ($A_{ca}^{ser} = -\Delta_R G_{ca}^{ser}$) is

$$A_{ca}^{ser} = 2\left(R\,T\,\ln\left(\frac{[Ca^{2+}]_c}{[Ca^{2+}]_r}\right) + z_{ca}\,F(-\Delta\phi_r)\right)\left(A_{ca}^{ser} < 0,\ z_{ca} = 2.0\right) \text{ in J/mol.}$$

The first term of the right side of the above equation results from the chemical potential difference of the Ca^{2+} ions of the lumen and sarcosol:

$$\Delta\mu_{ca}^{ser} = -R\,T\,\ln\left(\frac{[Ca^{2+}]_c}{[Ca^{2+}]_r}\right)(\text{in J/mol}).$$

On comparison with a chemical reaction shows that the $\Delta_R G^\circ$ term is no longer listed. This is omitted because the standard potentials (here of Ca^{2+} in the reticulum lumen and in the sarcosol) can be considered as equal. In addition, the mass action quotient Γ contains only the concentration ratio of the concentrations separated by a membrane of the respective compartment.

https://doi.org/10.1515/9783110650501-007

The second term must be added in principle. It refers to charged particles that are transported by an electric potential difference. As a result, electrical work can be performed on them which must be taken into account by the expression $z_{ca}F\Delta\phi_r$. Both terms can be summarized to the electrochemical potential difference of a reaction

$$\Delta\tilde{\mu} = \Delta\mu + zF\Delta\phi \quad \text{in J/mol.} \tag{7.1}$$

Thus, the following is applied:

$$A_{ca}^{ser} = -2\Delta\tilde{\mu}_{ca}^{ser}.$$

The potential of the input reaction ($A_2 = A_{ATP}^{c} = -\Delta_R G_{ATP}^{c}$) is

$$A_{ATP}^{c} = R\,T\,\ln\left(\frac{[ATP]}{[ADP][P_i]}\,K'_{ATP}\right)\ (A_{ATP}^{c} > 0)\ \text{J/mol.}$$

K'_{ATP} is the equilibrium constant of ATP hydrolysis:

$$ATP + H_2O \rightarrow ADP + P_i\,, \tag{R7.2}$$

with

$$K'_{atp} = \frac{[ADP]_{eq}\,[P_i]_{eq}}{[ATP]_{eq}}$$

The square brackets indicate that it refers to the respective concentrations of all species occurring under the given conditions (biochemical notation). These conditions include a certain constant temperature, a predetermined range for pH and pMg and a certain ionic strength. For example, for a cytosolic pH range of 6.0–8.0 and a sarcosolic magnesium ion concentration ($[Mg^{2+}]_c$) of about 1.0 mM (pMg = 3.0), the following ATP species can be estimated:

$$[ATP] = \left[ATP^{4-} + HATP^{3-} + H_2ATP^{2-} + MgATP^{2-} + MgHATP^{-} + Mg_2ATP\right].$$

The chemical notation is based on only very specific species involved in the reaction, for example,

$$MgATP^{2-} + H_2O \rightarrow MgADP^{-} + H_2PO_4{}^{-} \tag{R7.3}$$

with

$$K_{MgATP} = \frac{[MgADP^{-}]_{eq}[H_2PO_4{}^{-}]_{eq}}{[MgATP^{2-}]_{eq}}.$$

The $\Delta_R G$ values resulting from the different notations are identical, but the corresponding $\Delta_R G^{\circ}$ values are different. A more detailed discussion of these relationships is provided in Chapter 10.1.

The H_2O concentration does not appear in the equilibrium constant and Γ, as it practically does not change during the course of the reaction and therefore can be included in the constant. This also applies to all other reactions that contain H_2O as a reactant.

Therefore, for the coupled reaction

$$A_{\text{ser}} = R\,T\,\ln\left(\frac{[\text{MgATP}^{2-}]}{[\text{MgADP}^{-}][\text{H}_2\text{PO}_4{}^{-}]}\,K_{\text{MgATP}}\right) + 2\left(R\,T\,\ln\left(\frac{[\text{Ca}^{2+}]_c}{[\text{Ca}^{2+}]_r}\right) + z_{\text{ca}}\,F(-\Delta\phi_r)\right)$$

is applied.

The following values for the sarcosol of a skeletal muscle cell (SMF) under resting conditions result: $[\text{Ca}^{2+}]_c$ = 0.29 μM and $[\text{Ca}^{2+}]_r$ = 0.317 mM, as well as $\Delta\phi_r$ = 0 mV. Therefore,

$$A_{\text{ca}}^{\text{ser}} = 2R\,T\,\ln\left(\frac{0.29\times10^{-6}}{0.317\times10^{-3}}\right) = -36.086\ \text{kJ/mol}.$$

In the presence of a low membrane potential of $\Delta\phi_r = \phi_r - \phi_c = 6.0$ mV and the same Ca^{2+} concentrations, an already significantly more negative value is obtained:

$$A_{\text{ca}}^{\text{ser}} = 2\left(R\,T\,\ln\left(\frac{0.29\times10^{-6}}{0.317\times10^{-3}}\right) - 2F\times6.0\times10^{-3}\right) = -38.402\ \text{kJ/mol}.$$

However, it can be assumed that in addition to Ca^{2+} ion channels, there are also K^+, H^+ and Cl^- channels of high conductance in the reticulum membrane, which always impede the formation of an electrical potential difference by Ca^{2+} transport immediately by charge neutralization.

For $A_{\text{ATP}}^{\text{c}}$ one obtains (with [ATP] = 9.0 mM, [ADP] = 0.1 mM and $[\text{P}_i]$ = 4.0 mM as well as $K'_{\text{ATP}} = 4.9687\times10^5$)

$$A_{\text{ATP}}^{\text{c}} = R\,T\,\ln\left(\frac{9\times10^{-3}}{0.1\times10^{-3}\times4.0\times10^{-3}}\ 4.9687\times10^5\right) = 59.665\ \text{kJ/mol}.$$

This then results in the affinity of the coupled reaction under resting conditions

$$A_{\text{res}} = A_{\text{ser}} = A_{\text{ca}}^{\text{ser}} + A_{\text{ATP}}^{\text{c}} = 23.579\ \text{kJ/mol}.$$

After a Ca^{2+} release, $[\text{Ca}^{2+}]_c = 20.0$ μM and $[\text{Ca}^{2+}]_r = 30.0$ μM. Under these conditions at the beginning

$$A_{\text{ser}} = 2R\,T\,\ln\left(\frac{20.0\times10^{-6}}{30.0\times10^{-6}}\right) + A_{\text{ATP}}^{\text{c}} = 57.574\ \text{kJ/mol},$$

but then decreases again in the course of the reaction to 23.579 kJ/mol.

In addition to the Ca^{2+} pumps, Ca^{2+} channels also exist in the reticulum membrane, through which the Ca^{2+} of the lumen can flow. This is triggered by an electrical stimulus, which is conducted as a membrane depolarization of the sarcolemma via transverse tubules up to the reticulum membranes. There the depolarization causes a drastic conductance increase of these channels, so that Ca^{2+} can flow massively from the reticulum into the sarcosol. The affinity of the Ca^{2+} efflux (CaR) is given by

$$A_{\text{cach}} = -\Delta\tilde{\mu}_{\text{cach}} = R\,T\,\ln\left(\frac{[Ca^{2+}]_r}{[Ca^{2+}]_c}\right) + z_{\text{ca}}F\Delta\phi_{\text{r}}.$$

It is essentially the interaction of these two structures of the reticulum membrane, that is, Ca^{2+} pumps and Ca^{2+} channels, which control the setting of $[Ca^{2+}]_c$ in the sarcosol. Figure 7.1 illustrates the time courses of CaR (A) and the back pumping process (CaP, B). The calculation was performed by a simulation of these reactions. The simulation is given in Appendix (A1).

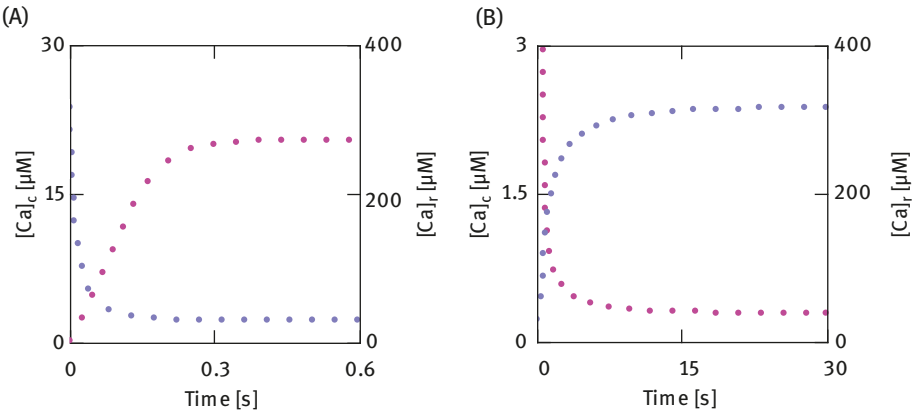

Figure 7.1: Time courses of Ca^{2+} release and uptake at the SR membrane. (A) Ca^{2+} release after increasing G_{cach} by a factor of $10^{3.8}$. Red points: changes of $[Ca^{2+}]_c$; blue points: changes of $[Ca^{2+}]_r$. B: Ca^{2+} uptake after decreasing G_{cach} by a factor of $10^{-3.8}$. Red points: changes of $[Ca^{2+}]_c$; blue points: changes of $[Ca^{2+}]_r$.

From Figure 7.1A it can be seen that after increasing the conductance (G_{cach}) of Ca^{2+} channels (CaCH) by a factor of $10^{3.8}$, Ca^{2+} ions of the reticulum are released into the sarcosol at high rate. Both there and in the reticulum, $[Ca^{2+}]_c$ and $[Ca^{2+}]_r$, respectively, are strongly buffered. In the reticular lumen, this is accomplished by calsequestrin, which is present there in high concentration. In the sarcosol, Ca^{2+} is mainly bound by troponin, a protein of the contractile filaments. $[Ca^{2+}]_c$ can increase in fractions of a second in the sarcosol from 0.29 to about 20.0 µM, while $[Ca^{2+}]_r$ drops in this period in the reticulum from 317.0 to about 30.0 µM (Figure 7.1A).

After decreasing G_{cach} by a factor of $10^{-3.8}$, the pumping action predominates, so that Ca^{2+} ions are now pumped back into the reticulum. This action is shown in Figure 7.1B. In approximately 30.0 s, the values of both initial concentrations are reached again, which means $[Ca^{2+}]_c = 0.29\ \mu M$ and $[Ca^{2+}]_r = 317\ \mu M$.

Figure 7.2 shows the time courses of ion currents and the membrane potential ($\Delta\phi_r$) at the reticulum membrane. Because Ca^{2+} ions are pumped across the membrane by CaP, this process has an electrogenic effect, that is, through it an electrical potential difference ($\Delta\phi_r$, lumen positive) can be built up at the reticulum membrane. An electrical potential difference with opposite sign ($-\Delta\phi_r$) is induced by CaR via CaCHs, which counteracts the electrogenic pumping reaction. In addition, the generation of a membrane potential is always immediately prevented by a

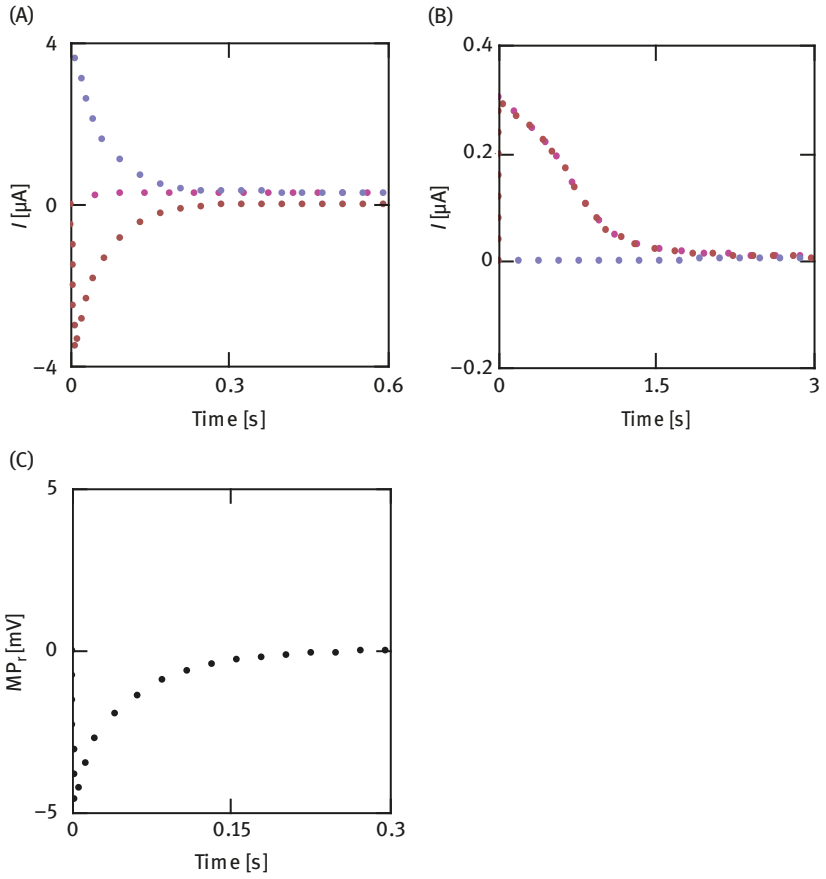

Figure 7.2: Currents and MP_r at the SR membrane. (A) During Ca^{2+} release, red points: I_{ser}; blue points: I_{cach}: brown points: I_K. B: during Ca^{2+} uptake, red points: I_{ser}; blue points: I_{cach}; brown points: I_K. C: during Ca^{2+} release, black points: MP_r.

compensating K^+ current via K^+ channels of high conductance. This is necessary because an electrical potential difference would inhibit the respective Ca^{2+} flux and thus slow down the process.

Figure 7.2C shows that during a massive Ca^{2+} efflux, a transient membrane potential of a few mV is generated. The induction of a far more negative membrane potential is evidently prevented by a strong K^+ influx. During increased backpumping after a drastic reduction of G_{cach} (B), this time a K^+ efflux prevents the sustained polarization of the reticulum membrane.

To calculate the currents, the respective driving force ($-\Delta\tilde{\mu}$ in J/mol) must be converted into V. It is absolutely necessary that both terms of $\Delta\tilde{\mu}$ have the same denominator, as only then can they be added or subtracted. For the representation as current in the form $I = G(-\Delta_{\mathrm{R}}\tilde{\mu}_{\mathrm{el}})$, this can be achieved, for example, with

$$A_{\mathrm{ca}}^{\mathrm{ser}} = 2\left(R\,T\,\ln\left(\frac{[\mathrm{Ca}^{2+}]_{\mathrm{c}}}{[\mathrm{Ca}^{2+}]_{\mathrm{r}}}\right) + z_{\mathrm{ca}}\,F(-\Delta\phi_{\mathrm{r}})\right)$$

by factoring out the term $z_{\mathrm{ca}}F$.

This leads to

$$A_{\mathrm{ca}}^{\mathrm{ser}} = z_{\mathrm{ca}}\,F \times 2\left(\frac{R\,T}{z_{\mathrm{ca}}\,F}\ln\left(\frac{[\mathrm{Ca}^{2+}]_{\mathrm{c}}}{[\mathrm{Ca}^{2+}]_{\mathrm{r}}}\right) + (-\Delta\phi_{\mathrm{r}})\right).$$

The term

$$\frac{R\,T}{z_{\mathrm{ca}}\,F}\ln\left(\frac{[\mathrm{Ca}^{2+}]_{c}}{[\mathrm{Ca}^{2+}]_{r}}\right)$$

is shown in J/C (=V). This becomes clear when the expression resulting from the chemical potential differences

$$(\text{here } R\,T\,\ln\left(\frac{[\mathrm{Ca}^{2+}]_{c}}{[\mathrm{Ca}^{2+}]_{r}}\right) \text{ in J/mol})$$

is to be expressed as the electric potential difference. For this purpose, for example,

$$R\,T\,\ln\left(\frac{[\mathrm{Ca}^{2+}]_{c}}{[\mathrm{Ca}^{2+}]_{r}}\right) = z_{\mathrm{ca}}\,F\Delta\phi$$

must be set (also in J/mol), resulting in the corresponding electrical potential difference

$$\Delta\phi = \frac{R\,T}{z_{\mathrm{ca}}\,F}\ln\left(\frac{[\mathrm{Ca}^{2+}]_{\mathrm{c}}}{[\mathrm{Ca}^{2+}]_{\mathrm{r}}}\right) \text{ in J/C or V.}$$

In a similar way, the term

$$R\,T\,\ln\left(\frac{[\mathrm{MgATP}^{2-}]}{[\mathrm{MgADP}^{-}][\mathrm{H_2PO_4}^{-}]}\,K_{MgATP}\right)$$

can be treated, so that for the affinity of the coupled reaction in electrical units, the expression

$$A^{\mathrm{el}}_{\mathrm{ser}} = \frac{A_{\mathrm{ser}}}{z_{\mathrm{ca}}\,F} = \frac{R\,T}{z_{\mathrm{ca}}\,F}\ln\left(\frac{[\mathrm{MgATP}^{2-}]}{[\mathrm{MgADP}^{-}][\mathrm{H_2PO_4}^{-}]}\,K_{MgATP}\right) + 2\left(\frac{R\,T}{z_{\mathrm{ca}}\,F}\ln\left(\frac{[\mathrm{Ca}^{2+}]_{\mathrm{c}}}{[\mathrm{Ca}^{2+}]_{\mathrm{r}}}\right) + (-\Delta\phi_{\mathrm{r}})\right)$$

(in V) results.

A similar result can be achieved if instead of $z_{\mathrm{ca}}\,F$ only F is excluded. This results in

$$\frac{A_{\mathrm{ser}}}{F} = z_{\mathrm{ca}}A^{\mathrm{el}}_{\mathrm{ser}} = \frac{R\,T}{F}\ln\left(\frac{[\mathrm{MgATP}^{2-}]}{[\mathrm{MgADP}^{-}][\mathrm{H_2PO_4}^{-}]}K_{MgATP}\right) + 2\left(\frac{R\,T}{F}\ln\left(\frac{[\mathrm{Ca}^{2+}]_{\mathrm{c}}}{[\mathrm{Ca}^{2+}]_{\mathrm{r}}}\right) + z_{\mathrm{ca}}(-\Delta\phi_{\mathrm{r}})\right).$$

Both results fulfil the identity $I_{\mathrm{ser}}A^{\mathrm{el}}_{\mathrm{ser}} = \left(I_{\mathrm{ser}}/z_{\mathrm{ca}}\right)\times\left(z_{\mathrm{ca}}A^{\mathrm{el}}_{\mathrm{ser}}\right) \equiv J_{\mathrm{ser}}A_{\mathrm{ser}}$

From $A^{\mathrm{el}}_{\mathrm{ser}} = A_{\mathrm{ser}}/z_{\mathrm{ca}}\,F$ and with $\alpha = 1/(z_{\mathrm{ca}}\,F)$, the flux can be determined from the membrane current as $J_{\mathrm{ser}} = \alpha I_{\mathrm{ser}}$. For this purpose, $I_{\mathrm{ser}}A^{\mathrm{el}}_{\mathrm{ser}} = J_{\mathrm{ser}}A_{\mathrm{ser}}$ has been used. On the other hand, $\alpha I_{\mathrm{ser}} = \alpha\,G_{\mathrm{ser}}\,A^{\mathrm{el}}_{\mathrm{ser}} = L_{\mathrm{ser}}\,z_{\mathrm{ca}}F\,A^{\mathrm{el}}_{\mathrm{ser}}$ must apply, from which $L_{\mathrm{ser}} = 1/(z_{\mathrm{ca}}F)^2\,G_{\mathrm{ser}}$ follows.

Since cells often differ greatly in shape and size, a normalized quantity is often referred to such as to 1 L of sarcosol, which can be included in α. The membrane current is given in simulations in fA (=10^{-18} C/ms) and the flux should be in mM/s. With $V_{\mathrm{c}} = 1.615\times10^{-9}$ L, this yields

$$\alpha = \frac{1}{z_{\mathrm{ca}}F\,V_{\mathrm{c}}} = 3.209\times10^{3}\ \mathrm{mol/(L\,C)}.$$

For the flux $J_{\mathrm{ser}} = \alpha I\times10^{-18}\ \mathrm{mol}/(L\ ms)$ is obtained (I is the dimensionless amount of the current I_{ser}). In order to achieve the result μM/ms = mM/s, the factor 10^{-12} must be used instead of 10^{-18} for multiplication.

For $V_{\mathrm{c}} = 1.615\times10^{-9}$ and $V_{\mathrm{r}} = 0.19\times10^{-9}$ L, the result is $\alpha_c = 10^{-12}/z_{ca}F\,V_{\mathrm{c}} = 3.209\times10^{-9}$ and $\alpha_{\mathrm{r}} = 10^{-12}/z_{\mathrm{ca}}F\,V_{\mathrm{r}} = 0.273\times10^{-9}\ (\mu M/C)$.

A Ca^{2+} current via Ca^{2+} channels of $I_{\mathrm{cach}} = 0.24758\times10^{9}$ fA (=0.24758 μA, see Figure 7.2B) corresponds to a Ca^{2+} flux from the reticulum into the sarcosol of $J_{\mathrm{cach}} = \alpha_c I_{\mathrm{cach}} = 0.7945$ mM/s

The condition

$$\Psi_{\mathrm{cach}} = J_{\mathrm{cach}}A_{\mathrm{cach}} \equiv \frac{I_{\mathrm{cach}}}{V_c}A^{\mathrm{el}}_{\mathrm{cach}} = \Psi^{\mathrm{el}}_{\mathrm{cach}}$$

is fulfilled at all times of CaR.

With the values resulting from the simulation the following one obtains $0.7945(\mathrm{mM/s}) \times 796.26(\mathrm{J/mol}) \equiv 1.533 \times 10^2(\mathrm{C/(Ls)}) \times 4.1263(\mathrm{mJ/C}) = 632.6\mathrm{mJ/(Ls)}$.

Figure 7.3 shows the $\Delta_R G$ (A) and ΔG values (B) of the SERCA pump (ATP splitting plus Ca^{2+} transport) and of CaR as functions of ξ (extent of reaction). The corresponding affinity values have opposite signs. With increasing ξ the $\Delta_R G$ values of the pumping reaction become increasingly more positive. The reason for this is the continuous increase of the positive $\Delta\tilde{\mu}_{ca}^{ser}$ (A, blue curve) with almost constant and negative $\Delta_R G_{ATP}^{c}$ (A, red curve). This means that ΔG_{ser} in the course of the pumping process becomes more and more positive (B, green curve), while ΔG_{ATP}^{c} almost linearly becomes more negative (B, red curve).

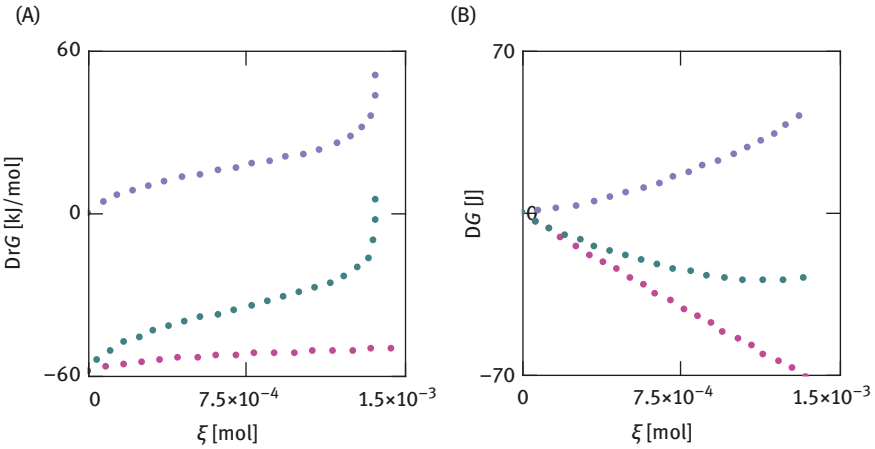

Figure 7.3: $\Delta_R G$ and ΔG values of Ca^{2+} pumping. (A) $\Delta_R G$s as a function of ξ, red points: $\Delta_R G_{ATP}^{c}$; blue points: $\Delta_R G_{ser}^{ca}$; green points: $\Delta_R G_{ser}$. (B) Respective ΔGs as a function of ξ.

The curves shown in Figures 7.3A and B only approximate the results of the simulation, because for the calculations a constant Ca^{2+} buffering was assumed, whereas in the simulation these are considered as a function of $[Ca^{2+}]_c$ or $[Ca^{2+}]_r$. This influences J_{ser} and A_{ser} of the pumping reaction through the coupled portion A_{ca}^{ser}, which depends on both concentrations.

Figure 7.4 shows that a steady state is achieved as well under conditions of a massive CaR as under high Ca^{2+} conditions. This situation is characterized by the fact that both Ca^{2+} fluxes J_{ca}^{ser} and J_{cach} assume equal magnitudes. However, the flux through the SERCA ATPase, that is, the rate of ATP splitting of the Ca^{2+} pump (J_{ser}), is always only half as large, that is, $J_{ser} = 1/2\, J_{ca}^{ser}$.

For a simple circuit consisting of a battery with external branch, it has been shown that the partial conductance of the coupled redox reaction of the battery is opposite equal to the conductance of the external branch, meaning $G_{ex} = -G_{c1}$.

The interaction of CaP and CaR at the reticulum membrane occurs in an analogous manner. The charge transport coupled to the redox reaction of the battery

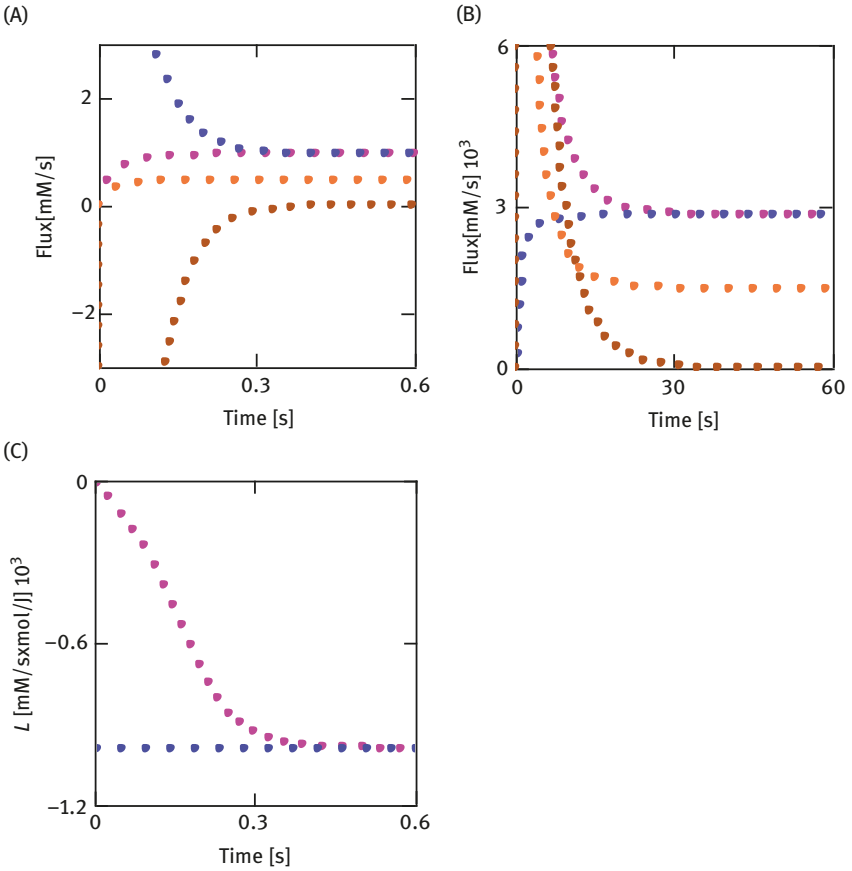

Figure 7.4: Fluxes and conductances at the SR membrane. (A) Fluxes during Ca^{2+} release, red points: J^{ca}_{ser}; blue points: J_{cach}; light brown: J^{atp}_{ser}; brown: J_K. (B) Same fluxes during Ca^{2+} uptake. (C) Conductances during Ca^{2+} release, red points: partial conductance L^{ser}_{c1}; blue points: $-L_{cach}$.

corresponds to the Ca^{2+} transport from the sarcosol into the lumen of the reticulum coupled to ATP hydrolysis. The outer branch of the current corresponds to the Ca^{2+} efflux through Ca^{2+} channels.

Here, with $\Psi_{ser} = J_{ser} A_{ser}$, L^{ser}_c can always be obtained from

$$L^{ser}_c = \frac{\Psi_{ser}}{\left(A^{ser}_{ca} + A^{c}_{ATP}\right)^2} \quad \text{(here } L^{ser}_c \text{ is however given)}.$$

For the partial conductance one obtains

$$L^{ser}_{c1} = 4L^{ser}_c \frac{\left(A^{ser}_{ca} + A^{c}_{ATP}\right)}{A^{ser}_{ca}}.$$

The following relation is fulfilled:

$$L_{ex} = L_{cach} = -L_{c1}^{ser}.$$

L_{c1}^{ser} (<0) is opposite equal to the conductance L_{cach} (>0). $4L_c^{ser}$must be taken, because it results from the twofold flux (J_{cach} instead of J_{ser}) and the half affinity ($-A_{cach}$ instead of A_{ca}^{ser}), that is

$$2J_{ser}/\left(1/2\,A_{ca}^{ser}\right) = 4J_{ser}/A_{ca}^{ser} = 4L_c^{ser}.$$

As the results of simulations show, these conditions are fulfilled for the Ca^{2+} cycle at the reticulum membrane. As a result, the total resistance of the cycle must disappear at steady state.

Figure 7.4 shows how and after which time period a steady state for CaR ($L_{cach} = 9.98 \times 10^{-4}$ mM/s × mol/J, under the conditions shown in A) or CaP ($L_{cach} = 1.582 \times 10^{-7}$ mM/s × mol/J, under the conditions shown in B) is reached. Under the conditions of a massive Ca^{2+} efflux, J_{ca}^{ser} (red) and J_{cach} (blue) take on the same values after approximately 0.5 s, which do not change any more. As Ca^{2+} is transported out of the sarcosol by J_{ca}^{ser} and flows back by J_{cach}, these two fluxes describe a cycle, which, when equal in magnitude, cause steady-state cycling (SSC) of Ca^{2+}. As a result of this equality, the cycle must be electroneutral, so that also J_K (brown) must disappear (Figure 7.4A). Figure 7.4B shows the same operations under CaP conditions. As shown in Figure 7.4B, this time, the flux magnitudes are reduced by a factor of 0.003, and the time to reach SSC is approximately 50 s. Also J_K must vanish; however, under these conditions arising from a K^+ influx into the sarcosol, whereas during CaR an opposite K^+ flux approaches zero.

In Figure 7.4C, the time courses of the conductances L_{c1}^{ser} and L_{cach} during CaR are shown (the same applies to CaP, not shown). The comparison with the corresponding flux (Figure 7.4A) shows that the relationship $L_{c1}^{ser} = -L_{cach}$ is valid only after reaching a steady state. For the total resistance of the SSC, this means that it only disappears at steady state. This behavior is also shown by the dissipation functions, as shown in Figure 7.5A and B. This is remarkable in that, in such a cycle, chemical reactions occur at finite reaction rates and affinities without producing entropy $\Delta_{Ri}S$.

The dissipation functions of the cycle are also opposite at SSC (Figure 7.5A–C). The outcome of this determines the behavior of the functionally related parameters such as fluxes, affinities and conductances or resistances.

Figure 7.5C shows that

$$\Psi_{tot} = \Psi_{ser} + \Psi_{cach} = J_{ser}\left(A_{ca}^{ser} + A_{ATP}^{c}\right) + J_{cach}\,A_{cach},$$

when a steady state is reached it coincides with $\Psi_{ATP} = J_{ser}A_{ATP}^{c}$.

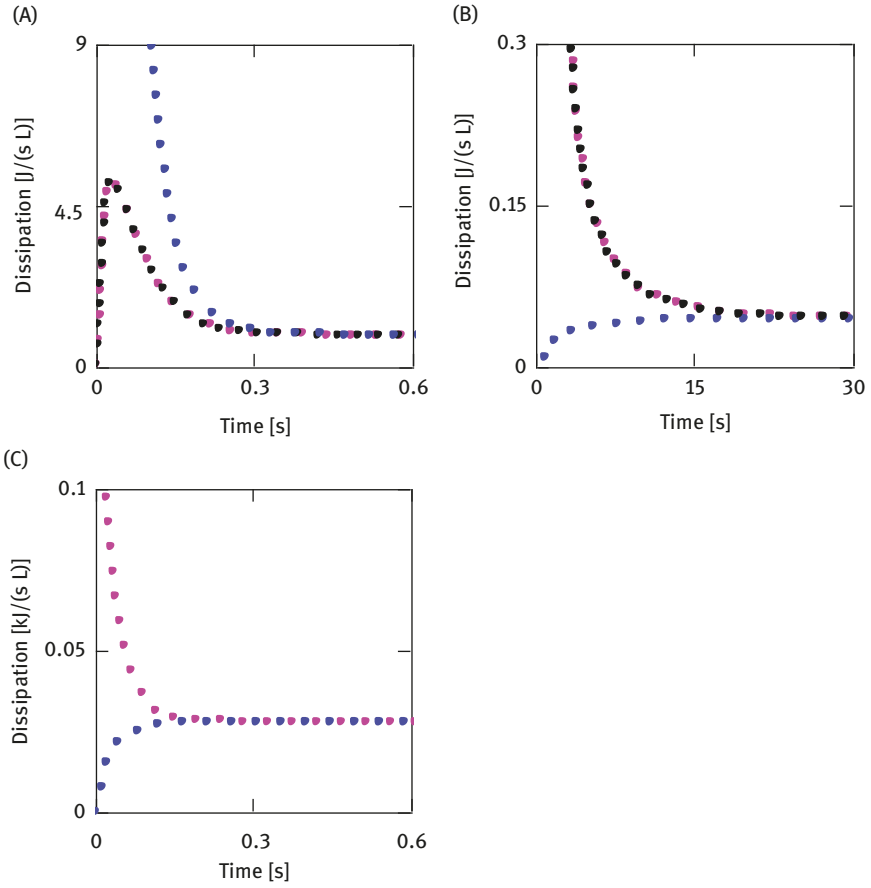

Figure 7.5: Dissipation functions during Ca^{2+} release and Ca^{2+} uptake at the SR membrane. (A) During Ca^{2+} release, red points: $-\Psi^{ca}_{ser}$; blue points: Ψ_{cach}; black points: $-\Psi^{ca}_{ser}$ in electrical units. (B) Same Ψs during Ca^{2+} uptake. (C) During Ca^{2+} release, red points: total dissipation function of Ca^{2+} cycling Ψ_{tot}; blue points: Ψ_{ATP}.

This demonstrates very impressively that at SSC the total dissipation disappears because it is composed of $J_{ser}A^{ser}_{ca}$ (<0) plus $J_{cach}A_{cach}$ (>0), which must vanish when both dissipation functions become opposite equal.

As will be discussed further in Chapter 9, cellular ATP consumption and ATP resynthesis through metabolism also demonstrate this behavior. As will be shown, on reaching an SSC of the ATP cycle, this one and all the cycles coupled to it – as here the Ca^{2+} cycle at the reticulum membrane – proceed without any dissipation. This finding is particularly important with regard to the entire energy metabolism and associated heat production.

7.2 Na/K ATPase and membrane potential

Like the SERCA pump, the Na/K ATPase or Na/K pump of cell membranes is driven by ATP hydrolysis and a high affinity (A^{c}_{ATP} = 59.665 kJ/mol). The reaction equation is

$$3Na_c^+ + 2K_e^+ + MgATP^{2-} + H_2O \rightarrow 3Na_e^+ + 2K_c^+ + MgADP^- + H_2PO_4^- . \qquad (R7.4)$$

In this active transport reaction, the ATP splitting is coupled to the outward transport of three Na^+ and the inward transport of two K^+ ions. The Na/K pump is therefore also electrogenic and as a result can charge the cell membrane electrically. In Figure 7.6A, such a charging process is shown at the sarcolemma of an SMF in the

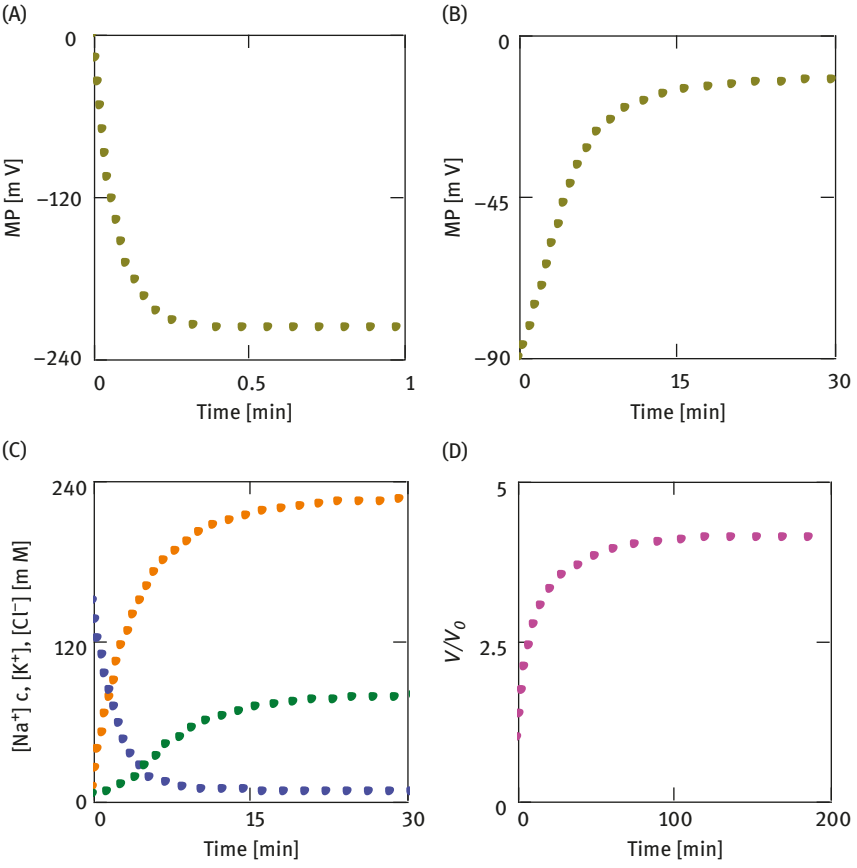

Figure 7.6: Membrane charging by the Na/K pump and Donnan effects. (A) MP generation by the Na/K pump in the absence of conductances. (B) Depolarization of MP in the absence of pump activity. (C) Concentration changes of permeable ions toward a Donnan equilibrium: yellow points, $[Na^+]_c$; blue points, $[K^+]_c$; green points, $[Cl^-]_c$. (D) Cell swelling by Donnan effects.

absence of any ionic conductance. After 30 s −217.44 mV is reached, which almost corresponds to the A_{NaK} value (217.44 mV $\triangleq$ 20.98 kJ/mol, see below) and arises from conditions at t = 0 ($[Na^+]_e = 143.0$ mM, $[Na^+]_c = 10.0$ mM, $[K^+]_e = 4.5$ mM and $[K^+]_c = 150.0$ mM). The required amount of charge is 1.064 nC (time integral of current). This corresponds to a concentration of $1.064/(F\,V_c) = 8.185\ \mu$M in the sarcosol ($V_{cell} = 2.72$ nL for 1.0 mm fiber length, $V_c = 1.35$ nL sarcosol), that is, $3 \times 8.158 = 24.56\ \mu$M of $[Na^+]_c$ is consumed. The pumping reaction is at equilibrium when the membrane potential generated in this way has reached −217.44 mV.

If the charging process would be done at the same respective concentrations, that is, if $[Na^+]_e = [Na^+]_c$ and $[K^+]_e = [K^+]_c$, then a membrane potential of

$$MP = -A^{el}_{ATP} = -618.4\ \text{mV}(\triangleq 59.665\text{kJ/molbyATPsplitting})$$

would result.

For the above calculations, the electrical capacitance of the sarcolemma must be known. It can be estimated from the surface to volume ratio, which has been found with stereological methods [8, 9] for $S_{sm}/V_{cell} = 0.116\ \mu^{-1}$ (smooth sarcolemma) and $S_{tt}/V_{cell} = 0.064\ \mu^{-1}$ (transverse tubuli), together 0.18 μ^{-1}. From this value a membrane capacitance of $C_M = 4.891 \times 10^6$ fF has been obtained by using 1.0 μF/cm^2 for the specific capacitance of cellular membranes.

In addition to this polarization by an active pumping reaction, the generation of an MP can occur also passively via ion channels. Therefore, the concentration distribution of the involved ions over the membrane is of great importance. The calculation is based on $\Delta\tilde{\mu}$ of the considered ion. For example, for the reaction via K^+ channels

$$K_c{}^+ \rightarrow K_e{}^+$$

and for the affinity ($= -\Delta\tilde{\mu}_K$) one obtains

$$-\Delta\tilde{\mu}_K = R\,T\,\ln\left(\frac{[K^+]_c}{[K^+]_e}\right) + z_K F \Delta\phi \quad (\text{inJ/mol}).$$

The reaction can reach equilibrium if $\Delta\tilde{\mu} = 0$, which leads to

$$\Delta\phi_K = -\frac{R\,T}{z_K F}\ln\left(\frac{[K^+]_c}{[K^+]_e}\right) = \frac{R\,T}{z_K F}\ln\left(\frac{[K^+]_e}{[K^+]_c}\right)\ (\text{in V}) \tag{7.2}$$

This is the Nernst equation, $\Delta\phi_K$ is also called the equilibrium potential E_k. In physiology, this is often given in mV, so eq. (7.2) reads

$$E_K = \frac{R\,T}{z_K F}\,10^3\,\ln\left(\frac{[K^+]_e}{[K^+]_c}\right)\ (\text{in mV}) \tag{7.3}$$

Since $\Delta\phi$ according to agreement is always given as a difference of electrical potentials $\phi_c - \phi_e$, the chemical potential difference

$$\Delta\mu = \mu_c - \mu_e = R\,T\,\ln\left(\frac{[\text{ion}]_c}{[\text{ion}]_e}\right)$$

must also be formulated accordingly.

For the K^+ distribution given above, $z_K = +1.0$ yields a K^+ equilibrium potential of

$$\Delta\phi_K = -\frac{RT}{z_K F}\ln\left(\frac{150}{4.5}\right) = -0.093719\text{V or } -9.043\text{kJ/mol.}$$

This result means that the reaction is at equilibrium when an MP of –93.719 mV has resulted from a K^+ efflux. Then no net efflux does occur. This also means that at a negative MP due to the agreed counting direction ("c"–"e"), the membrane outside is positively charged, while the inside carries negative charge.

For the Na^+ distribution the result is

$$\Delta\phi_{Na} = \frac{R\,T}{F}\ln\left(\frac{143}{10}\right) = 0.0711\text{V},$$

and for the Cl^- distribution

$$\Delta\phi_{Cl} = \frac{R\,T}{F}\ln\left(\frac{6}{126}\right) = -0.08137\text{V}.$$

The MP of an SMF at rest is around –90.0 mV. The respective $\Delta\tilde{\mu}$s are given through

$$\Delta\tilde{\mu}_K^{el} = 93.719 + (-90.0) = 3.719\,\text{mV},$$

$$\Delta\tilde{\mu}_{Na}^{el} = 71.1 - (-90.0) = 161.1\,\text{mV and}$$

$$\Delta\tilde{\mu}_{Cl}^{el} = -81.37 - (-90.0) = 8.63\,\text{mV}.$$

From this it can be seen that at an MP of –90.0 mV, K^+ ions flow out, Na^+ ions flow in and Cl ions have to flow out. Obviously, especially the Na^+ distribution is far from equilibrium, while those for K^+ and Cl^- are close to equilibrium. However, the strength of the ion currents is determined not only by the respective affinities, but also quite substantially by the associated conductance.

So far, only one type of ion and ion channel has ever been considered. However, cell membranes always have a whole range of different ion channels, all of which together influence the setting of a common MP. At equilibrium, the so-called Donnan equilibrium, every ion distribution is in equilibrium with that MP. This leads to

$$\frac{R\,T}{F}\ln\left(\frac{[K^+]_e}{[K^+]_c}\right) = \frac{R\,T}{F}\ln\left(\frac{[Cl^+]_c}{[Cl^+]_e}\right) = \frac{R\,T}{F}\ln\left(\frac{[Na^+]_e}{[Na^+]_c}\right)$$

and to

$$[K^+]_c \times [Cl^-]_c = [K^+]_e \times [Cl^-]_e$$

as well as

$$[Na^+]_c \times [Cl^-]_c = [Na^+]_e \times [Cl^-]_e.$$

Figure 7.6B and C shows the time courses of MP and of three intracellular ion concentrations. At equilibrium, which is reached very slowly via the concentration changes in the sarcosol, the above conditions are fulfilled for all types of ions. $[K^+]_c$ decreases from 150.0 to 7.13 mM, $[Na^+]_c$ increases from 10.0 to 226.44 mM and $[Cl^-]_c$ from 6.0 to 79.57 mM. The MP depolarizes from −90.0 to −12.29 mV. The values of the constantly held extracellular products $[K^+]_e \times [Cl^-]_e$ and $[Na^+]_e \times [Cl^-]_e$ are 0.567×10^3 and 18.018×10^3 (in $(mM)^2$), respectively.

It is noticeable that at equilibrium, the total concentration of the osmotically active particles (in this case K^+, Na^+ and Cl^-) has increased significantly under these conditions. As cell membranes have a high permeability to H_2O, it must be assumed that to maintain a constant osmolarity, additional inflow of water occurs, which is accompanied by an increase in volume. This considerably slows down the concentration increases of Na^+ und Cl^- and results in a more depolarized MP of only −1.54 mV at equilibrium. Figure 7.6D shows the volume increase (V/V_0) as a function of time. The osmolarity of the SMF is assumed as 310.0 mosM. Also with swelling ($V/V_0 = 4.134$), the equilibrium results in the same concentrations as in the absence of a volume increase.

The sarcolemma cannot endure such an increase in volume undamaged, despite a certain membrane reserve. However, even with considerably less swelling, damage occurs, because Ca^{2+} ions also flow into the sarcosol, which leads to lysis and cell death in many cell types.

Swelling could be prevented if the external concentrations were changed so that the respective products are equal to the corresponding products of the sarcosol. A possible outcome would be, for example, $30.0 \times 30.0 = 150.0 \times 6.0$ (for KCl) and $2.0 \times 30.0 = 10.0 \times 6.0$ (for NaCl). Such an external solution with 30.0 mM K^+, 2.0 mM Na^+ and 30.0 mM Cl^- is in electrochemical equilibrium with the internal concentrations. Under these conditions, no ion flows occur and swelling cannot occur as a result. Only MP is depolarized from −90.0 to −41.5 mV.

Donnan distribution and cell swelling must always occur when the Donnan products in the cyto/sarcosol are smaller than in the adjacent medium. In cells, this is mainly due to the relatively large amount of negative charges for which the cell membrane is impermeable. These are free moving and fixed proteins carrying negative net charge, membrane phospholipids and larger anions such as ATP (most ATP ion species), phosphocreatine (PCr) and nonpermeable metabolite anions. This, to a certain extent, fixed charge is not involved in the setting of a Donnan equilibrium,

but is responsible for the asymmetric distribution of the permeating ions and, consequently, for a low Donnan product of the cyto/sarcosol.

With the SERCA pump, the polarization of the membrane is prevented by the high conductance of K^+ channels. However, this was only possible because the K^+ concentrations in the sarcosol and in the reticulum lumen are approximately the same. This is not possible at the sarcolemma due to the different concentrations of the permeating cations and anions, as shown; nevertheless, a drastic depolarization also sets in here, but only after a longer reaction time.

Though the maintenance of a negative MP is imperative to trigger a contraction in an SMF, for example, as already mentioned, this occurs via a depolarization of the sarcolemma, which leads to the release of Ca^{2+} from the reticulum and finally to contraction. To maintain this ability of the membrane to be stimulated by depolarization, it must be charged to an appropriate MP of approximately −90 mV (SMF). Such a situation can persist only if Donnan effects are prevented or at least largely prevented. This occurs, on the one hand, by a reduction of all relevant conductances, so that the setting of a Donnan equilibrium with depolarization and swelling is strongly delayed. To a far greater extent, however, the Na/K pump can counteract these inevitable Donnan effects. Thus, by such a pumping activity, a loss of K^+, an accumulation of Na^+ and a depolarization can be compensated.

Figure 7.7 shows the time course of the MP (A) and $[Na^+]_c$, $[K^+]_c$ and $[Cl^-]_c$ (B) after continued depolarizations and corresponding mechanical power output of an SMF. The action potentials producing a tetanus are triggered by depolarizations that have to overcome a threshold of approximately −50 mV. This is followed by an abrupt and short-lived increase of the conductance of Na^+ channels (here by a factor of 45.7), while that for K^+ temporarily decreases (by a factor of 0.158). This initiates a strong

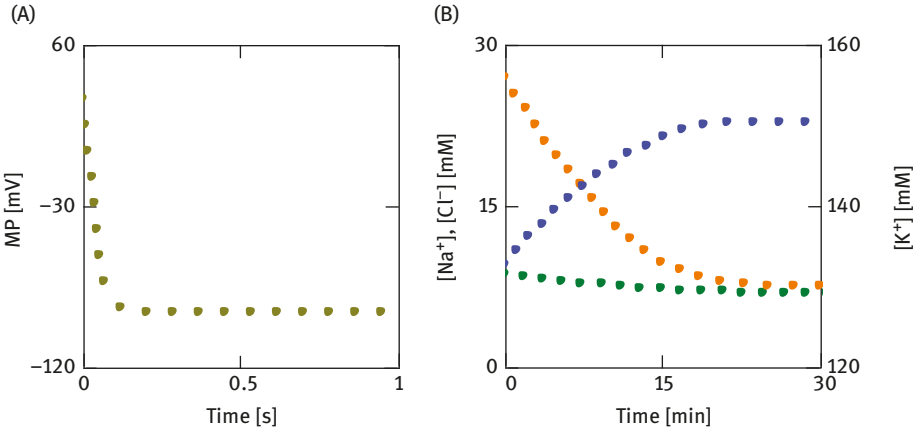

Figure 7.7: Recovery of MP and intracellular ion concentrations after sustained depolarizations. (A) MP; (B) yellow points, $[Na^+]_c$; blue points, $[K^+]_c$; green points, $[Cl^-]_c$.

depolarization (action potential) up to +30 mV. The increased Na^+ conductance then drops back to normal according to MP, while that for K^+ does not immediately return completely to resting values. Due to the many successive action potentials, it can be expected that the ion concentrations in the sarcosol also change. It is assumed that $[Na^+]_c$ increases from 7.0 to 27.0 mM, $[K^+]_c$ drops from 150.0 to 132.7 mM and $[Cl^-]_c$ increases from 6.0 to 8.7 mM. When stimulation is terminated, MP is repolarized within fractions of a second to almost the resting value (Figure 7.7A). This happens practically without involvement of the Na/K pump, so it is almost completely due to the reincreased K^+ conductance. However, the conductance must have reached its low resting value again. The following extending over a longer time period (here up to 30.0 min) process is due solely to the activity of the Na/K pump. During that activity, $[Na^+]_c$ and $[K^+]_c$ are pumped back to their original values.

The Cl^- conductance remains unchanged. An increased Cl^- influx during the action potentials is mainly due to the disappearance of the negative MP. After repolarization, this excess Cl^- leaves again passively the cell.

In the course of recovery (restoration of resting conditions), a steady state is reached after approximately 30.0 min (Figure 7.8). Then an SSC is reached, which is generated by the pumping reaction, on the one hand, and by the fluxes J_{Na} and J_K via Na^+ and K^+ channels, on the other hand.

The affinity of the pump reaction is

$$A_{NaK} = 3\left(RT\ln\left(\frac{[Na^+]_c}{[Na^+]_e}\right) + F\Delta\phi\right) + 2\left(RT\ln\left(\frac{[K^+]_e}{[K^+]_c}\right) - F\Delta\phi\right) + A^c_{ATP} = 9.8\ \text{kJ/mol},$$

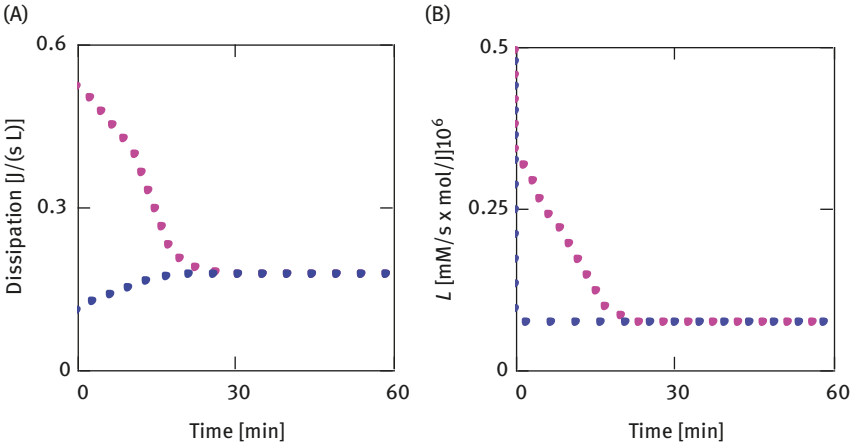

Figure 7.8: Matching of dissipation functions and conductances. (A) Dissipation functions. (red points, $-\Psi^{nk}_{ion}$; blue points, $\Psi_{Na} + \Psi_K$); (B) conductances (red points, $-L^{nk}_{c1}$; blue points, L^{ch}_{ex}).

$$A_1 = A_{\text{ion}}^{\text{nk}} = 3\left(R\,T\,\ln\left(\frac{[\text{Na}^+]_\text{c}}{[\text{Na}^+]_\text{e}}\right) + F\Delta\phi\right) + 2\left(R\,T\,\ln\left(\frac{[\text{K}^+]_\text{e}}{[\text{K}^+]_\text{c}}\right) - F\Delta\phi\right) = -49.86\ \text{kJ/mol}.$$

A_2 is given through $A_{\text{ATP}}^{\text{c}}$.

The efficiency under resting conditions at steady state is $\eta_{\text{NaK}} = -A_{\text{ion}}^{\text{nk}}/A_{\text{ATP}}^{\text{c}} = 0.836$. Under the conditions of a tetanus, it decreases to about 0.65, mainly due to the strong depolarization (MP = 30 mV) and in the presence of an additional increase in $[\text{Na}^+]_\text{c}$ and decrease of $[\text{K}^+]_c$ up to 0.4 down. The pumping speed increases because, on the one hand, $A_{\text{ion}}^{\text{nk}}$ becomes less negative (2.3 times at 30 mV), and on the other hand because of an increase of the $[\text{Na}^+]_\text{c}$ (4.46-fold at 27.0 mM, the change of a flux through activation factors is discussed in Section 15). When the resting state is reached again, the pump flux falls back to the resting value of 0.003 mM/s.

The flux through the pumping reaction is

$$J_{\text{NaK}} = L_\text{c}^{\text{nk}}\left(A_{\text{ion}}^{\text{nk}} + A_{\text{ATP}}^{\text{c}}\right).$$

The dissipation functions are

$$\Psi_1 = \Psi_{\text{ion}}^{\text{nk}} = J_{\text{NaK}}A_{\text{ion}}^{\text{nk}} \quad \text{and} \quad \Psi_2 = \Psi_{\text{ATP}}^{\text{nk}} = \text{J}_{\text{NaK}}\text{A}_{\text{ATP}}^{\text{c}}.$$

The partial conductances are then

$$L_{\text{c1}}^{\text{nk}} = L_\text{c}^{\text{nk}}\frac{A_{\text{ion}}^{\text{nk}} + A_{\text{ATP}}^{\text{c}}}{A_{\text{ion}}^{\text{nk}}}$$

and

$$L_{\text{c2}}^{\text{nk}} = L_\text{c}^{\text{nk}}\frac{A_{\text{ion}}^{\text{nk}} + A_{\text{ATP}}^{\text{c}}}{A_{\text{ATP}}^{\text{c}}}.$$

The requirement

$$L_\text{c}^{\text{nk}} = \frac{1}{\dfrac{1}{L_{\text{c1}}^{\text{nk}}} + \dfrac{1}{L_{\text{c2}}^{\text{nk}}}}$$

is fulfilled also for this coupled reaction.

The conductance $L_{\text{ex}}^{\text{nk}}$ associated with the Na/K cycle is obtained from the dissipation function for Na^+ and K^+ transport via both ion channels

$$\Psi_{\text{Na}} + \Psi_{\text{K}} = J_{\text{Na}}A_{\text{Na}} + J_{\text{K}}A_{\text{K}} = \left(J_{\text{Na}}\,\frac{A_{\text{Na}}}{-A_{\text{ion}}^{\text{nk}}} + J_{\text{K}}\,\frac{A_{\text{K}}}{-A_{\text{ion}}^{\text{nk}}}\right)\left(-A_{\text{ion}}^{\text{nk}}\right)$$

$$(\Psi_{\text{Na}} + \Psi_{\text{K}} > 0).$$

The expression in the first bracket is the flux that would result if J_{Na} plus J_K were caused together by the potential difference $-A_{ion}^{nk}$. The conductance for this flux is given by

$$L_{ex}^{ch} = \frac{\Psi_{Na} + \Psi_K}{\left(-A_{ion}^{nk}\right)^2}.$$

At steady state, both dissipation functions Ψ_{ion}^{nk} (red) and $\Psi_{Na} + \Psi_K$ (blue) are opposite equal (Figure 7.8A), and accordingly also the conductances L_{c1}^{nk} (<0) and L_{ex}^{ch} (>0) (Figure 7.8B). However, this means that when an SSC is reached, this cycle must also proceed virtually free of resistance and without dissipation.

An SSC can also be shown for other ion transport systems of the cell membrane such as the Ca^{2+} ATPase of the sarcolemma in conjunction with a Ca^{2+} leak flux or in myocardial cells in conjunction with Na/Ca exchange. It is therefore reasonable to suppose that in the presence of a steady state, that is, a constant MP over a longer period of time, an SSC is established for all ion transport systems at the membrane. Therefore, the entropy production of all involved ion transport processes at the membrane would go to zero. At constant MP, always the sum of all membrane currents must vanish, which is confirmed by the simulation. This does not mean, however, that this always has to be connected to one or more SSCs. On the other hand, SSCs include a state of zero current and therefore do not contradict the possibility that a constant MP has been brought about through the formation of one or more SSCs.

8 Oxidative phosphorylation

The oxidation of metabolic substrates such as glucose (Glu) and fatty acids such as palmitic acid (Palm) occurs in the mitochondria. In skeletal muscle, branched chain amino acids such as leucine, isoleucine and valine as α-keto acids can also be included in the oxidation to a small extent. A large part of the reaction steps in the metabolism of these different compounds is identical and ultimately leads to the reaction with O_2. As with all reactions of carbon containing compounds with oxygen, CO_2 and H_2O are produced, albeit with different stoichiometries. All common reaction steps are located in the CAC of the mitochondrial matrix. By decarboxylation, the product CO_2 is produced there and by dehydrogenation the hydrogen of the metabolites involved in the cycle is transferred to the oxidized redox compounds nicotinamide adenine dinucleotide (NAD_{ox}) and flavin adenine dinucleotide (FAD_{ox}), which are converted by H_2 uptake into the reduced forms NAD_{red} and FAD_{red}, respectively. In the glucose oxidation (4/12) as well as in the fatty acid oxidation (Palm, 7/23) NAD_{red} and FAD_{red} are produced also outside of CAC. All reduced redox compounds in the matrix reach the inside of the inner mitochondrial membrane, where the oxidation of these compounds takes place. This is where the process of oxidative phosphorylation (OP) begins. The reaction with oxygen for both NAD_{red} and FAD_{red} is coupled to the transport of protons from the matrix into the intermembrane space (IMS) of the mitochondria. For the NAD_{red} oxidation, the reaction equation is

$$NAD_{red} + \frac{1}{2}\,O_2 + 10\,H_m{}^+ \rightarrow NAD_{ox} + H_2O + 10\,H_c{}^+ \qquad \text{(R8.1)}$$

and for the FAD_{red} oxidation

$$FAD_{red} + \frac{1}{2}\,O_2 + 6\,H_m{}^+ \rightarrow FAD_{ox} + H_2O + 6\,H_c{}^+ \qquad \text{(R8.2)}$$

These are the overall reactions of a system consisting of several serial redox steps. All of the associated protein complexes are embedded in the bilayer structure of the inner mitochondrial membrane. The respiratory chain is the cooperation of four complexes, which accomplishes the gradual oxidation of the NAD_{red}. These are the NAD_{red} dehydrogenase (complex I), the succinate dehydrogenase (complex II), the cytochrome-bc_1 complex (complex III) and the cytochrome-c-oxidase (complex IV). FAD_{red} can react with the respiratory chain via complex II, ETF-ubiquinone-oxidoreductase or glycerol-3-phosphate dehydrogenase. In this process, the two electrons of the hydrogen bound to NAD_{red} or FAD_{red} are delivered to the respiratory chain, while the two associated protons are available for the reaction with oxygen. Both electrons remain in the membrane and pass through several increasingly positive redox potentials in series, and are transferred finally to oxygen in the last step. Without coupling to proton transport such a reaction system would correspond to a battery whose electrodes – for example

https://doi.org/10.1515/9783110650501-008

Complex I and IV for NAD_{red} oxidation – are short-circuited through the respiratory chain, so that the Gibbs energy of this redox reaction ($\Delta_R G_{NA}$) would be dissipated unused. By coupling to proton transport, part of this energy is transformed into the electrochemical potential difference of protons, which extends over the inner membrane. This coupled proton transfer from the matrix side to the outside of the inner mitochondrial membrane occurs at three sites in the respiratory chain. Complex I transports 4.0, complex III also transports 4.0 and complex IV 2.0 protons. In total, 10.0 H^+ are pumped over the inner membrane. Since FAD_{red} only feeds its electrons after complex I, this redox reaction is only coupled to the transport of 6.0 protons. The electrochemical potential difference across the membrane is given by

$$\Delta\tilde{\mu}_H = R\,T\,\ln\left(\frac{[H^+]_m}{[H^+]_c}\right) + F\Delta\phi_m \text{ (in J/mol)}. \tag{8.1}$$

With $\Delta\phi_m = \phi_m - \phi_c$, both $\Delta\phi_m < 0$ and $\Delta\mu_H = R\,T\,\ln([H^+]_m/[H^+]_c) < 0$.

The membrane potential of the inner membrane, $MP_m = \Delta\phi_m$, arises on the one hand by the H^+ withdrawal from the matrix, whereby anions attach on the matrix side of the membrane. These are predominantly HCO_3^- and HPO_4^{2-}, since these ion species have the highest concentration in the matrix. On the other hand, the membrane outside is positively charged by the transported protons. However, the H^+ ions do not remain in the phase boundary, but are replaced by K^+ ions, so that a large part of the protons appear as freely moving ions in the aqueous solution of the IMS. The exchange reaction is so much faster in comparison to proton pumping that it can be assumed that it is always at equilibrium and, consequently, does not need to be considered energetically.

In addition to the inner membrane, mitochondria also have an outer membrane which, together with the latter, encloses the IMS. This, in turn, contacts the sarcosol via a porin (voltage-dependent anion channel (VDAC)) in the outer membrane, which is permeable to ions and most metabolites (up to a molar mass of 10^4 g/mol). It can therefore be assumed that the H^+ ion concentrations in the IMS and sarcosol are virtually identical. That is the reason why, in $\Delta\tilde{\mu}_H$ the H^+ concentration of the sarcosol, $[H^+]_c$, may appear.

$\Delta\tilde{\mu}_H$ is in electrical units

$$\Delta\tilde{\mu}_H^{el} = \frac{R\,T}{F}\ln\left(\frac{[H^+]_m}{[H^+]_c}\right) + \Delta\phi_m \text{ (V)}$$

or

$$\Delta p = \ln(10)\,\frac{R\,T}{F}\lg\left(\frac{[H^+]_m}{[H^+]_c}\right) + \Delta\phi_m = \ln(10)\,\frac{R\,T}{F}\,(pH_c - pH_m) + \Delta\phi_m(V). \tag{8.2}$$

This last term (often in mV) is the designation chosen by Peter Mitchell [8–10] for $\Delta\tilde{\mu}_H$, where "Δp" stands for proton motive force.

For the flux through the coupled NAD_{red} oxidation applies

$$J_{NA} = L_c^{na}\left(\nu_{NA}\,\Delta\tilde{\mu}_H + R\,T\,\ln\left(\frac{[NAD_{red}]}{[NAD_{ox}]}\,[O_2]^{0.5}\,K'_{NA}\right)\right) \tag{8.3}$$

and for the coupled FAD_{red} oxidation

$$J_{FA} = L_c^{fa}\left(\nu_{FA}\,\Delta\tilde{\mu}_H + R\,T\,\ln\left(\frac{[FAD_{red}]}{[FAD_{ox}]}\,[O_2]^{0.5}\,K'_{FA}\right)\right)\ (\text{in mM/s}). \tag{8.4}$$

If only these two reactions of the respiratory chain were present in the inner membrane, without the possibility for a proton reflux, as was shown in the case of the Na/K ATPase, the membrane would be charged until equilibrium is reached between $A_1 = A_{NA}^{h} = \nu_{NA}\,\Delta\tilde{\mu}_H$ and

$$A_2 = A_{NA}^{ox} = R\,T\,\ln\left(\frac{[NAD_{red}]}{[NAD_{ox}]}\,[O_2]^{0.5}\,K'_{NA}\right)$$

as well as $A_1 = A_{FA}^{h} = \nu_{FA}\,\Delta\tilde{\mu}_H$ and

$$A_2 = A_{FA}^{ox} = R\,T\,\ln\left(\frac{[FAD_{red}]}{[FAD_{ox}]}\,[O_2]^{0.5}\,K'_{FA}\right).$$

The respective equilibrium values are $\Delta\tilde{\mu}_H = -211.8\text{mV}$ ($MP_M = -192.1\text{mV}$, for NAD_{red}), and $\Delta\tilde{\mu}_H = -226.5\text{mV}$ ($MP_M = -206.8\text{mV}$, for FAD_{red}). For calculation, constant pH values of $pH_c = 7.08$ and $pH_m = 7.4$ have been assumed. A capacitance of $C_{Mm} = 71.434 \times 10^6$ fF for the inner membrane has been derived from the fact that 0.75 nmol of H^+ can charge the membranes corresponding to 1.0 mg mitochondrial dry mass up to 0.2 V. The content of mitochondria is given by 1.9743×10^{-4} mg dry mass per SMF ($V_{cell} = 2.717\text{nL}$).

The values of FAD_{red} are more negative than those of NAD_{red} because the stoichiometric coefficient of coupled proton transport for FAD_{red} ($\nu_{FA} = 6.0$) is considerably smaller than that for NAD_{red} ($\nu_{NA} = 10.0$).

There exist several possibilities for a proton reflux at the inner mitochondrial membrane. In fact, most of the H^+ ions pumped in the IMS can be returned to the mitochondrial matrix via ATP synthase. In contrast to the reflux of Na^+ and K^+ ions, which have been pumped outward by the Na/K ATPase and have returned to the sarcosol through Na^+ and K^+ channels of the sarcolemma, the proton reflux via synthase, however, is coupled. In fact, the reflux is coupled with a specific proton stoichiometry to the synthesis of ATP from ADP and P_i. Due to the reversed flux direction opposite to the pump direction, $\Delta\tilde{\mu}_H$ must be used for this reaction with opposite sign. The coupled ATP synthase reaction is then

$$\nu_{SY}H_c^+ + MgADP_m^- + H_2PO_{4m}^- \rightleftharpoons MgATP_m^{2-} + H_2O + \nu_{SY}H_m^+. \tag{R8.3}$$

For the flux through this reaction, the following is applied

$$J_{SY} = L_c^{sy}\left(A_{ATP}^{m} + \nu_{SY}(-\Delta\tilde{\mu}_H)\right) \tag{8.5}$$

with

$$A_1 = A_{SY}^{p} = A_{ATP}^{m} = R\,T\ln\left(\frac{[MgADP^-]_m[H_2PO_4]_m}{[MgATP^{2-}]_m}\,\frac{1}{K_{MgATP}}\right)\ (\text{in J/mol})$$

and

$$A_2 = A_{SY}^{h} = \nu_{SY}(-\Delta\tilde{\mu}_H)\ (\text{in J/mol}).$$

To produce ATP continuously in the matrix, reactions (R8.1), (R8.2) and (R8.3) must be followed continuously. For the two redox reactions, the consistent outcoming of NAD_{ox} and FAD_{ox} must also be continuously reduced again. This is done through the metabolism and as already mentioned mainly by CAC in the mitochondrial matrix. For ATP synthesis, ATP synthase requires $MgADP^-$ and $H_2PO_4^-$ from the sarcosol, where ATP is continuously consumed through splitting and this ATP requirement must be constantly covered. Phosphate transport from the sarcosol to the matrix is electrically neutral by symport of $H_2PO_4^-$ and a H^+ ion. This is done by the H/P symporter of the inner membrane. ADP_c^{3-} from the sarcosol is exchanged against ATP_m^{4-} of the matrix electrogenically via adenine nucleotide antiport (ATP/ADP-Ex) of the inner membrane. For the H/P symport

$$J_{HP} = L_{P_i} R\,T\,\ln\left(\frac{[H_2PO_4^-]_c}{[H_2PO_4^-]_m}\,\frac{[H^+]_c}{[H^+]_m}\right) \tag{8.6}$$

is applied for the ATP/ADP antiport:

$$J_{AE} = L_{AE}\left(R\,T\,\ln\left(\frac{[ATP^{4-}]_m}{[ATP^{4-}]_c}\,\frac{[ADP^{3-}]_c}{[ADP^{3-}]_m}\right) + F(-\Delta\phi_m)\right)\ (\text{in mM/s}). \tag{8.7}$$

In the presence of a steady state, therefore, ATP could be continuously consumed in the sarcosol in order to access the mitochondrial matrix in split form. Here it is resynthesized via ATP synthase, but this can only occur with the contribution of a proton potential difference $\Delta\tilde{\mu}_H$ over the inner membrane. This in turn is generated by the coupled redox reactions with consumption of NAD_{red} and FAD_{red}. The resulting NAD_{ox} and FAD_{ox} must finally be reduced again by the metabolism. The reaction sequence from the O_2 consuming redox reactions to the ATP synthesis and subsequent replacement of ATP_m^{4-} for ADP_c^{3-} and $H_2PO_{4c}^-$ from the sarcosol is referred to as OP.

If A_{HP} and A_{AE} become contracted to a common affinity, one obtains

$$A_{HPAE} = A_{HP} + A_{AE} = R\,T\,\ln\left(\frac{[H_2PO_4^-]_c}{[H_2PO_4^-]_m}\,\frac{[H^+]_c}{[H^+]_m}\,\frac{[ATP^{4-}]_m}{[ATP^{4-}]_c}\,\frac{[ADP^{3-}]_c}{[ADP^{3-}]_m}\right) + F(-\Delta\phi_m)$$
$$= R\,T\,\ln\left(\frac{[H_2PO_4^-]_c}{[H_2PO_4^-]_m}\,\frac{[ATP^{4-}]_m}{[ATP^{4-}]_c}\,\frac{[ADP^{3-}]_c}{[ADP^{3-}]_m}\right) - \Delta\tilde{\mu}_H.$$

The sum of A^{m}_{ATP} and the first term (A^{p}_{HPAE}) from the above equation results in

$$A^{m}_{ATP} + A^{p}_{HPAE} = R\,T \ln\left(\left(\frac{[ADP^{3-}]_m [H_2PO_4^-]_m}{[ATP^{4-}]_m}\,\frac{1}{K_{ATP}}\right)\left(\frac{[H_2PO_4^-]_c}{[H_2PO_4^-]_m}\,\frac{[ATP^{4-}]_m}{[ATP^{4-}]_c}\,\frac{[ADP^{3-}]_c}{[ADP^{3-}]_m}\right)\right)$$
$$= -A^{c}_{ATP}. \qquad (8.8)$$

In the above derivation, the formula for A^{m}_{ATP} without Mg^{2+} containing species has been used; however, A^{m}_{ATP} is not changed. A more detailed discussion of these relationships is provided in Chapter 9.

For the resynthesis of the ATP from its splitting products via ATP synthase plus transport into the sarcosol, a total of $\nu_{SY} + 1$ protons are needed, which transfer their electrochemical energy when passing through the potential difference $\Delta\tilde{\mu}_H$ through coupling as well into ATP synthesis as into transport reactions (ATP/ADP-Ex plus H/P). While the stoichiometric factor is considered with respect to A_{HPAE} (1.0), there is less certainty regarding ν_{SY} of the ATP synthase reaction. Recently, 2.67 [11, 12] seems to be favored over the older value of 3.0. The following results have been calculated for a $\nu_{SY} = 3.0$.

The most noticeable change due to a reduction of ν_{SY} from the value 3.0 is a significant decrease of MP_M from −144 .0 to −58.0 mV. Thus $\Delta\tilde{\mu}_H$ also assumes a more negative value. The result of this is, as shown by simulations, ATP can be produced more efficiently with complete coupling, but when the respiratory chain is uncoupled, due to the more negative $\Delta\tilde{\mu}_H$ a larger proton leak flux occurs, so that less power can be produced under these conditions.

Figure 8.1 shows the most important affinities (A) and potential differences (B) of the inner membrane. In Figure 8.1C, the fluxes of H/P symport ($J_{HP} - J_{CAC}$, gray), ATP/ADP exchange ($J_{AE} - J_{CAC}$, dark red) and the ATP synthase (J_{SY}, red) are shown. The citric acid cycle derived ATP production must be removed, in order to account for only the associated fluxes belonging to OP. Figure 8.1A shows that at complete coupling (NAD_{red} oxidation) the efficiency η_{NA} is about 74.0%. Input affinity and output affinity thus differ significantly in this redox reaction. The same applies to the FAD_{red} oxidation (η_{FA} = 69.0%). In the ATP synthase reaction, however, input and output affinities are close together. Hence, the efficiency η_{SY} of this reaction is 98.5%. These conditions change only insignificantly when switching from rest to almost maximum power output. The fluxes through these almost constant affinities of OP, however, change considerably with increasing power output. However, this also depends strongly on the mitochondrial content of an SMF. For both fatty acid oxidation and Glu plus glycogen (Glgen) oxidation require mitochondria with the appropriate enzyme endowment for oxidative metabolism. It is primarily the reactions of β oxidation and of CAC that provide NAD_{red} and FAD_{red} for OP.

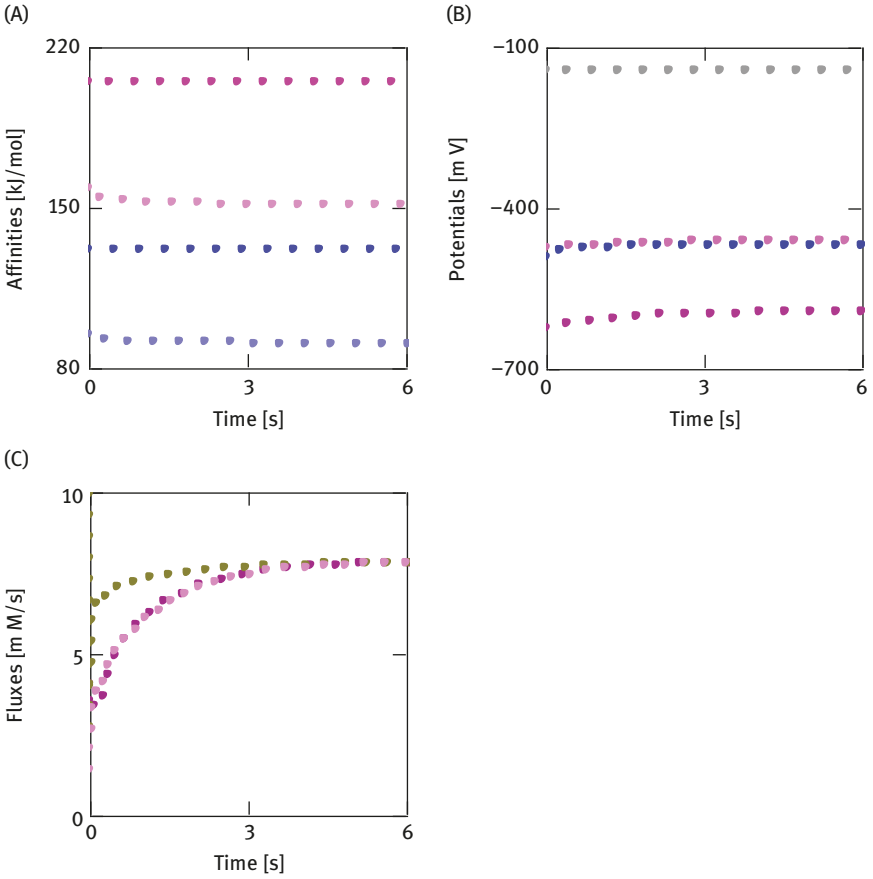

Figure 8.1: Affinities, potentials and fluxes at the inner mitochondrial membrane. (A) Red points, A^{ox}_{NA} and $-A^{h}_{NA}$; blue points, A^{ox}_{FA} and $-A^{h}_{FA}$. (B) Gray points, MP_M; red points, A^{m}_{ATP}/F and $-A^{c}_{ATP}/F$ (dark); blue points, $v_{SY}\Delta\tilde{\mu}_H$. (C) Gray points, $J_{HP} - J_{CAC}$; dark red points, $J_{AE} - J_{CAC}$; red points, J_{SY}.

The oxidative degradation of some amino acids is also possible, but under normal conditions (no increased protein degradation) it is relatively low, so it has not been included in simulations here.

The simulation ($SIM_{GLY/PAL}$, A3) chosen here for viewing the OP of an SMF assumes a moderate power output at $[Ca^{2+}]_c$ = 1.134 µM, as metabolism substrates Glu ($[Glu]_c$ = 4.0 mM), Glgen and Palm ($[Palm]_e$ = 0.1 µM) are present. Under these conditions, ATP (consumption = 4.103 mM/s) is derived to 22.58% from Palm and to 77.42% from Glu/Glgen degradation.

Figure 8.1C shows that for example the fluxes associated with ATP production increase significantly when switching from near resting conditions (at 0.3 µM $[Ca^{2+}]_c$) to a moderate power output at 1.134 µM $[Ca^{2+}]_c$ (2.24-fold). All three fluxes are identical at steady state after about 5.0 s.

In the following on the basis of the above simulation it should be demonstrated that the proton energy cycle already promoted by P. Mitchell [10] across the inner mitochondrial membrane is in fact achieved on reaching an SSC. In contrast to the previously introduced Ca^{2+} cycle at the reticulum membrane and the Na^+/K^+ cycle at the sarcolemma, the OP proton cycle proceeds through two coupled in series reactions. It therefore represents the analogue of the electrical circuit with two batteries connected against each other. To demonstrate this, the two proton fluxes resulting from the redox reactions must first be combined. This can be accomplished by the corresponding dissipation functions. It is

$$\Psi_1 = \Psi^{\mathrm{h}}_{\mathrm{NA}} = L^{\mathrm{na}}_{\mathrm{c}} \left(\left(1 + \lambda^{\mathrm{h}}_{\mathrm{NA}} \right) A^{\mathrm{h}}_{\mathrm{NA}} + A^{\mathrm{ox}}_{\mathrm{NA}} \right) A^{\mathrm{h}}_{\mathrm{NA}},$$

$$\Psi_2 = \Psi^{\mathrm{ox}}_{\mathrm{NA}} = L^{\mathrm{na}}_{\mathrm{c}} \left(A^{\mathrm{h}}_{\mathrm{NA}} + \left(1 + \lambda^{\mathrm{ox}}_{\mathrm{NA}} \right) A^{\mathrm{ox}}_{\mathrm{NA}} \right) A^{\mathrm{ox}}_{\mathrm{NA}},$$

$$\Psi_1 = \Psi^{\mathrm{h}}_{\mathrm{FA}} = L^{\mathrm{fa}}_{\mathrm{c}} \left(\left(1 + \lambda^{\mathrm{h}}_{\mathrm{FA}} \right) A^{\mathrm{h}}_{\mathrm{FA}} + A^{\mathrm{ox}}_{\mathrm{FA}} \right) A^{\mathrm{h}}_{\mathrm{FA}},$$

$$\Psi_2 = \Psi^{\mathrm{ox}}_{\mathrm{FA}} = L^{\mathrm{fa}}_{\mathrm{c}} \left(A^{\mathrm{ox}}_{\mathrm{FA}} + \left(1 + \lambda^{\mathrm{ox}}_{\mathrm{FA}} \right) A^{\mathrm{ox}}_{\mathrm{FA}} \right) A^{\mathrm{ox}}_{\mathrm{FA}}.$$

The equations include all possibilities of uncoupling, that is, all corresponding λ_s, so that any decoupling caused by this is also included, resulting in

$$\Psi^{\mathrm{h}}_{\mathrm{R}} = \Psi^{\mathrm{h}}_{\mathrm{NA}} + \Psi^{\mathrm{h}}_{\mathrm{FA}} \text{ and } \Psi^{\mathrm{ox}}_{\mathrm{R}} = \Psi^{\mathrm{ox}}_{\mathrm{NA}} + \Psi^{\mathrm{ox}}_{\mathrm{FA}}.$$

However, only the proportion $Q^{\mathrm{op}}_{\mathrm{H}}$ of all pumped protons flows into the OP. This is given by

$$Q^{\mathrm{op}}_{\mathrm{H}} = \frac{\nu_{\mathrm{NA}} J_{\mathrm{NA}} + \nu_{\mathrm{FA}} J_{\mathrm{FA}} - \left(J_{\mathrm{NAsh}} + J_{\mathrm{PL}} + 2J_{\mathrm{CaH}} + J_{\mathrm{CAC}} \right)}{\nu_{\mathrm{NA}} J^{\mathrm{h}}_{\mathrm{NA}} + \nu_{\mathrm{FA}} J^{\mathrm{h}}_{\mathrm{FA}}} = \frac{\nu_{\mathrm{SY}} J^{\mathrm{h}}_{\mathrm{SY}} + J^{\mathrm{p}}_{\mathrm{SY}}}{\nu_{\mathrm{NA}} J^{\mathrm{h}}_{\mathrm{NA}} + \nu_{\mathrm{FA}} J^{\mathrm{h}}_{\mathrm{FA}}} \tag{8.9}$$

where J_{NASH} describes the flux, which transports $\mathrm{NAD}_{\mathrm{red}}$ via malate-aspartate-shuttle from the sarcosol into the matrix, J_{PL} the proton leak flux, J_{CaH} the Ca/H exchange at the inner membrane and J_{CAC} the flux through CAC. The sum of these fluxes ($\Sigma^{\mathrm{rest}}_{\mathrm{H}} = J_{\mathrm{NAsh}} + J_{\mathrm{PL}} + 2J_{\mathrm{CaH}} + J_{\mathrm{CAC}}$) also flows back into the matrix, but on other reaction paths that are not directly related to the OP.

For the dissipation functions, one obtains

$$\Psi^{\mathrm{h}}_{\mathrm{Rop}} = Q^{\mathrm{op}}_{\mathrm{H}} \left(\Psi^{\mathrm{h}}_{\mathrm{NA}} + \Psi^{\mathrm{h}}_{\mathrm{FA}} \right) \text{ and } \Psi^{\mathrm{ox}}_{\mathrm{Rop}} = Q^{\mathrm{op}}_{\mathrm{H}} \left(\Psi^{\mathrm{ox}}_{\mathrm{NA}} + \Psi^{\mathrm{ox}}_{\mathrm{FA}} \right).$$

For the associated affinities and conductances the result is

$$A_{\mathrm{Rop}} = \frac{\Psi^{\mathrm{h}}_{\mathrm{Rop}} + \Psi^{\mathrm{ox}}_{\mathrm{Rop}}}{J^{\mathrm{p}}_{\mathrm{SY}}} \text{ and } L^{\mathrm{rop}}_{\mathrm{c}} = \frac{\Psi^{\mathrm{h}}_{\mathrm{Rop}} + \Psi^{\mathrm{ox}}_{\mathrm{Rop}}}{\left(A_{\mathrm{Rop}} \right)^2}$$

with

$$A^{\mathrm{h}}_{\mathrm{Rop}} = \frac{\Psi^{\mathrm{h}}_{\mathrm{Rop}}}{J^{\mathrm{p}}_{\mathrm{SY}}} \text{ and } A^{\mathrm{ox}}_{\mathrm{Rop}} = \frac{\Psi^{\mathrm{ox}}_{\mathrm{Rop}}}{J^{\mathrm{p}}_{\mathrm{SY}}}$$

The respective flux is given by

$$J_{\mathrm{Rop}} = L^{\mathrm{rop}}_{\mathrm{c}} \left(A^{\mathrm{h}}_{\mathrm{Rop}} + A^{\mathrm{ox}}_{\mathrm{Rop}} \right).$$

This is the flux through both redox reactions. The partial conductances can be determined from it. These are

$$L^{\mathrm{rop}}_{\mathrm{c1}} = L^{\mathrm{rop}}_{\mathrm{c}} \frac{A^{\mathrm{h}}_{\mathrm{Rop}} + A^{\mathrm{ox}}_{\mathrm{Rop}}}{A^{\mathrm{h}}_{\mathrm{Rop}}} (<0) \tag{8.10}$$

and

$$L^{\mathrm{rop}}_{\mathrm{c2}} = L^{\mathrm{rop}}_{\mathrm{c}} \frac{A^{\mathrm{h}}_{\mathrm{Rop}} + A^{\mathrm{ox}}_{\mathrm{Rop}}}{A^{\mathrm{ox}}_{\mathrm{Rop}}} (>0). \tag{8.11}$$

Also,

$$L^{\mathrm{rop}}_{\mathrm{c}} = \frac{1}{\frac{1}{L^{\mathrm{rop}}_{\mathrm{c1}}} + \frac{1}{L^{\mathrm{rop}}_{\mathrm{c2}}}}$$

is fulfilled.

Next, the common conductance of series reactions of ATP synthase and ATP transport must be found. The dissipation function is given by

$$\begin{aligned} \Psi_{\mathrm{SYTr}} &= J^{\mathrm{p}}_{\mathrm{SY}} A^{\mathrm{m}}_{\mathrm{ATP}} + J^{\mathrm{h}}_{\mathrm{SY}} A^{\mathrm{h}}_{\mathrm{SY}} + J^{\mathrm{p}}_{\mathrm{SY}} A_{\mathrm{HPAE}} + J^{\mathrm{p}}_{\mathrm{SY}} (-\Delta\tilde{\mu}_{\mathrm{H}}) \\ &= J^{\mathrm{p}}_{\mathrm{SY}} \left(-A^{\mathrm{c}}_{\mathrm{ATP}} + \frac{J^{\mathrm{h}}_{\mathrm{SY}}}{J^{\mathrm{p}}_{\mathrm{Sy}}} A^{\mathrm{h}}_{\mathrm{SY}} - \Delta\tilde{\mu}_{\mathrm{H}} \right) \end{aligned}$$

with

$$A_{\mathrm{SYTr}} = -A^{\mathrm{c}}_{\mathrm{ATP}} + \frac{J^{\mathrm{h}}_{\mathrm{SY}}}{J^{\mathrm{p}}_{\mathrm{Sy}}} A^{\mathrm{h}}_{\mathrm{SY}} - \Delta\tilde{\mu}_{\mathrm{H}}.$$

From this one obtains

$L^{\mathrm{sytr}}_{\mathrm{c}} = \Psi_{\mathrm{SYTr}} / {A_{\mathrm{SYTr}}}^2$ and finally

$$J_{\mathrm{SYTr}} = L^{\mathrm{sytr}}_{\mathrm{c}} \left(-A^{\mathrm{c}}_{\mathrm{ATP}} + \frac{J^{\mathrm{h}}_{\mathrm{SY}}}{J^{\mathrm{p}}_{\mathrm{Sy}}} A^{\mathrm{h}}_{\mathrm{SY}} - \Delta\tilde{\mu}_{\mathrm{H}} \right). \tag{8.12}$$

The partial conductances are given by

$$L_{c1}^{sytr} = L_c^{sytr} \frac{-A_{ATP}^c + \frac{J_{SY}^h}{J_{Sy}^p} A_{SY}^h - \Delta\tilde{\mu}_H}{-A_{ATP}^c} \quad (<0) \tag{8.13}$$

and

$$L_{c2}^{sytr} = L_c^{sytr} \frac{-A_{ATP}^c + \frac{J_{SY}^h}{J_{Sy}^p} A_{SY}^h - \Delta\tilde{\mu}_H}{\frac{J_{SY}^h}{J_{Sy}^p} A_{SY}^h - \Delta\tilde{\mu}_H} \quad (>0). \tag{8.14}$$

With complete coupling $J_{SY}^h = J_{SY}^p$. When $A_{SY}^h = -\nu_{SY}\,\Delta\tilde{\mu}_H$, this leads to

$$L_{c2}^{sytr} = L_c^{sytr} \frac{-A_{ATP}^c + (\nu_{SY}+1)(-\Delta\tilde{\mu}_H)}{(\nu_{SY}+1)(-\Delta\tilde{\mu}_H)}$$

and

$$L_{c2}^{sytr} = L_c^{sytr} \frac{-A_{ATP}^c + (\nu_{SY}+1)(-\Delta\tilde{\mu}_H)}{(\nu_{SY}+1)(-\Delta\tilde{\mu}_H)}.$$

The results of the simulation show that under fully coupled as well as under uncoupled conditions, $L_{c1}^{rop} = -L_{c2}^{sytr}$ is always fulfilled for the proton cycle of the OP.

For the determination of changes caused by uncoupling, the respective fluxes used in the simulations must also contain the corresponding λ values. These appear in the flux equations as factors $(\lambda_1 + 1)$ of the corresponding affinity A_1 or $(\lambda_2 + 1)$ for A_2, as already shown in eqs. (6.10) and (6.11). For example, these are the two flux equations for the NAD_{red} oxidation with uncoupling

$$J_{NA}^h = L_c^{na}\left(\nu_{NA}\left(\lambda_{NA}^h + 1\right)\Delta\tilde{\mu}_H + R\,T\,\ln\left(\frac{[NAD_{red}]}{[NAD_{ox}]}\,[O_2]^{0.5}\,K'_{NA}\right)\right)$$

and

$$J_{NA}^{ox} = L_c^{na}\left(\nu_{NA}\Delta\tilde{\mu}_H + \left(\lambda_{NA}^{ox} + 1\right)R\,T\,\ln\left(\frac{[NAD_{red}]}{[NAD_{ox}]}\,[O_2]^{0.5}\,K'_{NA}\right)\right).$$

The same applies to the fluxes involved in the OP J_{FA}^h and J_{FA}^{ox}, as well as J_{SY}^p and J_{SY}^h. Figure 8.2 shows that the dissipation functions of proton transport (A), the proton fluxes themselves (B) and their conductances (C) have identical time courses, but this time from the beginning onwards. Figure 8.2D shows the corresponding non-transformed fluxes of OP. These are the proton flux coupled to redox reactions (from the matrix into the IMS) and the proton reflux through the ATP synthase, including the H^+ reflux required for ATP exchange. With this presentation, it becomes clear that a certain amount of time is required even to reach an SSC for protons.

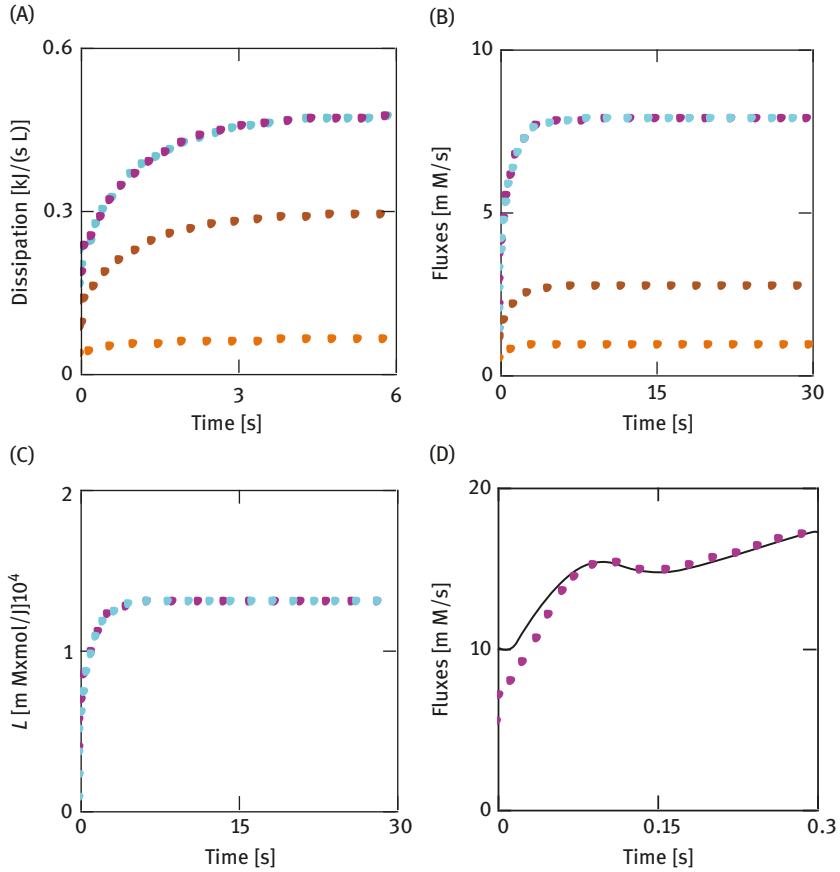

Figure 8.2: Matching of dissipation functions, fluxes and conductances. (A) Dissipation functions (cyan points, Ψ^{h}_{Pop}; red points, Ψ_{SYTr}; for comparison, brown points, $Q^{op}_{H}\,\Psi^{h}_{NA}$; yellow points, $Q^{op}_{H}\,\Psi^{h}_{FA}$). (B) Fluxes (cyan points, J_{Rop}; red points, J^{p}_{SY}; brown points, J^{h}_{NA}; yellow points, J^{h}_{FA}. (C) conductances (cyan points, L^{rop}_{c1}; red points, $-L^{sytr}_{c2}$). (D) Nontransformed proton fluxes of OP (black line, $v_{NA}J^{h}_{NA} + v_{FA}J^{h}_{FA} - (J_{NAsh} + J_{PL} + 2J_{CaH} + J_{CAC})$; red points, $v_{SY}J^{h}_{SY} + J^{p}_{SY}$.).

Apparently, however, an SSC is reached already before the setting of constant values for the fluxes involved. This behavior could be explained by the fact that the redox reactions at the inner membrane are supplied with NAD_{red} or FAD_{red} from a relatively slowly increasing metabolism and, as a result, can likewise only increase slowly. The proton fluxes at the membrane, however, can proceed considerably faster, so that they can reach SSC in a much shorter time.

The data needed for the OP are supplied by a simulation that calculates the total energy metabolism of an SMF. This includes all ATP-producing and ATP-consuming reactions of the metabolism. However, for the OP only the reactions involved in the Palm oxidation and Glu/Glgen oxidation are considered.

Their respective proportions can be determined by the following formulas:

$$Q_{\mathrm{H}}^{\mathrm{palm}} = \frac{\left(7J_\beta \nu_{\mathrm{NA}} + 8J_\beta 3\nu_{\mathrm{NA}}\right)\frac{J_{\mathrm{NA}}^{\mathrm{cp}}}{J_{\mathrm{NA}}^{\mathrm{ox}}} + \left(7J_\beta \nu_{\mathrm{FA}} + 8J_\beta \nu_{\mathrm{FA}}\right)\frac{J_{\mathrm{FA}}^{\mathrm{cp}}}{J_{\mathrm{FA}}^{\mathrm{ox}}}}{J_{\mathrm{NA}}^{\mathrm{ox}} \nu_{\mathrm{NA}} \frac{J_{\mathrm{NA}}^{\mathrm{cp}}}{J_{\mathrm{NA}}^{\mathrm{ox}}} + J_{\mathrm{FA}}^{\mathrm{ox}} \nu_{\mathrm{FA}} \frac{J_{\mathrm{FA}}^{\mathrm{cp}}}{J_{\mathrm{FA}}^{\mathrm{ox}}} - J_{\mathrm{NAsh}}} = 52.82\%$$

and

$$Q_{\mathrm{H}}^{\mathrm{gl}} = \frac{\left(4J_{\mathrm{PDH}} \nu_{\mathrm{NA}} + J_{\mathrm{NAsh}} \nu_{\mathrm{NA}}\right)\frac{J_{\mathrm{NA}}^{\mathrm{cp}}}{J_{\mathrm{NA}}^{\mathrm{ox}}} + \left(J_{\mathrm{PDH}} \nu_{\mathrm{FA}} + J_{\mathrm{FAsh}} \nu_{\mathrm{FA}}\right)\frac{J_{FA}^{cp}}{J_{\mathrm{FA}}^{\mathrm{ox}}} - J_{\mathrm{NAsh}}}{J_{\mathrm{NA}}^{\mathrm{ox}} \nu_{\mathrm{NA}} \frac{J_{\mathrm{NA}}^{\mathrm{cp}}}{J_{\mathrm{NA}}^{\mathrm{ox}}} + J_{\mathrm{FA}}^{\mathrm{ox}} \nu_{\mathrm{FA}} \frac{J_{\mathrm{FA}}^{\mathrm{cp}}}{J_{\mathrm{FA}}^{\mathrm{ox}}} - J_{\mathrm{NAsh}}} = 47.18\%.$$

where J_β describes the flux through the β-oxidation, and J_{PDH} the flux through the pyruvate dehydrogenase. $J_{\mathrm{NA}}^{\mathrm{cp}}/J_{\mathrm{NA}}^{\mathrm{ox}}$ describes the coupled share of $J_{\mathrm{NA}}^{\mathrm{ox}}$.

The above quotients indicate the respective mitochondrial fraction of the metabolic pathway considered. So, the proton transport coupled to Palm oxidation, for example, is related to the total, that is, from Palm plus Glu/Glgen produced H^+ flux. The associated ATP production is given then by $J_{\mathrm{ATP}}^{\mathrm{palm}} = Q_{\mathrm{H}}^{\mathrm{palm}} J_{\mathrm{SY}}^{\mathrm{p}}$ and $J_{\mathrm{ATP}}^{\mathrm{gl}} = Q_{\mathrm{H}}^{\mathrm{gl}} J_{\mathrm{SY}}^{\mathrm{p}}$.

It is

$$\frac{J_{\mathrm{ATP}}^{\mathrm{palm}}}{J_{\mathrm{ATP}}^{\mathrm{palm}} + J_{\mathrm{ATP}}^{\mathrm{gl}}} = \frac{J_{\mathrm{ATP}}^{\mathrm{palm}}}{J_{\mathrm{ATP}}^{\mathrm{tot}}} = 21.26\%$$

and

$$\frac{J_{\mathrm{ATP}}^{\mathrm{gl}}}{J_{\mathrm{ATP}}^{\mathrm{tot}}} = 18.99\ \%,$$

and thus 40.25% oxidative. $8J_\beta$ and $1J_{\mathrm{PDH}}$ (1.76 or 1.43%) are each additionally produced in the CAC of the matrix but not added to OP.

The total O_2 consumption is $J_{\mathrm{O}} = J_{\mathrm{NA}} + J_{\mathrm{FA}} = 3.66$ mM/s (related to 1.0 L matrix volume), resulting in $J_{\mathrm{O}_2}^{\mathrm{c}} = 0.5 J_{\mathrm{O}}/Q_{\mathrm{V}} = 0.383$ mM/s (related to 1.0 L of sarcosol, $Q_{\mathrm{V}} = V_{\mathrm{c}}/V_{\mathrm{m}} = 4.77869$).

The respective relative oxygen consumption is

$$Q_{\mathrm{O}}^{\mathrm{palm}} = \frac{2 \times 7J_\beta + 8 \times 4J_\beta}{J_{\mathrm{O}}} = \frac{46J_\beta}{J_{\mathrm{O}}} = 54.08\%$$

and

$$Q_{\mathrm{O}}^{\mathrm{gl}} = \frac{J_{\mathrm{NAsh}} + J_{\mathrm{FYsh}} + 5J_{\mathrm{PDH}}}{J_{\mathrm{O}}} = \frac{6J_{\mathrm{PDH}}}{J_{\mathrm{O}}} = 45.92\%.$$

The total CO_2 consumption is given by

$J_{CO_2} = J_{PDH} + 2J_{CAC} = 1.5288$ mM/s (matrix), or $J^{c}_{CO_2} = J_{CO_2}/Q_V = 0.3199$ mM/s (sarcosol).

This results in a respiratory quotient of

$$RQ = J^{c}_{CO_2}\Big/J^{c}_{O_2} = 0.8354.$$

The respective relative CO_2 consumption is given by

$$J^{palm}_{ATP} = Q^{palm}_{H} J^{p}_{SY} \text{ and } J^{gl}_{ATP} = Q^{gl}_{H} J^{p}_{SY}. \text{ and } Q^{gl}_{CO_2} = 3J_{PDH}/(J_{PDH} + 2J_{CAC}) = 54.97\%.$$

The respiratory quotient for the Palm oxidation is given by $RQ^{palm} = 8 \times 2J_\beta / 0.5\left(2 \times 7J_\beta + 8 \times 4J_\beta\right) = 0.695652$. This value must be identical to the result from the reaction equation (R8.3) (16/23 = 0.695652):

$$\text{Palm} + 23\,O_2 \rightarrow 16\,CO_2 + 16H_2O \tag{R8.4}$$

For Glu/Glgen oxidation, the following is applied:

$$RQ^{gl} = 3J_{PDH}/0.5(J_{NAsh} + J_{FAsh} + 5J_{PDH}) = 1.0.$$

From (R4.1) the result is 6/6 = 1.0. The last two results are particularly well suited as controls for such simulations, which include mitochondrial reactions.

For the P/O quotients of the OP one obtains with

$$Q^{op}_{H} = \frac{\nu_{NA} J^{h}_{NA} + \nu_{FA} J^{h}_{FA} - (J_{NAsh} + J_{PL} + 2J_{CaH} + J_{CAC})}{\nu_{NA} J^{h}_{NA} + \nu_{FA} J^{h}_{FA} - J_{NAsh}} \tag{8.15}$$

$$Q_{PO} = \frac{J^{p}_{SY}}{Q^{op}_{H} J_O} = 2.2258.$$

The P/O quotient for palm oxidation is

$$Q^{palm}_{PO} = \frac{Q^{palm}_{H} J^{p}_{SY}}{Q^{op}_{H}\left(2 \times 7J_\beta + 8 \times 4J_\beta\right)} = 2.1739 \tag{8.16}$$

or

$$Q^{palm}_{PO} = \frac{\left(7J_\beta + 8 \times 3J_\beta\right)\nu_{NA} + \left(7J_\beta + 8J_\beta\right)\nu_{FA}}{\left(\nu_{SY} + 1\right)\left(2 \times 7J_\beta + 8 \times 3J_\beta\right)} = 2.1739, \tag{8.16a}$$

and that for Glu/Glgen oxidation

$$Q^{gl}_{PO} = \frac{Q^{gl}_{H} J^{p}_{SY}}{Q^{op}_{H}(J_{NAsh} + J_{FAsh} + 5 \times J_{PDH})} = 2.2868 \tag{8.17}$$

or

$$Q_{\mathrm{PO}}^{\mathrm{gl}} = \frac{J_{\mathrm{NAsh}}\,\nu_{\mathrm{NA}} - J_{\mathrm{NAsh}} + J_{\mathrm{FAsh}}\,\nu_{\mathrm{FA}} + 4J_{\mathrm{PDH}}\nu_{\mathrm{NA}} + J_{\mathrm{PDH}}\nu_{\mathrm{FA}}}{(\nu_{\mathrm{SY}} + 1)(J_{\mathrm{NAsh}} + J_{\mathrm{FAsh}} + 5 \times J_{\mathrm{PDH}})} = 2.2868. \tag{8.17a}$$

Formulas (8.16a)–(8.17a) are independent of coupling, while (8.16) and (8.17) in uncoupling are always accompanied by a reduction of the results given here for complete coupling. An external uncoupling by activation of the proton leak flux via UCP3 (uncoupling protein 3) of the inner membrane is also not indicated as uncoupling, so there is no reduction of the Q_{PO}, because J_{PL} in eq. (8.15) is also subtracted from the total flux of all pumped protons. Consequently, only the leak fluxes that flow through the coupled reaction itself are taken into account, which hence cause an inner uncoupling. For example, when changing J_{PL} from 0 to 5.532 mM/s (20.43% of the OP flux), ATP production remains nearly unchanged at 4.09 mM/s (vs. 4.103 mM/s). The O_2 consumption increases by 3.19%. However, the production of ATP solely by the OP drops significantly from 40.24 to 34.63%. $Q_{\mathrm{PO}}^{\mathrm{palm}}$, $Q_{\mathrm{PO}}^{\mathrm{gl}}$ and Q_{PO} remain unchanged.

With uncoupling of the respiratory chain ($\lambda_{\mathrm{NA}} = 0.15$, $\lambda_{\mathrm{FA}} = 0.3$, $J_{\mathrm{PL}} = 0$ mM/s), ATP production remains virtually unchanged, O_2 consumption increases by 8.67% and ATP production by OP decreases to 24.85%. $\mathrm{PO}^{\mathrm{palm}}$drops to 1.25, $\mathrm{PO}^{\mathrm{gl}}$ to 1.32 and PO to 1.283. A reduction of ν_{SY} from 3.0 to 2.67 ($\nu_{\mathrm{SY}}\mathrm{H}^+/\mathrm{ATP}$) increases the respective Q_{PO} s to 2.426, 2.369 and 2.493, respectively.

These results show that, above all, through inner uncoupling such as the respiratory chain always ATP production by OP becomes reduced, whereas O_2 consumption is increased, which must lead to a decrease in the respective Q_{PO} s.

However, the total ATP production is only marginally reduced, from which it can be concluded that the anoxic Glu/Glgen metabolism is able to compensate almost completely for the loss caused by uncoupling. Under these conditions, anoxic ATP production (Glu/Glgen) increases from 55.14% to 69.88%.

Like the P/O quotient, the efficiency also provides information regarding the extent to which the power of the redox reactions is utilized by OP for ATP production. The efficiency is obtained with

$$Q_{\mathrm{H}}^{\mathrm{op}'} = \frac{\nu_{\mathrm{NA}} J_{\mathrm{NA}}^{\mathrm{h}} + \nu_{FA} J_{FA}^{\mathrm{h}} - (J_{\mathrm{NAsh}} + J_{PL} + 2J_{\mathrm{CaH}} + J_{\mathrm{CAC}})}{\nu_{\mathrm{NA}} J_{\mathrm{NA}}^{h} + \nu_{\mathrm{FA}} J_{\mathrm{FA}}^{\mathrm{h}}}$$

as

$$\eta_{\mathrm{OP}} = -\frac{J_{\mathrm{SY}}^{\mathrm{p}}\left(-A_{\mathrm{atp}}^{\mathrm{c}}\right)}{Q_{\mathrm{H}}^{\mathrm{op}'}\left(J_{\mathrm{NA}}^{\mathrm{ox}} A_{\mathrm{NA}}^{\mathrm{ox}} + J_{\mathrm{FA}}^{\mathrm{ox}} A_{\mathrm{FA}}^{\mathrm{ox}}\right)} = 69.32\%. \tag{8.18}$$

The value associated with Palm oxidation is

$$\eta_{\mathrm{OP}}^{\mathrm{palm}} = -\frac{Q_{\mathrm{H}}^{\mathrm{palm}} J_{\mathrm{SY}}^{\mathrm{p}} \left(-A_{\mathrm{atp}}^{\mathrm{c}}\right)}{Q_{\mathrm{H}}^{\mathrm{op}'} \left(31 J_{\beta} AS + 15 J_{\beta} A_{\mathrm{FA}}^{\mathrm{ox}}\right)} = 69.63\%, \tag{8.19}$$

and that for Glu/Glgen

$$\eta_{\mathrm{OP}}^{\mathrm{gl}} = \frac{Q_{\mathrm{H}}^{\mathrm{gl}} J_{\mathrm{SY}}^{\mathrm{p}} \left(-A_{\mathrm{atp}}^{\mathrm{c}}\right)}{Q_{\mathrm{H}}^{\mathrm{op}'} \left((4J_{\mathrm{PDH}} + J_{\mathrm{NAsh}}) A_{\mathrm{NA}}^{\mathrm{ox}} + (J_{\mathrm{PDH}} + J_{\mathrm{FAsh}}) A_{\mathrm{FA}}^{\mathrm{ox}}\right)} = 68.97\%. \tag{8.20}$$

When the respiratory chain becomes uncoupled (see above), the above values are reduced to 40.0%, 39.62% and 39.8%, respectively.

The behavior of the respective uncoupled redox reactions of the respiratory chain is shown in Figure 8.3. The curve is determined by the corresponding λ values. For $\mathrm{NAD_{red}}$ oxidation (red; $\lambda_{\mathrm{NA}}^{\mathrm{h}} = 0.15$, $\lambda_{\mathrm{NA}}^{\mathrm{ox}} = 0$), the efficiency $\eta_{\mathrm{NA}} = 0.4435$ of this reaction at an abscissa value of $a = A_{\mathrm{NA}}^{\mathrm{h}}/A_{\mathrm{NA}}^{\mathrm{ox}} = -0.737$ obtained from simulation gives the point on the curve. For the $\mathrm{FAD_{red}}$ oxidation (blue), $\eta_{\mathrm{FA}} = 0.2593$ with $a = A_{\mathrm{FA}}^{\mathrm{h}}/A_{\mathrm{FA}}^{\mathrm{ox}} = -0.689$. When completely coupled, the points lie on the line $\eta = -a$. Then the result is, as already mentioned, $\eta_{\mathrm{NA}} = 0.737$ and $\eta_{\mathrm{FA}} = 0.689$.

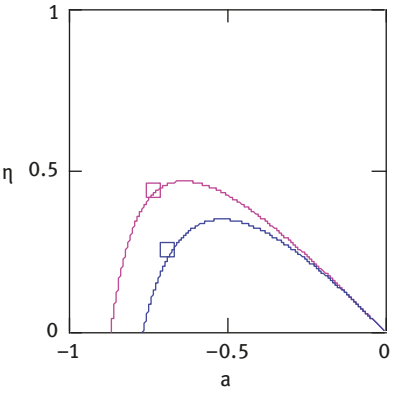

Figure 8.3: Uncoupling of the respiratory chain. Red line: efficiency of uncoupled $\mathrm{NAD_{red}}$-linked proton transport, $\lambda_{\mathrm{NA}} = 0.15$; red square: efficiency at $a = -\eta_{\mathrm{cp}} = -0.737$ under totally coupled conditions. Blue line: efficiency of uncoupled $\mathrm{FAD_{red}}$-linked proton transport, $\lambda_{\mathrm{NA}} = 0.3$; blue square: efficiency at $a = -\eta_{\mathrm{cp}} = -0.689$ under totally coupled conditions.

A reduction of the efficiencies with complete coupling can also be observed by increasing the power output (associated with about 11.0 mM/s ATP production, for instance). With $[\mathrm{Ca}^{2+}]_{\mathrm{c}} = 6.0\mu\mathrm{M}$, the above considered efficiencies of OP decrease to 65.49%, 65.08% and 65.19%.

With $\nu_{\mathrm{SY}} = 2.67$, efficiencies are higher (75.86%, 75.14% and 75.54%), however. The ATP production by OP is also increased (by 7.24%), but with uncoupling a significant reduction of efficiency is produced by a lower ν_{SY} value (50.99 instead of 61.74% at $\nu_{\mathrm{SY}} = 3.0$).

The values of the partial conductances are

$L_{c1}^{rop} = -1.3047 \times 10^{-4}$ and $L_{c2}^{sytr} = 1.3049 \times 10^{-4} (\mathrm{mM/s \times mol/J})$ at $\left[Ca^{2+}\right]_c = 1.136\,\mu\mathrm{M}$,

$L_{c1}^{rop} = -2.535 \times 10^{-4}$ and $L_{c2}^{sytr} = 2.535 \times 10^{-4}$ $(\mathrm{mM/s \times mol/J})$, at $\left[Ca^{2+}\right]_c = 6.0\,\mu\mathrm{M}$ and

$L_{c1}^{rop} = -0.821 \times 10^{-4}$ and $L_{c2}^{sytr} = 0.8211 \times 10^{-4}$ $(\mathrm{mM/s \times mol/J})$, *at* $[Ca^{2+}]_c = 1.136\,\mu\mathrm{M}$

in addition to uncoupling.

In analogy to the two batteries connected against each other, it is also possible with respect to the proton cycle of the OP at the inner mitochondrial membrane to differentiate between energy-delivering (redox reactions) and energy-consuming (ATP synthase and ATP transport) reactions. So Ψ_{Rop}^{h} is compared with the dissipation function Ψ_1^{Del}, and Ψ_{SYTr}^{h} to the dissipation function Ψ_2^{Dem}. Similarly L_{c1}^{rop} and L_{c1}^{Del} as well as L_{c2}^{sytr} and L_{c2}^{Dem}.

For the efficiencies the result is therefore

$$\eta_{OP} = \frac{\left(-\Psi_{Rop}^{h}\right)}{\Psi_{Rop}^{h}} \times \frac{\left(-\Psi_{SYTr}^{p}\right)}{\Psi_{SYTr}^{h}} = \frac{\left(-\Psi_1^{Del}\right)}{\Psi_2^{Del}} \times \frac{\left(-\Psi_1^{Dem}\right)}{\Psi_2^{Dem}} = \eta_{Del} \times \eta_{Dem}. \tag{8.21}$$

Since $\Psi_2^{Dem} = -\Psi_1^{Del}$, the following is obtained:

$$\eta_{OP} = \frac{\left(-\Psi_1^{Dem}\right)}{\Psi_2^{Del}} = 69.32\%.$$

The dissipation functions are given by

$$\Psi_1^{Dem} = J_{SY}^{p}\left(-A_{ATP}^{c}\right) \tag{8.22}$$

and

$$\Psi_2^{Del} = Q_H^{op}\left(J_{NA}^{op}A_{NA}^{ox} + J_{FA}^{ox}A_{FA}^{ox}\right). \tag{8.23}$$

For the total dissipation of OP one obtains

$$\begin{aligned}\Psi_{OP}^{tot} &= \Psi_1^{Del} + \Psi_2^{Del} + \Psi_1^{Dem} + \Psi_2^{Dem} \\ &= J_{SY}^{p}\left(-A_{ATP}^{c}\right) + Q_H^{op}\left(J_{NA}^{ox}A_{FA}^{ox}\right).\end{aligned} \tag{8.24}$$

Mitochondria can produce ATP also without the consumption of O_2 This comes about via CAC in the mitochondrial matrix through substrate-level phosphorylation in a similar way as glycolytic ATP formation in the sarcosol. At a mitochondrial ATP delivery rate of $J_{SY}^{p} + J_{CAC} = 1.636 + 0.129 = 1.7651$ mM/s about 92.7% is delivered by OP and 7.3% via CAC.

9 The ATP cycle of energy metabolism

So far, it has been shown that coupled reactions are of significant importance in cellular membrane transport processes. Upon reaching an SSC, there is a reaction cycle, which is characterized mainly by its dissipation-free progression. Characteristic of such a cycle gone through at a constant flux is always that Ψ_1^{Del} and Ψ_2^{Dem}, A_1^{Del} and A_2^{Dem} as well as L_1^{Del} and L_2^{Dem} are oppositely equal. This applies to cycles with only one coupled reaction and to those with two coupled reactions, whereby the second – as in the example of two batteries connected against each other – uses the output power of the first as input power.

In the following, it should be deduced that this principle can also be applied to the reactions of ATP delivery (production) and ATP demand (consumption) in energy metabolism.

As already mentioned, the mathematical simulation ($\mathrm{SIM_{GLY/PAL}}$) used here simulates the degradation of Palm, Glu and Glgen of an SMF. This results in several ways in which ATP can be produced. These are Palm oxidation and Glu/Glgen metabolism. The latter can be split into several different degradation pathways. Glucose and glucose-1-phosphate (G1P) from glycogen phosphorolysis can, on the one hand, pass through the OP in the mitochondria; on the other hand, these substances have the possibility of passing through glycolysis to pyruvate, to react under $\mathrm{NAD_{red}}$ consumption to lactate (Lac), which is released from the sarcosol into the interstitial space together with $\mathrm{H^+}$ via Lac/H cotransport. The simulation provides the metabolite concentrations by means of which the fluxes involved in the respective ATP production can be determined. In addition to OP, these are the fluxes through CAC and the ATP supplying part of glycolysis (J_{GAP}, from glyceraldehyde-3-phosphate to pyruvate), which has been contracted here to a single reaction step.

The ATP production rate via the metabolic pathway of Palm (PAL) is given by

$$J_{\mathrm{ATP}}^{\mathrm{palm}} = Q_{\mathrm{H}}^{\mathrm{palm}} \frac{J_{\mathrm{SY}}^{\mathrm{p}}}{Q_V} + \frac{8J_\beta}{Q_V} - 2J_{\mathrm{Pact}}\,(\mathrm{mM/s},\ 22.58\%), \tag{9.1}$$

and that via oxidative metabolism of Glu/Glgen by

$$J_{\mathrm{ATP}}^{\mathrm{glox}} = Q_{\mathrm{H}}^{\mathrm{gl}} \frac{J_{\mathrm{SY}}^{\mathrm{p}}}{Q_V} + \frac{J_{\mathrm{PDH}}}{Q_V} + \frac{J_{\mathrm{PDH}}}{Q_V J_{\mathrm{GAP}}} (2J_{\mathrm{GAP}} - J_{\mathrm{PFK}} - J_{\mathrm{HK}})\,(\mathrm{mM/s},\ 77.42\%) \tag{9.2}$$

where GAP represents glyceraldehyde-3-phosphate dehydrogenase, PFK phosphofructokinase and HK hexokinase).

The metabolic pathway of Glu/Glgen is made up of the paths $\mathrm{Glu_{ox}}$ and $\mathrm{Glgen_{ox}}$.

https://doi.org/10.1515/9783110650501-009

The ATP production rate via Glu_{ox} is given by

$$J_{\mathrm{ATP}}^{\mathrm{gluox}} = \frac{J_{\mathrm{HK}}}{J_{\mathrm{PGI}}}\left(Q_{\mathrm{H}}^{\mathrm{gl}}\frac{J_{\mathrm{SY}}^{\mathrm{p}}}{Q_V} + \frac{J_{\mathrm{PDH}}}{Q_V} + \frac{J_{\mathrm{PDH}}}{Q_V J_{\mathrm{GAP}}}(2J_{\mathrm{GAP}} - J_{\mathrm{PFK}})\right) - \frac{J_{\mathrm{PDH}}}{Q_V J_{\mathrm{GAP}}} J_{\mathrm{HK}}\ (\mathrm{mM/s},\ 8.06\%), \tag{9.3}$$

and that via $Glgen_{ox}$ by

$$J_{\mathrm{ATP}}^{\mathrm{glgox}} = \frac{J_{\mathrm{PGM}}}{J_{\mathrm{PGI}}}\left(Q_{\mathrm{H}}^{\mathrm{gl}}\frac{J_{\mathrm{SY}}^{\mathrm{p}}}{Q_V} + \frac{J_{\mathrm{PDH}}}{Q_V} + \frac{J_{\mathrm{PDH}}}{Q_V J_{\mathrm{GAP}}}(2J_{\mathrm{GAP}} - J_{\mathrm{PFK}})\right)\ (\mathrm{mM/s},\ 14.24\%). \tag{9.4}$$

In $J_{\mathrm{ATP}}^{\mathrm{glox}}$, $J_{\mathrm{ATP}}^{\mathrm{gluox}}$ and $J_{\mathrm{ATP}}^{\mathrm{glgox}}$, the ATP production via CAC is included.

The respective anoxic ATP production rates are

$$J_{\mathrm{ATP}}^{\mathrm{gluanox}} = \frac{J_{\mathrm{HK}}}{J_{\mathrm{PGI}}}\left(\frac{J_{\mathrm{LDH}}}{J_{\mathrm{GAP}}}(2J_{\mathrm{GAP}} - J_{\mathrm{PFK}})\right) - \frac{J_{\mathrm{LDH}}}{J_{\mathrm{GAP}}} J_{\mathrm{HK}}\ (\mathrm{mM/s},\ 15.46\%) \tag{9.5}$$

and

$$J_{\mathrm{ATP}}^{\mathrm{glganox}} = \frac{J_{\mathrm{LDH}}}{J_{\mathrm{GAP}}}\frac{J_{\mathrm{PGM}}}{J_{\mathrm{PGI}}}(2J_{\mathrm{GAP}} - J_{\mathrm{PFK}})\ (\mathrm{mM/s},\ 39.66\%), \tag{9.6}$$

where LDH represents lactate dehydrogenase, PGI phosphoglucose isomerase and PGM phosphoglucomutase. The fluxes $J_{\mathrm{ATP}}^{\mathrm{glox}}$ and $J_{\mathrm{ATP}}^{\mathrm{gluanox}} + J_{\mathrm{ATP}}^{\mathrm{glganox}}$ belong to the pathway denoted here with GLY.

The total ATP production rate then results as the sum of all these parallel fluxes:

$$J_{\mathrm{ATP}} = \frac{J_{\mathrm{AE}}}{Q_V} + 2J_{\mathrm{GAP}} - J_{\mathrm{PFK}} - J_{\mathrm{HK}} = 4.103\ \ (\mathrm{mM/s}). \tag{9.7}$$

Compared to the ATP production of OP, which is solely fed by oxidative input reactions, the reactions of Palm oxidation as well as of oxidative and anoxic Glu/Glgen metabolism contain the possibility to generate ATP without the direct participation of O_2. This occurs both in the CAC (J_{CAC}) of the mitochondrial matrix and in the second part of glycolysis (J_{GAP}) and is referred to as substrate-level phosphorylation.

The ATP production rate per substrate flux results in the ATP yield of a given metabolic pathway as follows:

$$\frac{J_{\mathrm{ATP}}^{\mathrm{palm}}}{J_\beta} = 102.89,\ \frac{J_{\mathrm{ATP}}^{\mathrm{gluox}}}{\frac{J_{\mathrm{PDH}}}{Q_V J_{\mathrm{GAP}}} J_{\mathrm{HK}}} = 30.588,\ \frac{J_{\mathrm{ATP}}^{\mathrm{glgox}}}{\frac{J_{\mathrm{PDH}}}{Q_V J_{\mathrm{GAP}}} J_{\mathrm{PGM}}} = 31.588,\ \frac{J_{\mathrm{ATP}}^{\mathrm{gluanox}}}{\frac{J_{\mathrm{LDH}}}{J_{\mathrm{GAP}}} J_{\mathrm{HK}}} = 2.0$$

and

$$\frac{J_{\mathrm{ATP}}^{\mathrm{glganox}}}{\frac{J_{\mathrm{LDH}}}{J_{\mathrm{GAP}}} J_{\mathrm{PGM}}} = 3.0.$$

In SMFs exist a number of ATP-consuming reactions that need the ATP delivered from the degradation of substrates to perform mechanical, chemical or electrochemical work. In all these coupled reactions, the affinity of ATP hydrolysis ($A^{c}_{ATP} > 0$) is used as an input potential. For muscle contraction, for example, this is coupled to a mechanical output potential. In addition to contraction, ATP splitting is required for chemical syntheses (e.g., protein biosynthesis and glycogen synthesis) as well as for ion transport (e.g., Na^+ and K^+ transport by Na/K ATPase or Ca^{2+} transport by SERCA). ATP hydrolysis always occurs in sarcosol. Its affinity is oppositely equal to the affinity of ATP synthesis of the ATP-producing reactions. Although the mitochondrial ATP production is determined by the reactants and products of the matrix, it is also given by the ATP potential of the sarcosol, as has already been shown (eq. (8.8)), by taking into account the associated transport affinities.

All ATP-splitting reactions proceeding in parallel in the sarcosol and being coupled to work are given by the flux

$$J_W = J_{Wb} + J_{ser} + J_{Str} + J_{Glgsy} + J_{Acc}.$$

where J_{Wb} denotes the sum of the fluxes by the Na/K ATPase and protein biosynthesis, J_{ser} the flux through SERCA, J_{Str} the flux through myosin ATPase of cross-bridges involved with stroking, J_{Glgsy} the flux through glycogen synthase and J_{Acc} the flux through acetyl coenzyme A (CoA) carboxylase.

The dissipation function Ψ_W is composed of

$$\Psi_W = \Psi^{ld}_W + \Psi^{p}_W, \text{ with } \Psi^{ld}_W = J_{Wb} A^{ld}_{Wb} + J_{ser} A^{ser}_{ca} + J_{Str} A^{ld}_{Str} + J_{Acc} A^{ld}_{Acc} \text{ and } \Psi^{p}_W = J_W A^{c}_{ATP}.$$

From these equations the dissipation functions Ψ^{Del} and Ψ^{Dem} of the total ATP production rate or the total consumption rate can be determined, from which the desired conductances L^{Del}_{c1} and L^{Dem}_{c2} can be obtained.

Ψ^{Del} equals the sum of dissipation functions, which are composed of all involved reactions of Palm oxidation and Glu/Glgen degradation:

$\Psi^{Del}_2 = \Psi_{ovt}$ describes the dissipation function without coupling to A^{c}_{ATP}; hence, Ψ^{Del}_1 is given by $\Psi^{Del}_1 = J_{ATP}\left(-A^{c}_{ATP}\right)$.

The transformed affinity related to J_{ATP} is given by $\bar{A}_{ovt} = \Psi_{ovt}/J_{ATP}$, and the corresponding transformed conductance is

$$\bar{L}^{Del}_{c} = \frac{J_{ovt}\left(-A^{c}_{ATP}\right) + \Psi_{ovt}}{\left(\left(-A^{c}_{ATP}\right) + \bar{A}_{ovt}\right)^2}. \tag{9.8}$$

The corresponding flux is then

$$J_{ovt} = J_{ATP} = \bar{L}^{Del}_{c}\left(\left(-A^{c}_{ATP}\right) + \bar{A}_{ovt}\right) \tag{9.9}$$

from which the partial conductances are

$$\bar{L}_{c1}^{Del} = \bar{L}_{c}^{Del} \frac{\left(-A_{ATP}^{c}\right) + \bar{A}_{ovt}}{\left(-A_{ATP}^{c}\right)} \; (<0) \tag{9.10}$$

and

$$\bar{L}_{c2}^{Del} = \bar{L}_{c}^{Del} \frac{\left(-A_{ATP}^{c}\right) + \bar{A}_{ovt}}{\bar{A}_{ovt}} \; (>0). \tag{9.11}$$

From $\Psi^{Dem} = \Psi_W = \Psi_W^{ld} + J_W A_{ATP}^{c}$, one obtains

$$\bar{A}_{W}^{ld} = \frac{\Psi_W^{ld}}{J_W}$$

and

$$\bar{L}_{c}^{Dem} = \frac{\Psi_W^{ld} + J_W A_{ATP}^{c}}{\left(\bar{A}_{W}^{ld} + A_{ATP}^{c}\right)^2}. \tag{9.12}$$

The corresponding flux is

$$J_W = J_{ATP} = \bar{L}_{c}^{Dem} \left(\bar{A}_{W}^{ld} + A_{ATP}^{c}\right), \tag{9.13}$$

from which

$$\bar{L}_{c1}^{Dem} = \bar{L}_{c}^{Dem} \; \frac{\bar{A}_{W}^{ld} + A_{ATP}^{c}}{\bar{A}_{W}^{ld}} \; (<0) \tag{9.14}$$

and

$$\bar{L}_{c2}^{Dem} = \bar{L}_{c}^{Dem} \; \frac{\bar{A}_{W}^{ld} + A_{ATP}^{c}}{A_{atp}^{c}} \; (>0) \tag{9.15}$$

are obtained.

Both partial conductances are at SSC (only after about 6.0 s, Figure 9.1C) with $\bar{L}_{c1}^{Del} = -7.1334 \times 10^{-5}$ and $\bar{L}_{c2}^{Dem} = 7.1334 \times 10^{-5}\,\mathrm{mM/s \times mol/J}$ again oppositely equal. For this situation, it becomes particularly apparent that the potentials of the cycle ($-A_{ATP}^{c}$ and A_{ATP}^{c}) must be oppositely equal at each point in time, since cycling is always connected with a change of sign of these potentials.

Figure 9.1 shows that the entire ATP production via PAL and GLY reaches an SSC (B). From this time on, ATP production and ATP consumption proceed at the same rates ($J_W = J_{ATP}$). Since the affinities of this ATP cycle are oppositely equal ($-A_{ATP}$ and A_{ATP}), the dissipation functions of the cycle must vanish ($J_W A_{ATP} + J_{ATP}(-A_{ATP}) = 0$).

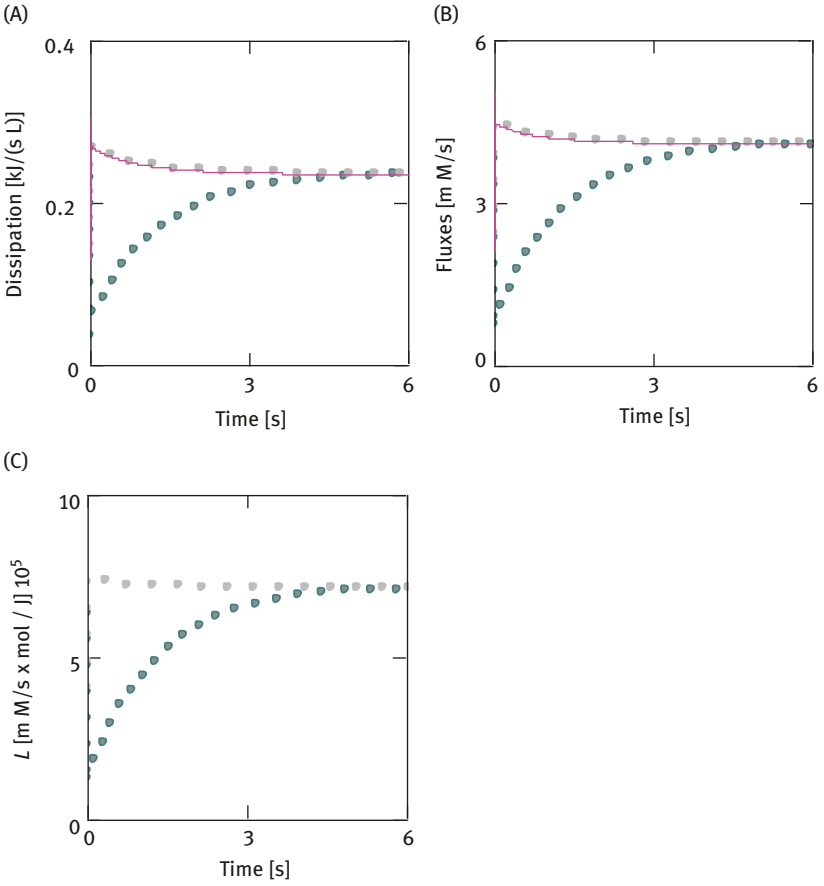

Figure 9.1: Dissipation functions, fluxes and conductances of PAL plus GLY. (A) Dissipation functions (gray points, Ψ_W^p; green points, $-\Psi_1^{Del}$; red line, ATP production by the PCr reaction is included). (B) Fluxes (gray points, J_W; green points, $J_{ovt} = J_{ATP}$; red line, $J_{ATP} + J_{PCr}$). (C) Conductances (gray points, L_{c2}^{Dem}; green points, $-L_{c1}^{Del}$).

Since the resistances also disappear, ATP synthesis coupled to metabolism as well as ATP splitting coupled to work taken as a whole occur without dissipation ($\Sigma \Delta_{Ri} S = 0$). This cycle is driven by the sum of the input potential ($\bar{A}_{ovt} > 0$) and the output potential ($\bar{A}_W^{ld} < 0$), which are both related to the ATP turnover rate.

The respective efficiencies of ATP production are

$$\eta_{ATPc}^{Del} = -\frac{\left(J_{atpc}^{palm} + J_{atpc}^{gl}\right)\left(-A_{ATP}^{c}\right)}{\Psi_{ov}^{palm} + \Psi_{ov}^{gl}} = 0.6146,$$

$$\eta_{\mathrm{ATPc}}^{\mathrm{palm}} = -\frac{\left(J_{\mathrm{atpc}}^{\mathrm{palm}}\right)\left(-A_{\mathrm{ATP}}^{\mathrm{c}}\right)}{\Psi_{\mathrm{ov}}^{\mathrm{palm}}} = 0.5954,$$

$$\eta_{\mathrm{ATPc}}^{\mathrm{glox}} = -\frac{\left(J_{\mathrm{atpc}}^{\mathrm{gluox}} + J_{\mathrm{atpc}}^{\mathrm{glgox}}\right)\left(-A_{\mathrm{ATP}}^{\mathrm{c}}\right)}{\Psi_{\mathrm{ov}}^{\mathrm{gluox}} + \Psi_{\mathrm{ov}}^{\mathrm{glgox}}} = 0.5942,$$

$$\eta_{\mathrm{ATPc}}^{\mathrm{gluox}} = -\frac{\left(J_{\mathrm{atpc}}^{\mathrm{gluox}}\right)\left(-A_{\mathrm{ATP}}^{\mathrm{c}}\right)}{\Psi_{\mathrm{ov}}^{\mathrm{gluox}}} = 0.5846,$$

$$\eta_{\mathrm{ATPc}}^{\mathrm{glgox}} = -\frac{\left(J_{\mathrm{atpc}}^{\mathrm{glgox}}\right)\left(-A_{\mathrm{ATP}}^{\mathrm{c}}\right)}{\Psi_{\mathrm{ov}}^{\mathrm{glgox}}} = 0.5998,$$

$$\eta_{\mathrm{ATPc}}^{\mathrm{glanox}} = -\frac{\left(J_{\mathrm{atpc}}^{\mathrm{gluanox}} + J_{\mathrm{atpc}}^{\mathrm{glganox}}\right)\left(-A_{\mathrm{ATP}}^{\mathrm{c}}\right)}{\Psi_{\mathrm{ov}}^{\mathrm{gluanox}} + \Psi_{\mathrm{ov}}^{\mathrm{glganox}}} = 0.6317,$$

$$\eta_{\mathrm{ATPc}}^{\mathrm{gluanox}} = -\frac{\left(J_{\mathrm{atpc}}^{\mathrm{gluanox}}\right)\left(-A_{\mathrm{ATP}}^{\mathrm{c}}\right)}{\Psi_{\mathrm{ov}}^{\mathrm{gluanox}}} = 0.5064 \text{ and}$$

$$\eta_{\mathrm{ATPc}}^{\mathrm{glganox}} = -\frac{\left(J_{\mathrm{atpc}}^{\mathrm{glganox}}\right)\left(-A_{\mathrm{ATP}}^{\mathrm{c}}\right)}{\Psi_{\mathrm{ov}}^{\mathrm{glganox}}} = 0.6991.$$

The activation of energy metabolism occurs in the SMF by an increase in the Ca^{2+} concentration of sarcosol. As described in Chapter 7, this occurs via depolarizations of the sarcolemma, which are triggered and controlled by nerve impulses. Most of the work reactions (J_{W}) and the muscular contraction are activated by $\left[Ca^{2+}\right]_{\mathrm{c}}$, so that with this activation also an increased ATP consumption begins, which is accompanied by an increase of $[\mathrm{ADP}]_{\mathrm{c}}$ and $[\mathrm{P_i}]$. The former is connected via the near-equilibrium reaction of adenylate kinase

$$2\,\mathrm{ADP}^{3-} \rightleftharpoons \mathrm{ATP}^{4-} + \mathrm{AMP}^{2-} \tag{R9.1}$$

with $[\mathrm{ATP}]_{\mathrm{c}}$ and $[\mathrm{AMP}]_{\mathrm{c}}$. The subsequent increase in $[\mathrm{AMP}]_{\mathrm{c}}$ now activates the PFK of glycolysis, which in turn leads to activation of both anoxic and oxidative Glu/Glgen degradation. The fatty acid metabolism (here Palm) is known to be not significantly affected by this activation through $[\mathrm{AMP}]_{\mathrm{c}}$. The ATP demand under these conditions must thus be covered mainly by ATP delivery via GLY.

At moderate power output ($\left[Ca^{2+}\right]_{\mathrm{c}} = 1.136\,\mu\mathrm{M}$), the ATP production and consumption rate, as already mentioned, is 4.103 mM/s. This would mean that even at this submaximal consumption rate, most of the ATP ($[\mathrm{ATP}]_{c} = 9.0\,\mathrm{mM}$) would be consumed within 2.0 s if this could not be resynthesized fast enough from splitting products. However, especially under conditions of high power output, ATP

production via GLY and PAL degradation pathways is no longer capable of doing this because the activation of all these reaction steps, which must occur, takes too much time to increase the ATP delivery rate (J_{ATP}) sufficiently to cover the ATP demand rate (J_W). In this short period of time between increased ATP demand and insufficient ATP delivery by the metabolism after a sudden switch from low power to high power output, ATP is supplied by the creatine kinase (CK) catalyzed reaction

$$PCr^{2-} + MgADP^{-} + H^{+} \rightleftharpoons Cr + MgATP^{2-} \qquad \text{(R9.2)}$$

(chemical notation, see Chapter 10). This buffers a significant decrease in $[ATP]_c$ and is shown in Figure 9.1. The solid line in red coincides practically from the beginning with the ATP demand rate, if the additional (parallel) ATP production via the PCr reaction has been taken into account. Apparently, this reaction ensures that $[ATP]_c$ does not drop significantly. This is achieved, on the one hand, by a high $[PCr]$ ($[MgPCr] + [PCr^{2-}] + [Cr] = 40.0\,mM$) and on the other by a high L_c^{pcr}.

However, this buffering of $[ATP]_c$ is not the only task of the PCr system. This latter system can also significantly increase the availability of ATP at locations of its consumption. Since ATP is not synthesized exactly where it is needed, in order to drive muscle contraction or Ca^{2+} transport, for example. There is a spatial distance between locations of production and consumption, which the ATP molecule has to overcome by diffusion. In the intracellular space, however, this diffusion process is apparently hindered by structural proteins of the cytoskeleton even for molecules of the size of the ATP, so that the diffusion path can become the limiting factor. The sarcosol itself, that is, the aqueous protein solution that surrounds these structures is not critical to this impediment of diffusion.

This particularly concerns cells with very high power output, such as fast skeletal muscle fibers, which have a very high turnover of ATP. But the too slow diffusion rate of ATP can be counterbalanced by a reaction cycle. It is the PCr shuttle, which does fulfil this task. This shuttle can be described as follows:

At sites of ATP production, PCr^{2-} is formed from Cr and $MgATP^{2-}$ according to

$$MgATP^{2-} + Cr_p \rightleftharpoons PCr_p{}^{2-} + MgADP^{-} + H^{+} \qquad \text{(R9.3)}$$

(index "p" indicates sites of ATP production).

The product $MgADP^{-}$ can be incorporated directly into the ATP synthesis coupled to metabolism according to $MgADP^{-} + H_2PO_4{}^{-} \rightarrow MgATP^{2-} + H_2O$.

In this way, $MgATP^{2-}$ and $MgADP^{-}$ are recycled by both reactions, while PCr^{2-}, Cr and $H_2PO_4{}^{-}$ form chemical potential differences between the sites of ATP production and ATP consumption. These respective potential differences are associated with corresponding concentration gradients that drive the diffusion of these substances.

PCr^{2-} can thus reach a site of ATP consumption via diffusion, where it reacts with $MgADP^{-}$ to $MgATP^{2-}$ and Cr. Reaction (R9.3) proceeds at this location in the opposite direction, according to

$$PCr_u^{2-} + MgADP^- + H^+ \rightleftharpoons MgATP^{2-} + Cr_u$$

(index "u" indicates sites of ATP utilization).

This is possible because, on the one hand, the value of the equilibrium constant of this reaction is relatively low ($K'_{PCr} = 177$), and, in addition, the concentrations of the reactants are close to their equilibrium concentrations.

The $MgATP^{2-}$ formed here can now be split again by the respective ATP coupled work reaction, thereby $MgADP^-$ and $H_2PO_4^-$ are produced according to $MgATP^{2-} + H_2O \rightarrow MgADP^- + H_2PO_4^-$.

Also at sites of ATP utilization, $MgATP^{2-}$ and $MgADP^-$ are recycled just as at sites of ATP production, while PCr^{2-}, Cr and $H_2PO_4^-$ take part in gradient formation. Diffusion proceeds in the direction of the negative gradient, which means PCr^{2-} diffuses from sites of ATP production to sites of ATP utilization, while Cr and HPO_4^{2-} diffuse from here into the opposite direction to sites of ATP production. At sites of ATP utilization, HPO_{4u}^{2-} is formed from $H_2PO_4^-$ of the ATP splitting reaction by release of a proton, which is taken up by the PCr reaction. At sites of ATP production, however, $H_2PO_4^-$ is required for ATP synthesis. It arises from the incoming HPO_{4p}^{2-} and the proton released at this site by the reverse PCr reaction.

PCr^{2-} and Cr thereby go through a cycle, the PCr shuttle. At SSC, also this reaction cycle must proceed without dissipation as follows:

$$\Phi_{cyc} = J \times RT \left(\begin{array}{c} \ln\left(\frac{[MgADP^-]_p [HPO_4^{2-}]_p [H^+]_p}{[MgATP^{2-}]_p} \frac{1}{K_{MgATP1}}\right) + \ln\left(\frac{[Cr]_p [MgATP^{2-}]_p}{[PCr^{2-}]_p [MgADP^-]_p [H^+]_p} \frac{1}{K_{PCr}}\right) \\ + \ln\left(\frac{[PCr^{2-}]_p}{[PCr^{2-}]_u}\right) \\ + \ln\left(\frac{[PCr^{2-}]_u [MgADP^-]_u [H^+]_u}{[Cr]_u [MgATP^{2-}]_u} K_{PCr}\right) + \ln\left(\frac{[MgATP^{2-}]_u}{[MgADP^-]_u [HPO_4^{2-}]_u [H^+]_u} K_{MgATP1}\right) \\ + \ln\left(\frac{[HPO_4^{2-}]_u}{[HPO_4^{2-}]_p}\right) + \ln\left(\frac{[Cr]_u}{[Cr]_p}\right) \end{array} \right) \equiv 0 \tag{9.16}$$

All affinities of the above formulation are given in chemical notation. The ATP splitting and synthesis reactions have been modified; instead of $H_2PO_4^-$, HPO_4^{2-} and H^+ are introduced. The interrelation is given by

$$[H_2PO_4^-] = [HPO_4^{2-}][H^+]/Kp1_H.$$

The resulting new equilibrium constant is K_{MgATP1}. A_{ATP} does not change as a result of this action (see Chapter 10). However, the equation can be simplified

because the potential difference for proton diffusion, $RT\ln([H^+]_u/[H^+]p)$ and $RT\ln([H_2PO_4^-]_u/[H_2PO_4^-]_p)$, can be replaced by $RT\ln([HPO_4^{2-}]_u/[HPO_4^{2-}]_p)$.

For the diffusion processes, the chemical potential difference of the respective substance was used, for example

$$\Delta\mu = -A_{PCr}^{dif} = RT\ln\left(\frac{[PCr^{2-}]_p}{[PCr^{2-}]_u}\right).$$

From this the potential gradient needed for the diffusional flux is obtained for the case of only one dimension by

$$-\operatorname{grad}(\mu(c)) = -\frac{d(\mu(c))}{dx}\vec{i} = -\frac{d(\mu(c))}{dc}\frac{dc}{dx}\vec{i} = -\frac{1}{c}\frac{dc}{dx}\vec{i} \approx -\frac{1}{\bar{c}}\frac{\Delta c}{\Delta x}$$

where Δx represents magnitude of the path coordinate toward $\vec{i}$ of the diffusion path, and $\bar{c}$ the mean concentration in the range Δx.

From this formula, it can be seen that as Δx decreases, the driving force for diffusion $\Delta c/\Delta x$, increases. This also seems to be essential for muscle cells. As can be seen on electron micrographs, locations of high ATP production such as mitochondria are frequent in the immediate vicinity of sites of high ATP demand such as myofibrils. Such a spatial arrangement ensures that diffusion paths are as short as possible, so that also as high as possible diffusional fluxes can be generated.

For further explanation, the PCr shuttle is described for the situation of increased ATP demand at the location of contracting myofibrils, and ATP delivery via mitochondrial metabolism (GLY plus PAL). The increased ATP demand is triggered by the Ca^{2+}-activated ATP splitting (contraction mechanism, see Chapter 11) in myofibrils. When $MgADP^-$ is combined with HPO_4^{2-} and H^+, $MgATP^{2-}$ is obtained. Since $MgATP^{2-}$ itself cannot diffuse fast enough from mitochondria into the myofibril, this is provided by the PCr reaction in myofibrils. One proton from ATP splitting is consumed by this reaction. Besides $MgATP^{2-}$ from PCr^{2-} and $MgADP^-$ derived from ATP splitting, Cr is obtained. By this initial ATP buffering, in the myofibrils $[PCr^{2-}]$ becomes decreased, while [Cr] and $[HPO_4^{2-}]$ increase. By this way, the gradients for these substances increase so that PCr^{2-} can now increasingly diffuse from the mitochondrion into the fibril, whereas Cr and HPO_4^{2-} diffuse in the opposite direction. In order for PCr^{2-} to be not used up as an ATP supplier in the fibrils, it has to be constantly replenished. This is accomplished by PCr^{2-} synthesis from $MgATP^{2-}$ and Cr in the intermembrane space (IMS) of the mitochondrion. This compartment communicates with the sarcosol via VDAC pores that are well permeable to Cr and HPO_4^{2-}. The resulting $MgADP^-$ is exchanged between ADP^{3-} and ATP^{4-} from the matrix via ATP/ADP-Ex of the inner membrane. Mg^{2+} becomes merely exchanged between ADP^{3-} and ATP^{4-}. The released proton can be taken up by the diffusion delivered HPO_4^{2-} and then be transported as $H_2PO_4^-$ together with an additional proton from the IMS by H/P symport into the matrix. There, the proton taken up from the IMS is

released into the matrix. $MgADP^-$ (after taking up a Mg^{2+} ion from $MgATP^{2-}$ of the matrix), HPO_4^{2-} and a proton from $H_2PO_4^-$ enter into ATP formation via ATP synthase and CaC. As already explained, mitochondrial ATP synthesis and transport energetically correspond to the ATP synthesis outside the inner membrane and can thus be treated as if this reaction were to take place in the IMS or the sarcosol. Therefore, the cycle is closed and can be treated based on eq. (9.16).

One of the tasks of the PCr shuttle is to replace the poorer diffusion properties of $MgATP^{2-}$ and $MgADP^-$ with the better properties in this effect of PCr^{2-} and Cr. These two substances in the shuttle take over the exchange via diffusion of cleaved ATP against resynthesized ATP. An additional and very important task of the PCr system is that with PCr^{2-} and Cr significantly higher gradients can be generated than with ATP and ADP species. It can be assumed that $MgATP^{2-}$ is present as well in fibrils, in the sarcosol and in the IMS under resting conditions in a concentration of 7.2 mM ([ATP] = 9.0 mM, pH = 7.0, pMg = 3.1). The concentrations of PCr^{2-} and Cr under these conditions are 17.3 and 22.3 mM, respectively. When switching to high power output, however, these resting concentrations in the fibrils can change significantly in contrast to the ATP concentration. For example, $[PCr^{2-}]$ can decrease to 7.3 mM here, while [Cr] must increase at that location by the same amount. Such a strong reduction of $[MgATP^{2-}]$ is not possible, however. But even a moderate drop of only a few millimolar is not tolerated by the SMF (see Chapter 11). The generation of a sufficiently high $MgATP^{2-}$ gradient would thus be impossible, which makes the existence of the PCr shuttle absolutely necessary, even if the diffusional properties of ATP would be sufficient to allow a direct supply.

This assessment is supported by the fact that cell types with far less power output like liver cells possess neither a PCr shuttle nor the required enzyme (CK). Obviously, in these cells the supply of ATP can occur directly via ATP/ADP diffusion. Although liver cells have no fibrils whose structural peculiarities are responsible for the hindered diffusion, they have, like SMFs, a cell membrane that is stabilized at its inner aspect by a cytoskeleton. This network of protein filaments certainly also restricts the diffusibility of ATP-sized molecules, so that undersupply could easily occur if the ATP-coupled ion pumps located in the cell membrane (e.g., the Na/K ATPase) would have a too large ATP consumption. Obviously, this is not the case. It can be concluded that although structures of this type represent a diffusion hindrance for ATP, they are not completely inaccessible for these and similar compounds. The ATP consumption rate may not exceed a certain threshold to allow delivery. In this respect, it should also be considered that such cells may tolerate a much greater reduction of their $[ATP]_c$. Thus, such cells would be able to create high gradients for this compound with the result that also in this way a sufficiently high diffusion flux may be generated.

10 ATP species, pH and pMg

10.1 Biochemical versus chemical notation

Weak acids such as lactic acid may occur in different forms, both as undissociated acid LacH and as lactate anion Lac^-. The relationship between both molecular species is described by the law of mass action. This dissociation reaction is described by

$$LacH + H_2O \rightleftharpoons Lac^- + H_3O^+$$

or displayed simplified as

$$LacH \rightleftharpoons Lac^- + H^+.$$

At equilibrium

$$\frac{[Lac^-]_{eq}[H^+]_{eq}}{[LacH]_{eq}} = K_{Diss} (= \text{dissociation constant in mol/L}).$$

Given the total concentration $[Lac] = [Lac^-] + [LacH]$ and known K_{Diss}, $[Lac^-]$ and $[LacH]$ can be calculated (the index "eq" has been omitted for simplicity). For example,

$$[Lac] = [Lac^-]\left(1 + \frac{[LacH]}{[Lac^-]}\right) = [Lac^-]\left(1 + \frac{[H^+]}{K_{Diss}}\right)$$

and

$$[Lac] = [LacH]\left(\frac{[Lac^-]}{[LacH]} + 1\right) = [LacH]\left(\frac{K_{Diss}}{[H^+]} + 1\right).$$

The result from this is

$$[Lac^-] = \frac{[Lac]}{\left(1 + \frac{[H^+]}{K_{Diss}}\right)}$$

and

$$[LacH] = \frac{[Lac]}{\left(\frac{K_{Diss}}{[H^+]} + 1\right)} (\text{both concentrations in mol/L}).$$

With $K_{Diss} = 1.38 \times 10^{-4}$, $[Lac] = 5 \times 10^{-3}$ and $[H^+] = 10^{-7}\text{mol/L} (pH = 7.0)$ the result is $[Lac^-] = 4.996379 \times 10^{-3}$ and $[LacH] = 3.62 \times 10^{-6}\text{mol/L}$.

At a weighed total concentration of, for example, 5.0 mM lactic acid and a pH = 7.0, lactic acid is almost completely dissociated. If $[H^+] = K_{Diss}$, $[Lac]$ is present at 50.0% as $[Lac^-] = 2.5\text{mM}$.

https://doi.org/10.1515/9783110650501-010

Species formation of phosphoric acid offers more possibilities. The total concentration is given as follows:

$$[\mathrm{P_i}] = \mathrm{H_3PO_4} + \mathrm{H_2PO_4^-} + \mathrm{HPO_4^{2-}} + \mathrm{PO_4^{3-}} + \mathrm{MgHPO_4} + \mathrm{MgPO_4^-}.$$

For further simplification, the concentration brackets of the various species have been omitted. Only the total concentration is indicated by this. In sarcosol, the concentrations of $\mathrm{H^+}$ and $\mathrm{Mg^{2+}}$ are present in certain concentration ranges. For $\mathrm{H^+}$ this lies between pH = 6.0 and pH = 8.0. For this pH range, three P_i species can be neglected, which leads to

$$[\mathrm{P_i}] = \mathrm{H_2PO_4^-} + \mathrm{HPO_4^{2-}} + \mathrm{MgHPO_4}\ \mathrm{mol/L}.$$

The corresponding constants are

$$K\mathrm{p1_H} = \frac{\mathrm{HPO_4^{2-}}\ \mathrm{H^+}}{\mathrm{H_2PO_4^-}} \text{ and } K\mathrm{p2_{Mg}} = \frac{\mathrm{HPO_4^{2-}}\ \mathrm{Mg^{2+}}}{\mathrm{MgHPO_4}}.$$

Thus, the following three conditional equations can be established:

$$[\mathrm{P_i}] = \mathrm{H_2PO_4^-}\left(1 + \frac{\mathrm{HPO_4^{2-}}}{\mathrm{H_2PO_4^-}} + 1 + \frac{\mathrm{MgHPO_4}}{\mathrm{H_2PO_4^-}}\right) = \mathrm{H_2PO_4^-}\left(1 + \frac{\mathrm{Kp1_H}}{\mathrm{H^+}} + \frac{\mathrm{Mg^{2+}}}{\mathrm{Kp2_{Mg}}}\frac{\mathrm{Kp1_H}}{\mathrm{H^+}}\right),$$

$$[\mathrm{P_i}] = \mathrm{HPO_4^{2-}}\left(\frac{\mathrm{H_2PO_4^-}}{\mathrm{HPO_4^{2-}}} + 1 + \frac{\mathrm{MgHPO_4}}{\mathrm{HPO_4^{2-}}}\right) = \mathrm{HPO_4^{2-}}\left(\frac{\mathrm{H^+}}{K\mathrm{p1_H}} + 1 + \frac{\mathrm{Mg^{2+}}}{K\mathrm{p2_{Mg}}}\right)$$

and

$$[\mathrm{P_i}] = \mathrm{MgHPO_4}\left(\frac{\mathrm{H_2PO_4^-}}{\mathrm{MgHPO_4}} + \frac{\mathrm{HPO_4^{2-}}}{\mathrm{MgHPO_4}} + 1\right) = \mathrm{MgHPO_4}\left(\frac{K\mathrm{p2_{Mg}}}{\mathrm{Mg^{2+}}}\frac{\mathrm{H^+}}{K\mathrm{p1_H}} + \frac{K\mathrm{p2_{Mg}}}{\mathrm{Mg^{2+}}} + 1\right).$$

The terms in parentheses are somewhat similar to polynomials. Hence, the description $P_{\mathrm{H_2PO_4}}$ for the polynomial has arisen by excluding $\mathrm{H_2PO_4^-}$. The species of phosphoric acid can thus be determined as follows:

$$[\mathrm{H_2PO_4^-}] = \frac{[\mathrm{P_i}]}{P_{\mathrm{H_2PO_4}}}\left[\mathrm{HPO_4^{2-}}\right] = \frac{[\mathrm{P_i}]}{P_{\mathrm{HPO_4}}} \text{ and } [\mathrm{MgHPO_4}] = \frac{[\mathrm{P_i}]}{P_{\mathrm{MgHPO_4}}}\ (\mathrm{mol/L}).$$

They are functions of the respective polynomials with the variables $[\mathrm{H^+}]$ and $\left[\mathrm{Mg^{2+}}\right]$. For pH = 7.0, $[\mathrm{Mg^{2+}}] = 0.8 \times 10^{-3}$ and $[P_i] = 4 \times 10^{-3}\mathrm{mol/L}$, the result is $[\mathrm{H_2PO_4^-}] = 1.4314\,(35.79\,\%)$, $\left[\mathrm{HPO_4^{2-}}\right] = 2.4937\,(62.34\,\%)$ and $[\mathrm{MgHPO_4}] = 75\ 10\text{^}{-3}$ (1.88%) mM.

You can also obtain the respective species by exclusion. For example, you obtain

$$[\mathrm{P_i}] = \mathrm{H_2PO_4}^- \left(1 + \frac{K\mathrm{p1_H}}{\mathrm{H}^+} + \frac{\mathrm{Mg}^{2+}}{K\mathrm{p2_{Mg}}} \frac{K\mathrm{p1_H}}{\mathrm{H}^+}\right)$$

from exclusion of $\frac{K\mathrm{p1_H}}{\mathrm{H}^+}$

$$[\mathrm{P_i}] = \mathrm{H_2PO_4}^- \left(\frac{K\mathrm{p1_H}}{\mathrm{H}^+}\right) \left(\frac{\mathrm{H}^+}{K\mathrm{p1_H}} + 1 + \frac{\mathrm{Mg}^{2+}}{K\mathrm{p2_{Mg}}}\right) = \mathrm{HPO_4}^{2-} \left(\frac{\mathrm{H}^+}{K\mathrm{p1_H}} + 1 + \frac{\mathrm{Mg}^{2+}}{K\mathrm{p2_{Mg}}}\right)$$

of from

$$\frac{\mathrm{Mg}^{2+}}{K\mathrm{p2_{Mg}}} \frac{K\mathrm{p1_H}}{\mathrm{H}^+}$$

$$\begin{aligned}[\mathrm{P_i}] &= \mathrm{H_2PO_4}^- \left(\frac{\mathrm{Mg}^{2+}}{K\mathrm{p2_{Mg}}} \frac{K\mathrm{p1_H}}{\mathrm{H}^+}\right) \left(\frac{K\mathrm{p2_{Mg}}}{\mathrm{Mg}^{2+}} \frac{\mathrm{H}^+}{K\mathrm{p1_H}} + \frac{K\mathrm{p2_{Mg}}}{\mathrm{Mg}^{2+}} + 1\right) \\ &= \mathrm{MgHPO_4} \left(\frac{K\mathrm{p2_{Mg}}}{\mathrm{Mg}^{2+}} \frac{\mathrm{H}^+}{K\mathrm{p1_H}} + \frac{K\mathrm{p2_{Mg}}}{\mathrm{Mg}^{2+}} + 1\right)\end{aligned}$$

ATP species in the pH range 6.0–8.0 and pMg range 4–3.5 are

$$[\mathrm{ATP}] = \mathrm{ATP}^{4-} + \mathrm{HATP}^{3-} + \mathrm{H_2ATP}^{2-} + \mathrm{MgATP}^{2-} + \mathrm{MgHATP}^- + \mathrm{Mg_2ATP}.$$

The result is

$$\begin{aligned}[\mathrm{ATP}] &= \mathrm{ATP}^{4-} \left(1 + \frac{\mathrm{H}^+}{K\mathrm{at1_H}} + \frac{(\mathrm{H}^+)^2}{K\mathrm{at1_H}\,K\mathrm{at2_H}} + \frac{\mathrm{Mg}^{2+}}{K\mathrm{at3_{Mg}}} + \frac{\mathrm{Mg}^{2+}\,\mathrm{H}^+}{K\mathrm{at4_{Mg}}\,K\mathrm{at1_H}} + \frac{\left(\mathrm{Mg}^{2+}\right)^2}{K\mathrm{at3_{Mg}}\,K\mathrm{at5_{Mg}}}\right). \\ &= \left[\mathrm{ATP}^{4-}\right] P_{\mathrm{ATP}}\end{aligned}$$

Excluding $\mathrm{Mg}^{2+}/K\mathrm{at3_{Mg}}$ the following is obtained:

$$\begin{aligned}[\mathrm{ATP}] &= \mathrm{ATP}^{4-} \left(\frac{\mathrm{Mg}^{2+}}{K3_{\mathrm{Mg}}}\right) \\ &\left(\frac{K\mathrm{at3_{Mg}}}{\mathrm{Mg}^{2+}} + \frac{\mathrm{H}^+}{K\mathrm{at1_H}} \frac{K\mathrm{at3_{Mg}}}{\mathrm{Mg}^{2+}} + \frac{(\mathrm{H}^+)^2}{K\mathrm{at1_H}\,K\mathrm{at2_H}} \frac{K\mathrm{at3_{Mg}}}{\mathrm{Mg}^{2+}} + 1 + \frac{\mathrm{H}^+}{K\mathrm{at1_H}} \frac{K\mathrm{at3_{Mg}}}{K\mathrm{at4_{Mg}}} + \frac{\mathrm{Mg}^{2+}}{K\mathrm{at5_{Mg}}}\right) \\ &= \left[\mathrm{MgATP}^{2-}\right] P_{\mathrm{MgATP}}\end{aligned}$$

For the ADP species, the result is

$$[\mathrm{ADP}] = \mathrm{ADP}^{3-} + \mathrm{HADP}^{2-} + \mathrm{H_2ADP}^- + \mathrm{MgADP}^- + \mathrm{MgHADP}, \text{ and from there}$$

$$\begin{aligned}[\mathrm{ADP}] &= \mathrm{ADP}^{3-} \left(1 + \frac{\mathrm{H}^+}{K\mathrm{ad1_H}} + \frac{(\mathrm{H}^+)^2}{K\mathrm{ad1_H}\,K\mathrm{ad2_H}} + \frac{\mathrm{Mg}^{2+}}{K\mathrm{ad3_{Mg}}} + \frac{\mathrm{H}^+}{K\mathrm{ad1_H}} \frac{\mathrm{Mg}^{2+}}{K\mathrm{ad4_{Mg}}}\right) \\ &= \left[\mathrm{ADP}^{3-}\right] P_{\mathrm{MgADP}}\end{aligned}$$

or

$$[\mathrm{ADP}] = \mathrm{ADP}^{3-}\left(\frac{\mathrm{Mg}^{2+}}{K\mathrm{ad3}_{\mathrm{Mg}}}\right)\left(\frac{K\mathrm{ad3}_{\mathrm{Mg}}}{\mathrm{Mg}^{2+}} + \frac{\mathrm{H}^{+}}{K\mathrm{ad1}_{\mathrm{H}}}\frac{K\mathrm{ad3}_{\mathrm{Mg}}}{\mathrm{Mg}^{2+}} + \frac{(\mathrm{H}^{+})^{2}}{K\mathrm{ad1}_{\mathrm{H}}\,K\mathrm{ad2}_{\mathrm{H}}}\frac{K\mathrm{ad3}_{\mathrm{Mg}}}{\mathrm{Mg}^{2+}} + 1 + \frac{\mathrm{H}^{+}}{K\mathrm{ad1}_{\mathrm{H}}}\frac{K\mathrm{ad3}_{\mathrm{Mg}}}{K\mathrm{ad4}_{\mathrm{Mg}}}\right) = [\mathrm{MgADP}^{-}]P_{\mathrm{MgADP}}$$

According to this pattern, all other species can be determined.

In biochemistry, the equilibrium constant of a reaction is defined as follows:

For the ATP cleavage

$$\mathrm{ATP} + \mathrm{H_2O} \rightarrow \mathrm{ADP} + \mathrm{P_i},$$

$K'_{\mathrm{ATP}} = \frac{[\mathrm{ADP}]_{\mathrm{eq}}[\mathrm{P_i}]_{\mathrm{eq}}}{[\mathrm{ATP}]_{\mathrm{eq}}}$ is valid (the above index on K indicates the biochemical notation).

The concentration brackets thus contain the sum of all species concentrations that come into question for this substance. On the other hand, only specific species involved in the reaction appear in the chemical notation, for example,

$$\mathrm{ATP}^{4-} + \mathrm{H_2O} \rightarrow \mathrm{ADP}^{3-} + \mathrm{HPO_4}^{2-} + \mathrm{H}^{+}$$

results in

$$K_{\mathrm{ATP1}} = \frac{\left[\mathrm{ADP}^{3-}\right]_{\mathrm{eq}}\left[\mathrm{HPO_4}^{2-}\right]_{\mathrm{eq}}[\mathrm{H}^{+}]_{\mathrm{eq}}}{\left[\mathrm{ATP}^{4-}\right]_{\mathrm{eq}}}.$$

Care must be taken with this formulation because in addition to the conservation of mass, the electrical charge is also maintained.

Both constants are related to each other. This can be recognized if, for example, for [ADP] the corresponding expression $[\mathrm{ADP}] = \mathrm{ADP}^{3-}\,P_{\mathrm{ADP}}$ is used. This leads to

$$K'_{\mathrm{ATP}} = \frac{\left[\mathrm{ADP}^{3-}\right]_{\mathrm{eq}}\left[\mathrm{HPO_4}^{2-}\right]_{\mathrm{eq}}}{\left[\mathrm{ATP}^{4-}\right]_{\mathrm{eq}}}\,\frac{P_{\mathrm{ADP}}\,P_{\mathrm{HPO_4}}}{P_{\mathrm{ATP}}} = \frac{K_{\mathrm{ATP1}}}{[\mathrm{H}^{+}]}\,\frac{P_{\mathrm{ADP}}\,P_{\mathrm{HPO_4}}}{P_{\mathrm{ATP}}}.$$

$$\text{For } \mathrm{ATP}^{4-} + \mathrm{H_2O} \rightarrow \mathrm{ADP}^{3-} + \mathrm{H_2PO_4}^{-},$$

$$K_{\mathrm{ATP}} = \frac{\left[\mathrm{ADP}^{3-}\right]_{\mathrm{eq}}\left[\mathrm{H_2PO_4}^{2-}\right]_{\mathrm{eq}}}{\left[\mathrm{ATP}^{4-}\right]_{\mathrm{eq}}}$$

is valid, and

$$K'_{\mathrm{ATP}} = \frac{\left[\mathrm{ADP}^{3-}\right]_{\mathrm{eq}}[\mathrm{H_2PO_4}^{-}]_{\mathrm{eq}}}{\left[\mathrm{ATP}^{4-}\right]_{\mathrm{eq}}}\,\frac{P_{\mathrm{ADP}}\,P_{\mathrm{H_2PO_4}}}{P_{\mathrm{ATP}}} = K_{\mathrm{ATP}}\,\frac{P_{\mathrm{ADP}}\,P_{\mathrm{H_2PO_4}}}{P_{\mathrm{ATP}}}.$$

Another possibility is given through

$\mathrm{MgATP^{2-} + H_2O \rightarrow MgADP^{-} + H_2PO_4{}^{-}}$ with

$$K_{\mathrm{MgATP}} = \frac{[\mathrm{MgADP^{-}}]_{\mathrm{eq}}[\mathrm{H_2PO_4{}^{-}}]_{\mathrm{eq}}}{[\mathrm{MgATP^{2-}}]_{\mathrm{eq}}}.$$

The relationship with K'_{ATP} at this time is

$$K'_{\mathrm{ATP}} = \frac{[\mathrm{MgADP^{-}}]_{\mathrm{eq}}[\mathrm{H_2PO_4{}^{-}}]_{\mathrm{eq}}}{[\mathrm{MgATP^{2-}}]_{\mathrm{eq}}} \frac{P_{\mathrm{MgADP}} P_{\mathrm{H_2PO_4}}}{P_{\mathrm{MgATP}}} = K_{\mathrm{MgATP}} \frac{P_{\mathrm{MgADP}} P_{\mathrm{H_2PO_4}}}{P_{\mathrm{MgATP}}}.$$

Furthermore, with $K_{\mathrm{ATP}} = K_{\mathrm{Ref}}$ as the reference constant the result is

$$K_{\mathrm{MgATP}} \frac{P_{\mathrm{MgADP}} P_{\mathrm{H_2PO_4}}}{P_{\mathrm{MgATP}}} = \frac{K_{\mathrm{ATP}}}{[\mathrm{H^{+}}]} \frac{P_{\mathrm{ADP}} P_{\mathrm{HPO_4}}}{P_{\mathrm{ATP}}},$$

from which

$$K_{\mathrm{MgATP}} = K_{\mathrm{ATP}} \frac{P_{\mathrm{ADP}} P_{\mathrm{HPO_4}}}{[\mathrm{H^{+}}] P_{\mathrm{ATP}}} \frac{P_{\mathrm{MgATP}}}{P_{\mathrm{MgADP}} P_{\mathrm{H_2PO_4}}} = K_{\mathrm{Ref}} \frac{K\mathrm{at3_{Mg}}}{K\mathrm{ad3_{Mg}}\, K\mathrm{p1_H}}$$

is obtained.

For the reaction, $\mathrm{MgATP^{2-} + H_2O \rightarrow MgADP^{-} + HPO_4{}^{2-} + H^{+}}$ the result is

$$K_{\mathrm{MgATP1}} = \frac{[\mathrm{MgADP^{-}}]_{\mathrm{eq}} [\mathrm{HPO_4{}^{2-}}]_{\mathrm{eq}} [\mathrm{H^{+}}]}{[\mathrm{MgATP^{2-}}]_{\mathrm{eq}}}$$

and

$$K'_{\mathrm{ATP}} = \frac{[\mathrm{MgADP^{-}}]_{\mathrm{eq}} [\mathrm{HPO_4{}^{2-}}]_{\mathrm{eq}}}{[\mathrm{MgATP^{2-}}]_{\mathrm{eq}}} \frac{P_{\mathrm{MgADP}} P_{\mathrm{HPO_4}}}{P_{\mathrm{MgATP}}} = \frac{K_{\mathrm{MgATP1}}}{[\mathrm{H^{+}}]} \frac{P_{\mathrm{MgADP}} P_{\mathrm{HPO_4}}}{P_{\mathrm{MgATP}}}.$$

$$K_{\mathrm{MgATP1}} = K_{\mathrm{ATP}} \frac{P_{\mathrm{ADP}}}{P_{\mathrm{MgADP}}} \frac{P_{\mathrm{MgATP}}}{P_{\mathrm{ATP}}} = K_{\mathrm{Ref}} \frac{K\mathrm{at3_{Mg}}}{K\mathrm{ad3_{Mg}}}.$$

The $\Delta_{\mathrm{R}}G$ values of the different ATP splitting reactions must be identical. This is demonstrated by the following example:

$$A_{\mathrm{ATP}} = -\Delta_{\mathrm{R}}G = RT \ln\left(\frac{[\mathrm{ATP}]}{[\mathrm{ADP}][\mathrm{P_i}]} K'_{\mathrm{ATP}}\right) = RT \ln\left(\frac{[\mathrm{ATP}]}{[\mathrm{ADP}][\mathrm{P_i}]} \frac{[\mathrm{ADP}]_{\mathrm{eq}}[\mathrm{P_i}]_{\mathrm{eq}}}{[\mathrm{ATP}]_{\mathrm{eq}}}\right). \quad (10.1)$$

If the total concentrations are replaced by the corresponding polynomial expressions such as $[\mathrm{ATP}]/P_{\mathrm{MgATP}} = [\mathrm{MgATP^{2-}}]$ the result is obtained for example for the $Mg\mathrm{ATP^{2-}}$ reaction

$$A_{\mathrm{MgATP}} = RT\,\ln\left(\frac{[\mathrm{ATP}]}{[\mathrm{ADP}][P_i]}\,\frac{P_{\mathrm{MgADP}}\,P_{\mathrm{H_2PO_4}}}{P_{\mathrm{MgATP}}}\,\frac{[\mathrm{ADP}]_{\mathrm{eq}}[P_i]_{\mathrm{eq}}}{[\mathrm{ATP}]_{\mathrm{eq}}}\,\frac{P_{\mathrm{MgATP}}}{P_{\mathrm{MgADP}}\,P_{\mathrm{H_2PO_4}}}\right)$$
$$= RT\,\ln\left(\frac{[\mathrm{MgATP}^{2-}]}{[\mathrm{MgADP}^{-}][\mathrm{H_2PO_4}^{-}]}\,K_{\mathrm{MgATP}}\right) \tag{10.2}$$

Since the two polynomial terms stand out, A_{ATP} must be equal to A_{SPEC} (as, e.g., $A_{\mathrm{SPEC}} = A_{\mathrm{MgATP}}$). All the possible affinities in chemical notation must always be identical to the affinity in biochemical notation, which contains the total concentrations and K'.

In Chapter 8 it has been shown that

$$A^{\mathrm{m}}_{\mathrm{ATP}} + A^{\mathrm{p}}_{\mathrm{HPAE}} = -A^{\mathrm{c}}_{\mathrm{ATP}}.$$

The derivation contains $A^{\mathrm{m}}_{\mathrm{ATP}}$ and $A^{\mathrm{c}}_{\mathrm{ATP}}$ regarding K_{ATP}, without the participation of Mg^{2+} ions. The PCr shuttle, on the other hand, has been formulated for affinities regarding K_{MgATP1} . Therefore, the exchange reactions between $MgATP^{2-}$ and ADP^{3-} in the matrix and $MgADP^{-}$ and ATP^{4-} in the IMS must be taken into account. The following is valid for the matrix

$$\mathrm{MgATP}^{2-} + \mathrm{ADP}^{3-} \rightleftharpoons \mathrm{ATP}^{4-} + \mathrm{MgADP}^{-}$$

The result from this is

$$K^{\mathrm{m}}_{\mathrm{Mgex}} = \frac{[\mathrm{ATP}^{4-}]_{\mathrm{eqm}}[\mathrm{MgADP}^{-}]_{\mathrm{eqm}}}{[\mathrm{MgATP}^{2-}]_{\mathrm{eqm}}[\mathrm{ADP}^{3-}]_{\mathrm{eqm}}} = \frac{[\mathrm{ATP}]_{\mathrm{eqm}}}{P_{\mathrm{ATPm}}}\,\frac{[\mathrm{ADP}]_{\mathrm{eqm}}}{P_{\mathrm{MgADPm}}}\,\frac{P_{\mathrm{MgATPm}}}{[\mathrm{ATP}]_{\mathrm{eqm}}}\,\frac{P_{\mathrm{ADPm}}}{[\mathrm{ADP}]_{\mathrm{eqm}}}.$$
$$= \frac{P_{\mathrm{MgATPm}}}{P_{\mathrm{ATPm}}}\,\frac{P_{\mathrm{ADPm}}}{P_{\mathrm{MgADPm}}} = \frac{K\mathrm{at3}}{K\mathrm{ad3}}$$

As

$$\Gamma = \frac{[\mathrm{MgATP}^{2-}]_m[\mathrm{ADP}^{3-}]_m}{[\mathrm{ATP}^{4-}]_m[\mathrm{MgADP}^{-}]_m} = \frac{P_{\mathrm{ATPm}}}{P_{\mathrm{MgATPm}}}\frac{P_{\mathrm{MgADPm}}}{P_{\mathrm{ADPm}}} = \frac{K\mathrm{ad3}}{K\mathrm{at3}},$$

this leads to

$$A^{\mathrm{m}}_{\mathrm{Mgex}} = RT\,\ln\left(\Gamma_{\mathrm{m}}\,K^{\mathrm{m}}_{\mathrm{Mgex}}\right) = 0.$$

The same applies to the reaction occurring in the reverse direction in the IMS

$$\mathrm{ATP}^{4-} + \mathrm{MgADP}^{-} \rightleftharpoons \mathrm{MgATP}^{2-} + \mathrm{ADP}^{3-}.$$

Their affinity must also be zero. This is the reason why in the derivation of the relation $A^{\mathrm{m}}_{\mathrm{ATP}} + A^{\mathrm{p}}_{\mathrm{HPAE}} = -A^{\mathrm{c}}_{\mathrm{ATP}}$ (Chapter 8) of the Mg^{2+} exchange need not be considered.

To support the above derivations, numerical values are given for the differently formulated but identical ATP affinities. At moderate power output ($[Ca^{2+}]_c$ = 1.136μM), the simulation results ($SIM_{GLY/PAL}$, [13–15]) for $[H^+]_c = 0.079258\ 10^{-6}$ (pH = 7.101) and $[Mg^{2+}]_c = 0.8172\ 10^{-3}$mol/L. The calculation from there is K'_{ATP} $(0.0793\times\ 10^{-6}, 0.8172\ \times 10^{-3}) = 4.92569\ \times 10^5$. The total concentrations are therefore [ATP] = 8.8845, [ADP] = 0.1147 and $[P_i]$ = 7.8426 mM. This leads to

$$A_{ATP} = RT\ \ln\left(\frac{8.8845\times 10^{-3}}{0.1147\ \times 10^{-3}\times 7.8426\times\ 10^{-3}}\times 4.92569\times 10^5\right) = 57.519\ \text{kJ/mol}$$

(biochemical notation).

For chemical notation with $K_{ATP} = K_{ref} = 0.109174$, $[ATP^{4-}] = 1.082831\ \times 10^{-3}$, $[ADP^{3-}] = 0.058094\times 10^{-3}$ and $[HPO_4{}^{2-}] = 5.2789\times\ 10^{-3}$mol/L, the result is

$$A_{ATP} = RT\ \ln\left(\frac{1.082831\times 10^{-3}}{0.058094\times 10^{-3}\times 5.2789\times 10^{-3}\times 0.079258\times 10^{-6}}\times 0.109174\right)$$
$$= 57.519\text{kJ/mol}.$$

For $K_{ATP1} = 6.266559\ \times 10^5$, $[ATP^{4-}] = 1.082831\ \times 10^{-3}$, $[ADP^{3-}] = 0.058094\ \times 10^{-3}$ and $[H_2PO_4{}^-] = 2.401562\ \times 10^{-3}$mol/L, the result is

$$A_{ATP} = RT\ \ln\left(\frac{1.082831\times 10^{-3}}{0.058094\times 10^{-3}\times 2.401562\times 10^{-3}}\times 6.266559\times 10^5\right) = 57.519\ \text{kJ/mol}.$$

For $K_{MgATP} = 6.827661\ \times 10^4$ as well as $[MgATP^{2-}] = 7.200128\times\ 10^{-3}$, $[MgADP^-] =\ 0.0421$ and $[H_2PO_4{}^-] = 2.401562$mol/L, the result is

$$A_{ATP} = RT\ \ln\left(\frac{7.200128\times 10^{-3}}{0.0421\times 10^{-3}\times 2.401562\times 10^{-3}}\times 6.827661\times 10^4\right) = 57.519\text{kJ/mol}.$$

For $K_{MgATP1} = 0.011895$ as well as $[MgATP^{2-}] = 7.200128\ \times 10^{-3}$, $[MgADP^-] = 0.0421$ and $[HPO_4{}^{2-}] = 5.2789\ \times 10^{-3}$mol/L the following is obtained:

$$A_{ATP} = RT\ \ln\left(\frac{7.200128\times 10^{-3}}{0.0421\times 10^{-3}\times 5.2789\times 10^{-3}\times 0.079258\times 10^{-6}}\times 0.011895\right)$$
$$= 57.519\text{kJ/mol}$$

The calculations demonstrate that both notations lead to the same results. For simulations, especially the following formulation is advantageous because, on the one hand, easily manageable total concentrations can be used, and on the other hand the functional dependence of $[H^+]$ and $[Mg^{2+}]$ is ensured:

$$A_{\mathrm{MgATP}} = RT\,\ln\left(\frac{[\mathrm{ATP}]}{[\mathrm{ADP}][P_i]}\,\frac{P_{\mathrm{MgADP}}\,P_{\mathrm{H_2PO_4}}}{P_{\mathrm{MgATP}}}\,K_{\mathrm{MgATP}}\right)$$

with

$$K'_{\mathrm{ATP}}\left(\mathrm{H}^+, \mathrm{Mg}^{2+}\right) = K_{\mathrm{MgATP}}\,\frac{P_{\mathrm{MgADP}}\,P_{\mathrm{H_2PO_4}}}{P_{\mathrm{MgATP}}}.$$

$$A_{\mathrm{ATP}} = RT\,\ln\left(\frac{8.8845\times10^{-3}}{0.1147\ 10^{-3}\times\ 7.8426\ 10^{-3}}\,\times\,\frac{2.725972\times3.26563}{1.23394}\times6.827661\times10^{4}\right)$$
$$= 57.519\,\mathrm{kJ/mol},$$

and

$$K'_{\mathrm{ATP}}\left(0.079258\times10^{-6},\ 0.8172\times10^{-3}\right) = \frac{2.725972\times3.26563}{1.23394}\times6.827661\times10^{4}$$
$$= 4.925681\times10^{5}$$

(for comparison, $K'_{\mathrm{ATP}}\left(10^{-7.0}, 0.8\times10^{-3}\right) = 4.351127\ \times10^{5}$).

If changes in these variables occur as a result of changing metabolism, these changes are automatically taken into account in A_{ATP}.

10.2 Ion activities

Up to now, concentrations have always been used as the starting point for the calculation of $\Delta_R G$ or affinities and the associated K_{eq}. Strictly speaking, however, this is only acceptable when the other parameters besides the temperature are also given. Therefore, in aqueous electrolyte solutions, the ionic strength I_{Ion} is exceedingly important. It is defined as

$$I_{\mathrm{Ion}} = \frac{1}{2}\sum z_i^2 c_i\ (c = \text{ion concentration in mol}/L,\ z = \text{charge number}). \qquad (10.3)$$

A physiological NaCl solution (150.0 mM) has, for example, an ionic strength of $I_{\mathrm{Ion}} = \frac{1}{2}(1.0\times0.15 + 1.0\times0.15) = 0.15\mathrm{mol}/L$.

A Krebs–Ringer bicarbonate (KRB) solution has the following composition (in mM, pH = 7.4 at 310.15 K): 143.0 Na^+, 5.0 K^+, 1.2 Mg^{2+}, 1.2 Ca^{2+}, 124.65 Cl^-, 24.0 HCO_3^-, 0.1794 $H_2PO_4^-$, 0.7852 HPO_4^{2-} (0.0354 $MgPO_4$), 1.2 SO_4^{2-}.

Its ionic strength is

$$I_{\mathrm{Ion}} = \frac{1}{2}\begin{pmatrix}1.0\times143.0 + 1.0\times5.0 + 4.0\times1.2 + 4.0\times1.2 + 1.0\times124.65 + 1.0\times24.0\\ +\,1.0\times0.18 + 4.0\times0.785 + 4.0\times1.2\end{pmatrix}$$
$$= 0.1572\,\mathrm{mol}/L.$$

The influence of I_{Ion} on the concentration is described according to Debye and Hückel [4, 16] using the following approximation formula: $a = \gamma c$, whereby γ is linked via

$$\ln(\gamma) = -Az^2(I_{\text{ion}})^{\frac{1}{2}} \tag{10.4}$$

to the ionic strength. At the same time, a is the activity of the relevant ion (in mol/L), γ the dimensionless activity coefficient and A is a temperature-dependent constant in $(\text{mol/L})^{-\frac{1}{2}}$ [16]. But this approximation only applies to very dilute electrolyte solutions. For ionic strengths such as those calculated for cells (0.2–0.25 mol/L), eq. (10.4) must be expanded. An expanded form is (Alberty, Goldberg and Tewari, 1991)

$$\ln(\gamma) = -Az^2(I_{\text{ion}})^{\frac{1}{2}} \frac{1}{1 + B\,(I_{\text{ion}})^{\frac{1}{2}}} \tag{10.5}$$

with $B = 1.6\,(\text{mol}/L)^{-\frac{1}{2}}$.

The activity of a monovalent ion in KRB is calculated using the above formula with

$$\ln(\gamma) = -\frac{1.2 \times 1.0^2 \times (0.157.2)^{\frac{1}{2}}}{1 + 1.6 \times (0.157.2)^{\frac{1}{2}}} = -0.2913 \text{ and } \gamma = \text{e}^{-0.2913} = 0.7473$$

to

$$a_K = \gamma[\text{K}^+]_{\text{e}} = 0.7473 \times 0.005 = 0.00374\,\text{mol/L (at 310.15K)}.$$

The formula does not differentiate between cations and anions. The type of ion is also not taken into consideration. Likewise, γ can thus be applied to, for example $[\text{H}^+]$, $[\text{K}^+]$ or $[\text{Cl}^-]$ to obtain the corresponding ionic activity. The charge number, however, considerably influences γ and therefore, the ionic activity.

In the sarcosol, $I_{\text{Ion}} = 0.25\text{mol}/L$. Under these conditions, the results are

$$\ln(\gamma) = -\frac{1.2 \times 1.0^2 \times (0.25)^{\frac{1}{2}}}{1 + 1.6 \times (0.25)^{\frac{1}{2}}} = -0.3336 \text{ and } \gamma = \text{e}^{-0.3336} = 0.7164$$

as well as

$$a_{\text{K}} = \gamma[\text{K}^+]_{\text{c}} = 0.7164 \times 0.15 = 0.1075\text{mol/L}.$$

For $[\text{Ca}^{2+}] = 3.0\,\mu\text{M}$ with

$$\ln(\gamma) = -\frac{1.2 \times 2.0^2 \times (0.25)^{\frac{1}{2}}}{1 + 1.6 \times (0.25)^{\frac{1}{2}}} = -1.3342\,(I_{\text{Ion}} = 0.25\text{mol/L}) \text{ and } \gamma = \text{e}^{-1.3342} = 0.2634,$$

one obtains

$$a_{\text{Ca}} = \gamma\left[\text{Ca}^{2+}\right]_c = 0.2634 \times 0.3 \times 10^{-6} = 0.079 \times 10^{-6}\text{mol/L}.$$

Differences between activity and concentration are also noticeable when determining the equilibrium constants. When calculating $\Delta_R G$s or affinities for chemical and biochemical reactions, this is, however, superfluous, because respective γs are factored out again. However, often when determining $\Delta_R G$, a tabulated K_{eq} value is taken. When doing this, care must be taken that the ionic strengths match. If this is not the case, the tabulated value must be recalculated for the desired ionic strength with the aid of the activity coefficients.

The activity of H^+ in this context, however, possesses a special position, because the proton concentration of an electrolyte solution is determined generally using a pH electrode. During such an electrochemical measurement, it must be assumed that the result of the measurement, the pH value, results from the H^+ activity, because the pH value is defined as

$$\mathrm{pH} = \log\left(\frac{1}{a_H}\right).$$

Therefore, it has become accepted, especially in biochemistry, that the equilibrium constants of reactions involving protons can be defined by proton activity. This results in so-called mixed constants. They include all the reactants except protons in concentration units; however, the latter, as activity.

Such mixed constants are also used here in all the simulations, so that the proton concentration of the sarcosol or the mitochondrial matrix generated by a simulation is also obtained as H^+ activity or as pH. To convert the proton concentration into activity

$a_H = \gamma_H\,[H^+]$ can be used.

For $I_{Ion} = 0.25\mathrm{mol}/L$ and $T = 310.15\mathrm{K}$, $\gamma_H = 0.7164$.

For the pH value, the following relation with the p[H] value gives

$\mathrm{pH} = p[H] - \log(\gamma_H) = p[H] + 0.14486$ with $\log(\gamma_H) = -0.14486$.

For the determination of $\Delta\mu_{Ca}$ at the sarcolemma, for example, different γ_{Ca}s emerge because the corresponding ionic strengths in the sarcosol and interstitial space have different values. One assumes that in the sarcosol $I_c = 0.25$ and in the interstitium $I_e = 0.163\mathrm{mol/L}$, thus giving a concentration of

$$\Delta\mu_{Ca} = RT\,\ln\left(\frac{[Ca]_c}{[Ca]_e}\right) = RT\,\ln\left(\frac{0.3\times10^{-6}}{1.2\times10^{-3}}\right) = -2.1388\times10^4$$

and for ionic activities

$$\Delta\mu^a_{Ca} = RT\,\ln\left(\frac{\gamma^c_{Ca}[Ca]_c}{\gamma E[Ca]_e}\right) = \Delta\mu_{Ca} + RT\,\ln\left(\frac{0.2634}{0.308}\right) = (-21.388 - 0.4034)\,10^4$$

$$= -20.985\ \mathrm{kJ/mol}.$$

The relative error is approximately –2.0%.

Finally, the following can be determined about the effect of the ionic strength on the ionic concentration: In an electrolyte solution, the ionic concentrations of all the present and freely moving ions have an effect on the concentration of one specific ion in such a way that the "effective" concentration of this ion is reduced by a specific factor, the activity coefficient ($\gamma_{\mathrm{Ion}} < 1.0$). This effective concentration is the ionic activity.

10.3 H^+ and Mg^{2+} binding

The reaction equation commonly used in biochemistry for ATP hydrolysis ($ATP^{4-} + H_2O \rightarrow ADP^{3-} + HPO_4{}^{2-} + H^+$) has a proton as product. This must not be interpreted, however, to the effect that H^+ is also created as a product during every reaction run. ATP cleavage itself does not create protons, as it emerged from the biochemical notation. The chemical formulation using protons presents only one of several equivalent formulation possibilities, as has already been shown. These relate primarily to the energetic consideration of the reaction.

To record a possible proton, change through the products created and the reactants depleted during ATP cleavage, the proton binding on products and reactants must be determined before and after a reaction run. This is possible via the calculation of the individual species. For example

$$\frac{[\mathrm{HATP}^{3-}]}{[\mathrm{ATP}]} = \frac{1}{P_{\mathrm{HATP}}} = \frac{1}{\frac{K\mathrm{at1_H}}{[\mathrm{H}^+]}\,P_{\mathrm{ATP}}} = \frac{\frac{[\mathrm{H}^+]}{K\mathrm{at1_H}}}{P_{\mathrm{ATP}}} = 0.04191,$$

or

$$\frac{[\mathrm{MgATP}^{2-}]}{[\mathrm{ATP}]} = \frac{\frac{[\mathrm{Mg}^{2+}]}{K3\mathrm{at_{Mg}}}}{P_{\mathrm{ATP}}} = 0.808 \;\; (\mathrm{pH} = \; 7.1,\; [\mathrm{Mg}^{2+}] = 0.8\; 10^{-3} \;\hat{=}\; \mathrm{pMg} = \; 3.0969)$$

The expressions give the proportion of respective ATP species in the sum of all the relevant species in the given pH and Mg range. This leads to

$$\frac{\sum(\mathrm{ATP\;\; species})}{[\mathrm{ATP}]} = 1 = \frac{\frac{[\mathrm{H}^+]}{K1\mathrm{at_H}} + \frac{[\mathrm{H}^+]^2}{K\mathrm{at1_H}K\mathrm{at2_H}} + \frac{[\mathrm{Mg}^{2+}]}{K3\mathrm{at_{Mg}}} + \frac{[\mathrm{H}^+][\mathrm{Mg}^{2+}]}{K1\mathrm{at_H}\,K4\mathrm{at_{Mg}}} + \frac{[\mathrm{Mg}^{2+}]^2}{K3\mathrm{at_{Mg}}\,K5\mathrm{at_{Mg}}}}{P_{\mathrm{ATP}}}.$$

By counting the hydrogen atoms bound to the respective species, one obtains

$$N_{\mathrm{H}}^{\mathrm{ATP}} = \frac{1\times\frac{[\mathrm{H}^+]}{K1\mathrm{at}_{\mathrm{H}}} + 2\times\frac{[\mathrm{H}^+]^2}{K\mathrm{at}1_{\mathrm{H}}K\mathrm{at}2_{\mathrm{H}}} + 0\times\frac{[\mathrm{Mg}^{2+}]}{K3\mathrm{at}_{\mathrm{Mg}}} + 1\times\frac{[\mathrm{H}^+][\mathrm{Mg}^{2+}]}{K1\mathrm{at}_{\mathrm{H}}\,K4\mathrm{at}_{\mathrm{Mg}}} + 0\times\frac{[\mathrm{Mg}^{2+}]^2}{K3\mathrm{at}_{\mathrm{Mg}}\,K5\mathrm{at}_{\mathrm{Mg}}}}{P_{\mathrm{ATP}}}$$

$$= \frac{1\times\frac{[\mathrm{H}^+]}{K1\mathrm{at}_{\mathrm{H}}} + 2\times\frac{[\mathrm{H}^+]^2}{K\mathrm{at}1_{\mathrm{H}}K\mathrm{at}2_{\mathrm{H}}} + 1\times\frac{[\mathrm{H}^+][\mathrm{Mg}^{2+}]}{K1\mathrm{at}_{\mathrm{H}}\,K4\mathrm{at}_{\mathrm{Mg}}}}{P_{\mathrm{ATP}}}.$$

Only the dissociable H atoms of the phosphate residues were counted.

One can see that the result of the numerator can be obtained also through differentiation of P_{ATP} with respect to $[\mathrm{H}^+]$ and subsequent multiplication with $[\mathrm{H}^+]$. It is in fact

$$\frac{\partial(P_{\mathrm{ATP}})}{\partial[\mathrm{H}^+]}\,[\mathrm{H}^+] = \frac{[\mathrm{H}^+]}{K1\mathrm{at}_{\mathrm{H}}} + \frac{2\,[\mathrm{H}^+]^2}{K\mathrm{at}1_{\mathrm{H}}K\mathrm{at}2_{\mathrm{H}}} + \frac{[\mathrm{H}^+][\mathrm{Mg}^{2+}]}{K1\mathrm{at}_{\mathrm{H}}\,K4\mathrm{at}_{\mathrm{Mg}}}.$$

Thus, for N_{H} there is

$$N_{\mathrm{H}}^{\mathrm{ATP}} = \frac{\partial(P_{\mathrm{ATP}})}{P_{\mathrm{ATP}}}\,\frac{[\mathrm{H}^+]}{\partial[\mathrm{H}^+]} = \frac{d\ln(P_{\mathrm{ATP}})}{d\ln([\mathrm{H}^+])}. \tag{10.6}$$

N_{H} is a function of $[\mathrm{H}^+]$ and $[\mathrm{Mg}^{2+}]$. For pH = 7.1 and $[\mathrm{Mg}^{2+}] = 0.8\times10^{-3}$, one obtains, for example,

$$N_{\mathrm{H}}^{\mathrm{ATP}}\left(10^{-7.1}, 0.8\times10^{-3}\right) = 0.0448.$$

This result shows that for the given values, the proportion of hydrogen bound to ATP is 0.0448. This number changes at different pH and Mg^{2+} values. For example, $N_{\mathrm{H}}^{\mathrm{ATP}}(10^{-7.4}, 0.8\times10^{-3}) = 0.023$, $N_{\mathrm{H}}^{\mathrm{ATP}}(10^{-6.8}, 0.8\times10^{-3}) = 0.0857$ and $N_{\mathrm{H}}^{\mathrm{ATP}}(10^{-6.8}, 1.5\times10^{-3}) = 0.052$.

In the same way, the binding proportion of $N_{\mathrm{H}}^{\mathrm{ADP}}$ and $N_{\mathrm{H}}^{P_i}$ can be determined. One then obtains from the difference between products and reactants, the changes caused by the reaction to bound hydrogen $\Delta_{\mathrm{R}}N_{\mathrm{H}}^{\mathrm{ATP}} = N_{\mathrm{H}}^{\mathrm{ADP}} + N_{\mathrm{H}}^{\mathrm{Pi}} - N_{\mathrm{H}}^{\mathrm{ATP}} - 1$.

The two hydrogen atoms of the reactant H_2O are also included in the count. But as one hydrogen atom is bound during hydrolysis by the resulting phosphate and is no longer involved in consecutive reactions (in the considered pH range), only one hydrogen atom of H_2O has to be counted. This fact is taken into consideration through the occurrence of "–1" (instead of "–2") in the above formula.

The different N_{H}s can be expressed through their differential quotients. This leads to

$$\Delta_{\mathrm{R}}N_{\mathrm{H}}^{\mathrm{ATP}} = [\mathrm{H}^+]\;\frac{\partial\left(\ln\left(\frac{P_{\mathrm{ADP}}\,P_{\mathrm{HPO_4}}}{P_{\mathrm{ATP}}}\right)\right)}{\partial([\mathrm{H}^+])} - 1. \tag{10.7}$$

The logarithmic argument can be expressed through

$$\frac{P_{\mathrm{ADP}}\,P_{\mathrm{HPO_4}}}{P_{\mathrm{ATP}}} = K'_{\mathrm{ATP}}\;\frac{[\mathrm{H}^+]}{K^{\mathrm{ref}}_{\mathrm{ATP}}}.$$

Taking the logarithm leads to

$$\ln\left(\frac{P_{\mathrm{ADP}}\,P_{\mathrm{HPO_4}}}{P_{\mathrm{ATP}}}\right) = \ln\left(K'_{\mathrm{ATP}}\right) + \ln([\mathrm{H}^+]) - \ln\left(K^{\mathrm{ref}}_{\mathrm{ATP}}\right)$$

and

$$[\mathrm{H}^+]\;\frac{\partial\left(\ln\left(\frac{P_{\mathrm{ADP}}\,P_{\mathrm{HPO_4}}}{P_{ATP}}\right)\right)}{\partial([\mathrm{H}^+])} = \frac{\partial\left(\ln\left(K'_{\mathrm{ATP}}\right)\right)}{\partial(\ln([\mathrm{H}^+]))} + 1,$$

where K_{Ref} is independent of $[\mathrm{H}^+]$ and $[\mathrm{Mg}^{2+}]$.

This consequently gives

$$\Delta_{\mathrm{R}}N^{\mathrm{ATP}}_{\mathrm{H}} = \frac{\partial\left(\ln\left(K'_{\mathrm{ATP}}\right)\right)}{\partial(\ln([\mathrm{H}^+]))}. \tag{10.8}$$

For example, one finds for

$$\Delta_{\mathrm{R}}N^{\mathrm{ATP}}_{\mathrm{H}}\left(10^{-7.1}, 0.8\times10^{-3}\right) = 0.128055 + 0.306821 - 1.0 - 0.044797 \;=\; -\;0.61.$$

$\frac{\partial\left(\ln\left(K'_{\mathrm{ATP}}\left(10^{-7.1}, 0.8\times10^{-3}\right)\right)\right)}{\partial(\ln([\mathrm{H}^+]))}$ is also equal to −0.61.

The negative result means that at pH = 7.1 and $[\mathrm{Mg}^{2+}] = 0.8\mathrm{mM}$, 0.61 mol H^+ per $\xi = 1.0\mathrm{mol}$ of reaction extension (ATP cleavage) is released from the reaction. The minus also shows, therefore, a reduction in bound hydrogen atoms. These no longer bound atoms appear as protons in the surrounding media and there reduce its pH. A positive $\Delta_{\mathrm{R}}N_{\mathrm{H}}$ would result in an increase in pH.

In a similar manner, one can find the Mg^{2+} binding for ATP

$$N^{\mathrm{ATP}}_{\mathrm{Mg}} = \frac{\partial(P_{\mathrm{ATP}})}{P_{\mathrm{ATP}}}\;\frac{[\mathrm{Mg}^{2+}]}{\partial([\mathrm{Mg}^{2+}])} = \frac{d\ln(P_{\mathrm{ATP}})}{d\ln([\mathrm{Mg}^{2+}])}. \tag{10.9}$$

For $\Delta_{\mathrm{R}}N^{\mathrm{ATP}}_{\mathrm{Mg}}$, one sees

$$\Delta_{\mathrm{R}}N^{\mathrm{ATP}}_{\mathrm{Mg}} = N^{\mathrm{ADP}}_{\mathrm{Mg}} + N^{\mathrm{Pi}}_{\mathrm{Mg}} - N^{\mathrm{ATP}}_{\mathrm{Mg}} = \left[\mathrm{Mg}^{2+}\right]\;\frac{\partial\left(\ln\left(\frac{P_{\mathrm{ADP}}\,P_{\mathrm{HPO_4}}}{P_{\mathrm{ATP}}}\right)\right)}{\partial([\mathrm{Mg}^{2+}])}. \tag{10.10}$$

With

$$\ln\left(\frac{P_{\mathrm{ADP}}\,P_{\mathrm{HPO_4}}}{P_{\mathrm{ATP}}}\right) = \ln\left(K'_{\mathrm{ATP}}\right) + \ln([\mathrm{H}^+]) - \ln(K_{\mathrm{Ref}})$$

it results in

$$\frac{\partial\left(\ln\left(\frac{P_{\mathrm{ADP}}\,P_{\mathrm{HPO_4}}}{P_{\mathrm{ATP}}}\right)\right)}{\partial([\mathrm{Mg^{2+}}])} = \frac{\partial\left(\ln\left(K'_{\mathrm{ATP}}\right)\right)}{\partial([\mathrm{Mg^{2+}}])}$$

and for $\Delta_{\mathrm{R}}N_{\mathrm{Mg}}^{\mathrm{ATP}}$

$$\Delta_{\mathrm{R}}N_{\mathrm{Mg}}^{\mathrm{ATP}} = \frac{\partial\left(\ln\left(K'_{\mathrm{ATP}}\right)\right)}{\partial(\ln([\mathrm{Mg^{2+}}]))}. \tag{10.11}$$

For example

$$\Delta_{\mathrm{R}}N_{\mathrm{Mg}}^{\mathrm{ATP}}\left(10^{-7.1}, 0.8\times10^{-3}\right) = -0.47276.$$

This means that $[\mathrm{Mg^{2+}}]$ must also increase during ATP cleavage. The pH can also be influenced by the PCr reaction. For PCr + ADP $\rightleftharpoons$ ATP + Cr applies that

$$\Delta_{\mathrm{R}}N_{\mathrm{H}}^{\mathrm{PCr}} = N_{\mathrm{H}}^{\mathrm{ATP}} - N_{\mathrm{H}}^{\mathrm{ADP}} - \left(N_{\mathrm{H}}^{\mathrm{PCr}} - 1\right) = 0.0448 - 0.12806 - \left(2.2127\times\ 10^{-3} - 1.0\right)\ =\ 0.9145.$$

One can achieve the same result with

$$K'_{\mathrm{PCr}} = K_{\mathrm{PCr}}^{\mathrm{ref}}\,[\mathrm{H^+}]\ \frac{P_{\mathrm{ATP}}}{P_{\mathrm{ADP}}\,P_{\mathrm{PCr}}}\ \left(K_{PCr}^{ref} = 3.77\ 10^{8}\right)$$

to obtain

$$\Delta_{\mathrm{R}}N_{\mathrm{H}}^{\mathrm{PCr}} = \frac{\partial\left(\ln\left(K'_{\mathrm{PCr}}\right)\right)}{\partial(\ln([\mathrm{H^+}]))}\ \left(K'_{\mathrm{PCr}}\left(10^{-7.1}, 0.8\times10^{-3}\right) = 121.04\right)$$

and

$$\Delta_{\mathrm{R}}N_{\mathrm{H}}^{\mathrm{PCr}}\left(10^{-7.1}, 0.8\times10^{-3}\right) = 0.9145.$$

Here, the result is positive so that protons from the environment are taken up if this reaction runs in the given direction. It runs in the SMF – as already discussed – in that direction at sites of ATP consumption. Thus, the protons are used there. At sites of $\mathrm{PCr^{2-}}$ production, such as in the IMS, the direction is reversed, that is protons are produced under these conditions. That can also be taken directly from $\Delta_{\mathrm{R}}N_{\mathrm{H}}$. Then, for the PCr reaction in the opposite direction, it must hold

$$\Delta_{\mathrm{R}}N_{\mathrm{H}}^{\mathrm{rCP}} = N_{\mathrm{H}}^{\mathrm{ADP}} + \left(N_{\mathrm{H}}^{\mathrm{PCr}} - 1\right) - N_{\mathrm{H}}^{\mathrm{ATP}} = 0.12806 + \left(2.2127\times10^{-3} - 1.0\right) - 0.0448\ =\ -0.9145.$$

This naturally also comes from

$$\frac{\partial\left(\ln\left(K'_{\mathrm{PCr}}{}^{-1}\right)\right)}{\partial(\ln([\mathrm{H^+}]))} = -\frac{\partial\left(\ln\left(K'_{\mathrm{PCr}}\right)\right)}{\partial(\ln([\mathrm{H^+}]))}.$$

Here, use is made of the fact that by reversing the direction of the reaction, the reciprocal value of K' comes into operation. This must be valid for every reaction, and therefore also to ATP cleavage and synthesis.

For the SSC of ATP, this means that due to the sign reversal, proton production must always be compensated through proton consumption, so that the pH at SSC remains constant.

If mitochondria are involved in ATP production, the approach becomes more complicated. The transport of $H_2PO_4^-$ via H/P symport from the sarcosol into the matrix corresponds to proton binding, as H^+ ions disappear from the sarcosol. Only $H_2PO_4^-$ ions are transported. The proportion N_H^{Pi} is already present as $H_2PO_4^-$ in the sarcosol. Therefore, only the proportion $1 - N_H^{Pi}$ for the transport must be removed.

During ATP/ADP-Ex, only "naked" species of ATP and ADP are transported. In doing so, the ATP^{4-} ion binds the proportion N_H^{ATP} (when arriving in the IMS), while ADP (when starting from the IMS) must dissociate its bound H atoms in order to be able to be transported as ADP^{3-} ions. At the same time, the N_H^{ADP} proportion of protons remains in the sarcosol. The binding related to the sarcosol through both transport processes is then

$$\Delta_R N_H^{ATPrev}\left(10^{-7.1}, 0.8 \times 10^{-3}\right) = N_H^{ATP} - N_H^{ADP} + 1 - N_H^{Pi} = -\Delta_R N_H^{ATP}\left(10^{-7.1}, 800\right)$$
$$= 0.0448 - 0.12806 + 1.0 - 0.3068 = 0.61.$$

So at SSC, the protons produced though ATP cleavage are completely consumed again by the transport processes ATP/ADP-Ex and H/P at the inner membrane, so that this path also keeps the pH constant.

The cleavage and transport processes in the matrix run both in the reverse direction. Consequently, only the signs must be changed, which also leads to complete compensation. This includes, in addition to the ATP synthesis reaction, the ATP formation through CAC. However, these reactions run in the matrix at a higher pH. This is $-\Delta_R N_H^{ATP}\left(10^{-7.3}, 0.8 \times 10^{-3}\right) = 0.72565$, and at this pH $-\left(N_H^{ATP} - N_H^{ADP} + 1 - N_H^{Pi}\right) = -(0.02873 - 0.08477 + 1.0 - 0.2183) = 0.72565$.

At this point, it must be mentioned that the proton needed for the H/P symport is not included in the binding calculation. Together with the positive electrical charge, which runs through the inner membrane with ATP/ADP-Ex, this belongs to the pumped, electrochemical protons, some of which also pass back into the matrix in this way (see Chapter 8).

For the Mg^{2+} binding through mitochondrial transport processes

$$\Delta_R N_{Mg}^{ATPrev}\left(10^{-7.1}, 0.8 \times 10^{-3}\right) = N_{Mg}^{ATP} - N_{Mg}^{ADP} - N_{Mg}^{Pi} = -\Delta_R N_{Mg}^{ATP}\left(10^{-7.1}, 0.8 \times 10^{-3}\right)$$
$$= -(0.36416 + 0.02024 - 0.85716) = 0.47276.$$

To the PCr^{2-} shuttle this applies in the same way as to ATP cleavage and formation in the sarcosol because

$$\frac{\partial\left(\ln\left(K'_{PCr}{}^{-1}\right)\right)}{\partial(\ln([Mg^+]))} = -\frac{\partial(\ln(K'_{PCr}))}{\partial(\ln([Mg^+]))},\ \Delta_R N_{Mg}^{PCrrev} = -\Delta_R N_{Mg}^{PCr}.$$

Therefore, it was demonstrated that all the reactions involved in the ATP cycle, including those of the PCr shuttle at SSC, are not capable of inducing a change in pH or the Mg^{2+} concentration, either in the sarcosol or in the mitochondrial matrix. This does not apply, however, when no SSC is present. It can be expected, particularly after a change from low to high power output, that a short-term situation may arise during which ion binding may not be compensated, when the ATP supply via the metabolism, therefore, is not sufficient to cover the ATP demand at high power output. This situation is discussed in the scope of muscle contraction (see Chapter 8).

10.4 Buffering

If a specific amount of protons is added or taken from an aqueous solution, then its pH changes. However, often this does not correspond to the change in concentration, which would be caused solely through the addition or extraction of the proton amount. The resulting change in proton activity is generally considerably lower. This effect is known as buffering. In the cyto/sarcosol, in addition to H^+, also Mg^{2+} and Ca^{2+} are buffered to a greater or lesser extent.

In physical chemistry, H^+ buffering β is described as follows:

$$\begin{aligned}\beta = \frac{d([H^+]_{tot})}{-d(pH)} &= \ln(10)\ \frac{d(\{H^+\}+[H]_b)}{d(\ln(\{H^+\}))} = \ln(10)\ \{H^+\}\ \frac{d(\{H^+\}+[H]_b)}{d\{H^+\}} \\ &= \ln(10)\ \{H^+\}\ \left(1+\frac{d([H]_b)}{d\{H^+\}}\right)\end{aligned}. \quad (10.12)$$

The curly brackets indicate proton activity, $[H]_b$ is the concentration of hydrogen bound to H^+ binding molecules or molecular groups. Furthermore,

$$[H]_b = N_H\left[BU^h\right],$$

and

$$\frac{d[H]_b}{d\{H^+\}} = \frac{d(N_H)}{d\{H^+\}}\ \left[BU^h\right].$$

$\left[BU^h\right]$ is the total concentration of H^+ binding molecules or molecular groups.

The time rate of change of proton concentration in a cell is important. This can be determined with the aid of the fluxes J^h, which produce or consume one or more protons. This is

$$\frac{d[\mathrm{H}]_{tot}}{dt} = \sum \nu_i J_i^h = \frac{d[\mathrm{H}]_\mathrm{b}}{dt} + \frac{d\{\mathrm{H}^+\}}{dt}$$

and due to

$$\frac{d[\mathrm{H}]_b}{dt} = \frac{d[\mathrm{H}]_b}{d\{\mathrm{H}^+\}} \frac{d\{\mathrm{H}^+\}}{dt}$$

$$\sum \nu_i J_i^h = \frac{d[\mathrm{H}]_b}{d\{\mathrm{H}^+\}} \frac{d\{\mathrm{H}^+\}}{dt} + \frac{d\{\mathrm{H}^+\}}{dt} = \frac{d\{\mathrm{H}^+\}}{dt} \left(\frac{dN_\mathrm{H}}{d\{\mathrm{H}^+\}} \left[\mathrm{BU^h}\right] + 1 \right).$$

Thus, for $d\{\mathrm{H}^+\}/dt$, one obtains

$$\frac{d\{\mathrm{H}^+\}}{dt} = \frac{\sum \nu_i J_i^h}{\left(\frac{dN_\mathrm{H}}{d\{\mathrm{H}^+\}} \left[\mathrm{BU^h}\right] + 1 \right)}.$$

To demonstrate the buffering effect of the denominator in the above equation, the carbonic anhydrase reaction is considered as follows:

$$\mathrm{CO_2 + H_2O \rightleftharpoons HCO_3^- + H^+}. \tag{R10.1}$$

For this reaction $d[\mathrm{H}]_\mathrm{b}/d\{\mathrm{H}^+\}$ is given by

$$\frac{d[\mathrm{H}]_\mathrm{b}}{d\{\mathrm{H}^+\}} = \frac{d(N_H)}{d\{\mathrm{H}^+\}} \left[\mathrm{BU^h}\right] = \frac{K_D}{(K_\mathrm{D} + \{\mathrm{H}^+\})^2} \left[\mathrm{BU^h}\right].$$

With $K_\mathrm{D} = 10^{-6.17}$, $[\mathrm{BU^h}] = [\mathrm{HCO_3^-}] + [\mathrm{CO_2}] = 0.011916 + 1.4 \times 10^{-3} = 0.013316\,\mathrm{M}$ (at pH = 7.1) and $d\{\mathrm{H}^+\}_\mathrm{tot}/dt = 10^{-3}\,\mathrm{mM/s}$, one obtains $d\{\mathrm{H}^+\}/dt = 6.339981 \times 10^{-8}\,\mathrm{mM/s}$ at $\{\mathrm{H}^+\} \sim 10^{-7.1}$. At the same time, the pH would drop slightly from 7.1 to 7.0997 in 1 s. With a K_D of $10^{-4.0}$, this would yield a pH drop to 7.061.

Two intrinsic buffers with the dissociation constants $K_\mathrm{D}^{\mathrm{bu1}} = 10^{-6.03}$ and $K_\mathrm{D}^{\mathrm{bu2}} = 10^{-7.57}$ M have been found for cardiac cells [17]. Both constants are also used here in simulations. The concentrations of these buffers are estimated as $\left[\mathrm{BU}_1^h\right] = 84.22 \times 10^{-3}$ and $\left[\mathrm{BU}_2^h\right] = 29.38 \times 10^{-3}\,\mathrm{M}$, respectively. The result from this is

$$\frac{d\{\mathrm{H}^+\}}{dt} = \frac{\sum \nu_i J_i}{\left(\frac{dN_{\mathrm{H1}}}{d\{\mathrm{H}^+\}} \left[\mathrm{BU}_1^h\right] + \frac{dN_{\mathrm{H2}}}{d\{\mathrm{H}^+\}} \left[\mathrm{BU}_2^h\right] + 1 \right)}.$$

However, the above equation is still not complete because the changes on proton binding caused by reactions are still not included. These are added to $\sum \nu_i J_i^h$ so that for the rate of $\{\mathrm{H}^+\}$ changes ultimately

$$\frac{d\{\mathrm{H}^+\}}{dt} = \frac{d\{\mathrm{H}^+\}}{dt} + \frac{d_{\mathrm{R}}\{\mathrm{H}^+\}}{dt}$$
$$= \frac{1}{\left(\frac{dN_{\mathrm{H1}}}{d\{\mathrm{H}^+\}}\ [\mathrm{BU}_1^h] + \frac{dN_{\mathrm{H2}}}{d\{\mathrm{H}^+\}}\ [\mathrm{BU}_2^h] + 1\right)}\ \left(\sum \nu_i J_i^h + \sum \left(-\Delta_{\mathrm{R}} N_{\mathrm{H}}\right)_k J_k^{rh}\right) \tag{10.13}$$

is obtained, where index "*R*" represents the change caused by a reaction.

The time rate change of Mg^{2+} binding can also be treated in exactly the same way. This is

$$[\mathrm{Mg}]_{\mathrm{b}} = N_{\mathrm{Mg}}[\mathrm{BU}^{\mathrm{mg}}] \text{ and } \frac{d[\mathrm{Mg}]_{\mathrm{b}}}{d[\mathrm{Mg}^{2+}]} = \frac{d\left(N_{\mathrm{Mg}}\right)}{d[\mathrm{Mg}^{2+}]}\ [\mathrm{BU}^{\mathrm{mg}}]$$

and

$$\frac{d[\mathrm{Mg}]_{tot}}{dt} = \sum \left(-\Delta_{\mathrm{R}} N_{\mathrm{Mg}}\right)_i J_i^{\mathrm{rmg}} = \frac{d[\mathrm{Mg}]_{\mathrm{b}}}{dt} + \frac{d\left[\mathrm{Mg}^{2+}\right]}{dt}$$

which leads to

$$\frac{d_R\left[\mathrm{Mg}^{2+}\right]}{dt} = \frac{\sum \left(-\Delta_{\mathrm{R}} N_{\mathrm{Mg}}\right)_k J_k^{\mathrm{rmg}}}{\left(\frac{dN_{\mathrm{Mg}}}{d\left[\mathrm{Mg}^{2+}\right]}\ [\mathrm{BU}^{\mathrm{mg}}] + 1\right)}.$$

Furthermore, Mg^{2+} binding is influenced by the change in pH, which gives

$$\frac{d[\mathrm{Mg}^{2+}]}{dt} = \frac{d[\mathrm{Mg}]_{\mathrm{b}}}{d\{\mathrm{H}^+\}}\frac{d\{\mathrm{H}^+\}}{dt} = \frac{-\partial\left(N_{\mathrm{Mg}}\right)}{\partial\{\mathrm{H}^+\}}\ [\mathrm{BU}^{\mathrm{mg}}]\ \frac{d\{\mathrm{H}^+\}}{dt}.$$

This Mg^{2+} release corresponds to a H^+ binding of at least one proton at the Mg^{2+} binding site. The resulting negative H^+ flux must be taken into consideration in $\sum \nu_i J_i^h$.

For the total $\left[\mathrm{Mg}^{2+}\right]$ change/unit time one then obtains

$$\frac{d\left[\mathrm{Mg}^{2+}\right]}{dt} = \frac{1}{\left(\frac{dN_{\mathrm{Mg}}}{d[\mathrm{Mg}^{2+}]}\ [\mathrm{BU}^{\mathrm{mg}}] + 1\right)}$$
$$\times \left(\frac{\frac{-\partial N_{\mathrm{Mg}}}{\partial\{\mathrm{H}^+\}}\ [\mathrm{BU}^{\mathrm{mg}}]}{\left(\frac{dN_{\mathrm{H1}}}{d\{\mathrm{H}^+\}}\ [\mathrm{BU}_1^h] + \frac{dN_{H2}}{d\{\mathrm{H}^+\}}\ [\mathrm{BU}_2^h] + 1\right)}\ \sum \nu_i J_i^h + \sum \left(-\Delta_{\mathrm{R}} N_{\mathrm{Mg}}\right)_k J_k^{\mathrm{rmg}}\right). \tag{10.14}$$

Figure 10.1 shows to what extent the respective H^+ and Mg^{2+} fluxes can cause changes in pH and pMg. The red line shows the total proton production (Figure 10.1A), which contains the H^+ ions produced though the metabolism via CO_2 and Lac production. The flux (blue) produced by the ATP cleavage reaction remains constant. This corresponds to an SSC of ATP. The sinking curve (gray) comprises all the ATP resynthesis

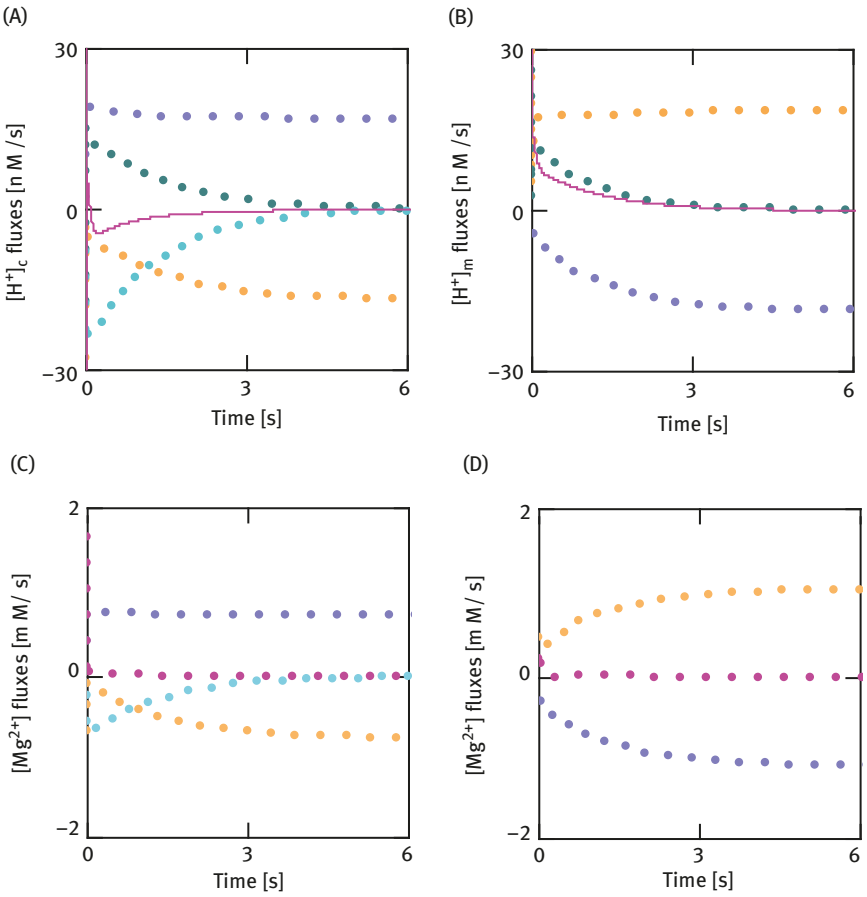

Figure 10.1: Time courses of proton and magnesium ion fluxes generated by reactions. (A) Rate of $[H^+]_c$ changes in the sarcosol (blue points, ATP splitting; yellow points, ATP/ADP-Ex plus H/P symport; green points, ATP splitting plus ATP/ADP-Ex plus H/P symport; cyan points, rate of $\{H^+\}_c$ changes during the PCr reaction; red line, total rate of all). (B) Rate of $\{H^+\}_m$ changes in the matrix (blue points, ATP_m formation; yellow points, ATP/ADP-Ex plus H/P symport; green points, ATP_m formation plus ATP/ADP-Ex plus H/P symport; red line, total rate of all). (C) Rate of $[Mg^{2+}]_c$ changes in the sarcosol (blue points, ATP splitting; yellow points, ATP/ADP-Ex plus H/P symport; cyan points, the PCr reaction; red points, total rate of all). (D) Rate of $[Mg^{2+}]_m$ changes in the matrix (blue points, ATP_m formation; yellow points, ATP/ADP-Ex plus H/P symport; red points, ATP_m formation plus ATP/ADP-Ex plus H/P symport).

reactions including those running via the mitochondrial synthesis pathway. The curve moving from positive to zero (red) is the sum of these two processes. The PCr reaction (in the direction of ATP formation, cyan) is part of the curve rising from the negative to zero. At the same time, [PCr] decreases from 20.0 to 15.529×10^{-3} mol/L under these conditions. This process (ATP buffering) lasts around 6.0 s. Afterward, the ATP delivery via the metabolism (PAL and GLU) is sufficiently fast so that the ATP production by J_{PCr} can be reduced. Proton consumption by J_{PCr} is taken into consideration in the black curve. This curve also includes proton production and proton consumption by the LDH reaction or Lac transport, as well as $[H^+]_c$ reduction through the Na/H exchanger. The main cause of acidification of the sarcosol through ATP cleavage is abolished particularly clearly by the PCr reaction.

Figure 10.1B shows the proton fluxes linked with ATP formation and its transport from the matrix into the sarcosol. These run, as expected, in the reverse direction. The proton consumption through ATP synthesis is compensated here alone through ATP/ADP exchange and H/P symport.

The $[Mg^{2+}]_c$ fluxes in the sarcosol are presented in Figure 10.1C. Here the PCr reaction is also significantly involved, although the Mg^{2+} binding of PCr^{2-} is low ($N_{Mg}(10^{-7.1}, 0.8 \times 10^{-3}) = 0.0145$ compared with 0.8572 for ATP). In the matrix (Figure 10.1D), the signs are opposite again, though the PCr reaction is not present there.

The acidification of the sarcosol and alkalization of the mitochondrial matrix linked mainly to ATP cycling (other reactions such as J_{AK} can be ignored) can clearly always be compensated through the respective opposing reactions, so that the resulting pH changes are not significant. The same applies to the Mg^{2+} concentration. Only when ATP demand exceeds ATP supply by the metabolism does this compensation break down (see Chapter 11).

11 Contraction

11.1 Fibril architecture

One of the most important prerequisites for muscle mechanics is the structural composition of protein filaments responsible for contraction and their organization in the SMF. Muscle fibers vary greatly in their length and radius. These are primarily dependent not only on the muscle being considered (e.g., biceps or ocular muscle), but also on the animal species to which the muscle belongs. The diameter of a typical muscle fiber is usually between 20.0 and 40.0 μm, with the length ranging from a few millimeters to several decimeters.

The contractile protein filaments are organized into fibrils, which run the entire length of the fiber, from the end of one tendon to the end of the opposite tendon. There they are anchored in such a way that contraction exerts a tensile force on both tendon ends. A single fibril has a diameter of approximately 1.0 μm. Each fibril is made up of a multitude of identical units, each with the same diameter but considerably shorter length of approximately 1.0 μm. These sarcomeres are separated longitudinally by Z-disks. Actin filaments (thin filaments) extend from these in both directions, reaching almost to the center of each sarcomere. The contractile force acts on these actin filaments as a tensile force pulling toward the center of the sarcomere. As the actin filaments are anchored in Z-disks, each of these structures stretching across the entire cross section of the fibril can accept tensile force from both sides. The tensile force itself is generated by myosin heads, which are organized at regular distances along the myosin filaments (thick filaments). The myosin filaments run, in contrast to the actin filaments, through the center of every sarcomere, but do not reach up to the Z-disks. Actin filaments extend from opposite Z-disks, and in doing so partly overlap the myosin filaments in the respective half. Characteristic transverse striation can be recognized in longitudinal sections of fibrils, which can in part be traced back to this overlapping. A visually darker anisotropic band (A-band) is created, where the actin and myosin filaments overlap; while on either side of the Z-disk lighter isotropic zones (I-bands) can be seen. This appearance in cardiac and skeletal muscles has led to muscles being known as "striated muscles." The H-band situated in the center of the sarcomere contains predominantly myosin filaments and not actin filaments. Also present in the center is the M-line, with its protein structure which contributes to mechanical stabilization of the whole actomyosin system. Furthermore, each sarcomere contains other protein filaments, such as titin and nebulin, which are responsible for the stabilization and positioning of the myosin and actin filaments.

The length of the thick filaments is 1.6 μm, and a half sarcomere (HS) is approximately 1.1 μm. Therefore, the distance available for shortening is approximately 0.5 μm or 25.0%. A sarcomere can therefore contract by around 50.0%, while at the

https://doi.org/10.1515/9783110650501-011

same time its volume remains almost constant. This is achieved by the thin filaments sliding over the anchored thick filaments (sliding filament theory according to Huxley [18–21]). This interlocking sliding is accomplished through the interaction of the myosin filaments with the actin filaments, aided by energized myosin heads. These become temporarily linked to the actin filaments, resulting in a short-term mechanical unit made up of actin and myosin filaments. These cross-bridges (CBs) bend toward the center of the sarcomere while releasing energy, thereby a tensile force is applied to the actin filaments, which transmit this to the Z-disks. As this bending of the CBs takes place in both halves of the sarcomere in opposing directions, therefore always toward the center of the sarcomere, the opposite Z-disks are pulled toward each other, so that the sarcomere is shortened. As the sarcomeres are arranged in series within the fibril, this results in shortening of the fibril. The simultaneous shortening of all parallel-arranged fibrils leads to contraction of the whole fiber.

The energy required for contracting against a force is supplied by ATP cleavage. The basic reaction for this process, during which the chemical energy of ATP hydrolysis is partly converted into mechanical work, can be treated as a coupled reaction. The mechanical output potential required for this can be calculated from the number of CBs involved in the contraction processes as follows:

The number of myosin heads of the respective half of a myosin filament within an HS is 294. This number can be taken from cross-sectional images of the A-band. Myosin filaments are organized into regular hexagons, which are composed of six equilateral triangles with side lengths of $l_{\mathrm{Tri}} = 41.0\mathrm{nm}$. The radius of a typical fibril is $R_{\mathrm{Fibr}} = 18.0 \times l_{\mathrm{Tri}} = 738.0\mathrm{nm}$. Due to the regular hexagonal geometry of the fibril, this is also the value of their side length. The smallest hexagon is made up of six triangles, and therefore, six corners. The next size up appears at a distance of $l_{\mathrm{Tri}} \sin(60^\circ)$. Thus, $R_{\mathrm{Fibr}} = 18.0 \times l_{\mathrm{Tri}}$ is created from 18 enlarging hexagons, with their additional corners on their hexagon sides. The number of points increases with the hexagons. This is because each subsequently larger hexagon has one point per side more than the previous one, and the growth is therefore six points per hexagon. This gives

$$6(1+2+3+\cdots+n) = \sum_{1}^{18} n_i = 6\ \frac{n(n+1)}{2} = 1,026.$$

As the point in the center must also be counted, the result for the number of myofilaments per fibril equals

$$\mathrm{MF}_{\mathrm{Fibr}} = 3n(n+1) + 1 = 1,027.$$

The volume of a 1.0 mm long fibril is calculated as

$$V_{\mathrm{Fibr}} = A_{\mathrm{Fibr}} \times 10^3 = 6\ \frac{(18 \times l_{\mathrm{Tri}})^2}{2} \sin(60^\circ) \times 10^3 = 1.415027 \times 10^3\ \mu\mathrm{m}^3$$

with the cross-sectional area

$$A_{\mathrm{Fibr}} = 6\ \frac{(18 \times l_{\mathrm{Tri}})^2}{2} \sin(60^\circ) = 1.415027\,\mu\mathrm{m}^2.$$

An HS of length $l_{\mathrm{HS}} = 1.1\,\mu$m has a volume of

$$V_{\mathrm{HS}} = A_{\mathrm{Fibr}}\, l_{\mathrm{HS}} = 1.55653\,\mu\mathrm{m}^3.$$

If one takes the total fibril volume of an SMF as $V_{\mathrm{Fibr}}^{\mathrm{tot}} = 0.866 \times V_{\mathrm{Cell}}$, then the number of fibrils/SMF is $N_{\mathrm{Fibr}} = 0.866\ \frac{V_{\mathrm{Cell}}}{V_{\mathrm{Fibr}}}$.

To determine the volume of a 1.0 mm long muscle fiber, cylindrical geometry is assumed. A fiber radius of $R_{\mathrm{Cell}} = 25.76\,\mu$m results in a reference volume of $V_{\mathrm{Cell}}^{\mathrm{ref}} = 2.0847 \times 10^6\,\mu\mathrm{m}^3$. From this, one can calculate the fibril number

$$N_{\mathrm{Fibr}} = 1.275842 \times 10^3.$$

An HS therefore contains

$N_{\mathrm{MH}}^{\mathrm{hs}} = 294.0 \times \mathrm{MF}_{\mathrm{Fibr}} = 3.01938 \times 10^5$ myosin heads.

In order to find the concentration of MHs in mol/L, first, $N_{\mathrm{MH}}^{\mathrm{hs}}$ must be divided by $N_{\mathrm{A}} = 6.022142 \times 10^{23}$ particles/mol. $\left[N_{\mathrm{MH}}^{\mathrm{hs}}\right]$ is obtained then by dividing the volume of water diffusible space (WDS) containing all MHs of an HS. About 77.0 nm of every myosin filament demonstrates no MHs in the H-band region. The resulting volume for the MH concentration thereby becomes reduced. The half-length of a myosin filament is 763.0 nm, of which 686.0 nm is occupied by MHs [22, 23]. This gives a volume fraction related to the HS length of $f_{\mathrm{MH}} = 0.686/1.1 = 0.62364$. Therefore, only approximately 62.0% of the HS volume must be considered and, in turn, from that only the fraction of that can be attributed to WDS. This fraction is determined using the factor $f_{\mathrm{WDS}} = 0.7852$ [24]. Thus, the specified volume to determine the MH concentration is given by $V_{\mathrm{HS}}^{\mathrm{mh}} = f_{\mathrm{WDS}}(A_{\mathrm{Fibr}} \times f_{\mathrm{MH}}\, l_{\mathrm{HS}}) = 0.7622048\ \mu\mathrm{m}^3$ or $0.7622048 \times 10^{-15}$L.

The MH concentration then is

$$[\mathrm{MH}] = \frac{N_{\mathrm{MH}}^{\mathrm{hs}}}{N_{\mathrm{A}}\, V_{\mathrm{HS}}^{\mathrm{mh}}} = 6.578 \times 10^{-4}\mathrm{mol/L} \text{ or } 657.8\,\mu\mathrm{M}.$$

11.2 The cross-bridge cycle

During both isotonic and isometric contractions, the MHs run through a reaction cycle with presumably several configurations, each of which differs from the other not only energetically but also in the macromolecular conformation. Only two different MH conformations are considered here.

The cycle begins with the detachment of deenergized CBs from actin by MgATP^{2-}, and subsequent splitting of that compound bound to MH. The energy released by these reactions is coupled to energize MHs, which is accompanied by a change in

conformation. This energized state is described here as MH_{En}. MH_{En} contains the products of ATP splitting, $MgADP^-$ and $H_2PO_4{}^-$, in the bound form. Through the dissociation of $MgADP^-$ and subsequently $H_2PO_4{}^-$, MH_{En}s can bind again to actin and form energized CBs (CB_{En}). These once again become deenergized CBs through a recurrent change in conformation. In the process, the energy from the energy-rich conformation is either converted to mechanical work and heat energy (isotonic contraction with shortening), or is completely dissipated as heat (isometric contraction with constant fiber length). In the first case, the process corresponds to a coupled reaction, while in the latter case it relates to uncoupling. Therefore, during isotonic contraction, the chemical energy is transferred to MHs through coupling, in order to transfer this energy in a second coupled reaction in part as mechanical energy to the actin filaments, from where it can be transmitted into the environment.

The reaction steps of one cycle can be concentrated to four reactions:

$$A - M + MgATP^{2-} \rightarrow A^{2-} + M^{2+} \bullet MgATP^{2-}. \tag{R11.1}$$

This first reaction of the cycle describes the splitting of the deenergized actomyosin complex by $MgATP^{2-}$. This creates two negative charges on actin (A^{2-}, binding site), and MHs with bound $MgATP^{2-}$. Both negative charges of the $MgATP^{2-}$ molecule were neutralized prior to ATP binding through two positive ions (e.g., K^+). These cations now neutralize the newly created binding site on actin (A^{2-}). Through the splitting reaction, myosin with two positive charges (M^{2+}) is created, which is neutralized by $MgATP^{2-}$. In this way it is ensured that the reaction can take place without charge separation. In the next reaction step, the bound $MgATP^{2-}$ becomes hydrolyzed:

$$M^{2+} \bullet MgATP^{2-} + H_2O \rightarrow \tilde{M}^{2+} \bullet MgADP^- \bullet H_2PO_4{}^-. \tag{R11.2}$$

In the process, energized MH_{En}s are created through coupling. The energization is expressed as $\tilde{M}^{2+}$ compared to M^{2+}.

The subsequent reaction describes the association of MH_{En} with a new binding site on the actin filament to form a temporary instable actomyosin complex (CB_{En}):

$$\tilde{M}^{2+} \bullet MgADP^- \bullet H_2PO^-{}_4 + A^{2-} \rightarrow \{A - \tilde{M}^{2+} \bullet MgADP^- \bullet H_2PO_4{}^-\}^{2-}. \tag{R11.3}$$

This instability is caused by the resulting double-negative charge. This is indicated by the curly brackets.

In the last step, the created energized CBs are stabilized by releasing the bound ATP cleavage products, $MgADP^-$ and $H_2PO_4{}^-$. In the process, on the one hand, the actomyosin complex becomes neutralized again; moreover, the two K^+ ions from A^{2-} are available to neutralize ATP cleavage products:

$$\{A - \tilde{M}^{2+} \bullet MgADP^- \bullet H_2PO_4{}^-\}^{2-} \rightarrow A - M + MgADP^- + H_2PO_4{}^-. \tag{R11.4}$$

This final reaction step is coupled to the release of mechanical energy. This is accomplished through the recurrent change in conformation of the energized CBs ($A - \tilde{M}^{2+}$) to deenergized CBs ($A - M$). This then closes the cycle.

The following affinities emerge:

$$A_{R1} = RT \ln\left(\frac{[A-M]\left[MgATP^{2-}\right]}{\left[A^{2-}\right]\left[M^{2+} \bullet MgATP^{2-}\right]} K_{R1}\right) = RT \ln\left(\frac{\left[MgATP^{2-}\right]}{\left[M^{2+} \bullet MgATP^{2-}\right]} K_{R1}\right),$$

$$A_{R2} = RT \ln\left(\frac{\left[M^{2+} \bullet MgATP^{2-}\right]}{\left[\tilde{M}^{2+} \bullet MgADP^{-} \bullet H_2PO_4{}^{-}\right] K_{R2}}\right),$$

$$A_{R3} = RT \ln\left(\frac{\left[\tilde{M}^{2+} \bullet MgADP^{-} \bullet H_2PO_4{}^{-}\right]\left[A^{2-}\right]}{\left[\{A-\tilde{M}^{2+} \bullet MgADP^{-} \bullet H_2PO_4{}^{-}\}^{2-}\right]} K_{R3}\right)$$

$$= RT \ln\left(\left[\tilde{M}^{2+} \bullet MgADP^{-} \bullet H_2PO_4{}^{-}\right] K_{R3}\right)$$

and

$$A_{R4} = RT \ln\left(\frac{\left[\{A-\tilde{M}^{2+} \bullet MgADP^{-} \bullet H_2PO_4{}^{-}\}^{2-}\right]}{[A-M][MgADP^{-}][H_2PO_4{}^{-}]} K_{R4}\right)$$

$$= RT \ln\left(\frac{1}{[MgADP^{-}][H_2PO_4{}^{-}]} K_{R4}\right).$$

Adding A_{R1} and A_{R2} yields

$$A_{R12} = RT \ln\left(\frac{\left[MgATP^{2-}\right]}{\left[M^{2+} \bullet MgATP^{2-}\right]} K_{R1}\right) + RT \ln\left(\frac{\left[M^{2+} \bullet MgATP^{2-}\right]}{\left[\tilde{M}^{2+} \bullet MgADP^{-} H_2PO_4{}^{-}\right]} K_{R2}\right),$$

$$= RT \ln\left(\frac{\left[MgATP^{2-}\right]}{\left[\tilde{M}^{2+} \bullet MgADP^{-} \bullet H_2PO_4{}^{-}\right]} K_{R1} K_{R2}\right)$$

and adding A_{R3} and A_{R4} gives

$$A_{R34} = RT \ln\left(\left[\tilde{M}^{2+} \bullet MgADP^{-} \bullet H_2PO_4{}^{-}\right] K_{R3}\right) + RT \ln\left(\frac{1}{[MgADP^{-}][H_2PO_4{}^{-}]} K_{R4}\right)$$

$$= RT \ln\left(\frac{\left[\tilde{M}^{2+} \bullet MgADP^{-} \bullet H_2PO_4{}^{-}\right]}{[MgADP^{-}][H_2PO_4{}^{-}]} K_{R3} K_{R4}\right).$$

Then, the result of A_{R12} plus A_{R34} is

$$\begin{aligned} A_{1234} &= RT\ln\left(\frac{[\mathrm{MgATP}^{2-}]}{[\tilde{\mathrm{M}}^{2+}\bullet\mathrm{MgADP}^{-}\bullet\mathrm{H_2PO_4}^{-}]}K_{R1}K_{R2}\right) \\ &+ RT\ln\left(\frac{[\tilde{\mathrm{M}}^{2+}\bullet\mathrm{MgADP}^{-}\bullet\mathrm{H_2PO_4}^{-}]}{[\mathrm{MgADP}^{-}][\mathrm{H_2PO_4}^{-}]}K_{R3}K_{R4}\right) \\ &= RT\ln\left(\frac{[\mathrm{MgATP}^{2-}]}{[\mathrm{MgADP}^{-}][\mathrm{H_2PO_4}^{-}]}K_{R1}K_{R2}K_{R3}K_{R4}\right) \\ &= A^{c}_{ATP}. \end{aligned}$$

The concentration of the MHs involved in the cycle always remains the same, irrespective of their conformation. Furthermore, obviously $K_{R1}\times K_{R2}\times K_{R3}\times K_{R4} = K^{ref}_{ATP}$ is valid. Therefore, the constraint that the sum of all the affinities ($-\Delta_R Gs$) of a reaction cycle must vanish is fulfilled. The input affinity A_{ATPc} is not involved in the CB cycle itself, in the same way, for example, as in the case of the Ca^{2+} cycle at the reticulum membrane.

The four reactions of the cycle are coupled at two points, that is, at these coupling points the energy from ATP cleavage is transferred to the MHs, so that these become energized (MH_{EN}). In the first coupling step, 3.2×10^4 J/mol is transferred, and the corresponding affinity is set to

$$A^{ldI}_{En} = RT\ln(K_{Tr}) = -3.2\times10^4\ \mathrm{J/mol}.$$

This represents the output affinity of the first coupled reaction. It is coupled to the input affinity

$$A_{R12} = A^{pI}_{En} = RT\ln\left(\frac{[\mathrm{MgATP}^{2-}]}{[\tilde{\mathrm{M}}^{2+}\bullet\mathrm{MgADP}^{-}\bullet\mathrm{H_2PO_4}^{-}]}K_{R1}K_{R2}\right)$$

(A_{R1} plus A_{R2}).

A second time energy from the affinities A_{R3} plus A_{R4} is transferred to the CBs, which have formed through the binding of the MH_{EN}s with actin. Thus,

$$A^{ldII}_{En} = -\varphi A_{R34} = -\varphi RT\ln\left(\frac{[\tilde{\mathrm{M}}^{2+}\bullet\mathrm{MgADP}^{-}\bullet\mathrm{H_2PO_4}^{-}]}{[\mathrm{MgADP}^{-}][\mathrm{H_2PO_4}^{-}]}K_{R3}K_{R4}\right)$$

Here, the factor $\varphi < 1.0$ is set to 0.9, so that only 90.0% of the A_{34} can be transferred to the CBs. The remaining 10.0% is dissipated and released as heat energy. The total CB energization is therefore,

$$A^{ldI}_{En} + A^{ldII}_{En} (\leq 0).$$

This affinity with inverted sign ($A^p_{Str} = -\left(A^{ldI}_{En} + A^{ldII}_{En}\right) > 0$) is available then for the power stroke of the CBs.

The flux for the energization can be summarized as

$$J_{\mathrm{En}} = L_{\mathrm{En}}\left(A^{ldI}_{\mathrm{En}} + A^{ldII}_{\mathrm{En}} + A_{R12} + A_{R34}\right) = L_{\mathrm{En}}\left(-A^p_{Str} + A^c_{ATP}\right)$$

The flux through the power stroke is

$$J_{Str} = L_{Str}\left(A^{ld}_{Str} + A^p_{Str}\right).$$

$A^{ld}_{Str}(\leq 0)$ is the affinity related to the (variable) force exerted on the SMF. This is coupled as the output affinity to the input affinity $A^p_{Str}(>0)$.

At steady state, both these fluxes are equal, so that the cycle can be expressed through only one flux:

$$J_{\mathrm{cyc}} = L_{\mathrm{cyc}}\left(-A^p_{\mathrm{Str}} + A^c_{\mathrm{ATP}} + A^{ld}_{\mathrm{Str}} + A^p_{\mathrm{Str}}\right) = L_{\mathrm{cyc}}\left(A^{ld}_{\mathrm{Str}} + A^c_{\mathrm{ATP}}\right).$$

A^{ld}_{Str}, in the same way as A^c_{ATP}, is not involved with the cycle itself. As with all the considered cycles, this cycle also runs in complete analogy to the cycle of electrical charges between two oppositely connected batteries. Here, $\mathrm{EMF_{Del}}$ ($\hat{=} A^{\mathrm{c}}_{\mathrm{ATP}}$) and $\mathrm{EMF_{Dem}}$ ($\hat{=} A^{\mathrm{ld}}_{\mathrm{Str}}$) are also not directly involved in the cycling of electrical charge. The cyclical behavior of the CB cycle is given in that the deenergized CBs are energized via MHs to $\mathrm{MH_{En}}$s, which subsequently deenergizes through energy release as energized $\mathrm{CB_{En}}$s during the power stroke.

To be able to calculate the force development of an SMF, the concentration of CBs taking part in the power stroke [CB] must be known. It results from two fluxes of the cycle, which differ in their functional attribution in the sequence while containing all the reactions and affinities of the process described earlier. The energizing flux is given through reactions R1 and R2; it increases $[\mathrm{MH_{En}}]$ and reduces [CB]. This flux is given by

$J_{\mathrm{CM}} = L_{\mathrm{CM}}\left(A^{\mathrm{ld\,I}}_{\mathrm{En}} + A_{\mathrm{R12}}\right)$ (Index "CM" indicates CB → MH).

The opposing flux reduces $[\mathrm{MH_{En}}]$ and increases [CB]. It contains the reaction for bond formation with actin (R3) and those of the power stroke (R4). The cycle is completed With this final reaction the cycle is closed. This flux is given by

$$J_{MC} = L_{MC}\left(A^{ld}_{Str} + A^p_{Str}\right) \text{ (Index "}MC\text{" indicates MH} \rightarrow \text{CB)}.$$

These last two fluxes are included in simulations. At steady state, $[\mathrm{MH_{En}}]$ and [CB] are constant. [CB] is obtained then from the relationship

$$[\mathrm{CB}] = [\mathrm{MH_{tot}}] - [\mathrm{MH_{En}}] \text{ with } [\mathrm{MH_{tot}}] = 657.8\,\mu\mathrm{M}$$

11.3 The Ca^{2+} dependence of CB formation

The muscle contraction is essentially activated by $[Ca^{2+}]_c$. In the process, Ca^{2+} ions are bound by troponin C on the actin filament, where the inhibition of bond

formation between MH_{En}s and the binding sites on the actin filament is abolished. This forces CB formation so that $[CB_{En}]$ increases; furthermore, the frequency of the cycle becomes increased by an increase in contraction velocity.

First, Ca^{2+}-dependent adjustment of $[CB_{En}]$ occurs. The contraction force is determined by the number of CBs working in an HS, and thus, by their concentration. This in turn is influenced primarily by the constants K_{R1} and K_{R3} (see R1 and R3). Therefore, a relationship must be found, which creates different $[CB_{En}]$s through a Ca^{2+}-dependent variation of the constants and namely in such a form that from it the known (from measurements) Ca^{2+} dependence of contractile force can be obtained.

The dependency of the contractile force on pCa measured under isometric conditions can be described by the following equation:

$$\frac{F}{F_{max}} = \frac{1}{1+10^{\left(\frac{pCa-pCa_{05}}{S}\right)}} = \frac{1}{1+10^{\left(\log\left(\left(\frac{[Ca_{05}]}{[Ca]}\right)^{\frac{1}{S}}\right)\right)}} = \frac{[Ca]^h}{[Ca_{05}]^h+[Ca]^h}$$

("$^{2+}$" for calcium ions is not included for the sake of clarity). $[Ca_{05}]$ ($pCa_{05} = 5.82$) is $[Ca^{2+}]_c$, where F/F_{max} is equal to 0.5; the constant $1/S = h = 3.65$ determines the slope of this sigmoidal curve.

The fluxes J_{CM} and J_{MC} include in the respective affinities A_{R12} and A^p_{Str} the products of the constants $K_{R1} \times K_{R2}$ and $K_{R3} \times K_{R4}$, which are interrelated through

$$K_{R1}\,K_{R2} = \frac{K^{ref}_{ATP}}{K_{R3}\,K_{R4}}.$$

Therefore, if $K_{R3} \times K_{R4}$ increases by a Ca^{2+}-dependent factor, then $K_{R1} \times K_{R2}$ must be reduced through the reciprocal value of the same factor in order to leave K^{ref}_{ATP} unaltered. Ca^2 dependency on $K_{R3} \times K_{R4}$ is given here by

$$f_{K3K4}(Ca) = \frac{Ca^h}{Ca^h_{05}+Ca^h} + 3.0,$$

with $\left[Ca^{2+}_{05}\right] = 1.5438\,\mu M$ and $h = 3.285$.

Each individual constant must be known to obtain the corresponding affinities. However, this is only possible through specification of a specific value. If it is assumed that both the affinities of the association reaction to actomyosin and its dissociation through ATP proceed near equilibrium, then the corresponding affinities A_{R1} and A_{R3} must approach zero. This means that under these conditions, the dissociation of actomyosin and the subsequent energization are practically reversible in the first coupling step. By varying K_{R1}, this situation can only be changed marginally, as several conditions must be fulfilled at the same time. All the affinities involved in the cycle must be positive, $A_{R2} > -A^{ld\,I}_{En}$ and $A_{R4} > -A^{ld\,II}_{En}$ must hold and certainly $A_{R1} + A_{R2} + A_{R3} + A_{R4} = A^c_{ATP}$ must be fulfilled. For the association of actomyosin, much larger variations

in all the involved constants and affinities (A_{R3} plus A_{R4}) are possible. In the process, energy from both affinities is transferred into further energization of the CBs in the second coupling step. Up to that point, only around 5% ($A^{p}_{Str}/A^{c}_{ATP} = 0.955$) of the energy from ATP cleavage is dissipated. This only occurs in appreciable amounts during the power stroke in that only a percentage of A^{p}_{Str} is used in order to work against the mechanical load potential ($A^{ld}_{Str} < 0$). The unused residue ($A^{p}_{Str} + A^{ld}_{Str}$) is released as heat energy.

The Ca^{2+} activation through the constants is, however, not sufficient to bring $[CB_{En}]$ to the desired maximum value for Ca^{2+} saturation ($[CB_{En}] = 170.7\,\mu M$ at $[Ca^{2+}]_c = 6.0\,\mu M$). For this, the activation factor $Ca^{h}/(Ca^{h}_{05} + Ca^{h})$ must also be included in the conductance L_{Str} of flux J_{Str}. Only then will the maximum $[CB_{En}]$ of 170.7 µM (approx. 26.0% of $[MH_{tot}]$) be achieved.

11.4 The load dependence of contraction

Besides the Ca^{2+}-dependent adjustment of $[CB_{En}]$ and the related force development, the contraction velocity is also very important for performance of an SMF. This is given by the cycling frequency of the synchronously working CBs. The relationship between force and velocity during isotonic contraction was recognized by Hill [25, 26]. The following equation is named after him:

$$v(F_{Ld}) = b\ \frac{F_{max} - F_{Ld}}{a + F_{Ld}}. \tag{11.1}$$

It represents the shortening velocity (in m/s) as a function of the force F_{Ld} (or load in Newton (N)), which has to be overcome during shortening. a is given in N so that the fraction is dimensionless. Then, b must have the dimension of a velocity in m/s. As can be seen from the equation, its function follows a hyperbolic course. The above equation should now be brought into relationship with the flux equation in mM/s

$$J\left(A^{ld}_{Str}\right) = L_{Str}\left(A^{ld}_{Str} + A^{p}_{Str}\right) \tag{11.2}$$

is used here. As a function of A^{ld}_{Str}, the latter represents a straight line, the ordinates ($J_{Str}\left(A^{ld}_{Str}\right)$) of which approach zero with A^{ld}_{Str} becoming more negative. At $A^{ld}_{Str} = -A^{p}_{Str}$, $J\left(-A^{p}_{Str}\right) = 0$ (Figure 11.1A). In order to achieve a hyperbolic dependency, a factor is introduced that has the mathematical structure of a Michaelis–Menten inhibitor. This leads to

$$J\left(A^{ld}_{Str}\right) = L_{Str}\ \frac{K^{ld}_{MI}}{K^{ld}_{MI} + A^{ld}_{Str}}\ \left(A^{ld}_{Str} + A^{p}_{Str}\right).$$

$J\left(A^{ld}_{Str}\right)$ also shows a hyperbolic dependency (Figure 11.1A).

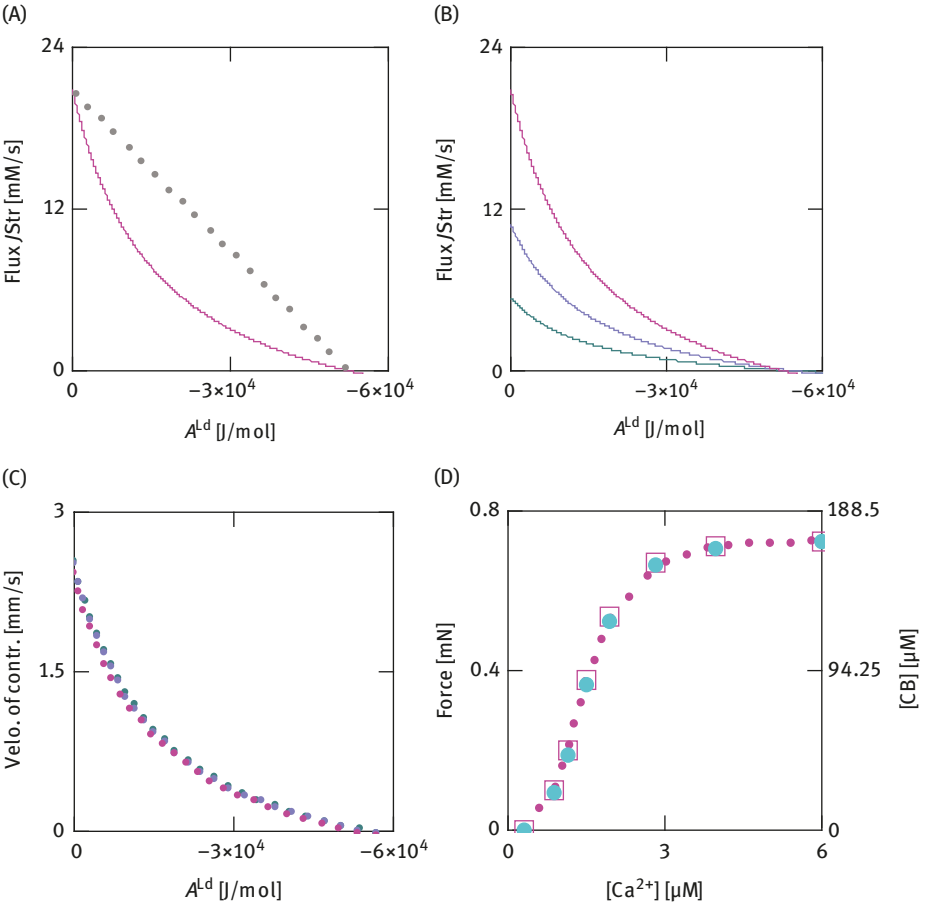

Figure 11.1: Performance of SMF. (A) The effect of the hyperbolic inhibition factor on $J_{\mathrm{Str}}(A^{\mathrm{ld}}_{\mathrm{Str}})$ (gray points, without inhibition; red line, inhibition through a Michaelis–Menten-like dimensionless factor). (B) The effect of $[\mathrm{Ca}^{2+}]_c$ (red line, $[\mathrm{Ca}^{2+}]_c = 6.0\mu\mathrm{M}$; blue line, $[\mathrm{Ca}^{2+}]_c = 1.514\mu\mathrm{M}$; green line, $[\mathrm{Ca}^{2+}]_c = 1.134\ \mu\mathrm{M}$).(C) Shortening velocity (red points, $[\mathrm{Ca}^{2+}]_c = 6.0\,\mu\mathrm{M}$; blue points, $[\mathrm{Ca}^{2+}]_c = 1.514\,\mu\mathrm{M}$; green points, $[\mathrm{Ca}^{2+}]_c = 1.134\,\mu\mathrm{M}$).(D) Force of contraction and [CB] as functions of $[\mathrm{Ca}^{2+}]_c$ (red points, the approximating function $F(\mathrm{Ca})$; red squares results from $\mathrm{SIM}_{\mathrm{GLY/PAL}}$; filled circles in cyan: $[\mathrm{Ca}^{2+}]_c$-dependent [CB], and the [CB] axis has been adjusted to match $F(\mathrm{Ca})$).

The inhibitor constant ($K^{\mathrm{ld}}_{\mathrm{MI}}$) according to Michaelis–Menten is set to $K^{\mathrm{ld}}_{\mathrm{MI}} = -1.6\ 10^4\mathrm{J/mol}$. An increase in its value strengthens the curve curvature, which in turn would strengthen the inhibitory effect on the reaction velocity.

In order to transform it into the shortening velocity $v(A^{\mathrm{ld}}_{\mathrm{Str}})$ (or contraction velocity in m/s), $J(A^{\mathrm{ld}}_{\mathrm{Str}})$ in mM/s must first be divided by $[\mathrm{CB_{En}}]$ (in mM). As a result, the frequency $v(A^{\mathrm{ld}}_{\mathrm{Str}})$ in 1/s is obtained. By multiplying with the stroke length $l_{\mathrm{Str}} = 12.0 \times 10^{-9}\mathrm{m}$, this gives

$$v\left(A_{\mathrm{Str}}^{\mathrm{ld}}\right) = L_{\mathrm{Str}} \frac{l_{\mathrm{Str}}}{[\mathrm{CB_{En}}]} \frac{K_{\mathrm{MI}}^{\mathrm{ld}}}{K_{\mathrm{MI}}^{\mathrm{ld}} + A_{\mathrm{Str}}^{\mathrm{ld}}} \left(A_{\mathrm{Str}}^{\mathrm{ld}} + A_{\mathrm{Str}}^{\mathrm{p}}\right) (\text{in m/s}).$$

To check this, a dimensional check is started from

$$v\left(A_{\mathrm{Str}}^{\mathrm{ld}}\right) = L_{\mathrm{Str}} \frac{l_{\mathrm{Str}} K_{\mathrm{MI}}^{\mathrm{ld}}}{[\mathrm{CB_{En}}]} \frac{A_{\mathrm{Str}}^{\mathrm{ld}} + A_{\mathrm{Str}}^{\mathrm{p}}}{K_{\mathrm{MI}}^{\mathrm{ld}} + A_{\mathrm{Str}}^{\mathrm{ld}}}.$$

The dimensional check gives

$$L_{\mathrm{Str}} \times \frac{Kmi_{\mathrm{Ld}}}{[\mathrm{CB_{En}}]} \times l_{\mathrm{Str}} \stackrel{\wedge}{=} \frac{\mathrm{mM}}{\mathrm{s}} \frac{\mathrm{mol}}{\mathrm{J}} \times \frac{\mathrm{J/mol}}{\mathrm{mM}} \times \mathrm{m} = \frac{\mathrm{m}}{\mathrm{s}},$$

as

$$\frac{A_{\mathrm{Str}}^{\mathrm{ld}} + A_{\mathrm{Str}}^{\mathrm{p}}}{K_{\mathrm{MI}}^{\mathrm{ld}} + A_{\mathrm{Str}}^{\mathrm{ld}}} \text{is dimensionless.}$$

$v\left(A_{\mathrm{Str}}^{\mathrm{ld}}\right)$ of an SMF is created through the active CBs in one HS (approx. 26% at Ca^{2+} saturation). Hence, $v\left(A_{\mathrm{Str}}^{\mathrm{ld}}\right)$ is related to the length of only one HS. In order to achieve the shortening velocity in relation to the total SMF length (here 1.0 mm), the velocity must still be multiplied by the number $N_{\mathrm{HS}} = 1,000/1.1 = 909.09$. Thus, the shortening velocity of a 1.0 mm long SMF is given by

$$v\left(A_{\mathrm{Str}}^{\mathrm{ld}}\right) = L_{\mathrm{Str}} \frac{l_{\mathrm{Str}}}{[\mathrm{CB_{En}}]} K_{\mathrm{MI}}^{\mathrm{ld}} N_{\mathrm{HS}} \frac{A_{\mathrm{Str}}^{\mathrm{ld}} + A_{\mathrm{Str}}^{\mathrm{p}}}{K_{\mathrm{MI}}^{\mathrm{ld}} + A_{\mathrm{Str}}^{\mathrm{ld}}}. \tag{11.3}$$

For $A_{\mathrm{Str}}^{\mathrm{ld}} = -1.68 \times 10^4$, $v(-1.68 \times 10^4) = 0.8053 \mathrm{mm/s}$. The maximum speed is reached when $A_{\mathrm{Str}}^{\mathrm{ld}}$ approaches zero. Then $v_{max} = 2.43 \mathrm{mm/s}$ (Figure 11.1C). A 10.0 cm long fiber would have a $v_{\max}$ of 24.3 cm/s.

Figure 11.1B demonstrates that the flux through the coupled affinities $\left(A_{\mathrm{Str}}^{\mathrm{ld}} + A_{\mathrm{Str}}^{\mathrm{p}}\right)$ depends on $[Ca^{2+}]_c$. With increasing $[Ca^{2+}]_c$, $J_{\mathrm{Str}}^{\mathrm{ld}}\left(A_{\mathrm{Str}}^{\mathrm{ld}}\right)$ also increases. At the same time, the functional dependency from $A_{\mathrm{Str}}^{\mathrm{ld}}$ is maintained. In contrast to $J_{\mathrm{Str}}^{\mathrm{ld}}\left(A_{\mathrm{Str}}^{\mathrm{ld}}\right)$, the shortening velocity is, however, not dependent on $[Ca^{2+}]_c$. Under the same conditions, this time all the $v\left(A_{\mathrm{Str}}^{\mathrm{ld}}\right)$s at different $[Ca^{2+}]_c$s are represented by practically one and the same curve (Figure 11.1C). This different behavior is to be expected because for $v\left(A_{\mathrm{Str}}^{\mathrm{ld}}\right)$, only the load-dependent cycle frequency can really be effective, while for $J_{\mathrm{Str}}^{\mathrm{ld}}\left(A_{\mathrm{Str}}^{\mathrm{ld}}\right)$, the proportion of involved CBs working with this frequency is also crucial. Thus, ATP consumption of contraction is given by $J_{\mathrm{Str}}^{\mathrm{p}}$ ($= J_{\mathrm{Str}}^{\mathrm{ld}}$ for complete coupling). In order to yield $v\left(A_{\mathrm{Str}}^{\mathrm{ld}}\right)$, it must be divided by [CB] (see eq. (11.2)), giving the term

$$\frac{L_{\mathrm{Str}}}{[\mathrm{CB_{En}}]}.$$

But as L_{Str} and [CB] possess the same $[Ca^{2+}]_c$ dependency, these must cancel so that in contrast to $J_{Str}^{ld}(A_{Str}^{ld})$, $v(A_{Str}^{ld})$ is influenced only by A_{Str}^{ld} alone.

To finally achieve v as a function of force,

$\frac{A_{Str}^{ld}+A_{Str}^{p}}{K_{MI}^{ld}+A_{Str}^{ld}}$ must be expanded with $1/l_{Str}$. This gives

$\frac{\bar{F}_{Str}^{ld}+\bar{F}_{Str}^{p}}{K_{MI}^{ldf}+\bar{F}_{Str}^{ld}}$ and with $\bar{F}_{Str}^{ld}=-\bar{F}_{Str}^{ld\prime}$, this leads to

$\frac{-\bar{F}_{Str}^{ld\prime}+\bar{F}_{Str}^{p}}{K_{MI}^{ldf}-\bar{F}_{Str}^{ld\prime}}=(-1)\frac{\bar{F}_{Str}^{p}-\bar{F}_{Str}^{ld\prime}}{(-K_{MI}^{ldf})+\bar{F}_{Str}^{ld}}$, and therefore to

$$v(\bar{F}_{Str}^{ld\prime})=L_{Str}\frac{l_{Str}}{[CB_{En}]}\ (-K_{MI}^{ld})\,N_{HS}\times\frac{\bar{F}_{Str}^{p}-\bar{F}_{Str}^{ld\prime}}{(-K_{MI}^{ldf})+\bar{F}_{Str}^{ld\prime}}.$$

One realizes that

$$L_{Str}\frac{l_{Str}}{[CB_{En}]}\ (-K_{MI}^{ldf})\,N_{HS}=b,\text{ and }-K_{MI}^{ldf}=a.$$

Both a and b are positive. Furthermore, b varies with [CB] ($=[CB_{En}]$) and is therefore dependent on $[Ca^{2+}]_c$.

Thus, the equation is

$$v(\bar{F}_{Str}^{ld\prime})=b\times\frac{\bar{F}_{Str}^{p}-\bar{F}_{Str}^{ld\prime}}{a+\bar{F}_{Str}^{ld\prime}}. \tag{11.4}$$

In this way, a direct relationship has been established between Hill's equation and the thermodynamic flux equation developed here. The conformity of both derivations can primarily be attributed to the fact that a dimensionless factor has been incorporated into the conductance of the flux equation, which induces the hyperbolic progression of that function. For this reason, the conductance is not only a constant, which functionally combines the flux J with the affinity A, but also becomes a variable through the additional inclusion of a variable quantity. L_{Str} therefore possesses two variable factors: one for Ca^{2+} activation and one for the load-induced inhibition of J_{Str} (see Chapter 16, in conjunction with enzyme-catalyzed reactions).

The molar force of the input affinity is given by

$$\bar{F}=\frac{A_{Str}^{p}}{l_{Str}}\text{in}\frac{J}{mol\times m}=\frac{N}{mol}.$$

The force of an individual CB is obtained by inserting Avogadro's constant N_A (= 6.022142 particle/mol). This gives

$$F_{CB} = \frac{A^p_{Str}}{l_{Str} N_A} = \frac{5.24 \times 10^4}{1.1 \times 10^{-9} \times N_A} \left[\frac{\text{Nm}}{\text{mol} \times \text{m} \times \frac{\text{Particle}}{\text{mol}}} \right] = 7.251 \times 10^{-12}\text{N}.$$

The force of an SMF can then be calculated as

$$F_{Cell} = \left([CB] \times V^{mh}_{HS} \times N_{Fibr} \times N_A\right) F_{CB} = 585.6265 \times 10^9 \times F_{CB} \times [CB] = 0.7251\text{mN}.$$

This result refers to an $A^p_{Str} = 52.4023\text{kJ/mol}$, which was found for $[Ca^{2+}]_c = 6.0\,\mu\text{M}$ and a corresponding [CB] of 170.74 µM. At a considerably lower power output, for example at $[Ca^{2+}]_c = 1.134\,\mu\text{M}$, A^p_{Str} is larger due to A^c_{ATP} also being higher under such moderate conditions. Under these latter conditions, with $[CB] = 44.47\mu\text{M}$ and $F_{CB} = 7.595\text{pN}$, $F_{Cell} = 0.1987\text{mN}$.

The force of the individual CBs may be somewhat raised under these conditions; however, the force development of the SMF is considerably reduced because [CB] is substantially lower than Ca^{2+} saturation. Figure 11.1D presents this relationship between the force [CB] and $[Ca^{2+}]_c$. The points corresponding to force and [CB], respectively, fulfil with sufficient precision the function (red points in Figure 11.1D)

$$F(\text{Ca}) = F_{max} \frac{[\text{Ca}]^h}{[\text{Ca}_{05}]^h + [\text{Ca}]^h}.$$

It is known from many experimental results that the efficiency of muscle contraction as a function of relative affinities (A_1/A_2) does not demonstrate linear behavior. The corresponding curve shows a maximum typical for uncoupled processes [5]. This means, however, that eq. (11.2) is not complete, as the determined efficiency as a function of A^{ld}_{Str} shows no maximum. To achieve such a dependency, uncoupling parameters must be introduced. This means that the affinity term $\left(A^{ld}_{Str} + A^p_{Str}\right)$ (without uncoupling)
must be converted into expressions with uncoupling

$$\left(\left(\lambda^{ld}_{Str} + 1\right)A^{ld}_{Str} + A^p_{Str}\right) \text{ and } \left(A^{ld}_{Str} + \left(\lambda^p_{Str} + 1\right)A^p_{Str}\right),$$

for only from such terms the efficiency function

$$\eta_{Str}(a) = \frac{\left(\lambda^{ld}_{Str} + 1\right)a + 1}{1 + \frac{\left(\lambda^p_{Str} + 1\right)}{a}} \text{ (see Chapter 6)},$$

can be obtained, which possesses a maximum.

For the uncoupling mechanism it is assumed that it is based on a shortening of the stroke length l_{Str}. The change of the corresponding dissipation functions through shortening of l_{Str} ($\Delta l_{Str}/l_{Str} < 0$) is given by

$$\Delta\Psi_{\mathrm{Str}}^{\mathrm{ld}} = L_{\mathrm{Str}}\left(A_{\mathrm{Str}}^{\mathrm{ld}} + A_{\mathrm{Str}}^{\mathrm{p}}\right)A_{\mathrm{Str}}^{\mathrm{ld}}\,\frac{\Delta l_{\mathrm{Str}}}{l_{\mathrm{Str}}}\,(>0)$$

and

$$\Delta\Psi_{\mathrm{Str}}^{\mathrm{p}} = L_{\mathrm{Str}}\left(A_{\mathrm{Str}}^{\mathrm{ld}} + A_{\mathrm{Str}}^{\mathrm{p}}\right)A_{\mathrm{Str}}^{\mathrm{p}}\,\frac{\Delta l_{\mathrm{Str}}}{l_{\mathrm{Str}}} + L_{\mathrm{StrL}}A_{\mathrm{Str}}^{\mathrm{p}}\left(-\frac{\Delta l_{\mathrm{Str}}}{l_{\mathrm{Str}}}\right)\,(<0).$$

The additional term in the second equation arises from the fact that the CB dissociated by $MgATP^{2-}$ from actin works without load. In the process, the energy originating from the input potential becomes dissipated as a function of relative shortening (first term < 0, second term > 0). If the leak conductance L_{StrL} is set to equal $a \times L_{\mathrm{Str}}$, this leads to

$$\Delta\Psi_{\mathrm{Str}}^{\mathrm{p}} = L_{\mathrm{Str}}\,\frac{\Delta l_{\mathrm{Str}}}{l_{\mathrm{Str}}}\left(\frac{A_{\mathrm{Str}}^{\mathrm{ld}}}{A_{\mathrm{Str}}^{\mathrm{p}}} + 1 - a\right)\left(A_{\mathrm{Str}}^{\mathrm{p}}\right)^2 \text{ and with } a \approx 1 \text{ to}$$

$$\Delta\Psi_{\mathrm{Str}}^{\mathrm{p}} \approx L_{\mathrm{Str}}\,\frac{\Delta l_{\mathrm{Str}}}{l_{\mathrm{Str}}}\left(\frac{A_{\mathrm{Str}}^{\mathrm{ld}}}{A_{\mathrm{Str}}^{\mathrm{p}}}\right)\left(A_{\mathrm{Str}}^{\mathrm{p}}\right)^2.$$

With $\Delta\Psi = \Psi - \Psi_{\mathrm{cp}}$ (Ψ_{cp} refers to the fully coupled proportion of Ψ), then one achieves

$$\Psi_{\mathrm{Str}}^{\mathrm{ld}} = L_{\mathrm{Str}}\left(A_{\mathrm{Str}}^{\mathrm{ld}} + A_{\mathrm{Str}}^{\mathrm{p}}\right)A_{\mathrm{Str}}^{\mathrm{ld}} + L_{\mathrm{Str}}\,\frac{\Delta l_{\mathrm{Str}}}{l_{\mathrm{Str}}}\left(\frac{A_{\mathrm{Str}}^{\mathrm{p}}}{A_{\mathrm{Str}}^{\mathrm{ld}}} + 1\right)\left(A_{\mathrm{Str}}^{\mathrm{ld}}\right)^2$$

and

$$\Psi_{\mathrm{Str}}^{\mathrm{p}} = L_{\mathrm{Str}}\left(A_{\mathrm{Str}}^{\mathrm{ld}} + A_{\mathrm{Str}}^{\mathrm{p}}\right)A_{\mathrm{Str}}^{\mathrm{p}} + L_{\mathrm{Str}}\,\frac{\Delta l_{\mathrm{Str}}}{l_{\mathrm{Str}}}\left(\frac{A_{\mathrm{Str}}^{\mathrm{ld}}}{A_{\mathrm{Str}}^{\mathrm{p}}}\right)\left(A_{\mathrm{Str}}^{\mathrm{p}}\right)^2.$$

By comparison one finds

$$\Psi_{\mathrm{Str}}^{\mathrm{ld}} = L_{\mathrm{Str}}\left(\left(\lambda_{\mathrm{Str}}^{\mathrm{ld}} + 1\right)A_{\mathrm{Str}}^{\mathrm{ld}} + A_{\mathrm{Str}}^{\mathrm{p}}\right)A_{\mathrm{Str}}^{\mathrm{ld}} = L_{\mathrm{Str}}\left(A_{\mathrm{Str}}^{\mathrm{ld}} + A_{\mathrm{Str}}^{\mathrm{p}}\right)A_{\mathrm{Str}}^{\mathrm{ld}} + L_{\mathrm{Str}}\,\lambda_{\mathrm{Str}}^{\mathrm{ld}}\left(A_{\mathrm{Str}}^{\mathrm{ld}}\right)^2$$

and

$$\Psi_{\mathrm{Str}}^{\mathrm{p}} = L_{\mathrm{Str}}\left(A_{\mathrm{Str}}^{\mathrm{ld}} + \left(\lambda_{\mathrm{Str}}^{\mathrm{p}} + 1\right)A_{\mathrm{Str}}^{\mathrm{p}}\right)A_{\mathrm{Str}}^{\mathrm{p}} = L_{\mathrm{Str}}\left(A_{\mathrm{Str}}^{\mathrm{ld}} + A_{\mathrm{Str}}^{\mathrm{p}}\right)A_{\mathrm{Str}}^{\mathrm{p}} + L_{\mathrm{Str}}\,\lambda_{\mathrm{Str}}^{\mathrm{p}}\left(A_{\mathrm{Str}}^{\mathrm{p}}\right)^2;$$

finally

$$\lambda_{\mathrm{Str}}^{\mathrm{ld}} = \frac{\Delta l_{\mathrm{Str}}}{l_{\mathrm{Str}}}\left(\frac{A_{\mathrm{Str}}^{\mathrm{p}}}{A_{\mathrm{Str}}^{\mathrm{ld}}} + 1\right)$$

and

$$\lambda_{\mathrm{Str}}^{\mathrm{p}} = \frac{\Delta l_{\mathrm{Str}}}{l_{\mathrm{Str}}}\left(\frac{A_{\mathrm{Str}}^{\mathrm{ld}}}{A_{\mathrm{Str}}^{\mathrm{p}}}\right).$$

Already from the last two equations, it can be seen that both λ values are functions of the variable load potential $A_{\mathrm{Str}}^{\mathrm{ld}}$, as well as the relative stroke shortening. It is, therefore, obvious that $\Delta l_{\mathrm{Str}}/l_{\mathrm{Str}}$ can also be expressed as a function of $A_{\mathrm{Str}}^{\mathrm{ld}}$. For this, the probability factors

$$P_{\mathrm{Str}}^{\mathrm{I}}\left(A_{\mathrm{Str}}^{\mathrm{ld}}\right) = \frac{1}{1+\exp\left(\frac{A_{\mathrm{Str}}^{\mathrm{ld}} - A_{05}^{\mathrm{I}}}{S_{\lambda \mathrm{I}}}\right)}$$

and

$$P_{\mathrm{Str}}^{\mathrm{II}}\left(A_{\mathrm{Str}}^{\mathrm{ld}}\right) = \frac{1}{1+\exp\left(\frac{A_{\mathrm{Str}}^{\mathrm{ld}} - A_{05}^{\mathrm{II}}}{S_{\lambda \mathrm{II}}}\right)}$$

are introduced.

It is assumed that the shortening can take place in several successively occurring steps. Here, however, only two identical step lengths of $\Delta_{\mathrm{I}} l_{\mathrm{Str}}/l_{\mathrm{Str}} = \Delta_{\mathrm{II}} l_{\mathrm{Str}}/l_{\mathrm{Str}} = -0.5$ are assumed.

Thus, one ultimately obtains for the $A_{\mathrm{Str}}^{\mathrm{ld}}$-dependent λ values

$$\lambda_{\mathrm{Str}}^{\mathrm{ld}}\left(A_{\mathrm{Str}}^{\mathrm{ld}}\right) = \left(\frac{\Delta_{\mathrm{I}} l_{\mathrm{Str}}}{l_{\mathrm{Str}}} P_{\mathrm{Str}}^{\mathrm{I}}\left(A_{\mathrm{Str}}^{\mathrm{ld}}\right) + \frac{\Delta_{\mathrm{II}} l_{\mathrm{Str}}}{l_{\mathrm{Str}}} P_{\mathrm{Str}}^{\mathrm{II}}\left(A_{\mathrm{Str}}^{\mathrm{ld}}\right)\right)\left(\frac{A_{\mathrm{Str}}^{\mathrm{p}}}{A_{\mathrm{Str}}^{\mathrm{ld}}} + 1\right)$$

and

$$\lambda_{\mathrm{Str}}^{\mathrm{p}}\left(A_{\mathrm{Str}}^{\mathrm{ld}}\right) = \left(\frac{\Delta_{\mathrm{I}} l_{\mathrm{Str}}}{l_{\mathrm{Str}}} P_{\mathrm{Str}}^{\mathrm{I}}\left(A_{\mathrm{Str}}^{\mathrm{ld}}\right) + \frac{\Delta_{\mathrm{II}} l_{\mathrm{Str}}}{l_{\mathrm{Str}}} P_{\mathrm{Str}}^{\mathrm{II}}\left(A_{\mathrm{Str}}^{\mathrm{ld}}\right)\right)\left(\frac{A_{\mathrm{Str}}^{\mathrm{ld}}}{A_{\mathrm{Str}}^{\mathrm{p}}}\right).$$

In simulations, the fluxes $J_{\mathrm{Str}}^{\mathrm{ld}}$ and $J_{\mathrm{Str}}^{\mathrm{p}}$ containing these $\lambda\left(A_{\mathrm{Str}}^{\mathrm{ld}}\right)$s determine the behavior of an SMF during contraction.

Figure 11.2A and B shows the differences arising from this compared with fully coupled SMFs (A). From both figures, it can be seen that efficiency ($\eta_{\mathrm{Str}}(a)$ and $\eta_{\mathrm{Str}}(j)$, with $j = J_{\mathrm{Str}}^{\mathrm{ld}}/J_{\max}$ actually deviates from linearity by uncoupling and a maximum is developed. At $A_{\mathrm{Str}}^{\mathrm{ld}}/A_{\mathrm{Str}}^{\mathrm{p}} > -0.5$, the uncoupled efficiency curve (squares in A) only deviates marginally from the coupled curve (blue points in A), which has also been found experimentally.

But only the curve progression of the efficiency function clearly shows that uncoupling must be present. The power curve, in contrast, must always show a maximum, which is independent of whether coupled or uncoupled conditions are present (Figure 11.3C and D). As expected, the maximum power lies in the coupled range of the respective function. It can be determined through setting the derivative equal to zero:

$$\Psi_{\mathrm{Str}}^{\mathrm{ld}}\left(A_{\mathrm{Str}}^{\mathrm{ld}}\right) = L_{\mathrm{Str}}\left(A_{\mathrm{Str}}^{\mathrm{ld}} + A_{\mathrm{Str}}^{\mathrm{p}}\right) A_{\mathrm{Str}}^{\mathrm{ld}}$$

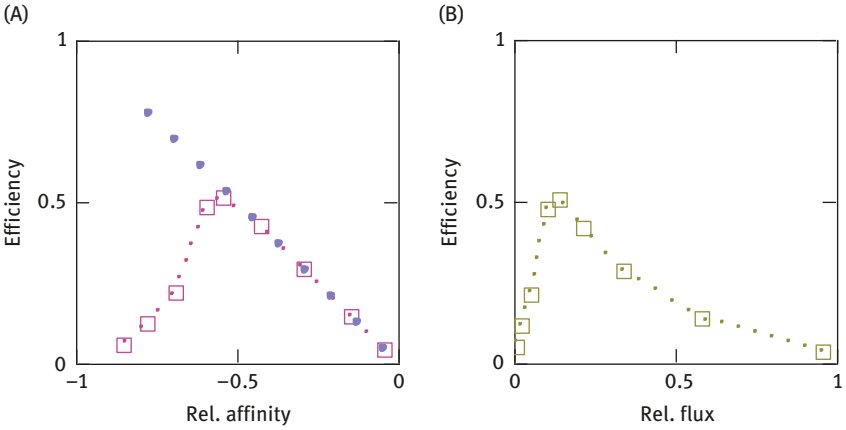

Figure 11.2: Efficiency as functions of A^{ld}_{Str}/A^{p}_{Str} and J^{ld}_{Str}/J_{max}. (A) Red squares: results from $SIM_{GLY/PAL}$ in dependence of A^{ld}_{Str}/A^{p}_{Str}, and a maximal efficiency is obtained by uncoupling contraction; blue points: efficiency that could be reached with a totally coupled SMF. (B) Efficiency in dependence of J^{ld}_{Str}/J_{max}.

However, this time L_{Str} is not constant, but contains the factor $K^{ld}_{MI}/\left(K^{ld}_{MI}+A^{ld}_{Str}\right)$ with the variable A^{ld}_{Str}. This leads to

$$\left(A^{ld}_{Str}\right)^2+2\,K^{ld}_{MI}\,A^{ld}_{Str}+A^{p}_{Str}\,K^{ld}_{MI}=0$$

and

$$A^{ld}_{max}=-1.7082\times10^{4}\,\mathrm{J/mol}\ (\triangleq\ 32.6\,\%\text{of the maximal value}).$$

The same applies to the mechanical power output as a function of the load force (Figure 11.3D). Also here, the maximum occurs at 32.6% of the maximal force.

Uncoupling begins at a load potential of about -3.0×10^{4} J/mol ($\triangleq\ -4.151\times10^{-4}$N). A continuous increase in uncoupling is achieved through the probability factors $P^{I}_{Str}\left(A^{ld}_{Str}\right)$ and $P^{II}_{Str}\left(A^{ld}_{Str}\right)$. This can be interpreted in such a way that, from this load potential onward, already a few of the total number of CBs involved in the cycle work with a shortened stroke length (initially to −50.0%). With increasingly negative A^{ld}_{Str}, all CBs become affected. Afterward, the second step of uncoupling begins, which is added to the first so that stroke shortening now can approach 100.0%. With a $\Delta l_{Str}/l_{Str}=-1.0$, the contraction is no longer accompanied by a change in length of the sarcomeres. The power output, therefore, approaches zero. The probability factors are adjusted in such a way that this is achieved when reaching the input potential A^{p}_{Str}. Therefore, if

$$A^{ld}_{Str}=-A^{p}_{Str},\ \text{then}\ \lambda^{ld}_{Str}\left(-A^{p}_{Str}\right)=0,\ \text{and}\ \lambda^{p}_{Str}\left(-A^{p}_{Str}\right)=1.0.$$

Then, also $\Psi^{ld}_{Str}\left(-A^{p}_{Str}\right)=0$.

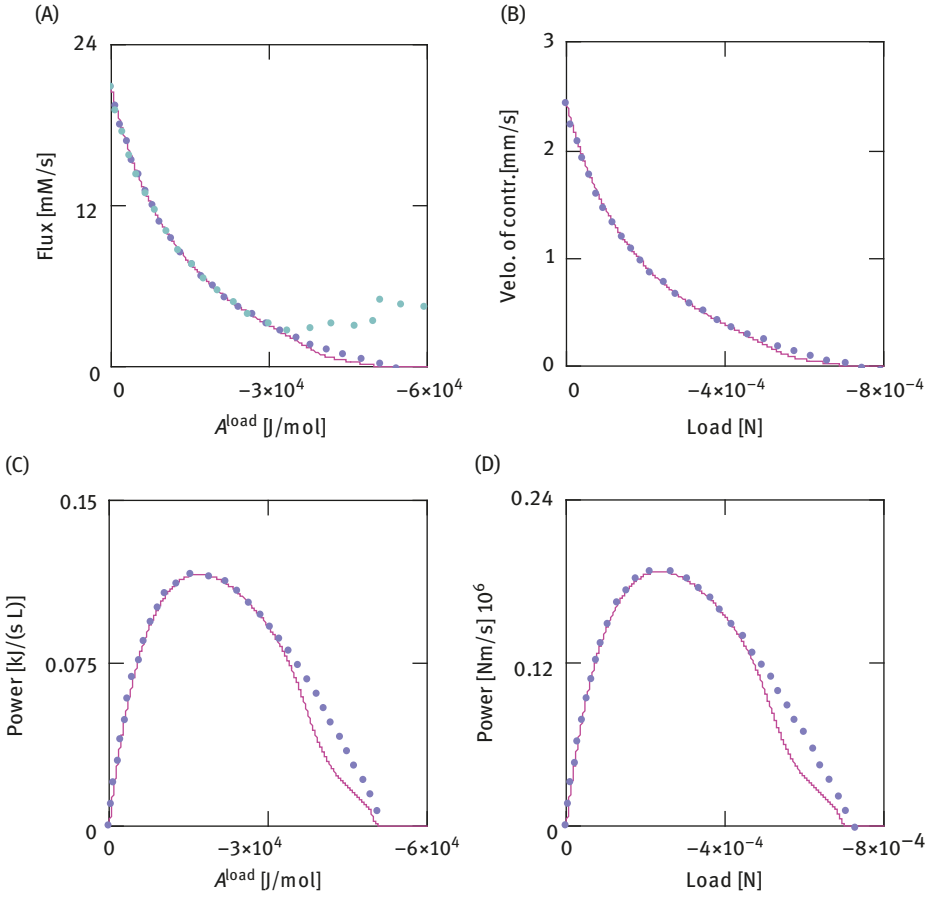

Figure 11.3: Effects of uncoupling on flux, velocity of shortening and power output at $[Ca^{2+}]_c = 6.0\,\mu M$. (A) Generation of three different fluxes (red line: uncoupled flux J^{ld}_{Str}; blue points: J^{ld}_{Str} under totally coupled conditions; green points: uncoupled input flux J^{p}_{Str}. (B) Uncoupling effects on shortening velocity as a function of load force (red line: uncoupled $v(F^{ld}_{Str}{}')$; blue points: under totally coupled conditions). (C) Metabolic power output (red line: uncoupled conditions; blue points: totally coupled conditions). (D) Mechanical power output (red line: uncoupled conditions; blue points: totally coupled conditions).

Ψ^{p}_{Str} is, however, not zero, but is given by

$$\Psi^{p}_{Str}\left(-A^{p}_{Str}\right) = L_{Str}\left(A^{ld}_{Str} + A^{p}_{Str}\right)A^{p}_{Str} + L_{Str}\frac{\Delta l_{Str}}{l_{Str}}\left(\frac{A^{ld}_{Str}}{A^{p}_{Str}}\right)\left(A^{p}_{Str}\right)^2 = L_{Str}\left(A^{p}_{Str}\right)^2 (>0).$$

The corresponding fluxes under these conditions are then

$$J^{ld}_{Str}\left(-A^{p}_{Str}\right) = L_{Str}\left(A^{ld}_{Str} + A^{p}_{Str}\right) + L_{Str}\lambda^{ld}_{Str}\left(-A^{p}_{Str}\right)A^{ld}_{Str} = 0 \text{ and}$$

$$J^{p}_{Str}\left(-A^{p}_{Str}\right) = L_{Str}\left(A^{ld}_{Str} + A^{p}_{Str}\right) + L_{Str}\lambda^{p}_{Str}\left(-A^{p}_{Str}\right)A^{p}_{Str} = L_{Str}A^{p}_{Str}\,(>0).$$

Figure 11.3A and B shows this relationship. Up to $A^{ld}_{Str} \approx -3.0 \times 10^4$, J^{ld}_{Str} and J^{p}_{Str} are practically identical because there is complete coupling of the load potential. With increasingly negative A^{ld}_{Str}, J^{ld}_{Str} approaches zero, while J^{p}_{Str} reaches the value $J^{p}_{Str}(-A^{p}_{Str}) = 4.868\text{mM/s}$ in two steps. This is approx. 23% of the maximum flux at $A^{ld}_{Str} = 0$.

Molecularly, the coupling mechanism can be interpreted as follows:

Under fully coupled conditions, the actomyosin bond is always split by $MgATP^{2-}$ only after first achieving the maximal stroke length (here $l_{Str} = 12.0\text{nm}$). If a specific negative A^{ld}_{Str} value is exceeded, however, the bond cleavage already takes place at a lower stroke length, so that the shortening velocity must decrease. The now no longer coupled MH_{En}s ; however, still possess the fraction $1 - \Delta l_{Str}/l_{Str}$ of their original potential A^{p}_{Str}, which now becomes dissipated. The cleaved MH_{En}s are moving along the rest of their stroke length without load. Then the cycle continues as under coupled conditions.

If $A^{ld}_{Str} = -A^{p}_{Str}$, the actomyosin splitting already occurs immediately after bond formation, so that the whole input potential A^{p}_{Str} gained during coupling becomes dissipated. The MH_{En}s perform their conformational change now throughout the whole stroke length at zero load, so that in this situation the entire input potential must be released as heat energy. As v^{ld}_{Str} has vanished, then accordingly the mechanical power $F^{ld}_{Str} \times v^{ld}_{Str}$ must also be zero in the process. But this does not mean that the force F^{ld}_{Str} must also vanish. When actomyosin bonds are formed, it is possible that the force F^{ld}_{Str} is transferred via the action of a torque onto actin filaments, without mechanical work being performed. The result of such a mechanism would be a force development without shortening, that is, an isometric contraction. Experimentally, such a force can be determined if a muscle or an SMF is fixed at constant length in two supports, and the tensile strength is measured in one of them. Then, with a given $[Ca^{2+}]_c$, isometric contraction is activated when the CBs try to transfer their A^{p}_{Str} to actin filaments. This, however, can only by accomplished as torque because the length fixation does not allow sarcomere shortening and with it isotonic contraction. In the process, however, exactly that load is generated that allows $MgATP^{2-}$ to cleave actomyosin bonds already at $l_{Str} = 0$ or $\Delta l_{Str}/l_{Str} = -1.0$.

The $[Ca^{2+}]_c$ dependency under these isometric conditions results from the fact that, at a given $[Ca^{2+}]_c$, always a specific number of CBs works, which is related to the concentration of CB. At a low number, only these generate the maximum force per CB under isometric conditions, which results in splitting of actomyosin bonds at $l_{Str} = 0$. The resulting SMF total force must then be correspondingly low. At a high number and high $[Ca^{2+}]_c$, the bond cleavage at $l_{Str} = 0$ is triggered in the same way, only in this case that the total number is considerably higher, and hence, also a higher power development can be recorded.

As a special feature of the isometric contraction it can be realized though the mechanical power with

$$P_{\mathrm{Str}}^{\mathrm{mech}} = v_{\mathrm{Str}}^{\mathrm{ld}} \times K_{\mathrm{Str}}^{\mathrm{ld}} = 0$$

is zero, the metabolic power with

$$P_{Str}^{met} = J_{Str}^{p} \times A_{ATP}^{c}$$

however, has a positive value because the CB cycle also under isometric conditions is gone through with ATP consumption. For a $[\mathrm{Ca}^{2+}]_{\mathrm{c}}$ of 6.0 µM, for example, the consumption of $J_{Str}^{p} = 4.9$ mM/s. This value appears low when considering the fact that the uncoupled flux is driven by A_{Str}^{p} alone. The corresponding flux for an $A_{Str}^{ld} \to 0$ would be considerably higher. However, L_{Str} must also be taken into consideration. Through the incorporated factor $K_{MI}^{ld}/\left(K_{MI}^{ld} + A_{Str}^{ld}\right)$, the flux drops hyperbolically with an increasingly negative A_{Str}^{ld}. Also during uncoupling, the actomyosin bond is initially formed. But this reaction is inhibited through a strong negative load potential $(= -A_{Str}^{p})$, so that the flux resulting from a high affinity and a low conductance must assume a value between the maximal and very low flux. In comparison, the whole ATP consumption of an SMF under isometric conditions (at $[\mathrm{Ca}^{2+}]_{\mathrm{c}} = 6.0\,\mu\mathrm{M}$) is $J_{ATP}^{tot} = 8.9$ mM/s.

Regarding the uncoupling mechanism described here, it can be summarized such that while this may appear complicated in the derivation, the required efficiency maximum is obtained in this model without additional postulates. Furthermore, the deviation from the fully coupled flux produced in the uncoupled range is low and thus conforms to experimental results. Moreover, with the aid of this mechanism, isometric contraction and its associated ATP consumption can be explained.

The CB cycle also possesses opposite and equal partial conduction at SSC: The affinities are

$$A_1^{del} = A_{\mathrm{En}}^{ld} + \left(-A_{Str}^{p}\right) \text{ and } A_2^{dem} = A_{Str}^{p} + \left(-A_{\mathrm{En}}^{ld}\right),$$

from which

$$L_{c1}^{del} = 1.317\ \times 10^{-4} \text{ and } L_{c2}^{dem} = 1.317 \times\ 10^{-4}\,\mathrm{mM/s \times mol/J}$$

can be obtained. However, this only applies under coupled conditions.

11.5 Limitation of contractile performance

The best known limitation in the performance of a muscle is its fatigue during enduring demands. This phenomenon is extremely interesting for physiology and sport medicine. Numerous differing elicitors have been related to fatigue [21, 22], however, to date, there is no unequivocal evidence regarding whether there is one single

mechanism and which one this could be. This is certainly also due to the parameters, which come into question, for example, the sarcosolic concentration of $MgATP^{2-}$, which is being very difficult to determine experimentally, if at all. However, such a problem can be solved through the use of mathematical simulations, as nearly all the important metabolites of energy metabolism, including $[MgATP^{2-}]_c$, can be gathered.

In the present model of the CB cycle, $[MgATP^{2-}]_c$ is the substrate of myosin ATPase. It occurs in R1 as a reactant, and therefore is contained in A_{R12}. Therefore, there is a possibility that J_{En} can be influenced by a change in $[MgATP^{2-}]_c$. To change a flux by an alteration of its affinity is primarily possible if the respective reaction proceeds near equilibrium, which applies to J_{En}. But this can mean that a minor reduction in $[MgATP^{2-}]_c$ could make J_{En} smaller than J_{Str}, so that during the cycle fewer MH_{En}s are separated from actin than CBs are formed. Subsequently, [CB] must increase. This in turn leads to an even more pronounced ATP consumption, and hence to a further reduction of $[MgATP^{2-}]_c$. Through the increase in [CB], however, A_{Str}^{ld} becomes less negative (because of load reduction) so that as a result, the cycle frequency must also rise. This vicious circle only ends when all the MH_{En}s are present as CBs ($[CB] = 657.8\,\mu M$).

One such situation is presented in Figure 11.4. $[MgATP^{2-}]_c$ constantly decreases from the start (Figure 11.4A), while [CB] increases. At the beginning, J_{En} is only very slightly lower than J_{Str} (Figure 11.4B). What happens in detail can be seen from the course of the affinities involved (Figure 11.4C). The sudden collapse of A_{Str}^{ld} (blue points) is caused by the equally sudden increase in the CB concentration. The reduction in A_{Str}^{p} (red points) is caused by the reduction in $[MH_{En}]$ and the drastic increase in $[ADP]_c$ and $[P_i]_c$ (Figure 11.4D). The falling A_{Str}^{p} and rising A_{Str}^{ld} achieve opposite equal values, that is, their sum vanishes so that J_{Str} is also now zero.

Thus, the cycle comes to a standstill and from this point on, ATP consumption by these reactions vanishes. Now enough ATP can be resynthesized to reach the initial value of $[MgATP^{2-}]_c$ again (Figure 11.4A). Also PCr, which is consumed down to approx. 0.1 mM, can now be regenerated.

At $[Ca^{2+}]_c = 1.136\,\mu M$ and a given load potential of − 16.8 kJ/mol, the temporary collapse of $[MgATP^{2-}]_c$ and CB cycle still stand is triggered through lowering of the sarcosolic Mg^{2+} concentration from 0.8 (simulation starting value) to 0.55 mM. After around 15.0 ms, [CB] rises to 93.0 µM (instead of 44.6 µM). This results in A_{Str}^{ld} rising to approximately −8.05 kJ (instead of − 16.8 kJ/mol). After approximately 14.0 s, [CB] runs $\rightarrow$ 557.8 µM, $[MgATP^{2-}]_c \rightarrow 2.315$mM and $J_{Str} \rightarrow 0$, because $A_{Str}^{p} = -A_{Str}^{ld} = 11.4$kJ/mol has been reached. Due to the fact that the CB cycle is switched off, and no ATP is consumed by those reactions, ATP can be rapidly resupplied by the metabolism so that primarily PCr and $MgATP^{2-}$ are available again in sufficient quantities.

It is in fact only the reduction in $[MgATP^{2-}]_c$ triggers this process. However, both $[Ca^{2+}]_c$ and the height of the load potential play a role in this process. Due to a high $[Ca^{2+}]_c$, [CB] is also high, which at the given load potential leads to an

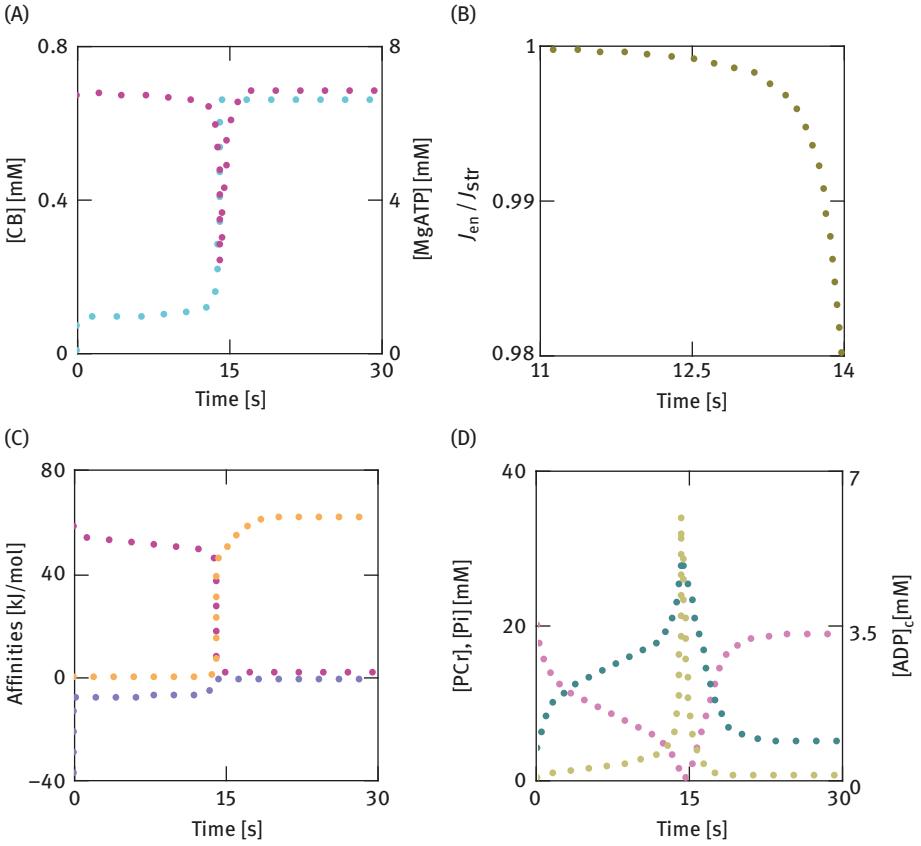

Figure 11.4: Collapse of muscular performance through a reduction of $[MgATP^{2-}]_c$. (A) Time courses of $[MgATP^{2-}]_c$ (red points) and [CB] (cyan points) after $[Mg^{2+}]_c$ has been reduced from 0.8 to 0.55 mM. (B) Time-dependent decrease of J_{En}/J_{Str}. (C) Changes of respective affinities with time, red points: A^p_{Str}; yellow points: A_{En}; blue points: A^{Id}_{Str}. (D) Changes of metabolites, red points: [PCr]; green points: $[ADP]_c$; dark green points: $[P_i]_c$.

increased ATP consumption rate and as a result favors the reduction of $MgATP^{2-}$. Thus, for $[Ca^{2+}]_c = 6.0\,\mu M$ and the same load potential (–16.8 kJ/mol), the process can already be triggered through a reduction of $[Mg^{2+}]_c$ to 0.65 mM. A lowering of the load potential at a given $[Ca^{2+}]_c$ aggravates the situation, because now the frequency becomes elevated, so that the ATP consumption rate is increased this time over this parameter. At $[Ca^{2+}]_c = 1.136\,\mu M$ and a load potential of only –3.0 kJ/mol, the process is already triggered at 0.76 mM. On the other hand, triggering can be prevented or at least delayed by raising $[MgATP^{2-}]_c$ through an elevation of the total ATP concentration and/or $[Mg^{2+}]_c$ (starting value).

A reduction in $[MgATP^{2-}]_c$ can be brought about by a whole series of mechanisms, which all have an indirect effect. It is in this context that the acidification of

the sarcosol is of particular importance insofar as this mechanism can be observed at an increased power – output. First of all, the fast SMFs are affected by this, whose ATP is primarily produced by GLY. The Lac plus proton created in the process is transported from the sarcosol into the interstitial space via the Lac/H symport, but not completely so that at steady state both $[Lac^-]_c$ and $[H^+]_c$ are elevated. Figure 11.5 shows the functional relationship between $[MgATP^{2-}]_c$, $[H^+]_c$ and $[Mg^{2+}]_c$.

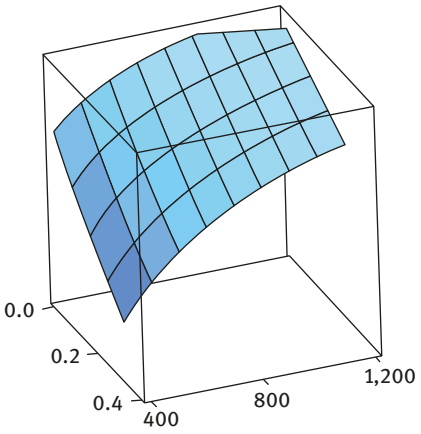

Figure 11.5: Three-dimensional representation of the function $MgATP^{2-}(H^+, Mg^{2+})$. *Z*-axis $\triangleq$ $[MgATP^{2-}]_c$ from 4,500 to 7,500 µM; *X*-axis $\triangleq$ $[H^+]_c$ from 0 to 0.4 µM; *Y*-axis $\triangleq$ $[Mg^{2+}]_c$ from 400 to 1,200 µM.

From the figure it can be seen that $[Mg^{2+}]_c$ has a particular influence on the level of $[MgATP^{2-}]_c$. An increase in $[H^+]_c$ is capable of reducing $[MgATP^{2-}]_c$, which may explain the metabolically caused reduction. However, this can be attributed in part back to a reduction of total ATP. All the reactions taking part with pH regulation, such as Na/H exchange (↓, downward pointing arrow indicates reduction), high buffering (↓), low Lac/H symport (↑), and proton production through ATP splitting itself (↑) are involved. The PCr reaction must also be mentioned in this context, because it promotes the formation of $MgATP^{2-}$ by raising pH. Lac accumulation in the interstitium and a resulting backpressure on glycolysis with a reduction in pH can also lead to lowering of $[MgATP^{2-}]_c$.

The in silico results obtained here suggest that this limitation of SMF function is the trigger for cramp, which is not restricted to a single muscle fibre, but extends in vivo across the whole muscle as a rule. The medical aid, for example, for cramp in the calf, is to apply an antagonistic force from the ankle to work against the contraction. This not only reduces the pain, but also helps to release the cramp. The CB cycle also normalizes correspondingly in the model. To set normal cycling into motion again, it is not sufficient that above all $[MgATP^{2-}]_c$, $[ADP]_c$ and $[P_i]_c$ reach their initial values again. This would produce the same simulation result with unchanged low $[Mg^{2+}]_c$ and/or $[ATP]_c$. Cycling must be started at a more negative load potential in

order to allow the CB cycle to run without contracture despite the still too low $[Mg^{2+}]_c$. Because at a more negative A_{Str}^{ld}, both $J_{Str}$and the ATP consumption rate are lowered so that under these conditions the ATP production rate (J_{ATP}) is sufficient to keep $[MgATP^{2-}]_c$ from decreasing. But a complete recovery can be expected only then if $[Mg^{2+}]_c$ again reaches its normal value (here approx. 0.8 mM).

A much more harmless and painless result of muscle fatigue in which training athletes ought to be particularly aware of is the gradual failure of the muscle or muscle group during exercises with repeated muscular activity, for example, pull-ups or squats. In doing so, a limit is always reached after which a continuation of the respective exercise is no longer possible. Painful cramp formation is however not triggered in such a situation. Therefore, it appears reasonable to suggest that a different mechanism may be involved, but one which likewise limits muscular performance.

An increase of J_{Str} is also always linked to a rise in $[ADP]_c$ (or $[MgADP^-]_c$) and $[P_i]_c$. Particularly, an increased $[ADP]_c$, as a reaction product, has an inhibitory effect on J_{Str}. At $[Ca^{2+}]_c = 6.0\,\mu M$ and a load – potential of –31.471 kJ/mol, $[ADP]_c$ increases from 72.0 to 130.26 µM. However, this is not sufficient to make J_{Str} slower than J_{En}. If this were the case, [CB] would reduce and at the same time A_{Str}^{ld} would become more negative, because the load would be distributed over fewer CBs. In the extreme case, the initial isotonic contraction would become isometric without power output.

$$\text{At } [Ca^{2+}]_c = 0.3\,\mu M \text{ is } (SIM_{GLY/PAL})$$

$$[MgATP^{2-}]_c = \frac{[ATP]_c}{P(H^+, Mg^{2+})} = \frac{8928.79}{P(10^{-1.0762}, 802.2)} = 7.198\text{mM},$$

and at 6.0 µM

$$[MgATP^{2-}]_c = \frac{[ATP]_c}{P(H^+, Mg^{2+})} = \frac{8868}{P(10^{-1.1097}, 827)} = 7.204.8\text{mM}.$$

Therefore, both values remain practically the same at a strong negative load potential ($A_{Str}^{ld} = -31.471\text{kJ/mol}$). The decisive reason for this is that, despite the high Ca^{2+} concentration and high force development, J_{Str} and therefore, also J_{ATP} are relatively low.

With repeatedly high muscular demands, however, ATP supply via the PCr shuttle may be delayed through an acidification at the sites of ATP and PCr^{2-} production, because at these locations of the sarcosol, the affinity of PCr formation (reverse reaction) may become reduced by a rise in $[H^+]$. The opposite is the case at the sites of ATP and PCr consumption (forward reaction), for example, in the fibrils. In this case, a reduction in $[H^+]$ has an inhibitory effect. As already mentioned, the functional differentiation between the sites of ATP consumption and those of ATP production were not included in the simulations. The following

example can help to estimate the possible consequences: At sites of PCr and ATP consumption (fibrils)

$$A_{CK} = RT \ln\left(\frac{[\mathrm{PCr}^{2-}][\mathrm{MgADP}^{-}][\mathrm{H}^{+}]}{[\mathrm{Cr}][\mathrm{MgATP}^{2-}]}\ K^{ref}_{PCr}\right)$$
$$= RT \ln\left(\frac{[11.7998][0.077959][10^{-7.15996}]}{[28.0][7.06917]}\ K^{ref}_{PCr}\right)$$
$$= 0.26102\,\mathrm{kJ/mol},\ \text{and}\ J_{CK} = 7.048\,\mathrm{mM/s}.$$

At sites of PCr production

$$A_{CK} = RT \ln\left(\frac{[\mathrm{Cr}][\mathrm{MgATP}^{2-}]}{[\mathrm{PCr}^{2-}][\mathrm{MgADP}^{-}][\mathrm{H}^{+}]}\ \frac{1}{K^{ref}_{PCr}}\right)$$
$$= RT \ln\left(\frac{[25.0][7.1516]}{[14.748][0.02879][10^{-6.9449}]}\ \frac{1}{K^{ref}_{PCr}}\right)$$
$$= 0.261025\mathrm{kJ/mol},\ \text{and}\ \overleftarrow{J}_{CK} = 7.048\mathrm{mM/s}.$$

If the pH_c would drop from 6.9449 to 6.93 (sites of production), this would lead to $A_{CK} = 0.1828\,\mathrm{kJ/mol}$ and $\overleftarrow{J}_{CK} = 4.935\,\mathrm{mM/s}$. Obviously, already a small drop in the pH_c value is sufficient to create a flux difference of about 30%. Even if this could be in part compensated in living muscle cells, so that the reduction would be less dramatic, a pH-related delay in ATP transport via the PCr shuttle must still be expected. The pH_c reduction under nonsteady-state conditions is caused by different proton binding of the two reactions ATP and PCr splitting and ATP and PCr formation. The result for cleavage (forward reaction) is

$$\Delta_R N_{ATP} + \Delta_R N_{PCr} = -0.648 + 0.924 = 0.276,$$

and for formation (reverse reaction) is

$$\Delta_R N_{ATP} + \Delta_R N_{PCr} = 0.502 + (-0.886) = -0.384.$$

The negative value for the reverse reaction shows that protons are lost ($pH_c \downarrow$) as both reactions progress. Furthermore, it must be assumed that an additional acidification, especially of the sarcosol due to the increased formation of Lac, could occur under these conditions. In the fibrillary space, a higher pH value is obtained and also shifts that occur in Mg^{2+} can be ignored.

It should be noted in connection with this that the above-mentioned processes are not dependent on the formulation of the reactions concerned, which means the PCr reaction could, for example, be equally well formulated without Mg^{2+}, the corresponding $\Delta_R \bar{N}_{PCr}$ would thereby remain unaffected, because it depends on the respective $K'(\mathrm{H}^{+}, \mathrm{Mg}^{2+})$, which is always related to all species.

On the basis of the CB model presented here, two different fatigue phenomena can be explained, which are associated with the fact that an SSC of the CB cycle occurring with constant [CB] is brought about by two opposing reactions. On the one hand, [CB] is decreased by actomyosin cleavage (J_{En}), on the other hand, [CB] is increased by actomyosin formation (J_{Str}). At SSC, both fluxes are equal. Already small deviations from this steady state can induce perturbation. Acidification at a sufficiently high $[MgATP^{2-}]_c$ is the less severe interference. However, it can be envisaged that after several episodes of fatigue and recovery, a lowered $[ATP]_c$ (ATP loss via AK and AMP deaminase) and a too low $[MgATP^{2-}]_c$ may be the result followed by cramp formation, as is seen in competitive sports. Severe damage with cell death is, however, not connected with this. Such a refusal of the muscles to work could also be seen as a protective mechanism, which prevents muscle cells from suffering irreversible damage through an overly high demand for contraction power.

The fact that muscle cells can maintain their $[ATP]_c$ almost constantly even at increased power output or more precisely at high J_{Str} is determined by the cycle behavior as this cycle does function only at a high $[MgATP^{2-}]_c$ (approx. 7.0 mM). As long as the muscle works with normal performance, no clear reduction of $[ATP]_c$ can be observed, even at high power. The development of a sufficiently high ATP gradient between the sites of consumption and production is therefore not possible. The task of energy transport via diffusion must be taken over, therefore, by the PCr shuttle, and the reactants of which can generate high gradients. Also for this reason, the PCr shuttle is indispensable for the SMF, as only in this way can the ATP cleavage energy diffuse to sites of consumption, without ATP and ADP themselves needing to form gradients for diffusion.

12 Recovery

By recovery, one means all those reactions that must occur within a particular timeframe to again reproduce the resting state with its characteristic values for predominantly $[Ca^{2+}]_c$, $[ATP]_c$, and [PCr], after a previous phase of high workload at elevated $[Ca^{2+}]_c$ and a high rate of ATP consumption. Coupled reactions are also of primary importance in this case. In simulations, a high-power output is induced by increasing $[Ca^{2+}]_c$ from near resting state conditions ($[Ca^{2+}]_c = 0.3\,\mu M$, $J_{ATP} = 1.0\,\mu M/s$) to 6.0 μM. In the process, the load potential is $A^{ld}_{Str} = -1.68\ 10^4 J/mol$. Figure 12.1A shows the effect such an abrupt change from rest to high power has on the glycolytic fluxes. Under these conditions, J_{ATP} consists of 8.5% J^{palm}_{ATP} and 91.5% J^{gl}_{ATP}, whereby the latter runs oxidative (J^{glox}_{ATP}) to 30.0% and anoxic to 70.0% (J^{glanox}_{ATP}). This in turn is made up almost completely from anoxic Glgen degradation. As long as Glgen is present, Glu is not used as a substrate under these conditions. This saving of Glu is enabled by increasing G – 6 – P from 483.0 to 582.0 μM and the associated inhibition of *HK* (Figure 12.1A black). Such a mechanism is essential to prevent the blood glucose concentration from falling below the critical value; otherwise, impairment of the brain as a result of such hypoglycemia cannot be ruled \out.

As can be seen in Figure 12.1A, all the glycolytic fl uxes (except J_{HK}) drastically increase by a factor of 10.53 for J_{ATP} and 20.33 for the glycolysis fluxes (J_{GLY}) after switching to high-power output. In the process, J_{GAP} (blue) is always twice as high as J_{GLY}. This high activation of GLY occurs nearly twice as fast as the production of ATP, and is associated with a different allocation of ATP between the PAL and GLY degradation pathways at a high ATP demand to that occurring under resting conditions. This switching process is depicted in Figure 12.1. Due to an increase in ATP consumption rate, $[ADP]_c$ increases so that [AMP] also considerably increases via the AK reaction (12.1B). This, in turn, activates the PFK reaction, which results in the activation of both J^{glox} and J^{glanox}, that is, of the entire metabolism proceeding via glycolysis.

The rate of PAL, on the other hand, only increases marginally.

[PCr] significantly decreases due to the high ATP demand (from approx. 20.0 to 10.28 mM), while $\left[MgATP^{2-}\right]_c$ only drops by 0.035 mM (from 7.198 to 7.163 mM). $[P_i]_c$ rises from approx. 4.0 to 12.3 mM (12.1 C). This value results predominantly (to 99.2%) from the initial ATP cleavage and the ATP buffering through the PCr reaction.

The pH values of the sarcosol and the mitochondrial matrix change in opposite directions (12.2A). pH_c increases marginally, while pH_m decreases.

In Figure 12.2B and C, the respective proton fluxes are shown. From these it can be seen that initially protons of the sarcosol disappear (B, red line) and are produced in the matrix (C, red line). The proton production rate through ATP cleavage in the sarcosol (blue) is compensated after approx. 5.0 s by the proton consumption rate via ATP/ADP – Ex plus H/Pi (yellow), so that a transient proton production rate

https://doi.org/10.1515/9783110650501-012

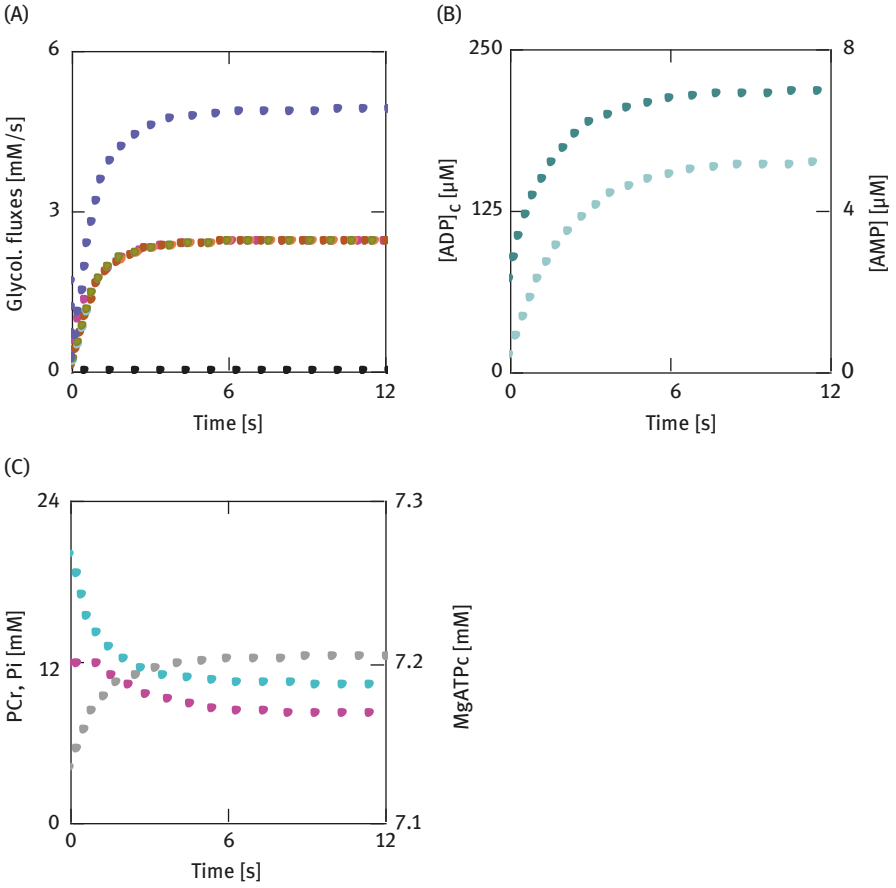

Figure 12.1: Effects of switching from low- to high-power output at $[Ca^{2+}]_c$ = 6.0 μM on glycolytic fluxes and metabolites. A: fluxes, J_{GAP} (blue); J_{HK} (black); J_{Glgen} (red); J_{PGI} (yellow); J_{PFK} (brown); J_{Ald} (cyan); J_{TIM} (gray). B: $[ADP]_c$ (green); [AMP] (light green). C: [PCr] (green); $[P_i]_c$ (gray); $[MgATP^{2-}]_c$ (red).

would be created (green) if in addition sarcosolic protons were not consumed by the PCr reaction (cyan). In addition to this are those metabolic reactions that generate protons, for example, the LDH reaction. However, this is clearly not sufficient to compensate for full alkalization, and so finally under these conditions, pH_c must initially increase slightly.

The opposite takes place in the mitochondrial matrix. In this case, the ATP synthesis taking place consumes protons (C, blue), which in turn is compensated through the transport reactions ATP/ADP – Ex plus H/Pi (yellow). While the carbonic anhydrase (CA) reaction may still reduce (C, red line) the remaining proton production rate (green) slightly, acidification of the matrix primarily remains because the PCr reaction does not take place.

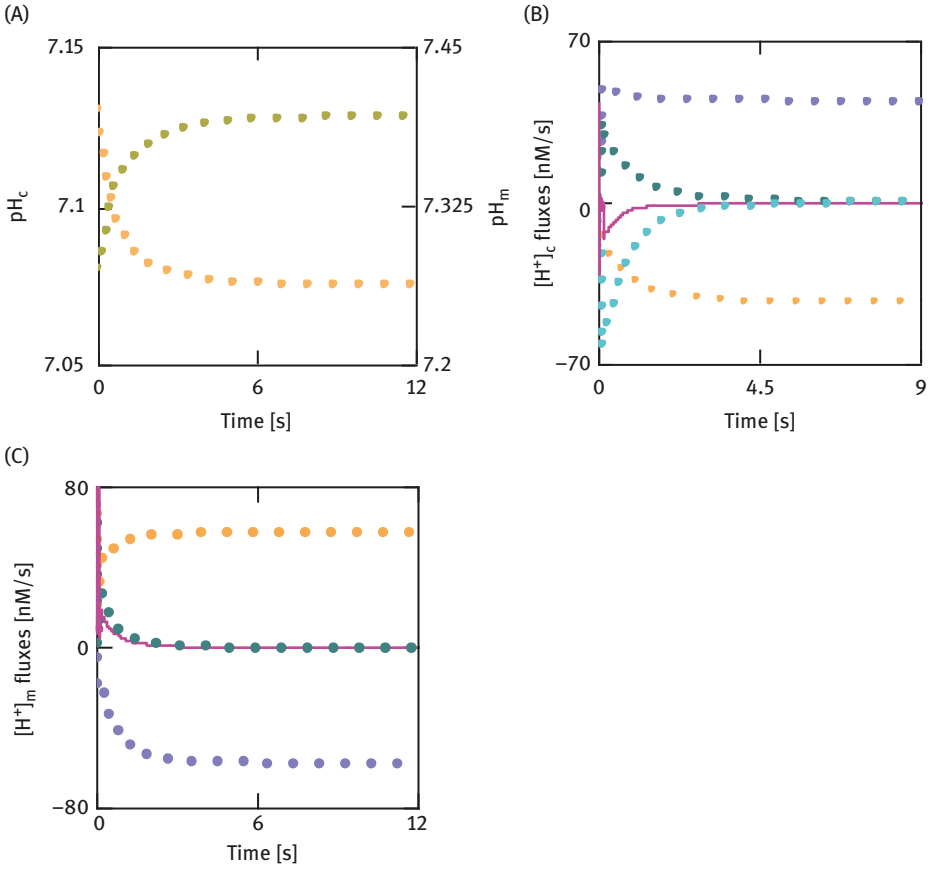

Figure 12.2: Effects of switching from low- to high-power output at $[Ca^{2+}]_c = 6.0\,\mu M$ on pH_c and pH_m, and rates of sarcosolic and mitochondrial proton generation and compensation reactions.
(A) pH_c (green); pH_m (yellow). (B) Sarcosolic proton fluxes, blue points: J^c_{ATP}; yellow points: J_{AE} plus J_{HP}; green points: J^c_{ATP}, J_{AE} and J_{HP}; cyan points: J_{Pcr}; red line: J^{tot}_{Hc}. (C) Mitochondrial proton fluxes, blue points: $J^m_{ATP} = J_{SY} + J_{CAC}$ (ATP formation); yellow points: J_{AE} and J_{HP} (in the matrix); green points: J^m_{ATP}, J_{AE} and J_{HP}; red line: J^{tot}_{Hm}.

Figure 12.3 shows the time courses of ATP production rates from PAL plus GLY ($= J_{ATP} = J^{Del}_{ATP}$, blue), from J_{PCr} (cyan), and the ATP consumption rate ($J_W = J^{Dem}_{ATP}$, gray). In addition, J^{Del}_{ATP} plus J_{PCr} (red line) is also depicted.

One sees that during the first 6.0 s, the metabolism is not able to cover the ATP demand (blue and gray). This is only guaranteed when there is also ATP production via the PCr reaction (red line). Only then is $J^{Del}_{ATP} = J^{Dem}_{ATP}$ fulfilled after about 0.2 s, and so a dangerous drop in $[MgATP^{2-}]_c$ can be prevented.

It seems likely from the early consistency of the fluxes that similar dissipation functions can also be suggested if these also contain the PCr reaction. Instead of

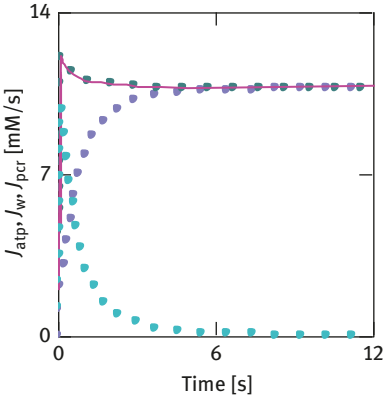

Figure 12.3: ATP-producing fluxes after switching from low- to high-power output at $[Ca^{2+}]_c = 6.0\,\mu$M. Gray points: J_W (all ATP demanding reactions); blue points: ATP delivery rate by PAL plus GLY (mainly via J_{Glgen}); cyan points: ATP production rate by J_{Pcr}; red line: ATP delivery rate by PAL plus GLY plus J_{Pcr}.

relating solely to J_{ATP} (see Chapter 9), $J_{ATP}^{pcrDel} = J_{ATP} + J_{Pcr}$ has to be taken. From this, one obtains the dissipation function

$$\Psi_{ATP}^{pcrDel} = J_{ATP}^{pcrDel}\left(-A_{ATP}^{c}\right) + \Psi_{ovt} \tag{12.1}$$

with respect to J_{ATP}^{pcrDel}-transformed parameters

$$\bar{A}_{ovt}^{pcr} = \frac{\Psi_{ovt}}{J_{ATP}^{pcrDel}}$$

and

$$\bar{L}_{c}^{pcrDel} = \frac{\Psi_{ovt}}{\left(\left(-A_{ATP}^{c}\right) + \bar{A}_{ovt}^{pcr}\right)^2}. \tag{12.2}$$

This results in

$$J_{ATP}^{pcrDel} = \bar{L}_{c}^{pcrDel}\left(\left(-A_{ATP}^{c}\right) + \bar{A}_{ovt}^{pcr}\right) \tag{12.3}$$

with the partial conductances

$$\bar{L}_{c1}^{pcrDel} = \bar{L}_{c}^{pcrDel}\frac{\left(-A_{ATP}^{c}\right) + \bar{A}_{ovt}^{pcr}}{-A_{ATP}^{c}} \tag{12.4}$$

and

$$\bar{L}_{c2}^{pcrDel} = \bar{L}_{c}^{pcrDel}\frac{\left(-A_{ATP}^{c}\right) + \bar{A}_{ovt}^{pcr}}{\bar{A}_{ovt}^{pcr}}. \tag{12.5}$$

The respective parameters for

$$\Psi^{Dem} = \Psi_W = \Psi_W^{ld} + J_W A_{ATP}^{c} \tag{12.6}$$

are the same as those in Chapter 9. These are

$$\bar{A}_W^{ld} = \frac{\Psi_W^{ld}}{J_W}$$

and

$$\bar{L}_c^{Dem} = \frac{\Psi_W^{ld} + J_W A_{ATP}^c}{\left(A_W^{ld} + A_{ATP}^c\right)^2}. \tag{12.7}$$

The corresponding flux is

$$J_W = J_{ATP} = \bar{L}_c^{Dem}\left(\bar{A}_W^{ld} + A_{ATP}^c\right), \tag{12.8}$$

from which

$$\bar{L}_{c1}^{Dem} = \bar{L}_c^{Dem}\ \frac{\bar{A}_W^{ld} + A_{ATP}^c}{\bar{A}_W^{ld}}\ (<0) \tag{12.9}$$

and

$$\bar{L}_{c2}^{Dem} = \bar{L}_c^{Dem}\ \frac{\bar{A}_W^{ld} + A_{ATP}^c}{A_{atp}^c}\ (>0) \tag{12.10}$$

are obtained.

As already demonstrated for moderate power output, under the conditions of considerably higher power output at $[Ca^{2+}]_c = 6.0\ \mu M$, $\bar{L}_{c1}^{pcrDel}$ is also oppositely equal to $\bar{L}_{c2}^{Dem}$ (-1.95473×10^4 and 1.95473×10^4). However, this time the PCr reaction is taken into consideration during the calculation of partial conductances. This leads to the result that not only the dissipation functions and fluxes, but also these quantities are oppositely equal practically from the start (Figures 12.3 and 12.4A–C). This result is solely due to the very high rate of the PCr reaction. As can also be seen in Figure 12.4, to achieve an SSC, it is clearly not essential that the involved reactions are at steady state. A very similar situation has already been observed while dealing with OP, where an SSC of protons can be develop early on, even if the involved redox reactions are not yet at steady state. It seems reasonable to assign responsibility for this to the effect of the intermediary $\Delta\tilde{\mu}_H$ and the PCr reaction, respectively, as both $\Delta\tilde{\mu}_H$ and the PCr potential μ_{PCr} appear as coupled energy carriers. Both quantities are involved in reactions with high conductances, which obviously enable the cycle to achieve an SSC already after a very short delay. This result is fundamentally important as it demonstrates that the ATP cycle linked to energy metabolism may proceed to be dissipation free under all possible conditions. The permanently progressing ATP splitting and formation reactions are energetically of no significance, as all the affinities or $\Delta_R G$s are fully compensated in the closed cycle. Neither entropy nor heat can be produced by such a cycle. Also $\Delta_{Re}S$ must disappear, as it is a circular process. The fact that $\Delta_{Ri}S$ also disappears may be surprising at first, for progressing chemical

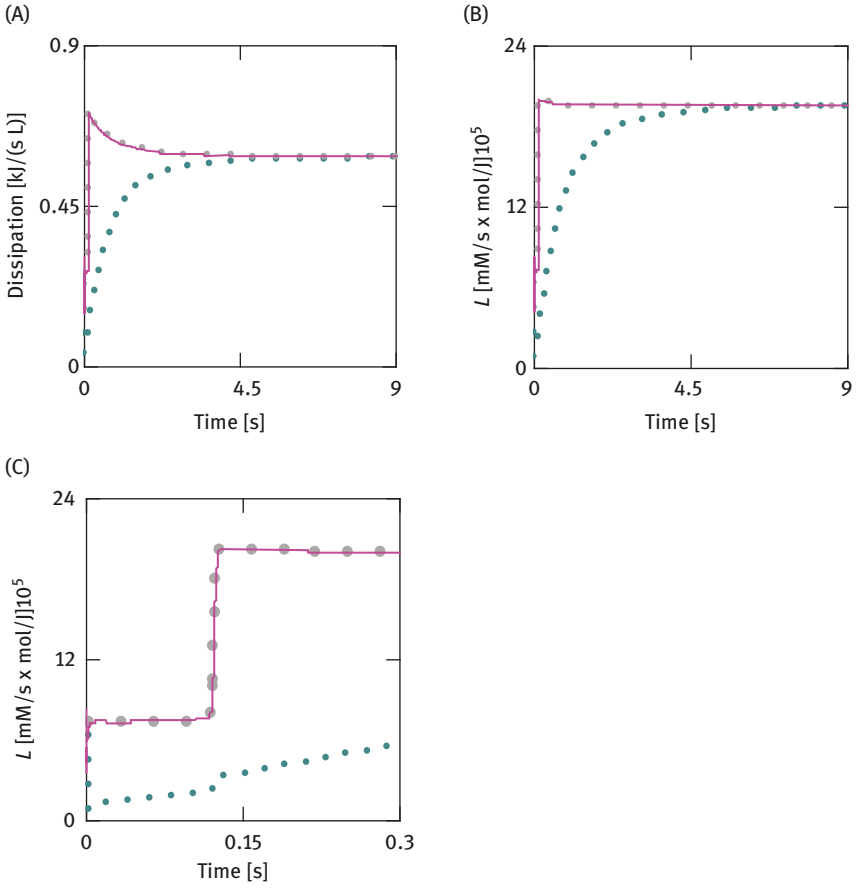

Figure 12.4: Matching of dissipation functions and conductances after switching to $[Ca^{2+}]_c$ = 6.0 µM. (A) Dissipation functions, gray points: Ψ_W; green points: Ψ_{PAL} and Ψ_{GLY}; red line: Ψ_{PAL}, Ψ_{GLY} and Ψ_{Pcr}. (B) Conductances, gray points $\bar{L}_{c2}^{Dem}$; green points: $-\bar{L}_{c1}^{Del}$; red line: $-\bar{L}_{c1}^{pcrDel}$ including L_{Pcr}. (C) Matching during the first 300.0 ms.

reactions are involved, each of which when considered separately must be linked to entropy production (positive). However, it should be remembered that such cycles are made up of two coupled reactions; of which, the input reaction is coupled to a negative potential (here $-A_{ATP}^c$), which now with opposite direction (A_{ATP}^c) can drive a second reaction due to coupling, so that ATP formation and cleavage results in a reaction cycle. The second reaction is usually composed of several parallel, ATP-coupled individual reactions.

The entropy production of ATP formation is negative and would be considered not compatible with the second law of thermodynamics, when assessed without coupling. As this reaction is, however, coupled to metabolism, for example Glu oxidation, with a considerably more positive $\Delta_{Ri}S$, the result for the total reaction is

also a $\Delta_{Ri}S > 0$, so that the second law is not violated. In the cyclical process, always only the opposing potentials, such as $-A^c_{ATP}$ and A^c_{ATP} are considered so that with identical fluxes, the respective dissipation functions must also compensate and, as a result, any entropy production in the cycle cannot occur. It follows that the resistance of the cycle must vanish and that the associated partial conductances of respective affinities (here $-A^c_{ATP}$ and A^c_{ATP}) are oppositely equal.

The inclusion of the PCr reaction in the calculation of partial conductances takes place only in connection with a high $[Ca^{2+}]_c$ = 6.0 μM, to demonstrate that an early conductance matching is operative even under conditions of an abrupt change from rest to very high power output. Under moderate conditions, as prevail when $[Ca^{2+}]_c$ = 1.136 μM, this mechanism naturally also comes into effect (see Figure 9.1).

Following the above-described relationships, the restoration of the conditions as seen at rest after a previous power output must apply mainly to the ATP cycle and the associated PCr shuttle. Hence, the next, fast delivery of contractile energy is often essential for the life of an individual. For this, $[ATP]_c$ and particularly [PCr] must be present in sufficiently high concentrations. From Figure 12.1C it can be seen that [PCr] drops down from approx. 20.0 to 10.28 mM during high power output. At the same time, $[ADP]_c$ increases to 308.0 μM. When a simulation ($SIM_{GLY/PAL}$, A3) is started from these initial values, then it can be seen that $[MgATP^{2-}]_c$ immediately decreases drastically, and the system switches to protection mode; in the same way as when triggered by too low $[Mg^{2+}]_c$ (see Figure 11.4). From this it follows that at least after a high power output, the resting condition must first be present again with high [PCr] and low $[ADP]_c$ before the SMF is able to give off high power once again.

Figure 12.5 shows the time courses of respective parameters approaching their resting values. A precondition for this is that the high contraction power becomes reduced again by a decrease of $[Ca^{2+}]_c$ from 6.0 to 3.0 μM. In a real SMF, this requires a certain length of time because initially MP must be repolarized and Ca^{2+} is pumped back into the SR. These processes are not included in the simulation. The curves relate purely to an abrupt reduction in the Ca^{2+} concentration.

From Figure 12.5A it can be seen that all the glycolytic fluxes reduce from originally high starting values to their resting values. At the same time, the Glgen consumption (red) decreases and is replaced again by Glu degradation (black). Also under these conditions, J_{GAP} is always twice as large as all the other fluxes of GLY.

From Figure 12.5B it can be seen that both $[ADP]_c$ and [AMP] return to their resting values within 30.0 s. Correspondingly, $[MgATP^{2-}]_c$ (C, red) rises.

Furthermore, Figure 12.5C demonstrates that [PCr] also achieves its starting value again. The affinity A_{PCr} of this reaction is always very low in the steady state; in other words, the PCr reaction is practically in equilibrium both under resting conditions ($A_{PCr} = 1.18\ 10^{-3}$ J/mol)) and at high power output ($A_{PCr} = 0.013$J/mol). When switching to high power, J_{PCr}increases primarily through the increase of $[ADP]_c$ at sites of ATP consumption. This is reflected in the simulation, although as has

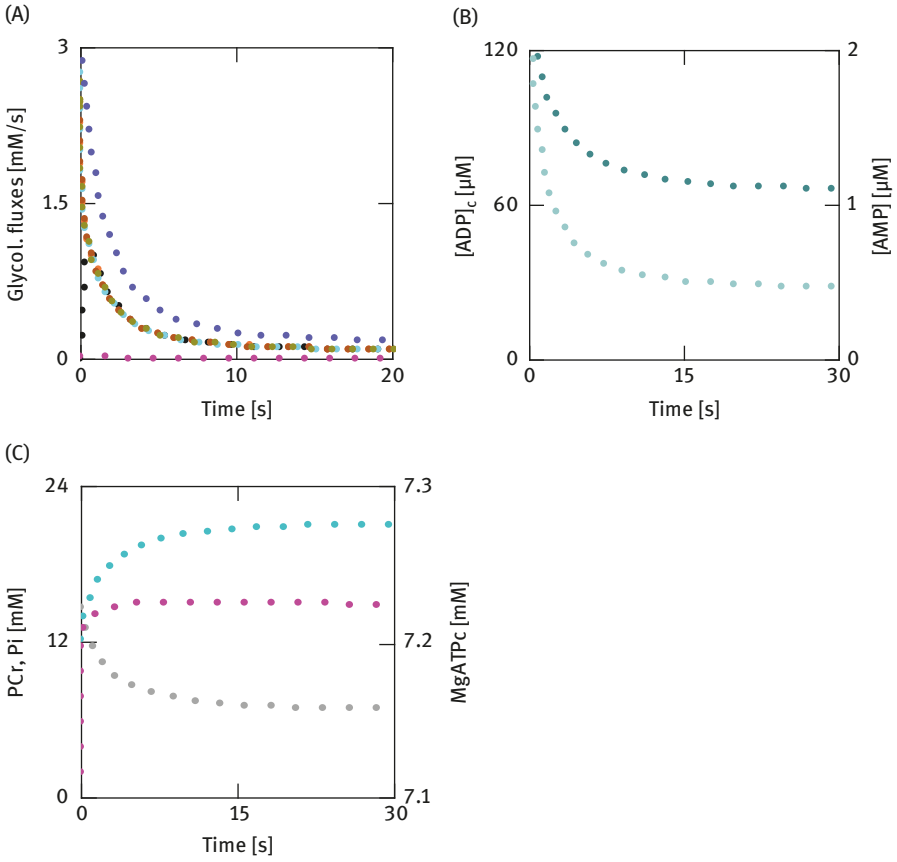

Figure 12.5: Recovery from high power output after switching from $[Ca^{2+}]_c = 6.0$ to 0.3 μM. Fluxes and metabolite concentrations reach their near resting values after about 30 s (see Figure 12.1 for designations).

already been mentioned, it cannot differentiate between the sites of ATP production and the sites of consumption.

Conversely, that is after switching off contraction power, the reaction is driven in the opposite direction through reduction of $[ADP]_c$ at a initially still high [Cr], so that PCr can be formed. That is the result of the simulation. However, this would lead to a contradiction in so far as PCr can only be resynthesized until this back reaction also approaches equilibrium. Then, J_{PCr} would be slightly negative instead of being positive as under resting conditions (A_{PCr} is then marginally greater than zero). Therefore, as a solution to this contradiction, it must be assumed that J^{p}_{PCr} (<0, "p" representing production site) and J^{u}_{PCr} (>0, "u" representing consumption site) retain their opposite directions at these sites. As the high $[ATP]_c$ and $[PCr^{2-}]$ consumption declines, $[PCr^{2-}]$ is replenished at sites of ATP consumption by

postdiffusion from sites of production until the starting conditions are reinstated, that is, until the forward and back reactions are again at near equilibrium. Then, A^u_{PCr} is slightly greater than zero and A^p_{PCr} is slightly less than zero.

Figure 12.6A shows that pH_c and pH_m have nearly reached their resting values after about 30.0 s. The shifting of pH_c to low values is primarily caused by the receding PCr reaction (B). Proton production and compensation remain principally the same; the corresponding fluxes and conductances, however, are displaced to considerably lower values (B, C).

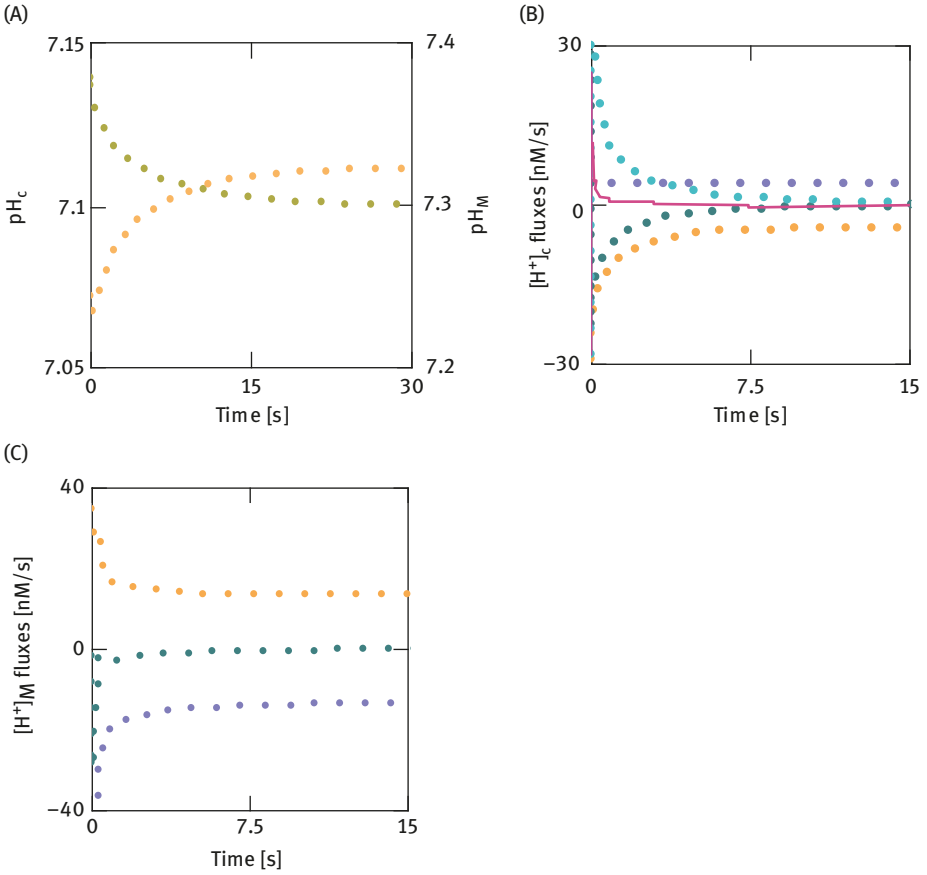

Figure 12.6: Effects of recovery at $[Ca^{2+}]_c = 0.3\,\mu M$ on pH_c and pH_m, and rates of sarcosolic and mitochondrial proton generation and compensation reactions. (A) pH_c (green) and pH_m (yellow) approach resting values during 30.0 s. (B) Sarcosolic proton fluxes, blue points: J^c_{ATP}; yellow points: J_{AE} and J_{HP}; green points: J^c_{ATP}, J_{AE} and J_{HP}; cyan points: J_{Pcr}; red line: J^{tot}_{Hc}. (C) Mitochondrial proton fluxes, blue points: $J^m_{ATP} = J_{SY} + J_{CAC}$ (ATP formation); yellow points: J_{AE} and J_{HP} (in the matrix); green points: J^m_{ATP}, J_{AE} and J_{HP}.

When the power output abruptly increases, the PCr reaction can also considerably shorten the adjustment time for achieving an SSC during reestablishment of resting conditions (Figure 12.7A–C). With regard to this situation, it can also be assumed that the ATP demand rate and ATP production rate already correspond early on, so that the ATP cycle can also run dissipation free under these conditions. However, recovery probably runs considerably slower than is expected from these simulation results because, as already mentioned, the membrane transport reactions for repolarization and the transport of Ca^{2+} through SERCA pumps are not taken into consideration in the simulation. A slower adjustment to a new steady state will certainly not obstruct conductance matching of partial conductances involved, but instead will facilitate it.

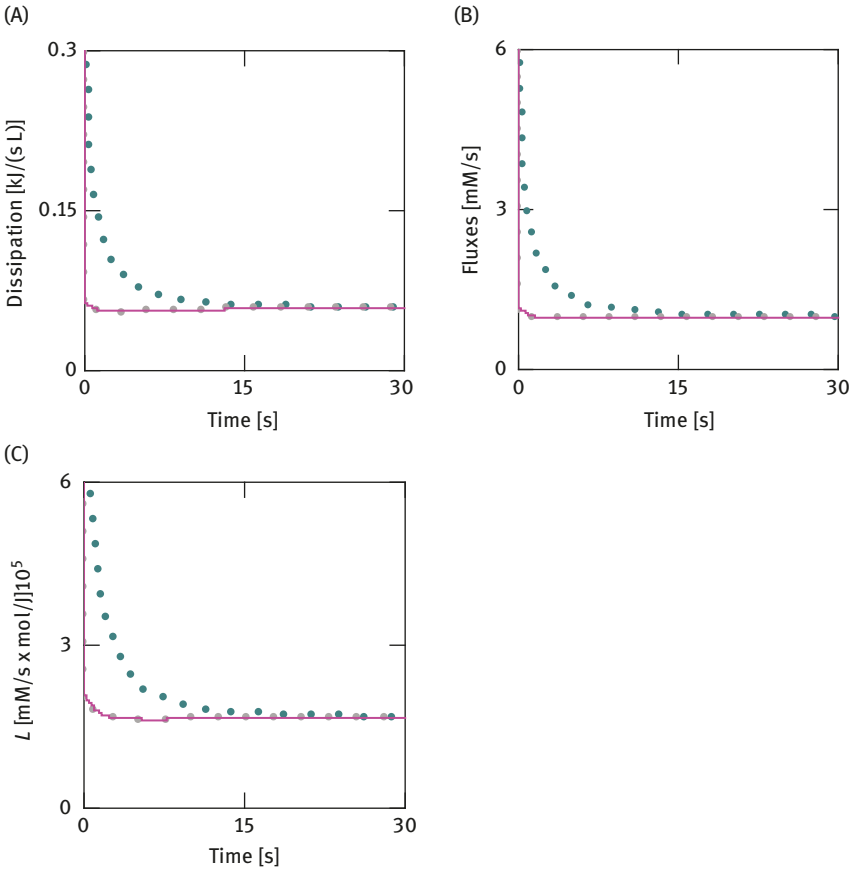

Figure 12.7: Matching of dissipation functions, fluxes and conductances during recovery at $[Ca^{2+}]_c = 3\,\mu M$. (A) Dissipation functions, gray points: Ψ_W; green points: Ψ_{PAL} and Ψ_{GLY}; red line: Ψ_{PAL}, Ψ_{GLY} and Ψ_{Pcr}. (B) Fluxes, gray points: J_W; green points: J_{PAL} and J_{GLY}; red line: J_{PAL} and J_{GLY} plus J_{Pcr}. (C) Conductances, gray points: $\bar{L}_{c2}^{Dem}$; green points: $-\bar{L}_{c1}^{Del}$; red line: $-\bar{L}_{c1}^{pcrDel}$ including L_{Pcr}.

Even if less reliable statements can be made on the basis of these simulation results, it does demonstrate, however, that the involvement of the PCr reaction during recovery guarantees an early SSC in a similar manner as under high power output conditions (Figure 12.7). It can be stated, therefore, that the PCr shuttle, which always includes both reaction directions, represents a necessary precondition for a rapid and possible restoration of the resting state, under the conditions of recovery.

13 The interaction between GLY and PAL

The preferred substrates of SMFs and VMs are fatty acids (FA) and Glu or (during Glgen breakdown) G–1–P, respectively. However, major differences arise during the metabolic utilization of these substances for ATP production, namely, FAs (here Palm) are metabolized primarily only under low-to-moderate power output conditions, while during high power output, the fuel is predominantly Glgen (via G–1–P). In the following, it will be shown with the aid of thermodynamic parameters, how such a switch from PAL to GLY pathway is accomplished in the process of a massively increased ATP demand.

With regard to this, an involvement of carnitine palmitoyltransferase I (CPT I) on the outer aspect of the inner mitochondrial membrane has already been discussed for some time [27, 28]. The transesterification of Palm–CoA to palm carnitine (Palm–Carn) takes place via this enzyme. This reaction is inhibited by malonyl-CoA (Mal–CoA). Only Palm–Carn can be transported via the inner membrane into the matrix in exchange for mitochondrial carnitine (Carn). Like Carn, this ester is electrically neutral, while Palm–CoA possesses several negative charges. The exchange reaction can, therefore, take place neutrally. As no additional proton is involved in the exchange, this process is only influenced by the concentration distribution of its reaction partners $[\mathrm{Palm-Carn}]_c$, $[\mathrm{Palm-Carn}]_m$, $[\mathrm{Carn}]_c$ and $[\mathrm{Carn}]_m$ over the inner membrane. The $[\mathrm{Palm-Carn}]_m$ transported into the matrix in this way can be converted again into Palm–CoA by the isoenzyme CPT II through backreaction on the inner aspect of the inner membrane, which then can enter β oxidation of the matrix and further degradation to CO_2 and H_2O. Merging the two transesterification events and the transport reaction, one sees that Carn transport occurs cyclically over the membrane; hence, it is not energetically relevant for Palm – CoA transport from the sarcosol into the matrix. The affinity of the overall reaction is given by

$$A_{CPT}^{ov} = RT \ln\left(\frac{[\mathrm{Palm-CoA}]_c}{[\mathrm{Palm-CoA}]_m}\frac{[\mathrm{CoA}]_m}{[\mathrm{CoA}]_c}\right). \tag{13.1}$$

The CoA originating from the matrix is again used in the Palm–CoA synthetase reaction in the sarcosol, while the CoA_m transported out of the matrix is released from Palm–CoA again via CAC.

Switching would now be possible by inhibition of the CPT I reaction through an increase in $[\mathrm{Mal-CoA}]$ in the sarcosol. In this way, Palm degradation would be inhibited. A rise in $[\mathrm{Mal-CoA}]$ may be accomplished through an increase in this metabolite via acetyl–CoA carboxylase (ACC). However, the deactivating phosphorylation by cAMP-activated protein kinase (cAMPK) has to be overcome. This principally takes place, however, under resting conditions at a high carbohydrate supply and low [cAMP]. A high power output, on the other hand, is generally accompanied with a rise in [cAMP] so that the ACC would be inactivated through the activated AMPK. As

https://doi.org/10.1515/9783110650501-013

a result, [Mal – CoA] should decrease, so that CTPT-I would be deinhibited and Palm degradation enhanced.

Such a deinhibition with the result of a strongly increasing β oxidation was, however, not observed. This can be explained in the following manner:

If one considers A_{CPT}^{ov}, then it is apparent that this affinity does not contain an equilibrium constant in contrast to, for example, the affinity of the PFK reaction. The affinity of this reaction, in simulations presented here, is

$$A_{PFK} = -\Delta_R G_{PFK} = 57.283\,\text{kJ/mol}\ (\left[Ca^{2+}\right]_c = 0.3\,\mu\text{M}).$$

With $K'_{PFK} = 1.16888\ 10^4$, the following is obtained: $-\Delta_R G^\circ = 23.219\,\text{kJ/mol}$.

This high proportion of A_{PFK} (=negative standard potential) is constant and can be changed only by an alteration of temperature. By increasing $[Ca^{2+}]_c$ from 0.3 to 6.0 µM, the power output is also increased. The conductance of the reaction is primarily raised due to [AMP] being greatly increased from 2.063×10^{-6} to 47.237×10^{-6} mM/s × mol/J under these conditions ($\Delta L_{PFK}/L_{PFKO} = 21.89724$). At the same time, J_{PFK} increases from 0.1182 to 2.441 mM/s ($\Delta J_{PFK}/J_{PFKO} = 19.6548$) and A_{PFK} drops from 57.283 to 51.673 kJ/mol ($\Delta A_{PFK}/A_{PFKO} = -0.097935$). Due to the fall in A_{PFK}, the rise in conduction cannot be fully transformed into a flux increase. In accordance with the general formulation of a flux, $J = L\,A$ is applied for the PFK reaction:

$$\frac{\Delta J_{PFK}}{J_{PFKO}} = \frac{\Delta A_{PFK}}{A_{PFKO}} + \frac{\Delta L_{PFK}}{L_{PFKO}}\left(1 + \frac{\Delta A_{PFK}}{A_{PFKO}}\right). \tag{13.2}$$

This formula is obtained from

$\Delta J_{PFK} = J_{PFK} - J_{PFKO}$, $\Delta L_{PFK} = L_{PFK} - L_{PFKO}$, and $\Delta A_{PFK} = A_{PFK} - A_{PFKO}$,
which leads to

$$\Delta J_{PFK} = (L_{PFKO} + \Delta L_{PFK})(A_{PFKO} + \Delta A_{PFK}) = L_{PFKO}\Delta A_{PFK} + \Delta L_{PFK}(A_{PFKO} + \Delta A_{PFK}). \tag{13.3}$$

This equation is achieved by dividing with J_{PFK0}. After applying the results from the simulation, one obtains

$$\frac{\Delta J_{PFK}}{J_{PFKO}} = 19.6548 \equiv -0.097935 + 21.89724 \times 0.902065.$$

The relative flux change achieved through the drastic increased conductance is obviously produced essentially by a conductance change. The affinity reduction is clearly caused by the increased flux going through the reaction, whereby the concentration ratio of products and reactants, that is Γ_{PFK}, becomes reduced. The lower this effect is, the more of the conductance increase has been transformed into a flux increase.

If the conductance of the Palm-CoA overall transport reaction is increased by a similar factor (20.63), then the following is obtained:

L^{ov}_{CPT} rises only from

$$7.452\ 10^{-6} \text{ to } 13.949\ 10^{-6}\ \text{mM/s} \times \text{mol/j}\ \left(\Delta L^{ov}_{CPT}/L^{ov}_{CPT0} = 0.87185\right)$$

(A^{ov}_{CPT}) drops from,

$$4.7123 \text{ to } 2.6766\ \text{Kj/mol}\ \left(\Delta A^{ov}_{CPT}/A^{ov}_{CPT0} = -0.432\right)$$

and J^{ov}_{CPT} is only raised from 0.0351 to 0.03734 mM/s ($\Delta J^{ov}_{CPT}/J^{ov}_{CPT0} = 0.0633$). Again it holds that

$$\frac{\Delta J^{ov}_{CPT}}{J^{ov}_{CPT0}} = 0.06321 \equiv -0.432 + 0.87185 \times 0.568.$$

For this reaction, obviously a flux increase by a factor of 1.063 is sufficient to considerably reduce the affinity. This is because the affinity of this reaction has a $\Delta_R G^\circ$ value of zero. Each change in Γ is directly apparent as a change in A^{ov}_{CPT}. In addition, $[\text{Palm} - \text{CoA}]_c$ (substrate) decreases, which also reduces the conductance of this reaction (see Chapter 15).

From the behavior of the two very different reactions, it can be seen that an adequate flux increase is only possible if the affected reactions have a high affinity, which has a high proportion of constant $-\Delta_R G^\circ$. Probably only this reaction step of the CPT I reaction, inhibitable by [Mal – CoA], is considered as a switching reaction for the pathway of whole Palm (and other FAs) metabolism, but as shown does not possess switching characteristics. It must be assumed that ATP production via PAL cannot be sufficiently activated to cover the ATP demand at high power output. This can only take place via GLY, as this metabolic pathway includes the PFK reaction, which, as has been demonstrated, can be switched from a very low to a high reaction rate by deinhibition.

The activability of a flux can be taken directly from eq. (13.1). If $\Delta A/A_0$ approaches 1.0, then the activation is primarily brought about by a conductance change, as is the case in the PFK reaction. On the contrary, if $\Delta A/A_0$ is markedly smaller than 1.0, then a drastic change in this parameter has practically no influence on the flux. Consequently, such a reaction is in principle unsuitable for regulatory interventions in metabolism.

If, however, the switching mechanism can be generated only via the GLY pathway, then the observed phenomena of ATP supply via PAL at low power output and via GLY at high power output can be explained without constraint. Palm degradation, and the thus achieved ATP production, is preset by the relative constant overall conductance of PAL. It is primarily determined by the mitochondrial content of an SMF. Under resting conditions, J^{pal}_{ATP} is sufficiently high to almost completely cover the ATP demand. After changing to high power output by raising $[Ca^{2+}]_c$, J^{pal}_{ATP} only changes marginally and is therefore not capable to deliver sufficient ATP. This task must be performed by GLY; in other words, J^{gl}_{ATP} must increase sufficiently to

cover the high ATP demand. This means that when the change of J_{ATP}^{pal} is negligible, the relative proportion of J_{ATP}^{gl} in the whole ATP production (J_{ATP}) must rise with increasing power output. Therefore, it is completely sufficient that the activation solely takes place via GLY, with J_{ATP}^{pal} remaining practically unchanged.

The simulation ($SIM_{GLY/PAL}$, A3) shows that for activation of total GLY, including both the oxidative and anoxic pathways, it obviously suffices to increase only one reaction step of glycolysis, namely that of the PFK reaction. With a Ca^{2+} increase of the sarcosol, however, $[Ca^{2+}]_m$ also rises (via Ca^{2+} uniporter of the inner membrane), which is accompanied by an activation of some mitochondrial dehydrogenases and ATP synthase. In this way, the activation of GLY_{ox} of mitochondria receives additional support.

Thus, the switching mechanism can be represented with only a few reaction steps:

Initially, $[ATP]_c$ falls marginally due to the Ca^{2+}-activated ATPases in the sarcosol (predominantly myosin ATPase), which is, however, associated with a strong increase in $[ADP]_c$. This, in turn, is transferred by the AK reaction due to the very low AMP concentration into an even greater relative increase of [AMP]. As the PFK reaction is very effectively deinhibited by [AMP], this results in an activation of the whole GLY pathway and thus to a sufficient ATP delivery primarily via this pathway. The important fact in conjunction with this is that the switching mechanism can also run in the opposite direction. Under the conditions of an abrupt reduction in ATP consumption after high power output, the recovery phase begins with the regeneration of PCr and a reduction of $[ADP]_c$. Thus, [AMP] also returns to its low resting value, so that PFK becomes increasingly inhibited. The result is an equally inactivated GLY. Also these reactions are aligned precisely by [AMP] to the declining ATP demand. When resting conditions are approached, the relative contribution via PAL increases again, although J_{ATP}^{pal} has hardly changed throughout the entire process of recovery.

The reason why activation of high power output, which is primarily concerned with the load reactions coupled to ATP, is brought about by an increase of $[Ca^{2+}]_c$ and does not involve [AMP] as a metabolism-dependent parameter is that ATP production is also required during recovery. Under such conditions, ATP delivery must be sufficient to meet the ATP demands also when $[Ca^{2+}]_c$ is already very low. Therefore, demand and delivery reactions must be activated by different messengers, namely the former by $[Ca^{2+}]_c$, and the latter by [AMP].

Figure 13.1A shows the ATP production rates of PAL (brown) and GLY (light blue). The percentage production rate via GLY (dark blue) is also shown. Figure 13.1B shows the time courses of RQ values (light blue), the fluxes J_{CO2} (gray) and J_{O2} (dark blue). In the processes, RQ changes from 0.7 to 0.915.

Figure 13.2 shows the same parameters under recovery conditions. In Figure 13.2A, the percentage progress of J_{ATP}^{pal} (brown) is shown rather than J_{ATP}^{gl} as in Figure 13.1A. Although J_{ATP}^{pal} barely changes, J_{ATP}^{pal}/J_{ATP} must increase because J_{ATP} decreases strongly.

The switching from Glu to Glgen consumption during the change to high power output has already been discussed. The metabolism of Glgen splits under these conditions into $J_{ATP}^{glgenox}$ (28.0%) and $J_{ATP}^{glgenanox}$ (72.0%). This fractionation is mainly

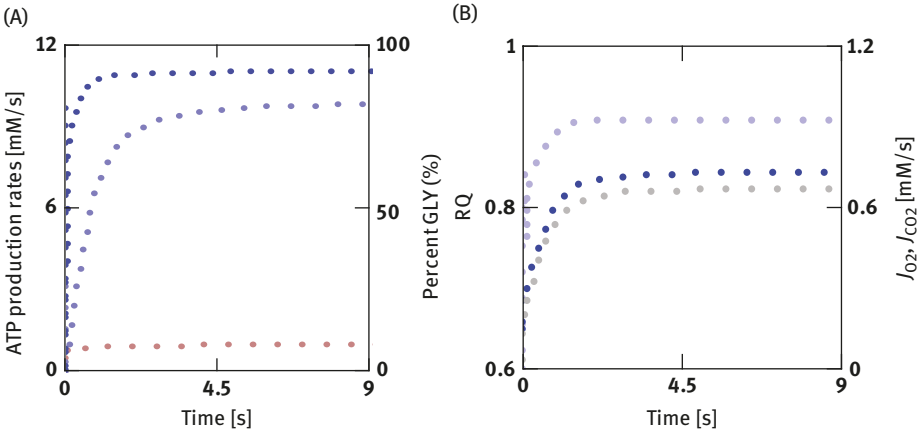

Figure 13.1: ATP production rates by PAL and GLY and respective rates of oxygen consumption during high power output at $[Ca^{2+}]_c$ = 6.0 µM. (A) Blue points: J_{ATP}^{gl} (Glu and Glgen); brown points: J_{ATP}^{palm}; dark blue points: fractional ATP production by GLY. (B) Blue points: RQ; dark blue points: J_{O2}; gray points: J_{CO2}.

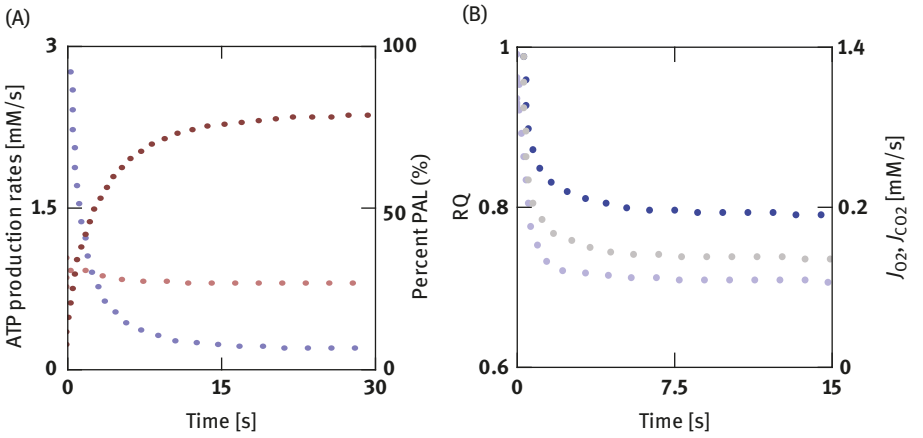

Figure 13.2: ATP production rates by PAL and GLY and respective rates of oxygen consumption during recovery at $[Ca^{2+}]_c$ = 0.3 µM. (A) Blue points: J_{ATP}^{gl} (Glu and Glgen); brown points: J_{ATP}^{palm}; dark brown points: fractional ATP production by PAL. (B) Blue points: RQ; dark blue points: J_{O2}; gray points: J_{CO2}.

determined by the mitochondrial content set for the simulation (here 20.0% (V_m/V_{Cell})). It is assumed that at a very high content of about 33.0%, practically the entire metabolism proceeds via mitochondria and that the anoxic pathway via GLY_{anox} and LDH is practically not possible. To achieve the same ATP production rate at only 20.0% mitochondria, ATP must also be produced in an appropriate

amount via GLY_{anox}. This situation is described in Figure 13.3. While Glu consumption already comes to a halt after only 1.0 s (A), Glgen consumption increases very quickly. At 20.0% of mitochondria, the predominant fraction of ATP production is supplied by the anoxic part via Lac production (B, green). In Figure 13.3B, J_{ATP}^{pal} (brown) is plotted once again for comparison.

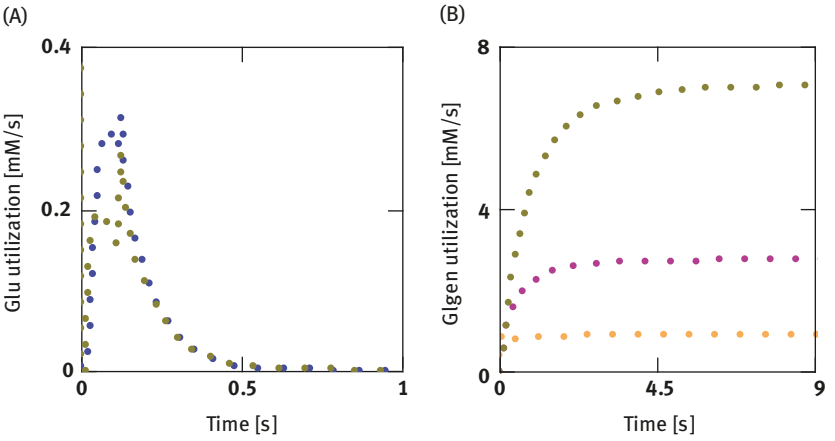

Figure 13.3: Glu and Glgen utilization during high power output at $[Ca^{2+}]_c$ = 6.0 µM. (A) Oxidative (blue, J_{ATP}^{gluox}) and anoxic (green, $J_{ATP}^{gluanox}$) Glu utilization. (B) Oxidative (blue, $J_{ATP}^{glgenox}$) and anoxic (green, $J_{ATP}^{glgenanox}$) Glgen utilization; yellow points: J_{ATP}^{pal}.

During recovery, J_{ATP}^{gl} falls to low values again. As a consequence of this, both J_{ATP}^{gluox} and $J_{ATP}^{gluanox}$ as well as $J_{ATP}^{glgenox}$ and $J_{ATP}^{glgenanox}$ are affected (Figure 13.4). The relations ox/(ox + anox) for Glu and Glgen, respectively, however, change considerably during switching. At high power output, the relation for Glu is insignificantly low (0.06%) and 28.0% for Glgen; during recovery about 9.0% for Glu and approx. 6.0% for Glgen. The corresponding resting values for the above relations are 8.0% and 5.2%. It can, therefore, be assumed that in the course of recovery, the different metabolic pathways of GLY once again approach the resting values, even after drastic changes were brought about by Ca^{2+} activation. As, at least in the simulation ($SIM_{GLY/PAL}$), no additional regulatory mechanism other than the [AMP] deinhibition of PFK has been addressed, the more complex metabolic branching of GLY must occur through this switching mechanism alone.

The clear difference in the oxidative GLY fraction between high and low power output primarily comes about through the very low overall conductance of Glu degradation under resting conditions and a $[Ca^{2+}]_m$ of approx. 0.2 µM. The Ca^{2+}-dependent conductance of CAC is equally low under these conditions, so that this metabolic pathway is supplied mainly via the acetyl-CoA concentration ($[Ac-CoA]_m$) produced

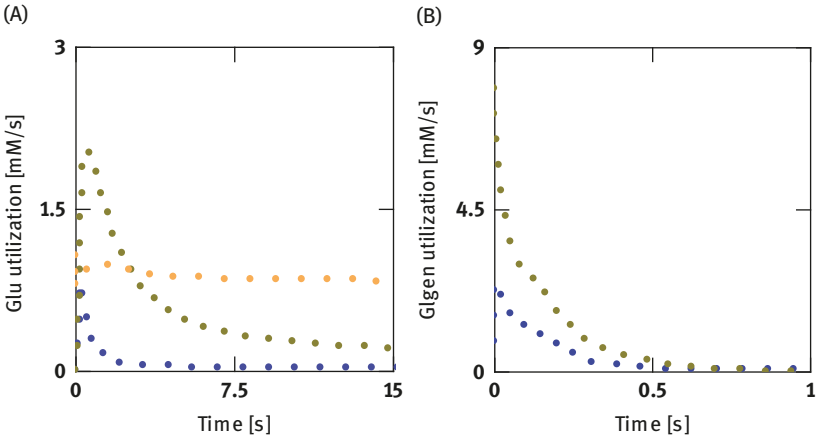

Figure 13.4: Glu and Glgen utilization during recovery at $[Ca^{2+}]_c$ = 0.3 µM. (A) Oxidative (blue, J_{ATP}^{gluox}) and anoxic (green, $J_{ATP}^{gluanox}$) Glu utilization; yellow points: J_{ATP}^{pal}. (B) Oxidative (blue, $J_{ATP}^{glgenox}$) and anoxic (green, $J_{ATP}^{glgenanox}$) Glgen utilization.

by PAL. The $[Ac-CoA]_m$ arising from Glu degradation is therefore relatively low, because the pathway via anoxic degradation is also available for Glu. By increasing the conductance of CAC by raising $[Ca^{2+}]_m$ (to about 6.8 µM) under high power output conditions, the pathway via glycolysis and CAC receives a higher conductance so that comparatively more Glgen can be oxidized, even if the anoxic degradation of Glgen still delivers the greatest proportion of ATP production.

A significant increase in PAL is possible if the conductance of the first reaction step is increased. This is the Palm transport reaction from the interstitium into the sarcosol via the FA translocase of the sarcolemma (J_{FAT}). The flux equation includes constant conductance because the extracellular Palm concentration ($[Palm]_e$) is taken to be constant in the simulation. This reduces, however, the reduction of both A_{FAT} and L_{FAT} so that an activation via conductance can proceed in a less damped manner. Under real conditions, it must be assumed that $[Palm]_e$ decreases through activation, whereas the relative flux change must be lower according to eq (13.1).

With $[Ca^{2+}]_c = 1.136\,\mu M$, J_{FAT} increases by doubling the conduction ($\Delta L_{FAT}/L_{FAT0} = 1.0$) from 8.997×10^{-3} to 15.614×10^{-3} mM/s ($\Delta J_{FAT}/J_{FAT0} = 0.7355$), while A_{FAT} decreases from 8.7811×10^3 to 7.62×10^3 ($\Delta A_{FAT}/A_{FAT0} = -0.1323$).

It has been demonstrated experimentally that during a power output of moderate but longer duration, the sarcolemma takes up a greater amount of transport proteins such as FAT/CD36 [29, 30]. This is accompanied by a higher FA flux into the sarcosol, which can be reduced again through retranslocation of the transport proteins into sarcosolic depots. Such an activation and deactivation cycle takes place over a longer time period and, therefore, does not play an important role during rapid switching to high power output.

14 Heat production

14.1 Heat production during high power output

The measurement of the heat output from an isolated SMF is comparable to the calorimetric determination of the ΔH value of a chemical or biochemical reaction. This takes place under the conditions of a closed system, that is, only thermal energy can pass the system boundaries. However, this does not apply to living cells. If one considers the isolated SMF as a system, then the incubation medium represents the surroundings. Substrates such as Glu permeate the cell membrane and enter the metabolism as reactants, while products such as CO_2 and H_2O are released by the cell into the surroundings through the cell membrane. Therefore, the isolated SMF system cannot be considered to be closed with respect to these substances, but rather must be viewed as an open system. Although this does not apply to the majority of the metabolites, it does appear necessary to analyze the possible resulting changes more closely. A muscle fiber bundle made up of several SMFs is fixed in a physiological medium (Krebs–Ringer bicarbonate buffer) in such a way that the contractile performance can be measured. The isotonic medium contained Glu (4.0 mM), O_2 (35 µM) and CO_2 (1.4 mM) in those concentrations, which are predominant in the sarcosol. Therefore, this should guarantee reversible transfer through the sarcolemma. Thus, no entropy can be produced through the associated transport reactions. At steady state, Glu and O_2 are taken up from the medium at constant rates in accordance with (R4.1), while CO_2 and H_2O are released into it from SMFs. The stoichiometric realization is given by the metabolism of Glu oxidation in the cell and by the corresponding transport reactions in the medium. At steady state, both are equal, that is, Glu plus 6.0 O_2 is continuously replaced by 6.0 CO_2 plus 6.0 H_2O in both compartments. However, the reactants are released and the products are continuously taken up by the medium, the corresponding concentrations in the sarcosol remain constant. As the volume of the medium is considerably larger than V_c and the experiment should only run for a short period, these concentrations in the medium remain practically unchanged. The temperature of the medium is controlled extremely sensitively.

The $\Delta_R G$ value of the Glu oxidation remains constant as the concentrations of reactants and products involved in this reaction do not change at steady state. The associated constant entropy $\Delta_{Ri}S$ is released as irreversible heat ($T\Delta_{Ri}S$) into surroundings. As $\Delta_{Re}S$ is positive for this reaction, heat must be released continuously from the medium into the system in order to balance the difference in the thermal energy content between products and reactants. In this case, the products require additional thermal energy because the thermal energy from the reactants is not sufficient to bring the products to the specified temperature. This heat originating from the medium is, however, returned to it quantitatively, in that precisely this

https://doi.org/10.1515/9783110650501-014

energy difference reappears in the medium through the exchange of reactants and products between surroundings and the system. In this case, the reactants are replaced by products, just as in the course of the reaction in the system. This exchange occurs only through transport in the medium. In contrast, the reaction-dependent exchange of reactants and products in the system is compensated through exchange by transport. The temperature changes occurring in the medium can be compensated to serve as a measurement signal.

Hence, for the open system

$$\Delta_{Re}S^o = \Delta_{Re}S^h + \Delta_{Re}S^m.$$

Here, the total exchange of entropy between the system and the environment can be divided into two fractions. $\Delta_{Re}S^h$ represents the fraction that occurs via reversible heat exchange (= $\Delta_{Re}S$ for closed systems), and $\Delta_{Re}S^m$ is the fraction associated with the transport of matter. At steady state, both fractions must be oppositely equal. This leads to

$$\Delta_R G = \Delta_R H = -\Delta_{Ri}S \quad \text{(open system at steady state)}. \tag{14.1}$$

As the reactants and products exchanged by transport between the system and surroundings are in thermal equilibrium with the medium, this process can influence neither the temperature of the system nor the temperature of the medium; however, thermal energy is associated with the transported matter. The result is that $\Delta_{Re}S^o$ must vanish for both the system and the surroundings. Therefore, only the irreversible heat $T\Delta_{Ri}S$ is produced by the system, which is reversibly released into surroundings. As a result, a change in temperature of the medium is registered, as would be expected for a closed system, because $T\Delta_{Re}S^m$ cannot cause a change in temperature. The change in enthalpy of the open system determined from the change in temperature $\Delta_R H^o = \Delta_R G = -T\Delta_{Ri}S$ differs, therefore, by the term

$$T\Delta_{Re}S^m = \Delta_R H^o - \Delta_R H^o = -T\Delta_{Re}S$$

from the change in enthalpy,

$$\Delta_R H^c = -T\Delta_{Ri}S + T\Delta_{Re}S,$$

of the closed system.

The measured heat production of the open system, on the other hand, is identical to that of a closed system $Q_R = \Delta_R H$ under these conditions (T and P const.).

The heat production for a coupled reaction can be calculated using the following: From

$$\begin{aligned} A_{res} = A_1 + A_2 &= -(\Delta_R G_1 + \Delta_R G_2) = -(\Delta_R H_1 - T\Delta_{Re}S_1) - (\Delta_R H_2 - T\Delta_{Re}S_2) \\ &= -(\Delta_R H_1 + \Delta_R H_2) + T(\Delta_{Re}S_1 + \Delta_{Re}S_2) \end{aligned}$$

one obtains

$$\begin{aligned} Q_R = \Delta_R H_1 + \Delta_R H_2 &= -(A_1 + A_2) + T(\Delta_{Re} S_1 + \Delta_{Re} S_2) \\ &= -T(\Delta_{Ri} S_1 + \Delta_{Ri} S_2) + T(\Delta_{Re} S_1 + \Delta_{Re} S_2). \end{aligned} \tag{14.2}$$

The released heat is made up of the negative coupled affinities and the sum of the two reversible heats from corresponding reactions. For the Glu oxidation coupled to ATP production, one obtains the following:

$$\mathrm{Glu} + 6\mathrm{O_2} + \mathrm{n^{gluox}ADP} + \mathrm{n^{gluox}P_i} \rightarrow 6\mathrm{CO_2} + 6\mathrm{H_2O} + \mathrm{n^{gluox}ATP},$$

with $[\mathrm{Ca}^{2+}]_c = 1.136\,\mu\mathrm{M}$, $[\mathrm{Glu}] = 4.0$ mM, $[\mathrm{O_2}] = 35.0\,\mu\mathrm{M}$, and

$$A_1 = -A_{ATP}^c = -60.42\,\mathrm{kJ/mol},$$

$$A_2 = A_{ov}^{gluox} = 3009.59\,\mathrm{kJ/mol},$$

$$n^{gluox} = 30.62,$$

$$\Delta_{Re} S_1 = \Delta_{Re} S_{ATP} = 7.7\,\mathrm{J/(mol\,K)},$$

and

$$\Delta_{Re} S_2 = \Delta_{Re} S^{gluox} = 259.1\,\mathrm{J/(mol\ K)}$$

$$\begin{aligned} Q_R &= -(A_1 + A_2) + T(\Delta_{Re} S_1 + \Delta_{Re} S_2) \\ &= -(-n^{gluox}\,60.42 + 3009.59) + 310.15\ (-n^{gluox} 7.7 + 259.1)\ 10^{-3} \\ Q_R &= -1159.53 + 7.235 = -1152.3\,\mathrm{kJ/mol}. \end{aligned}$$

Under these conditions,

$$\Delta_R G = \Delta_R H = -(A_1 + A_2) = -(-n^{gluox} 60.42 + 3009.59) = -1159.53\,\mathrm{kJ/mol}.$$

The difference between the released heat Q_R and actual change in enthalpy $\Delta_R G = \Delta_R H$ is not essential for the above reaction. The drop in entropy production through coupling, however, is appreciable. Without coupling,

$$\Delta_{Ri} S = -\frac{\Delta_R G}{T} = \frac{A_{ov}^{gluox}}{T} = 9.704\ 10^3\,\mathrm{J/(mol\,K)}$$

would be created, while in the presence of coupling, only

$$\Delta_{Ri} S = -\frac{\Delta_R G}{T} = \frac{1}{T}\left(-nA_{ATP}^c + A_{ov}^{gluox}\right) = 3.739\ 10^3\,\mathrm{J/(mol\,K)}$$

are produced.

Only the $\Delta_{Re} S$ values of ATP splitting are involved in ion transport reactions, for example, SERCA ATPase at the reticulum membrane, because ion transport takes

place in the system and, consequently, no entropy is exchanged with surroundings. The reduction of $\Delta_R G$ and $\Delta_{Ri} S$ through coupling to ion transport is, however, cancelled out by the Ca^{2+} release process so that the $\Delta_{Ri} S$ of the Ca^{2+} cycle disappears at SSC. As an isolated process, the ATP splitting alone would determine Q_R and all thermodynamic potentials, as well as $\Delta_{Ri} S$ of this reaction.

However, as already demonstrated, in the energy metabolism of an SMF, at SSC all ATP-consuming and ATP-producing reactions are oppositely equal. Thus, the ATP cycle undergoes without dissipation and also plays no part in the production of heat. The latter emerges from the following: the ATP production and ATP consumption reactions are

$$\begin{aligned} Q_R &= -\left(-nA^c_{ATP} + A^{gluox}_{ov}\right) + T\left(-n\Delta_{Re}S_{ATP} + \Delta_{Re}S^{gluox}\right) + \\ &\quad (-)\sum_1^n \left(A_n + A^c_{ATP}\right) + T\left(\sum_1^n \Delta_{Re}S_n + n\Delta_{Re}S_{ATP}\right) \\ &= -\left(\sum_1^n A_n + A^{gluox}_{ov}\right) + T\left(\sum_1^n \Delta_{Re}S_n + \Delta_{Re}S^{gluox}\right). \end{aligned} \tag{14.3}$$

$\sum_1^n A_n$ (with $A_n < 0$) representing all the load affinities of the sarcosol that are coupled to ATP splitting. If all the ATP originating from Glu oxidation were to flow into muscular contraction, then $\Delta_{Re} S_n$ would not apply, and the heat production would be given by

$$\begin{aligned} Q^{str}_R &= -\left(nA^{ld}_{Str} + A^{gluox}_{ov}\right) + T\Delta_{Re}S^{gluox} \\ &= -(-569.53 + 3009.59) + 310.15\left(295.1 \times 10^{-3}\right) = -2348.54\ \text{kJ/mol} \end{aligned}$$

(with $A^{ld}_{Str} = -1.86\ 10^4 \text{J/mol}$, $n = 30.62$). In this case the molar mechanical work (A^{ld}_{Str}) coupled to ATP splitting is released to the environment (surroundings), and thus does not remain in the system. Also under these conditions no appreciable difference arises between $\Delta_R G\ (= \Delta_R H)$ and Q_R. Thus,

$$\Delta_R G^{gluoxstr} = \Delta_R H^{gluoxstr} = -\left(nA^{ld}_{Str} + A^{gluox}_{ov}\right) = -(569.53 + 3009.59) = -2440.06\ \text{kJ/mol}.$$

This special situation can be explained as follows: At steady state, converted Glu is continuously substituted from the environment. Thus, there is a continuous conversion of chemical energy by the reaction that occurs at a constant potential difference ($\Delta_R G^{gluoxstr} = -\left(nA^{ld}_{Str} + A^{gluox}_{ov}\right)$). This is associated with a continuous entropy production as well. However, in contrast to a closed system, the converted energy is replaced, and the change in entropy resulting from heat exchange is compensated to zero by the entropy change occurring through exchange of matter. Therefore, a change of respective parameters under such conditions can only be observed in surroundings, while those of the system remains unchanged. The converted energy appears as performed work (nA^{ld}_{Str}) and irreversible heat ($T\Delta_{Ri}S = \Delta_R G^{gluoxstr} = nA^{ld}_{Str} + A^{gluox}_{ov}$, counted

as positive) in surroundings. As already mentioned, the total entropy change cannot be fully determined from a change in temperature.

The integral quantities of the system, such as ΔG^{gluox}, ΔH^{gluox} and ΔS^{gluox} must also disappear under these conditions.

The quantity Q_R describes the amount of heat released per reaction extent ξ = 1.0 mol. To retain the accumulated heat over a specified time period, its time integral must be determined. To do this, Q_R must be expressed as a function of time t. One such function is obtained by multiplying Q_R with the corresponding flux, yielding

$$J\Delta_R H = \frac{d\xi}{V_c dt}\left(\frac{dH}{d\xi}\right) = \frac{dH}{V_c dt} \tag{14.4}$$

(mJ/(L s), because J is given in mM/s).

The following equation

$$\dot{Q} = J\Delta_R H = J(-A + \Delta_{Re} S) \tag{14.5}$$

is used for calculation.

The rate of heat production calculated from this is represented here by $\dot{Q}$, with $\Delta_R H$ related to a closed system.

For Glu oxidation this gives

$$\dot{Q}^{gluoxstr} = J^{gluox}\left[-\left(nA_{Str}^{ld} + A_{ov}^{gluox}\right) + T\Delta_{Re}S^{gluox}\right] \text{ (in mJ/(L s)},$$

whereas $J^{gluox}(nA_{Str}^{ld} + A_{ov}^{gluox})$ represents the dissipation function $\Psi^{gluoxstr} = J^{gluox}(nA_{Str}^{ld} + A_{ov}^{gluox})$ for this reaction.

With $J^{gluox} = 0.01236$ mM/s (for $[Ca^{2+}]_c = 1.136\,\mu$M) there is

$$\dot{Q}^{gluoxstr} = 0.01236\left(-2348.5410^3\right) = -29028.0 \text{ mmol(L s)} \times \text{J/mol} = -29.028 \text{ J/(L s)}.$$

$$J^{gluox}\Delta_R G^{gluoxstr} = J^{gluox}\Delta_R H^{gluoxstr} = -J^{gluox}\left(nA_{Str}^{ld} + A_{ov}^{gluox}\right) = -\Psi^{gluoxstr} = -30.159 \text{ J/(L s)}.$$

In eq. (14.3), $\sum_1^n A_n + T\sum_1^n \Delta_{Re}S_n$ represents all the parallel reactions of the sarcosol coupled to ATP splitting, including muscular contraction. The fluxes through synthesis reactions, like glycogen synthesis, are, however, very low and can be neglected. The active ion transport reactions remain, primarily Ca^{2+} transport through SERCA pumps in the reticulum membrane and Na/K transport through Na/K pumps in the sarcolemma. At SSC, however, only their ATPase reaction has to be addressed, because the uncoupling fluxes via Ca^{2+} release and via Na^+ and K^+ channels of the sarcolemma, respectively, energetically compensate the work of ion transport. However, some of those potentials disappear, which could have decreased $\Delta_{Ri}S$ and heat production. Under these conditions, the contraction work released into

surroundings can alone reduce the entropy and heat production, respectively. But this simplifies the calculation considerably. Consequently, for the different metabolic pathways one obtains

$$\dot{Q}^{pal} = J^{pal}\left[-A_{ov}^{pal} + T\Delta_{Re}S^{pal}\right] - \frac{J_{ATP}^{pal}}{J_{ATP}+J_{ATPCK}} J_{Str}^{ld} A_{Str}^{ld}.$$

The quotient

$$\frac{J_{ATP}^{pal}}{J_{ATP}+J_{ATPcK}} = \frac{J_{ATP}^{pal}}{J_{ATP}^{tot}} \text{with}$$

$$J_{ATP}^{tot} = J_{ATP} + J_{ATPCK}$$

determines that fraction of the ATP production rate, which is delivered by PAL. Then,

$$\frac{J_{ATP}^{pal}}{J_{ATP}^{tot}} J_{Str}^{ld} A_{Str}^{ld}$$

represents the proportion of released contraction power delivered by PAL.

With $J^{pal} = 9.0972\ 10^{-3}\,\text{mM/s}$ (at $[Ca^{2+}]_c = 6.0\,\mu\text{M}$), $A_{ov}^{pal} = 9930.72\ 10^3\ \text{J/mol}$, $J_{Str}^{ld} A_{Str}^{ld} = -\ 1.159436\ 10^5 \text{mJ/(L s)}$ and $\Delta_{Re}S^{pal} = -7444.0\,\text{J/(mol K)}$ the following is obtained:

$$\dot{Q}^{pal} = 9.0972\ 10^{-3}\left(-9930.72\ 10^3 + 310.15 \times (-7444.0)\right) - 0.08523 \times \left(-1.159436\ 10^5\right)$$
$$= -1.014631\ 10^5 \text{mJ/(L s)} = -0.1015\,\text{kJ/(L s)}.$$

Correspondingly

$$\dot{Q}^{glgenox} = J^{glgenox}\left[-A_{ov}^{glgenox} + T\Delta_{Re}S^{glgenox}\right] - \frac{J_{ATP}^{glgenox}}{J_{ATP}^{tot}} J_{Str}^{ld} A_{Str}^{ld}.$$

With $J^{glgenox} = 0.090234\,\text{mM/s}$, $A_{ov}^{glgenox} = 3026.078\ 10^3\text{J/mol}$ and $\Delta_{Re}S^{glgenox} = 323.0$ we get

$$\dot{Q}^{glgenox} = -2.344\ 10^5\ \text{mJ/(L s)} = -0.2344\,\text{kJ/(L s)},$$

$$\dot{Q}^{glgenanox} = J^{glgenanox}\left[-A_{ov}^{glgenanox} + T\Delta_{Re}S^{glgenanox}\right] - \frac{J_{ATP}^{glgenanox}}{J_{ATP}^{tot}} J_{Str}^{ld} A_{Str}^{ld}.$$

With $J^{glgenanox} = 2.3491\,\text{mM/s}$, $A_{ov}^{glgenanox} = 246.676\ 10^3$ and $\Delta_{Re}S^{glgenanox} = 323.0$ the following are obtained:

$$\dot{Q}^{glgenanox} = -2.7935\ 10^5 \text{mJ/(L s)} = -0.27935\,\text{kJ/(L s)}.$$

$$\dot{Q}^{gluox} = -151.45\,\text{mJ/(L s)} = -0.1515\ 10^{-3}\ \text{kJ/(L s)}$$

and

$$\dot{Q}^{gluanox} = -166.35\,\mathrm{mJ/(L\,s)} = -0.16635\ 10^{-3}\mathrm{kJ/(L\ s)}.$$

The sum of the resulting heat release via the different metabolic pathways (PAL plus GLY) at high power output is

$$\dot{Q}^{Del} = \dot{Q}^{pal} + \dot{Q}^{glgenox} + \dot{Q}^{glgenanox} + \dot{Q}^{gluox} + \dot{Q}^{gluanox} = -0.61556\,\mathrm{kJ/(L\,s)}.$$

To be able to compare the heat production rates of different metabolic pathways, all respective $\dot{Q}$s have to be related to a given ATP production rate (here 1.0 mM/s). This is achieved by multiplying $\dot{Q}$ with $1.0/J^{pathway}$ (dimensionless). By dividing through $J^{pathway}_{ATP}/J^{pathway}$, the result is related to the yield of ATP by that pathway. For oxidative Glu degradation

$$\dot{Q}^{gluox}_{1.0} = \frac{1.0}{\frac{J^{gluox}_{ATP}}{J^{gluox}}}\left[-A^{gluox}_{ov} + T\Delta_{Re}S^{gluox}\right] - 1.0\ \frac{J^{ld}_{Str}}{J^{tot}_{ATP}}A^{ld}_{Str},$$

for oxidative Glgen degradation

$$\dot{Q}^{glgenox}_{1.0} = \frac{1.0}{\frac{J^{glgenox}_{ATP}}{J^{glgenox}}}\left[-A^{glgenox}_{ov} + T\Delta_{Re}S^{glgenox}\right] - 1.0\ \frac{J^{ld}_{Str}}{J^{tot}_{ATP}}A^{ld}_{Str},$$

for anoxic Glu degradation

$$\dot{Q}^{gluanox}_{1.0} = \frac{1.0}{\frac{J^{gluanox}_{ATP}}{J^{gluanox}}}\left[-A^{gluanox}_{ov} + T\Delta_{Re}S^{gluanox}\right] - 1.0\ \frac{J^{ld}_{Str}}{J^{tot}_{ATP}}A^{ld}_{Str},$$

for anoxic Glgen degradation

$$\dot{Q}^{glgenanox}_{1.0} = \frac{1.0}{\frac{J^{glgenanox}_{ATP}}{J^{glgenanox}}}\left[-A^{glgenanox}_{ov} + T\Delta_{Re}S^{glgenanox}\right] - 1.0\ \frac{J^{ld}_{Str}}{J^{tot}_{ATP}}A^{ld}_{Str}$$

and for Palm degradation

$$\dot{Q}^{palm}_{1.0} = \frac{1.0}{\frac{J^{palm}_{ATP}}{J^{palm}}}\left[-A^{palm}_{ov} + T\Delta_{Re}S^{palm}\right] - 1.0\ \frac{J^{ld}_{Str}}{J^{tot}_{ATP}}A^{ld}_{Str}.$$

In relation to $\dot{Q}^{gluox}_{1.0}$, one obtains the following quotients:

$$\frac{\dot{Q}^{palm}_{1.0}}{\dot{Q}^{gluox}_{1.0}} = 1.251,\ \frac{\dot{Q}^{glgenox}_{1.0}}{\dot{Q}^{gluox}_{1.0}} = 0.963,\ \frac{\dot{Q}^{gluanox}_{1.0}}{\dot{Q}^{gluox}_{1.0}} = 0.619 \text{ and } \frac{\dot{Q}^{glgenanox}_{1.0}}{\dot{Q}^{gluox}_{1.0}} = 0.446.$$

The factor

$$\frac{1.0}{\frac{J_{ATP}^{gluanox}}{J^{gluanox}}} = 0.5\,\mathrm{mM/s}$$

gives, for example, the value of the flux through glycolytic Glu degradation, which is required to produce 1.0 mM ATP/s.

$$\frac{J_{ATP}^{gluanox}}{J^{gluanox}} = 2.0$$

is therefore the ATP yield of this degradation pathway.

For Palm oxidation,

$$\frac{1.0}{\frac{J_{ATP}^{palm}}{J^{palm}}} = 9.976\ 10^{-3}\mathrm{mM/s}\ \text{with}\ \frac{J_{ATP}^{palm}}{J^{palm}} = 100.24.$$

The corresponding values for Glgen oxidation are

$$\frac{1.0}{\frac{J_{ATP}^{glgenox}}{J^{glgenox}}} = 0.033\,\mathrm{mM/s}\ \text{with}\ \frac{J_{ATP}^{glgenox}}{J^{glgenox}} = 30.316,$$

for Glu oxidation

$$\frac{1.0}{\frac{J_{ATP}^{gluox}}{J^{gluox}}} = 0.0341\,\mathrm{mM/s}\ \text{with}\ \frac{J_{ATP}^{gluox}}{J^{gluox}} = 29.316,$$

and for anoxic Glgen degradation

$$\frac{1.0}{\frac{J_{ATP}^{glgenanox}}{J^{glgenanox}}} = 0.3333\,\mathrm{mM/s}\ \text{with}\ \frac{J_{ATP}^{glgenanox}}{J^{glgenanox}} = 3.0,$$

The above results show that anoxic Glgen and Glu degradation produce considerably less heat than the oxidative pathways at the same ATP production rate. The greatest heat production takes place via the β-oxidative pathway. Therefore, it makes considerable sense that the power output from glycolysis of fast muscle fibers produces relatively little heat, whereas brown adipose tissue with the more heat yielding fatty acid degradation is used to provide the body with heat. With the latter, a particularly large amount of heat is also produced because there is no coupling to mechanical work in this process. The trigger for this type of heat production is the fatty acid-induced uncoupling of the respiratory chain. In this way, the proton cycle at the inner membrane is increased. However, that alone cannot lead to more heat production because, as has been shown (see Chapter 8), this cycle proceeds at SSC and consequently is dissipation free, that is, no release of heat takes place. The increased heat output is, therefore, caused primarily by the increased flux through β-oxidation and CAC with subsequent oxidation of NAD_{red} and FAD_{red}.

Heat production is also determined through the mechanical load potential. All the results given up to this point refer to an A^{ld}_{Str} of –1.68 10^4 J/mol. At even greater negative load potentials, the heat production rate drops (becomes less negative) (at the same ATP production rates of 1.0 mM/s), for example, at $A^{ld}_{Str} = -3.0\ 10^4$ and –1.728 10^4 J/mol to –84.39 and –85.55 J/(L s) compared with that at $A^{ld}_{Str} = -1.68\ 10^4\,\mathrm{J/mol}(-85.68)$. For more positive load potentials, heat production increases, for example, $A^{ld}_{Str} = -1.56\ 10^4$ increases to – 85.68 J/(L s). In contrast to mechanical power, it does not, however, go through a maximum. Under isometric conditions, the total ATP available for contraction is split without coupling. The heat production rate resulting from this is –97.0 J/(L s).

When measuring heat production, it is not the processes after reaching a steady state that are especially interesting, but rather primarily those that occur immediately after switching from low to high power, before a new steady state can be achieved. One such situation has already been discussed in connection with conductance matching and the PCr reaction (see Section 9). Figure 14.1 shows that the rate of heat production ($[Ca^{2+}]_c = 6.0\,\mu M$) in the first seconds is also strongly influenced by the ATP supplied by the PCr reaction and its cleavage (A). The corresponding fluxes are also included again for comparison (B).

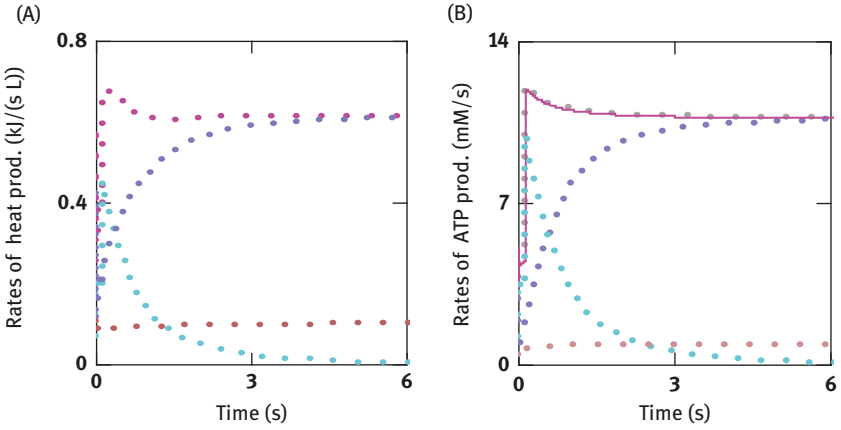

Figure 14.1: Rates of heat production and ATP delivery and demand during high power output at $[Ca^{2+}]_c = 6.0\,\mu M$. (A) Blue points: rate of heat production by metabolic ATP delivering reactions (GLY plus PAL, $\dot{Q}^{Del}$); brown points: by PAL ($\dot{Q}^{pal}$); cyan points: by the PCr reaction ($\dot{Q}^{pcr}$); red points: by GLY plus PAL plus PCr reaction ($\dot{Q}^{tot}$). (B) Corresponding ATP delivery and demand rates as shown in Figure 12.4C; cyan points: in addition, J^{pcr}_{ATP} is shown.

The heat production rates clearly show that these processes, as with those in ATP production, are also strongly influenced by the CK reaction in the first few seconds. Heat production $\dot{Q}_{tot}$ includes the heat produced via the metabolic pathways GLY and PAL, and also that from ATP splitting running downstream of the CK reaction,

that is, the PCr hydrolysis reaction (Figure 14.1A, red). However, the latter is only temporarily involved, namely only as long as the ATP consumption requires buffering (Figure 14.1A, cyan, $\dot{Q}^{pcr}$). Afterwards, heat is only produced from GLY and PAL (blue and brown) because ATP is only produced via these pathways.

Figure 14.2 shows the integrated heat output in kJ/L over time. The processes are almost linear (Figure 14.2A). From Figure 14.2B it can be seen that PCr hydrolysis is only involved in the first few seconds. The largest proportion is, however, during the first few fractions of a second (Figure 14.2A and B).

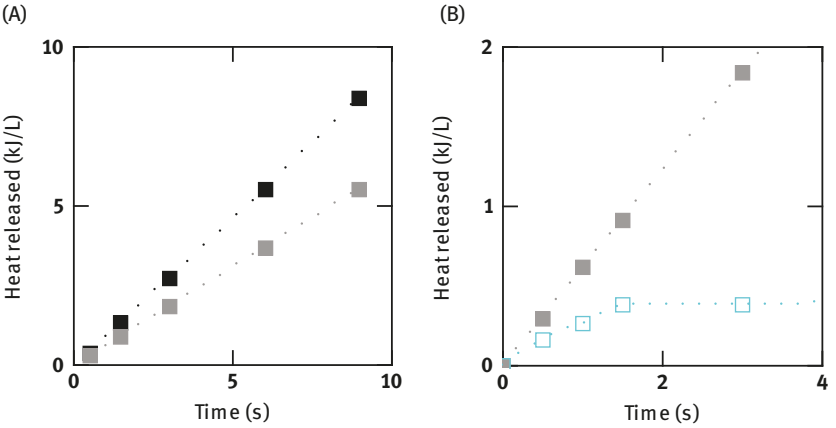

Figure 14.2: Time courses of heat release during high power output at 6.0 µM $[Ca^{2+}]_c$. (A) From SMFs containing 33.0% (black) and 20.0% (gray) mitochondria. (B) Composition of heat release during the first seconds from SMFs containing 20.0% mitochondria, gray points: by GLY plus PAL plus PCr reaction; cyan points: by the PCr reaction alone.

In Figure 14.2A, the heat output is shown from an SMF with a very high mitochondrial content (approx. 33%), which shows practically no anoxic ATP production. The entire ATP is delivered by $J_{ATP}^{glgenox}$ and J_{ATP}^{pal}. At the same ATP production rate, the heat output of this cell is, however, considerably higher than that of the cell with only approx. 20% mitochondrial content because metabolism under purely oxidative conditions produces more heat, as has already been shown.

14.2 Heat production during recovery

When switching to a very low power output by reducing $[Ca^{2+}]_c$ from 6.0 to 0.3 µM, all the fluxes involved in GLY reactions quickly drop to their resting values. Only PAL is barely affected. Under these conditions, the CK reaction runs in the opposite direction (Figure 14.3B, cyan). Now, PCr is formed. Therefore, ATP splitting must take place, that is, PCr hydrolysis must temporarily precede in the opposite direction.

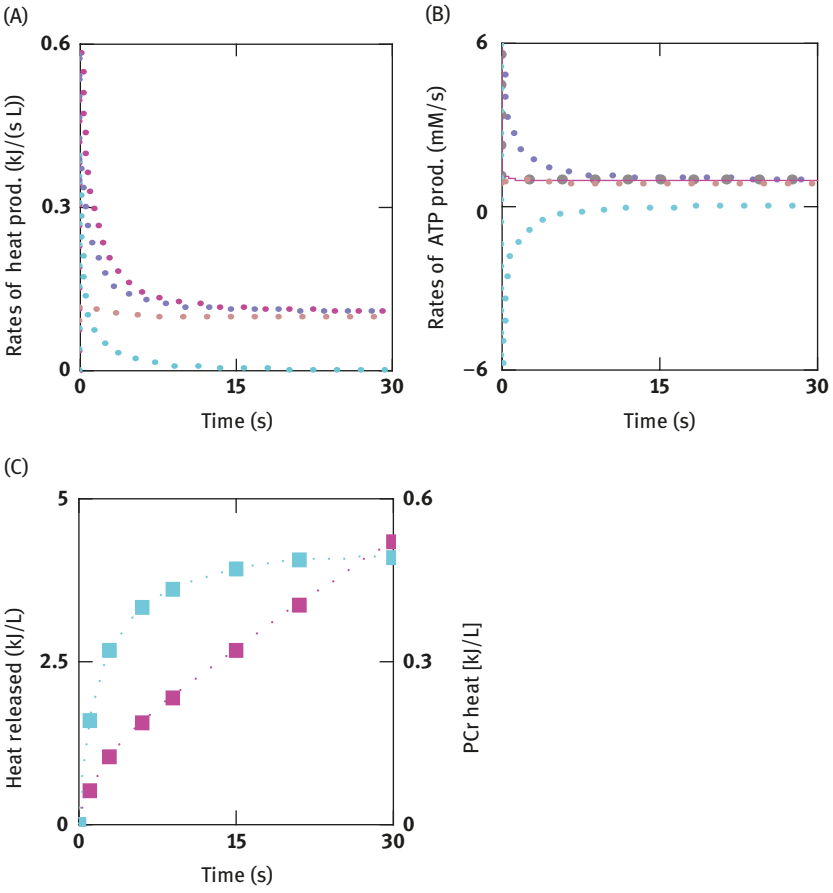

Figure 14.3: Rates of heat production, ATP delivery and demand, and heat release during recovery at $[Ca^{2+}]_c = 0.3\ \mu M$. (A) Blue points: rate of heat production by metabolic, ATP delivering reactions (GLY and PAL, $\dot{Q}^{Del}$); brown points: by PAL ($\dot{Q}^{pal}$); cyan points: by the PCr reaction ($\dot{Q}^{pcr}$); red points: by GLY plus PAL plus PCr reaction ($\dot{Q}^{tot}$). (B) Corresponding ATP delivery and demand rates as shown in Figure 14.2B. (C) Time courses of heat release during recovery at 0.3 µM $[Ca^{2+}]_c$, red points: by GLY plus PAL plus PCr reaction; cyan points: by the PCr reaction alone.

At steady state, ATP is supplied almost completely by PAL. Correspondingly, this also applies to the heat production under these conditions (Figure 14.3A). However, it should be noted that the negative J_{CK} is assumed as a positive value in the calculation of $\dot{Q}_{tot}$. Figure 14.3C shows the corresponding time integrals as heat output. In this case, linear progression of the curve is only observed after a steeper beginning (Figure 14.3C, red). This is due to the initial relatively high PCr formation rate. Therefore, [PCr] becomes elevated from initially about 9.0 mM after a high power output to its resting value of approx. 20 mM. The ATP required for this must be supplied

by GLY and PAL. That these reactions proceed relatively slowly compared to ATP delivery at sudden high power output, is due to the fact, that ATP formation initially proceeds via a high J_{PCr} (positive direction). During the first 6.0 ms, PCr and ATP are still formed via the CK reaction because $[ADP]_c$ is high (307.7 mM). However, after this, the direction of this reaction changes, and PCr is formed with ATP consumption. The PCr formation rate is initially high, but then slowly approaches zero, so that the time integral becomes a parallel to the time axis. During the first second, PCr formation contributes about 37% to the total heat released (C).

15 Fluxes and variable conductances

The simulations used here demonstrate a particular structure, which is determined fundamentally through the mathematical formulations of fluxes occurring within them. Each of these fluxes is principally given by

$$J = \frac{d[\mathrm{S}]}{dt} = L\,A\ (\text{in mM/s}), \tag{15.1}$$

that is, by the product of the conduction and the affinity of the reaction concerned. [S] designates the concentration of a metabolite, which is converted by the appropriate enzyme-catalyzed reaction.

To exemplify this, the glycolytic degradation of Glu to Lac is considered, and the concentrations of which are set to be constant at 4.0 and 1.2 mM. The first reaction is the conversion of Glu to G6P, catalyzed by HK. This is given by

$$J_{HK} = L_{\mathrm{HK}} A_{\mathrm{HK}}.$$

The temporal change from [G6P] is, however, determined through the ensuing conversion of G6P to F6P via PGI. This leads to

$$\frac{d[\mathrm{G6P}]}{dt} = J_{\mathrm{HK}} - J_{\mathrm{PGI}} = L_{HK} A_{HK} - L_{\mathrm{PGI}} A_{\mathrm{PGI}}.$$

Following this principle, one obtains the following for all the other metabolites involved in this reaction sequence:

$$\frac{d[\mathrm{F6P}]}{dt} = J_{\mathrm{PGI}} - J_{\mathrm{PFK}},$$

$$\frac{d[\mathrm{FBP}]}{dt} = J_{\mathrm{PFK}} - J_{\mathrm{Ald}},$$

$$\frac{d[\mathrm{DHAP}]}{dt} = J_{\mathrm{Ald}} - J_{\mathrm{TIM}},$$

$$\frac{d[\mathrm{GAP}]}{dt} = J_{\mathrm{Ald}} + J_{\mathrm{TIM}} - J_{\mathrm{GAP}},$$

$$\frac{d[\mathrm{Pyr}]}{dt} = J_{\mathrm{GAP}} - J_{\mathrm{LDH}},$$

$$\frac{d[\mathrm{ADP}]}{dt} = J_{\mathrm{Wb}} + J_{\mathrm{HK}} + J_{\mathrm{PFK}} - 2J_{\mathrm{GAP}} - 2J_{\mathrm{AK}},$$

$$\frac{d[\mathrm{P_i}]}{dt} = J_{\mathrm{Wb}} - J_{\mathrm{GAP}}$$

https://doi.org/10.1515/9783110650501-015

and

$$\frac{d[\mathrm{AMP}]}{dt} = J_{\mathrm{AK}}.$$

Such a set of differential equations can no longer be analytically solved. The solution must be found numerically with the aid of a solver. For this, the mathematical program *Mathcad 15.0* with the solver *AdamsBDF* was used. As a result, one obtains all the metabolite concentrations (e.g., [G6P] to [Pyr] and $[\mathrm{ADP}]_c$ to [AMP]) as functions of time, where the desired parameters, such as fluxes, affinities or dissipation functions, can be presented as time-dependent quantities.

The velocity of an enzyme-catalyzed reaction is generally presented according to Michaelis and Menten in the form [31, 32]

$$v = \frac{c}{K_{\mathrm{M}} + c}\, V_{\max}. \tag{15.2}$$

The *c*s denote the substrate concentration and K_{M} is the Michaelis–Menten constant of the catalyzing enzyme with the unit of substrate concentration. $V_{\max}$ designates the maximum or limiting velocity to be measured under given conditions (e.g., in mM/s). It depends on the used or present concentration of the respective enzyme. The function $v(c)$ represents a hyperbola with the asymptote $v(c_\infty) = V_{\max}$.

To be able to also present the flux $J = L\,A$ in a similar manner as a function of the substrate concentration, $V_{\max}$ is expressed as a product of a maximum conductance and the given affinity of the respective reaction, yielding $V_{\max} = L^{\max} A$.

The dimensionless Michaelis–Menten factor $c/(K_{\mathrm{M}} + c)$, therefore, maintains its effect on the reaction velocity in the same way as on the flux J when multiplied by $V_{\max}$. At constant affinity at steady state, both formulations should deliver the same numerical result. If, for example, $V_{\max} = 3.0\,\mathrm{mM/s}$, and the affinity starts at $A = 20.0 \times 10^3\,\mathrm{J/mol}$, then $L^{\max}$ must be set as equal to $V_{\max}/A = 3.0/\left(20.0\ 10^3\right) = 1.5\ 10^{-4}\,\mathrm{mM/s \times mol/J}$ in order to obtain the same result. This gives

$$v(c) = \frac{c}{K_{\mathrm{M}} + c}\, V_{\max} = \frac{c}{K_M + c} \times 3.0\ \mathrm{mM/s}$$

and for the flux

$$J(c) = \frac{c}{K_{\mathrm{M}} + c}\, L^{\max} A = \frac{c}{K_{\mathrm{M}} + c} \times 1.5 \times 10^{-4} \times 2.0 \times 10^4 = \frac{c}{K_{\mathrm{M}} + c} \times 3.0\,\mathrm{mM/s}. \tag{15.3}$$

But this only applies as long as A does not change. With an ongoing reaction, however, A decreases so that under such conditions, the Michaelis–Menten equation and the flux equation used here must deviate from each other. The dependency of the flux caused by the Michaelis–Menten factor is, however, retained in the process. Furthermore, this also offers the possibility of generating sigmoidal concentration dependencies, as are seen primarily by enzymes such as PFK. For this, the *c*s and K_{M} must be given the same exponents (>1.0), such as

$$\frac{c^3}{K_M{}^3 + c^3}.$$

However, besides this substrate activation, the by far more important possibility is the introduction of an additional Michaelis–Menten factor, which assumes a changing concentration of a metabolite not taking part in the enzyme reaction concerned, for instance, the activation of PFK through an increasing [AMP]. J_{PFK} can therefore be represented as follows:

$$J_{PFK} = L_{PFK} A_{PFK} = \frac{[AMP]^2}{\left(K_M^{amp}\right)^2 + [AMP]^2} \frac{[F6P]}{K_M^{f6p} + [F6P]} \; L_{PFK}^{max} \; A_{PFK}$$

with

$$L_{PFK} = \frac{[AMP]^2}{\left(K_M^{amp}\right)^2 + [AMP]^2} \frac{[F6P]}{K_M^{f6p} + [F6P]} \; L_{PFK}^{max}.$$

Figure 15.1A and B shows the two Michaelis–Menten factors as functions $f_1([F6P])$ and $f_2([AMP])$, respectively, which, from their course, can also be seen as probabilities. Thus, for a $[AMP] = K_M^{adp} = 2.0\ \mu M$, the value of the probability to achieve

$$\frac{[F6P]}{K_M^{f6p} + [F6P]} \; L_{PFK}^{max}$$

is equal to 0.5. For this [AMP], an $[F6P] = 96.36\,\mu M$, a $K_M^{f6p} = 90.0\,\mu M$ and an $L_{PFK}^{max} = 5.2 \times 10^{-4}\,mM/s \times mol/J$ are conductances of the PFK reaction

$$L = 0.5 \times 0.445 \times 5.2 \times 10^{-4} = 1.159 \times 10^{-4}\,mM/s \times mol/J.$$

In Figure 15.1C, the inhibition of HK by G6P is shown. The probability factor must run in the opposite direction during inhibition, that is, from 1.0 to zero. The conductance for this flux is

$$L_{HK} = \frac{1}{1 + \exp\left(\frac{[G6P] - G6P_{05}}{S_{G6P}}\right)} L_{HK}^{max}$$

with $G6P_{05} = 450\,\mu M$ and $S_{G6P} = 20.0\,\mu M$. At $[G6P] = 450.0\,\mu M$, L_{HK} is 50.0% of L_{HK}^{max}. With increasing substrate concentration, the conductances increase during activation (Figure 15.1A and B), whereas they decrease during inhibition (Figure 15.1C).

To better understand the mode of action of the above reaction sequence, this series of glycolytic reactions are at first examined for constant conductances. The total affinity A_{ov} (including ATP production) is constant. The change in flux at constant conductances is then

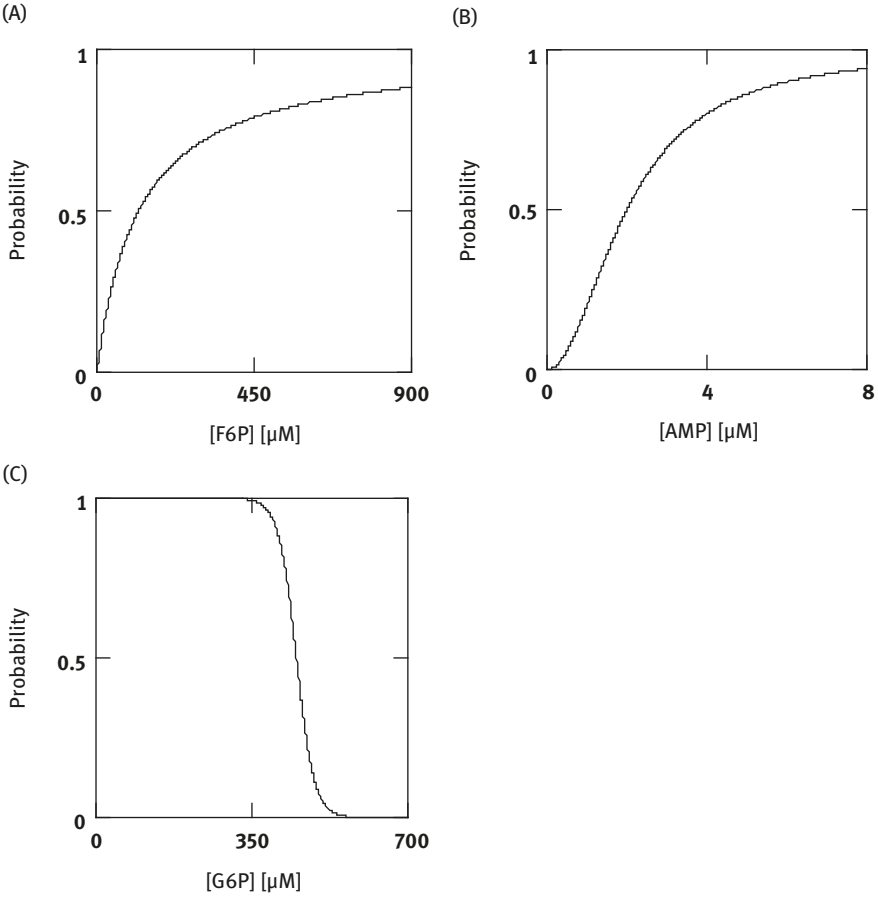

Figure 15.1: The introduction of Michaelis–Menten-like factors, which make conductances variable. (A) Hyperbolic activation through variable [F6P]. (B) Sigmoid activation through variable [AMP]. (C) Sigmoid inhibition through variable [G6P].

$$\Delta J = (L_{\mathrm{ov}0} + \Delta L_{\mathrm{ov}})A_{\mathrm{ov}} - L_{\mathrm{ov}0}A_{\mathrm{ov}} = \Delta L_{\mathrm{ov}}A_{\mathrm{ov}}.$$

If, for example, solely L_{PFK} changes by a factor of 2.0, then this adjusts to an elevated steady-state flux even at constant conductances. This is brought about solely through changes of the affinities involved, whereby their total value A_{ov} must, however, remain unchanged. The change in flux can also be expressed (with $L = 1/R$) as

$$\Delta J = \left(\frac{1}{R_{\mathrm{ov}}} - \frac{1}{R_{\mathrm{ov}0}}\right)A_{\mathrm{ov}} = -\frac{\Delta R}{R_{\mathrm{ov}0}(R_{\mathrm{ov}0} + \Delta R)}A_{\mathrm{ov}} = \Delta L_{\mathrm{ov}}A_{\mathrm{ov}}.$$

Since $R_{ov} = R_1 + R_2 + R_3 + \cdots + R_n$ and

$$\Delta R = R_{10} + R_{20} + (R_{30} + \Delta R) + \cdots + R_n$$
$$- R_{10} + R_{20} + R_{30} + \cdots + R_n.$$

This means that from the conduction change of each individual enzyme reaction, the corresponding change in resistance develops, which, in contrast to the first, is identical to the change in resistance of the entire reaction sequence. Thus, one can calculate the change in flux from the change in conductance. The overall conductance is given by

$$L_{ov} = \frac{1}{\frac{1}{L_{HK}} + \frac{1}{L_{PGI}} + \frac{1}{L_{PFK}} + \frac{1}{L_{Ald}} + \frac{1}{L_{TIM}} + \frac{1}{\bar{L}_{GAP}} + \frac{1}{\bar{L}_{LDH}}} = \frac{1}{R_{ov}}. \tag{15.4}$$

One obtains the overall affinity from

$$A_{ov} = A_{HK} + A_{PGI} + A_{PFK} + A_{Ald} + A_{TIM} + \bar{A}_{GAP} + \bar{A}_{LDH}. \tag{15.5}$$

The affinities and conductances with the bar represent transformed quantities. The reactions from GAPDH up to pyruvate kinase are contracted to one single reaction step. These and the LDH reaction go through the double reaction velocity compared with the flux through the reactions HK to TIM, so that one can no longer obtain A_{ov} simply as the sum of all affinities. For this, it would be necessary that every affinity goes through the same flux. To achieve this, one assumes the total dissipation function

$$\begin{aligned}\Psi_{ov} &= J_{HK}A_{HK} + J_{PGI}A_{PGI} + J_{PFK}A_{PFK} + J_{Ald}A_{Ald} + J_{TIM}A_{TIM} + J_{GAP}A_{GAP} + J_{LDH}A_{LDH} \\ &= 2.2 \times 10^2 \text{kJ}/(\text{Ls}).\end{aligned} \tag{15.6}$$

From this, one obtains A_{ov} by expressing Ψ_{ov} as the product from a given flux, for example J_{HK} and the total affinity. The overall affinity is then given by

$$A_{ov} = \frac{\Psi_{ov}}{J_{HK}} = 1.0274 \times 10^2 \text{ kJ/mol}.$$

As J_{GAP} and J_{LDH} are not identical to J_{HK}, their transformed affinities and conductances related to the selected flux (here J_{HK}) can be obtained from their respective dissipation function. For affinities, this gives

$$\bar{A}_{GAP} = \frac{J_{GAP}\, A_{GAP}}{J_{HK}} = \frac{\Psi_{GAP}}{J_{HK}} = 0.3595$$

and

$$\bar{A}_{LDH} = \frac{\Psi_{LDH}}{J_{HK}} = 17.467 \text{ kJ/mol}.$$

For conductances, one obtains

$$\bar{L}_{\mathrm{GAP}} = \frac{\Psi_{\mathrm{GAP}}}{\left(\bar{A}_{\mathrm{GAP}}\right)^2} = 5.7071 \times 10^{-3}$$

and

$$\bar{L}_{\mathrm{LDH}} = \frac{\Psi_{\mathrm{LDH}}}{\left(\bar{A}_{\mathrm{LDH}}\right)^2} = 1.1745 \times 10^{-4}\,\mathrm{mM/s \times mol/J}.$$

A perturbation of L_{PFK} by

$$\Delta L_{\mathrm{PFK}} = 2L_{\mathrm{PFK0}} - L_{\mathrm{PFK0}} = L_{\mathrm{PFK0}} = 4.5657 \times 10^{-5}\,\mathrm{mM/s \times mol/J}$$

gives a ΔR_{ov} of

$$\Delta R_{\mathrm{PFK}} = \Delta R_{\mathrm{ov}} = \frac{1}{2L_{\mathrm{PFK0}}} - \frac{1}{L_{\mathrm{PFK0}}} = -1.095 \times 10^{4}\ 1/(\mathrm{mM/s \times mol/J}),$$

from which results

$$\Delta J = -\frac{\Delta R}{R_{\mathrm{ov0}}(R_{\mathrm{ov0}} + \Delta R)} A_{\mathrm{ov}} = -\frac{\Delta R}{R_{\mathrm{ov1}}} J_{\mathrm{ov0}} = \frac{\Delta L_{\mathrm{ov}}}{L_{\mathrm{ov0}}} J_{\mathrm{ov0}} = 0.5437\,\mathrm{mM/s}$$

and

$$J_1 = J_0 + \Delta J = 2.0515 + 0.5437 = 2.9592\,\mathrm{mM/s}.$$

From this, all the changed affinities can be derived from $A_X = J_1/L_X$, as all the conductance values remain unchanged. For example,

$$A_{\mathrm{PFK1}} = 28.421\,\mathrm{kJ/mol}\ (A_{\mathrm{PFK0}} = 44.933\,\mathrm{kJ/mol}, \mathrm{factor}: 0.6325)$$

and

$$A_{\mathrm{HK1}} = 54.0\,\mathrm{kJ/mol}\ (A_{\mathrm{HK0}} = 42.687, \mathrm{factor}: 1.265).$$

The conductance elevated by a factor of 2.0 (here L_{PFK}) also does not change. The relative flux change obtained in this way for the whole pathway is

$$\frac{\Delta J}{J_0} = 26.5\%.$$

With the aid of the equations given above, all the ΔAs can be calculated. Their sum must be zero:

$$\sum_{i=1}^{n} \Delta A_i = 0.$$

This condition is fulfilled with sufficient accuracy by the simulation (SIM_{GLY}, see above) with a relative error of

$$\frac{\sum_{i=1}^{n} \Delta A_i - 0}{A_{ov}} = 6.4 \times 10^{-8}.$$

Figure 15.2 shows the time courses of the fluxes after a change of L_{PFK} by a factor of 2.0. The glycolytic ATP production rate is set at 4.103 mM/s. It is equal to J_{GAP} (blue line, Figure 15.2A). In Figure 15.2B, the time courses of the affinities A_{HK} (black) and A_{PFK} (red) are presented. This latter affinity becomes appreciably decreased by the increased flux going through it under these conditions. All the other affinities must increase because any increase in the respective fluxes to a new steady-state value can only be brought about with unchanged conductance values through an increase in their affinities. The lapse of time required for this processes is approximately 1.5 s, which is quite large. Although the relative change obtained for all the fluxes is substantial at 26.5%, it is considerably less pronounced than that, which can be obtained with variable conductances.

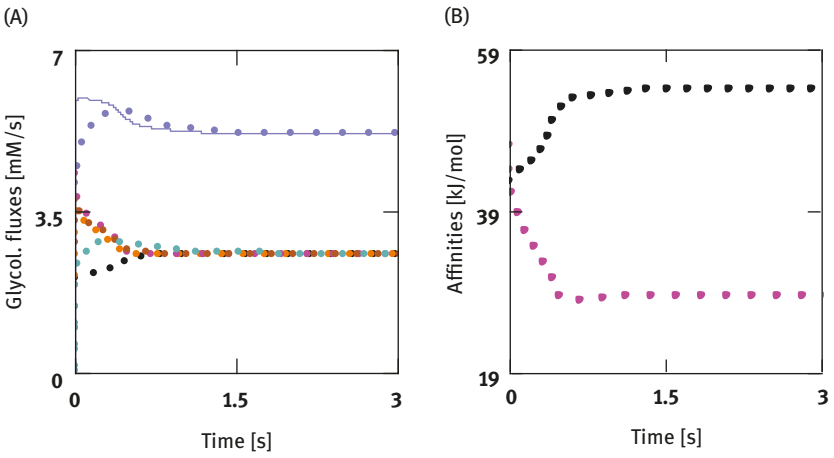

Figure 15.2: Metabolic activation by a conductance perturbance at constant conductances and provoked changes of affinities. (A) Effect of increasing L_{PFK}^{max} by a factor of 2.0 on fluxes, (blue line, J_{GAP}; black points, J_{HK}; yellow points, J_{PGI}; red points, J_{PFK}; brown points, J_{Ald}; green points, J_{TIM}; blue points, J_{LDH}). (B) Effect on affinities (black points, A_{HK}; red points, A_{PFK}); the other glycolytic affinities are much less affected.

The determination of the variable substance concentrations is only possible with the aid of the simulation. Their total concentration is 634.53 µM, and decreases considerably to 379.74 µM after activation of PFK. This is primarily due to the strong decrease in [G6P] and [F6P] (Figure 15.3, yellow and red).

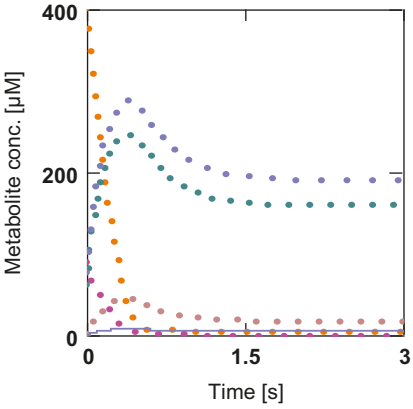

Figure 15.3: Concentration changes of metabolites by a conductance perturbance at constant conductances. Effect of increasing L_{PFK}^{max} by a factor of 2.0 on concentrations of glycolytic intermediates (yellow points, [G6P]; red points, [F6P]; brown points, [FBP]; green points, [DHAP]; blue line: [GAP]; blue points: $[Pyr]_c$).

When HK is activated rather than PFK, these concentrations must increase to very high values in order to achieve an increase in all the fluxes. Furthermore, a steady state would only be achieved after approximately 15.0 min. On the other hand, a reduction in these concentrations can be ruled out because J_{HK} must rise simply through the higher set conductance values. Additionally, a drop in [G6P] would lead to a reduction in [F6P] (A_{PGI} low) so that it would be impossible for J_{PFK} to increase by an increase in its affinity. This does not apply, however, for variable conductances because the HK reaction is inhibited by G6P so that its conductance must decrease with an increase of [G6P]. Activation of the metabolism via this first reaction step would consequently have little effect under these conditions.

At constant conductances, the greatest increase in the pathway flux is achieved by a higher set conductance of the PFK reaction. If all the enzymatic reactions of the pathway would be changed by the same factor at the same time, then the pathway flux would change exactly by this factor without time-consuming changes of concentrations as follows:

$$\frac{1}{\frac{1}{aL_1}+\frac{1}{aL_2}+\frac{1}{aL_3}+\cdots+\frac{1}{aL_n}} = a\ \frac{1}{\frac{1}{L_1}+\frac{1}{L_2}+\frac{1}{L_3}+\cdots+\frac{1}{L_n}} = aL_{ov}. \tag{15.7}$$

This possibility can, however, be excluded for fast activation because all concentrations of involved enzymes have to be increased through new syntheses, which would be extremely energy intensive and, furthermore, would require a lot of time.

For fast activation, as is necessary above all for the sudden increase in ATP demand during contraction, nature has found a much more effective possibility. This comes about due to the way enzymes operate. They catalyze not only the reaction concerned in that they offer a faster reaction pathway for, but also through their

substrate dependency they enable the conductance associated with them to be variable. In this way, the change in a single reaction, for example PFK, can propagate to all the other reaction steps involved in a reaction sequence. The transfer of the activation begins with an increase in the product concentration of the initially activated enzyme reaction, which then comes into effect for the following reaction step as an increase in the substrate. The result is that this also sees an increase in its reaction rate through substrate dependency in accordance with Michaelis–Menten or a similar enzyme kinetic. This process can continue through the last reaction in a sequence so that after achieving a new steady state, the pathway flux has an increased value, which does not fully equal the set change but is generally below it, so as if the original perturbation had been damped.

Unlike with constant conductances, the adjustment to a new steady state with variable conductances is achieved considerably faster (after approximately 0.06 s, Figure 15.4A). Furthermore, $\Delta J/J_0 = 0.7473$ and is therefore considerably higher than at constant conductances (Figure 15.4A). A marked reduction of affinity is only observed for A_{PFK}. A_{HK} hardly needs to change at all this time (compare Figures 15.3B and 15.4B). Under both conditions, the adjustment to a new steady state is dominated by the HK reaction (black).

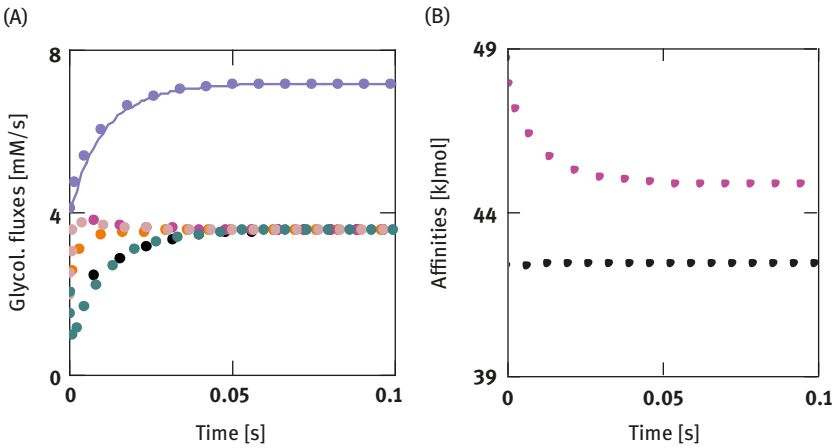

Figure 15.4: Metabolic activation by $[Ca^{2+}]_c = 1.134\,\mu M$ via [AMP] at variable conductances and provoked changes of affinities. (A) Effect on fluxes (blue line, J_{GAP}; black points, J_{HK}; yellow points, J_{PGI}; red points, J_{PFK}; brown points: J_{Ald}; green points, J_{TIM}; blue points, J_{LDH}. (B) Effect on affinities (black points, A_{HK}; red points, A_{PFK}); the other glycolytic affinities are much less affected, and only A_{GAP} does significantly increase.

As has been already mentioned, the greatest advantage that the achievement of variable conductance brings with it is given by the fact that not only the respective substrate concentrations can have additional influence on the reaction velocity, but

that the pathway flux can also be activated through the product of a reaction not involved in the pathway, like AMP from the AK reaction. It is known that the glycolysis enzyme PFK reacts to this product. Only another factor, which includes the activation function, must be added to the flux equation for the PFK reaction to establish this additional activation possibility. This is the dimensionless factor

$$\frac{[\mathrm{AMP}]^2}{\left(K_{\mathrm{M}}^{\mathrm{amp}}\right)^2 + [\mathrm{AMP}]^2},$$

represented in Figure 15.1B as a function of [AMP]. Furthermore, the constant set concentrations of $[\mathrm{ADP}]_c$, $[\mathrm{P_i}]_c$ and [AMP] appear as variables in simulation this time, so that $A_{\mathrm{ATP}}^{\mathrm{c}}$ is also a variable. Instead of direct activation of the PFK reaction with the factor 2.0, an increase in the pathway flux is induced by doubling power output. This causes $[\mathrm{ATP}]_c$ to drop initially from 8.9 to 8.746 mM ($\Delta[\mathrm{ATP}] = 25.11\,\mu\mathrm{M}$), while $[\mathrm{ADP}]_c$ increases from 100.0 to 124.52 µM (Figure 15.5B), This increase in $[\mathrm{ADP}]_c$ is transferred via the AK reaction into an increase in [AMP] from 1.0 to 1.594 (Figure 15.5B). This increase in [AMP] is sufficient to almost double the pathway flux ($\Delta J/J_0 = 0.964$). In contrast to the changes found for constant conductances, all the other concentrations change only marginally (Figure 15.5A).

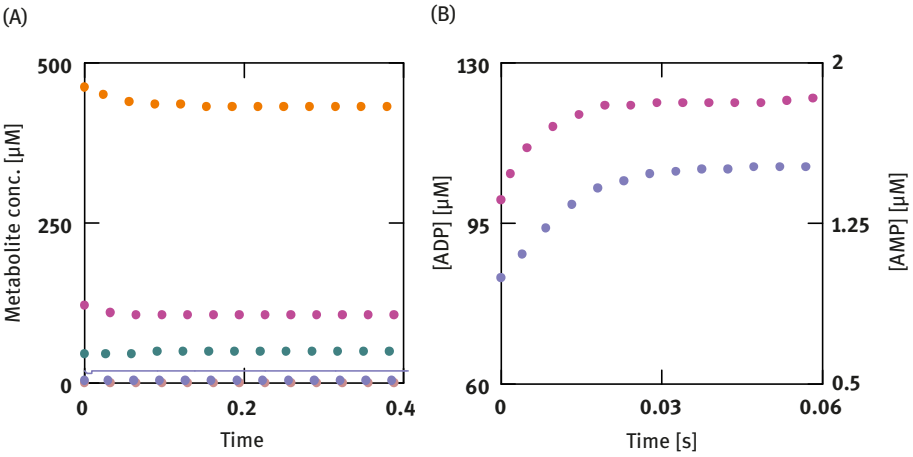

Figure 15.5: Concentration changes of metabolites by $[\mathrm{Ca}^{2+}]_c = 1.134$ mM at variable conductances. (A) Effect of [AMP] on concentrations of glycolytic intermediates (yellow points, [G6P]; red points, [F6P]; brown points, [FBP]; green points, [DHAP]; blue line, [GAP]; blue points, $[\mathrm{Pyr}]_c$). (B) Effect on $[\mathrm{ADP}]_c$ (red points) and [AMP] (blue points).

From Figure 15.5 it is seen that while somewhat more time is needed to achieve a new steady state with AMP activation (approx. 0.4 s, A), this indirect mechanism may more effectively raise the pathway flux than through direct perturbation of the

PFK conductance. The increase of [AMP] triggered by the increased power output corresponds to a factor of approximately 1.9 for the change in L_{PFK}.

Also under these conditions, the time required to reach the steady state is crucially determined by the HK reaction (Figure 15.4A), although A_{HK} is not markedly changed (Figure 15.4B).

The relative change of conductances shows particularly clearly which reaction steps of the sequence are specifically affected (Figure 15.6). These are the HK and PFK reactions, and the GAP and LDH reactions (Figure 15.6B).

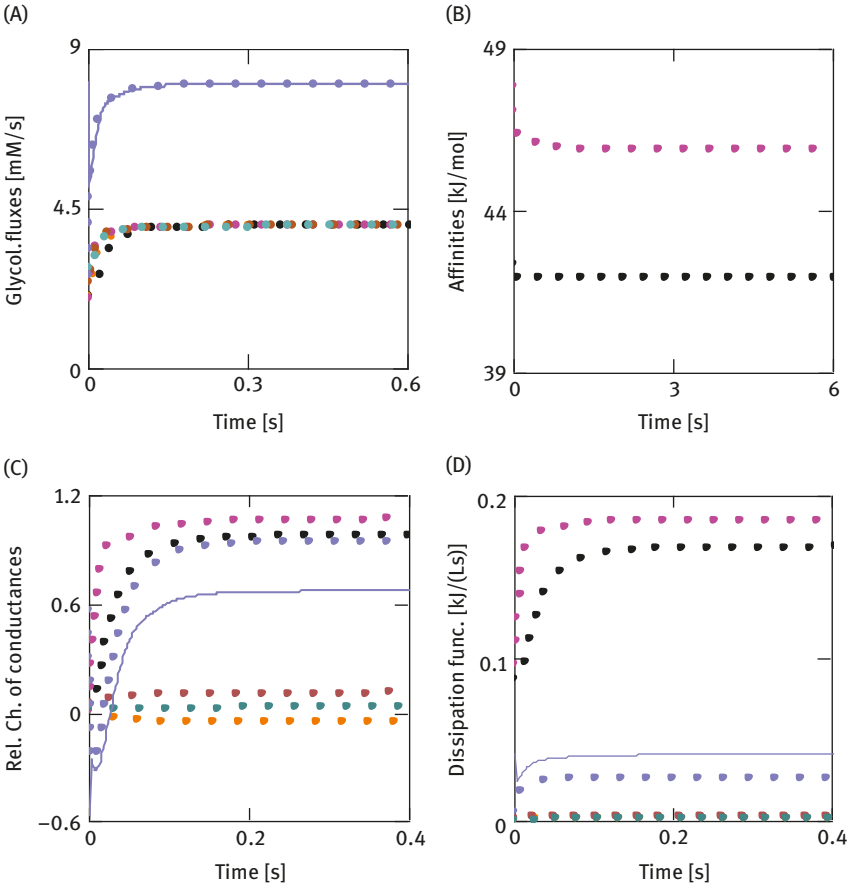

Figure 15.6: Effects of AMP activation. (A) and (B) as in Figure 15.4. (C) Effects on respective conductances ($\Delta L/L = \Delta_r L$) (red points,$\Delta_r L_{PFK}$; black points:$\Delta_r L_{HK}$; blue points:$\Delta_r L_{LDH}$; blue line:$\Delta_r L_{GAP}$; brown points:$\Delta_r L_{Ald}$; green points:$\Delta_r L_{TIM}$; yellow points:$\Delta_r L_{PGI}$). (D) Effects on dissipation functions of glycolytic reactions (red points,Ψ_{PFK}; black points:Ψ_{HK}; blue line:Ψ_{GAP}; blue points:Ψ_{LDH}; green points:Ψ_{TIM}).

Notable in connection with this is that L_{PGI} must decrease slightly. It emerges from the changes in the dissipation functions that the entropy production rates are essentially generated from the HK and PFK reactions (Figure 15.6D). These reactions are, therefore, also significantly involved in the heat production of this glycolytic reaction sequence.

To be able to achieve a highest possible pathway flux from a low flux under resting conditions, the conductance of the PFK reaction must allow a broad range of conductance values. This is guaranteed by a high L_{PFK}^{max}. Through a low [AMP] at low power output, the high conductance is, however, reduced, which can be taken as inhibition of PFK under these conditions. This inhibition becomes increasingly lower with increasing [AMP]. Therefore, it seems more appropriate to denote the activation of the PFK reaction as deinhibition.

Every individual reaction in the sequence must – as well as any chemical reaction – have a positive affinity or possess a positive $\Delta_{Ri}S$, respectively, so that at steady state the result is a flux, which does not differ from all the other fluxes and hence must be equal to the pathway flux. For every enzyme-catalyzed reaction in the sequence, the following equation must be fulfilled at steady state:

$$\frac{\Delta J}{J_0} = \frac{\Delta A}{A_0} + \frac{\Delta L}{L_0}\left(1 + \frac{\Delta A}{A_0}\right). \tag{15.8}$$

At constant conductance values, the second term on the right-hand side is vanishing. The result complies with Ohm's law. For variable conductances this law has to be merely expanded by the second term. The resulting effect of the pathway flux is, however, substantial. Without this additional specification, a rapid switch from low to high power output would hardly be possible.

In the phenomenological approach presented here, the flux is given as a combination of the classical flux equation from NET [5] and enzyme kinetics. Obviously, the obtained formulas with variable conductances are able to describe metabolic reactions in simulations including those, which are far from equilibrium.

The question regarding at which point in the sequence to place this switch in order to influence all the reactions the most cannot be answered clearly. This problem must not be solved by the solver, but instead is entered into the formulation of the PFK reaction as part of the differential equation block. As already discussed, this should be a reaction with a resting conductance that is as low as possible so that the associated affinity must be correspondingly high (to reach a given flux magnitude), as is the case with the PFK reaction. According to the above equation, a maximum $\Delta J/J_0$ should be reached in the extreme case if and only if ΔA changes from a negative value toward zero at an as much as possible high positive ΔL, so that

$$\frac{\Delta J_{max}}{J_0} = \lim_{\Delta A \to 0}\left(\frac{\Delta A}{A_0}\right) + \frac{\Delta L}{L_0}\left(1 + \lim_{\Delta A \to 0}\left(\frac{\Delta A}{A_0}\right)\right) = \frac{\Delta L}{L_0} \tag{15.9}$$

is applied.

Such activation, however, cannot be achieved under real conditions (A_{PFK} = 48.64 kJ/mol). To be able to guarantee a high power output despite this, the deinhibition of PFK must occur through a metabolite, which like AMP is present in a preferably low concentration so that changes in energy metabolism can be sensitively recorded. Only in this way it is possible to achieve a sufficiently high power output.

There are a number of procedures for presenting a branch of metabolism using differential equations and to solve them with the aid of an appropriate solver. The advantage of the flux equations used here is that this is based on the relationships of the thermodynamics of irreversible processes and consequently includes all the thermodynamic parameters, which are necessary for the evaluation and analysis of a pathway flux. A description based solely on kinetic equations would probably not be capable of permitting statements concerning such important quantities as entropy production, heat output and efficiency. Furthermore, it would be impossible to realize one of the fundamental and most prominent characteristics of living cells, the ability for reaction coupling. This achievement should be expected to the requirements for the generation and development of living systems.

16 Reaction coupling and the second law

Often, to supposedly facilitate understanding of the concept of entropy production in chemical and biochemical reactions, a comparison is made with the order of a system and its environment. An increase in entropy ($\Delta_{Ri}S > 0$) is put on a level with a decrease in order in the system and/or environment. This view has led to the following consideration: living systems are characterized particularly by the fact that, as for instance during growth, order is generated within them, as, in the process, large molecules and supramolecular structures are created from a huge number of small molecules, which is associated with an increase in order. This would mean, however, that the entropy of the system must be decreased. The production of such negentropy (=negative entropy) would, however, be inconsistent with the second law. The conclusion from this is that this thermodynamic law is not valid in living nature.

Such a situation is, however, unacceptable to many people. Hence, it has been looked for arguments that would support the validity of the second law also for living systems. To do this, one simply postulated that it is sufficient that only the entropy balance is positive. Consequently, the second law would not be violated, if a negentropic process could be balanced by an additional process associated with a more positive entropy production at another place, for example by solar irradiation. In this way, the requirements for the second law remained unviolated.

The scientific debate arising from it is, however, long settled. Not, however, because one opinion had prevailed. Both the recognition of the problem and its attempted solution show that the existence of coupled reactions and that these are found in particular in living systems have been completely ignored. The characteristic behavior of such reactions has been discussed in depth and explained on the basis of multiple calculated examples.

Regarding the term negentropy, it remains to be said that it refers to that entropy part, which due to coupling cannot appear separately. $A_{res} = A_1 + A_2 < A_2 > 0$ is the affinity, which is associated with entropy production. This entropy change is always positive so that the second law remains always fulfilled. The part of entropy production associated with A_1 (< 0) is referred to as negentropy.

The generation of complex structures also proceeds according to this principle. To synthesize a protein, for example, every chemical bond between the amino acids must be formed by reaction coupling. The input reaction available for this is given by the ATP splitting reaction so that every formed bond of the thus created macromolecule is associated with a positive change entropy.

A negative change in entropy cannot only become positive in the balance because a sufficient positive entropy change is occurring in the environment. This possibility only exists if both processes can be connected on a molecular level, that is, linked with each other by chemical bonds. For this, it is often necessary that an

https://doi.org/10.1515/9783110650501-016

enzyme-like protein complex consisting of several proteins is present, which brings about the quasicoupling as a molecular machine.

Well-known technological macroscopic machines, such as the combustion engine, also function according to the principle of reaction coupling. In the petrol engine, for example, fuel is burnt to generate a high temperature. Due to the temperature difference between the combustion chamber and the environment created in this way, heat is released into the environment via a Carnot cycle, which couples the heat transport to the generation of mechanical energy.

In the macroscopic as in the molecular process, the production of useful work via a coupled process can only work if energy uptake and release, entropy uptake and release and entropy production proceed all via the same machinery. In technical and many living systems, in the first instance it is not about gaining the maximal work as in the course of a reversible process, but rather about the power output. But an increase of power is always inevitably associated with an increase of irreversibility, and thus, also with an increased rate of entropy production. This situation is quantitatively realized by the dissipation function. In this relationship, the concept of order seems superfluous. It should be remembered that Boltzmann's derivation is related to the probability of systems, which provided the basis for a quantitative definition of entropy.

Appendix

Simulation of Ca^{2+} transport reactions at the SR membrane:

$$\mathrm{SIM}_{\mathrm{CaTr}}, \tag{A1}$$

$$\frac{d\,\mathrm{MP}_r}{dt} = \frac{1}{C_{\mathrm{Mr}}}(J_{\mathrm{ser}} - J_{\mathrm{cach}} - J_{\mathrm{K}}),$$

$$\frac{d[\mathrm{Ca}^{2+}]_{\mathrm{c}}}{dt} = \frac{1}{1 + [\mathrm{BU}_{\mathrm{tot}}]_{\mathrm{c}} \frac{K_{\mathrm{Buc}}}{\left(K_{\mathrm{Buc}} + [\mathrm{Ca}^{2+}]_{\mathrm{c}}\right)^2}}(J_{\mathrm{cach}} - J_{\mathrm{ser}}),$$

$$\frac{d[\mathrm{Ca}^{2+}]_{\mathrm{r}}}{dt} = \frac{1}{1 + [\mathrm{BU}_{\mathrm{tot}}]_{\mathrm{r}} \frac{K_{\mathrm{Bur}}}{\left(K_{\mathrm{Bur}} + [\mathrm{Ca}^{2+}]_{\mathrm{r}}\right)^2}}(J_{\mathrm{ser}} - J_{\mathrm{cach}}),$$

$$\frac{d[\mathrm{ATP}]_{\mathrm{c}}}{dt} = \frac{1}{2}J_{\mathrm{ser}}.$$

where membrane capacity of the SR membrane $C_{\mathrm{Mr}} = 0.2636\mathrm{nF}$, total buffer concentration of the sarcosol $[\mathrm{BU}_{\mathrm{tot}}]_{\mathrm{c}} = 1.0\mathrm{mM}$, $K_{\mathrm{Buc}} = 5.0\ \mu\mathrm{M}$, $[\mathrm{BU}_{\mathrm{tot}}]_{\mathrm{r}} = 15.0\mathrm{mM}$, $K_{\mathrm{Bur}} = 30.0\mu\mathrm{M}$.

Simulation of Na/K ATPase and of Na^+ and K^+ transport at the sarcolemma:

$$\mathrm{SIM}_{\mathrm{Na/K}}: \tag{A2}$$

$$\frac{d\,\mathrm{MP}}{dt} = J_{\mathrm{Na}} + J_{\mathrm{K}} - J_{\mathrm{Cl}} - J_{\mathrm{Na/K}},$$

$$\frac{d[\mathrm{Na}^+]_{\mathrm{c}}}{dt} = J_{\mathrm{Na}} - 3J_{\mathrm{Na/K}},$$

$$\frac{d[\mathrm{K}^+]_{\mathrm{c}}}{dt} = 2J_{\mathrm{Na/K}} - J_{\mathrm{K}}.$$

Simulating metabolism of GLY plus PAL ($\mathrm{SIM}_{\mathrm{GLY/PAL}}$) including ion concentrations of H^+ and Mg^{2+} of the sarcosol and the mitochondrial matrix, reactions of ATP formation and splitting, PCr formation and break down, and AK are formulated by using respective species:

https://doi.org/10.1515/9783110650501-017

$$\mathrm{SIM_{GLY/PAL}}: \tag{A3}$$

$$\frac{d\,\mathrm{MP_m}}{dt} = \frac{1}{C_{\mathrm{Mm}} \cdot \alpha_{\mathrm{m}}} (\nu_{\mathrm{SY}} J_{\mathrm{SY}} + J_{\mathrm{AE}} + 2J_{\mathrm{CU}} + J_{\mathrm{NAsh}} + J_{\mathrm{PL}} - \nu_{\mathrm{NA}} J_{\mathrm{NA}} - \nu_{\mathrm{FA}} J_{\mathrm{FA}}).$$

$$\frac{d[\mathrm{H}^+]_{\mathrm{m}}}{dt} = \frac{1}{1 + \kappa_{\mathrm{H1}}^{\mathrm{BU}} + \kappa_{\mathrm{H2}}^{\mathrm{BU}}} (\nu_{\mathrm{SY}} J_{\mathrm{SY}} + J_{\mathrm{Pi}} + J_{\mathrm{PL}} + J_{\mathrm{NAsh}} + 2J_{\mathrm{HC}} + J_{\mathrm{CAm}} - \nu_{\mathrm{NA}} J_{\mathrm{NA}} - \nu_{\mathrm{FA}} J_{\mathrm{FA}})$$

$$+ \frac{1}{1 + \kappa_{\mathrm{H1}}^{\mathrm{BU}} + \kappa_{\mathrm{H2}}^{\mathrm{BU}}} (\mathrm{H}^+ \text{ fluxes of the mitochondrial matrix}),$$

$$\frac{d[\mathrm{Ca}^{2+}]_{\mathrm{m}}}{dt} = \frac{1}{1 + \kappa_{\mathrm{Cam}}} \times (J_{\mathrm{CU}} - J_{\mathrm{HC}}),$$

$$\frac{d[\mathrm{NAD_{red}}]_{\mathrm{m}}}{dt} = J_{\mathrm{PDH}} + 7J_{\beta} + 3J_{\mathrm{CAC}} + J_{NAsh} - J_{\mathrm{NA}},$$

$$\frac{d[\mathrm{FAD_{red}}]_{\mathrm{m}}}{dt} = 7J_{\beta} + J_{\mathrm{CAC}} + J_{\mathrm{FAsh}} - J_{\mathrm{FA}},$$

$$\frac{d[\mathrm{ADP}]_{\mathrm{m}}}{dt} = J_{\mathrm{AE}} - J_{\mathrm{CAC}} - J_{\mathrm{SY}},$$

$$\frac{d[\mathrm{P_i}]_{\mathrm{m}}}{dt} = J_{\mathrm{HP}} - J_{\mathrm{SY}} - J_{\mathrm{CAC}},$$

$$\frac{d[\mathrm{ADP}]_{\mathrm{c}}}{dt} = J_{\mathrm{Str}}^{\mathrm{p}} + J_{\mathrm{ser}} + J_{\mathrm{Wb}} + J_{\mathrm{GK}} + J_{\mathrm{PFK}} + J_{\mathrm{Glgsy}} + J_{\mathrm{Acc}} - J_{\mathrm{AE}} - 2J_{\mathrm{GAP}} - 2J_{\mathrm{AK}} - J_{\mathrm{CK}},$$

$$\frac{d[\mathrm{P_i}]_{\mathrm{c}}}{dt} = J_{\mathrm{Str}}^{\mathrm{p}} + J_{\mathrm{ser}} + J_{\mathrm{Wb}} + 2J_{\mathrm{PPi}} + J_{\mathrm{Acc}} - J_{\mathrm{HP}} - J_{\mathrm{GAP}} - J_{\mathrm{Glgenph}},$$

$$\frac{d[\mathrm{Pyr}]_{\mathrm{m}}}{dt} = J_{\mathrm{Pym}} - J_{\mathrm{PDH}},$$

$$\frac{d[\mathrm{AcCoA}]_{\mathrm{m}}}{dt} = 8J_{\beta} + J_{\mathrm{PDH}} - J_{\mathrm{CAC}} - J_{\mathrm{Acco}},$$

$$\frac{d[\mathrm{AcCoA}]_{\mathrm{c}}}{dt} = J_{\mathrm{Acco}} + J_{\mathrm{Mcd}} - J_{\mathrm{Acc}},$$

$$\frac{d[\mathrm{Palm}]_{\mathrm{c}}}{dt} = J_{\mathrm{Palm}} - J_{\mathrm{Thk}},$$

$$\frac{d[\mathrm{PalmCoA}]_{\mathrm{c}}}{dt} = J_{\mathrm{Thk}} - J_{\mathrm{Cpt}},$$

$$\frac{d[\mathrm{PalmCoA}]_{\mathrm{m}}}{dt} = J_{\mathrm{Cpt}} - J_{\beta},$$

$$\frac{d[\mathrm{MalCoA}]}{dt} = J_{\mathrm{Acc}} - J_{\mathrm{Mcd}},$$

$$\frac{d[\mathrm{PP_i}]}{dt} = J_{\mathrm{Thk}} + J_{\mathrm{Gglsy}} - J_{\mathrm{PPi}},$$

$$\frac{d[\mathrm{Pyr}]_{\mathrm{c}}}{dt} = J_{\mathrm{GAP}} - J_{\mathrm{LDH}} - J_{\mathrm{Pym}},$$

$$\frac{d[\mathrm{Lac}]}{dt} = J_{\mathrm{LDH}} - J_{\mathrm{Lac}},$$

$$\frac{d[\mathrm{NAD_{red}}]_{\mathrm{c}}}{dt} = J_{\mathrm{GAP}} - J_{\mathrm{NAsh}} - J_{\mathrm{FAsh}},$$

$$\frac{d[\mathrm{G6P}]}{dt} = J_{\mathrm{HK}} + J_{\mathrm{PGM}} - J_{\mathrm{PGI}},$$

$$\frac{d[\mathrm{G1P}]}{dt} = J_{\mathrm{Glgenph}} - J_{\mathrm{PGM}},$$

$$\frac{d[\mathrm{F6P}]}{dt} = J_{\mathrm{PGI}} - J_{\mathrm{PFK}},$$

$$\frac{d[\mathrm{FBP}]}{dt} = J_{\mathrm{PFK}} - J_{\mathrm{Ald}},$$

$$\frac{d[\mathrm{GAP}]}{dt} = J_{\mathrm{Ald}} + J_{\mathrm{TIM}} - J_{\mathrm{GAP}},$$

$$\frac{d[\mathrm{DHAP}]}{dt} = J_{\mathrm{Ald}} - J_{\mathrm{TIM}},$$

$$\frac{d[\mathrm{CO_2}]_{\mathrm{m}}}{dt} = J_{\mathrm{PDH}} + 2J_{\mathrm{CAC}} - J_{\mathrm{CO_2m}} - J_{\mathrm{CAm}},$$

$$\frac{d[\mathrm{CO_2}]_{\mathrm{c}}}{dt} = J_{\mathrm{CO_2m}} - J_{\mathrm{CAc}} - J_{\mathrm{CO_2c}},$$

$$\frac{d\left[\mathrm{HCO_3^-}\right]_{\mathrm{m}}}{dt} = J_{\mathrm{CAm}},$$

$$\frac{d\left[\mathrm{HCO_3^-}\right]_{\mathrm{c}}}{dt} = J_{\mathrm{CAc}} + J_{\mathrm{Acc}} - J_{\mathrm{Mcd}} - J_{\mathrm{Anex}},$$

$$\frac{d[\mathrm{H^+}]_{\mathrm{c}}}{dt} = \frac{1}{1 + \kappa_{\mathrm{H1}}^{\mathrm{BU}} + \kappa_{\mathrm{H2}}^{\mathrm{BU}}} \left(J_{\mathrm{CAc}} + J_{\mathrm{Glgsy}} + J_{\mathrm{LDH}} - J_{\mathrm{CPK}} - J_{\mathrm{Lac}} - J_{\mathrm{NaH}}\right) + \frac{1}{1 + \kappa_{\mathrm{H1}}^{\mathrm{BU}} + \kappa_{\mathrm{H2}}^{\mathrm{BU}}} (\mathrm{H^+ fluxes\ of\ the\ sarcosol}),$$

$$\frac{d[\mathrm{PCr}]}{dt} = -J_{\mathrm{CK}},$$

$$\frac{d[\mathrm{AMP}]}{dt} = J_{\mathrm{Thk}} - J_{\mathrm{AK}},$$

$$\frac{d[\mathrm{Mg}^{2+}]_{\mathrm{c}}}{dt} = \frac{1}{1+\kappa_{\mathrm{Mg}}^{\mathrm{BU}}}\left(\mathrm{Mg}^{2+}\ \text{fluxes of the sarcosol}\right),$$

$$\frac{d[\mathrm{Mg}^{2+}]_{\mathrm{m}}}{dt} = \frac{1}{1+\kappa_{\mathrm{Mg}}^{\mathrm{BU}}}\left(\mathrm{Mg}^{2+}\ \text{fluxes of the mitochondrial matrix}\right).$$

References

[1] Noether, E. (1918) Invarianten beliebiger Differentialausdrücke. Nachrichten von der Gesellschaft der Wissenschaften zu Göttingen, Mathematisch-Physikalische Klasse, 37–44.
[2] Kondepudi, D., & Prigogine, I. (1998) Modern Thermodynamics: From Heat Engines to Dissipative Structures. Chichester, UK: John Wiley & Sons.
[3] Kondepudi, D., & Prigogine, I. (2015) Modern Thermodynamics: From Heat Engines to Dissipative Structures, Second Edition. Chichester, UK: John Wiley & Sons.
[4] Atkins, P., & De Paula, J. (2010) Atkins' Physical Chemistry. Oxford: University Press.
[5] Caplan, SR., & Essig, A. (1983) Bioenergetics and Linear Nonequilibrium Thermodynamics: The Steady State. Cambridge, MA, USA: Harvard University Press.
[6] Katchalsky, A., & Curran, PF. (1967) Nonequilibrium Thermodynamics in Biophysics. Cambridge Massachusetts UK: Harvard University Press.
[7] Pietrobon, D., & Caplan, SR. (1989) Use of nonequilibrium thermodynamics in the analysis of transport: general flow force relationships and the linear domain. Methods Enzymol. 171, 397–444.
[8] Mitchell, P. (1961) Coupling of phosphorylation to electron and hydrogen transfer by a chemiosmotic type of mechanism. Nature 191, 144–148.
[9] Mitchell, P., & Moyle, J. (1969) Estimation of membrane potential and pH difference across the cristae membrane of rat liver mitochondria. Eur. J. Biochem. 7, 471–484.
[10] Mitchell, P. (2011) Chemiosmotic coupling in oxidative and photosynthetic phosphorylation. Biochim. Biophys. Acta 1807, 1507–1538.
[11] Nicholls, DG., & Ferguson, SJ. (2013) Bioenergetics 4. Amsterdam, Boston, Heidelberg, London, New York, Oxford, Paris, San Diego, San Francisco, Singapore, Sydney, Tokyo: Academic Press.
[12] Hinkle, PC. (2005) P/O ratios of mitochondrial oxidative phosphorylation. Biochim. Biophys. Acta 1706, 1–11.
[13] Diederichs, F. (2010) Energetics of glucose metabolism: a phenomenological approach to metabolic network modeling. Int. J. Mol. Sci. 11, 2921–2961.
[14] Diederichs, F. (2012) From cycling between coupled reactions to the cross-bridge cycle: mechanical power output as an integral part of energy metabolism. Metabolites 2, 667–700.
[15] Diederichs, F. (2015) Substrate utilization in skeletal muscle under conditions of low and high power output: the thermodynamics of demand and delivery pathways. J. Basic App. Res. Int. 8, 126–154.
[16] Alberty, RA. (2003) Thermodynamics of Biochemical Reactions. New York NY, USA: Wiley Interscience.
[17] Vaughan – Jones, RD., Spitzer, KW., & Swietach, P. (2006) Spatial aspects of intracellular pH regulation in heart muscle. Prog. Biophys. Mol. Biol. 90, 207–224.
[18] Huxley, AF. (1957) Muscle structure and theories of contraction. Prog. Biophys. Biophys. Chem. 7, 255–318.
[19] Huxley, AF., & Simmons, RM. (1971) Proposed mechanism of force generation in striated muscle. Nature 233, 533–538.
[20] Huxley, AF. (2000) Mechanics and models of the myosin motor. Phil. Trans. R. Soc. Lond. B 355, 433–440.
[21] Huxley, HE. (2004) Fifty years of muscle and the sliding filament hypothesis. Eur. J. Biochem. 271, 1403–1415.
[22] Craig, R. (1977) Structure of A – segments from frog and rabbit skeletal muscle. J. Mol. Biol. 109, 69–81.
[23] Barclay, CJ. (2015) Energetics of contraction. Compr. Physiol. 5, 961–995.

https://doi.org/10.1515/9783110650501-018

[24] Aliev, MK., Dos Santos, P., Hoerter, JA., Soboll, S., Tikhonov, AN., & Saks, VA. (2002) Water content and its intracellular distribution in intact and saline perfused rat hearts revisited. Cardiovasc. Res. 53, 48–58.
[25] Hill, AV. (1938) The heat of shortening and the dynamic constants of muscle. Proc. Soc. Lond. B 126, 136–195.
[26] Hill, AV. (1964) The efficiency of mechanical power development during muscular shortening and its relation to load. Proc. Soc. Lond. B 159, 319–324.
[27] Saks, V., Favier, R., Guzun, R., Schlattner, U., & Wallimann, T. (2006) Molecular system bioenergetics: regulation of substrate supply in response to heart energy demands. J. Physiol. 577, 769–777.
[28] Jeppesen, J., & Kiens, B. (2012) Regulation and limitations to fatty acid oxidation during exercise. J. Physiol. 590, 1059–1068.
[29] Bonen, A., Luiken, JJFP., Arumugam, Y., Glatz, JFC., & Tandon, NN. (2000) Acute regulation of fatty acid uptake involves the cellular redistribution of fatty acid translocase. J. Biol. Chem. 275, 14501–14508.
[30] Holloway, GP., Luiken, JJFP., Glatz, JFC., Spriet, LL., & Bonen, A. (2008) Contribution of FAT/CD36 to the regulation of skeletal muscle fatty acid oxidation: an overview. Acta Physiol. 194, 293–309.
[31] Segel, IH. (1976) Biochemical Calculations 2nd Edition, New York, London, Sydney, Toronto: John Wiley & sons.
[32] Segel, IH. (1975) Enzyme kinetics, New York, London, Sydney, Toronto: John Wiley & sons.

Index

https://doi.org/10.1515/9783110650501-019